# PETROLOGIC IMPLICATIONS FROM THE CHEMISTRY OF OLIVINE PHENOCRYSTS

by

CHRISTOPHER A. VIDITO

A Dissertation submitted to the

Graduate School-New Brunswick

Rutgers, The State University of New Jersey

in partial fulfillment of the requirements

for the degree of

Doctor of Philosophy

Graduate Program in Geological Sciences

written under the direction of

Dr. Claude T. Herzberg

and approved by

_____

_____

_____

_____

New Brunswick, New Jersey

October, 2014

Abstract of the Dissertation

Petrologic Implications from the Chemistry of Olivine Phenocrysts

By Christopher A. Vidito

Dissertation Director:

Claude T. Herzberg

Source lithology of mantle plumes and other volcanic sources has been inferred from isotopic data for decades, however these studies cannot determine if the geochemical signature of pyroxenitic source is due to the presence of a pyroxenite, or if the geochemical signature had been imprinted upon peridotite by some metosomatic process (e.g. refertilization). Mn, Ca and Ni concentrations in olivines are used to infer the source lithology of primitive basalts. Secular cooling of the Galápagos hotspot has been established by petrologic modeling. An increase in the entrainment of relatively dense pyroxenite in the Galápagos plume over time may explain this trend in decreasing Tp with time, as pyroxenite entrainment would have a negative effect on the buoyancy of the plume. Analyses of olivines from Curacao indicates that pyroxenite was absent in the source of these Cretaceous age Galápagos plume lavas. Magmatism preserved at Quepos marks the transition of the Galápagos plume from the head (LIP) stage to the tail (hotspot track) stage. Major and trace element analyses of Quepos samples show a geochemical signal of a pyroxenite. The presence of pyroxenite as a distinct lithology in the source of these lavas is confirmed by olivine analyses. The extreme enrichment of radiogenic lead found in the lavas of Mangaia have long been interpreted as reflecting a component of ancient recycled crust and is representative of the isotopic endmember HIMU. Olivine

analyses of samples from Mangaia indicate that the source of these lavas is predominantly peridotite. If the source of Mangaia had a substantial pyroxenitic component, as inferred from isotopic data, then it is likely that it had its lithological identity destroyed. This may have been the result of the refertilization of mantle periditote by the injection of silicic, pyroxenite source melt. Ni excess observed in the chemistry of olivines from various LIPs and hotspots contrast their Mn and Ca concentrations which are indicative of a peridotite source. High $^{3}He/^{4}He$ found in samples for which He analysis has been done, suggest a deep lower mantle source. The Ni excess may be due to the interaction between the lower mantle and the core.

## Preface

The use of olivine trace element chemistry to infer source lithology first applied by Sobolev et al., 2005, constitutes the bulk of my PhD thesis work. This work as well as my masters thesis show that forward and inverse modeling of olivine chemistry is not only crucial for inferences of source lithology to be made, but also allows for the determination of magma chamber processes other than olivine crystallization (e.g. co-crystallization of other mineral phases, magma recharge and mixing). Below are summaries of my contributions to the 4 chapters of this dissertation as well as the contributions of other researchers.

**Chapter 1:**

This chapter is based on my modeling and interpretations of high precision EPMA olivine analyses I performed on samples from Curacao using the JXA-8200 superprobe at Rutgers University. These data were obtained from Curacao samples provided by A. Kerr from Cardiff University. Initial modeling of the pyroxenite primary magma was done by C. Herzberg and I performed all of the remaining petrologic modeling. I am responsible for the nterpretations and the writing of this text. Although it may not be published in a journal in this form, this work is expected to constitute part of an article in collaboration with E. Gazel and J. Trela at Virginia Tech, to be submitted for publication in late 2014 or early 2015.

**Chapter 2:**

The study of the accreted terranes at Quepos was made possible by the acquisition of samples by E. Gazel. I performed analyses of olivines from these samples on the JXA-8200 superprobe at Rutgers University. Thin sections of eight Quepos picrites were provided by E. Gazel, while I made the remaining 2 thin sections from chips supplied by E. Gazel. The initial modeling of the pyroxenite source primary magmas was done by C. Herzberg and I did all of the remaining petrologic modeling presented in the appendix. Interpretations and the writing of the appendix is my work. The bulk of the chapter was written by J. Trela at Virginia Tech. I also contributed to the writing of the body of the manuscript. Ar ages discussed in the chapter were obtained by B. Jicha at the University of Wisconsin-Madison. Pb, Nd and Sr isotopic measurements were performed by M. Bezimis at the University of South Carolina. All of the co-authors had intellectual input to the manuscript. Chapter 2 will be submitted to Earth and Planetary Science Letters for publication in 2014 with J. Trela as the first author.

**Chapter 3:**

Samples from Mangaia were provided by M. Jackson and R. Cabral. Olivine analyses were performed by R. Cabral and me on the JXA-8200 superprobe at Rutgers University. I was the author of the paragraphs on the analytical method in section 2 of this chapter. C. Herzberg was the first author of this manuscript. All of the co-authors had intellectual input to this manuscript. This chapter was originally published in Earth and Planetary Science letters.

Herzberg, C., R.A. Cabral, M.G. Jackson, C. Vidito, J.M.D. Day and E.H. Hauri, (2014), Phantom Archean crust in Mangaia hotspot lavas and the meaning of

heterogeneous mantle: Earth and Planetary Science Letters, v. 396, no. 0, p. 97-106.

**Chapter 4:**

My contribution to this chapter consists of olivine analyses of Fernandina sample D-38 which were performed on the JXA-8200 at Rutgers University. This sample was obtained from D. Geist at the University of Idaho. I authored the section of the analytical method for measurements of sample D-38 in the Supplimental Material. C. Herzberg was the first author of this manuscript. All of the co-authors had intellectual input to this manuscript. This chapter was originally published in Nature.

Herzberg, C., P.D. Asimow, D.A. Ionov, C. Vidito, M.G. Jackson and D. Geist, (2013), Nickel and helium evidence for melt above the core-mantle boundary: Nature, v. 493, no. 7432, p. 393-398.

**Acknowledgements**

First and foremost I would like to acknowledge my primary advisor Claude Herzberg. When Claude first approached me with the opportunity to work with him on the Galápagos project, I was in a position in which I did not know what I was going to do after my undergraduate degree. The opportunity to do extensive EPMA work in addition to doing a project in petrology immediately piqued my interest. However, given that I literally had no research experience the learning curve was very steep. Claude remained encouraging dispite the numerous ups and downs I experienced over the last 5 years. I do not know if I would have made it this far had it not been for his optimisim, extensive knowledge and confidence in me.

Esteban Gazel has been a collaborator of mine since the beginning and has always been willing to help me dispite the fact that he is at a different college. The introduction he gave me to LA-ICP-MS not only expanded my analytical repertoire, but also gave me ideas to improve my EPMA analytical protocols.

The department turned to me when the need for a EPMA manager was needed. The opportunity given to me allowed me to expand my abilities, as the position required me to work with both internal and external users who worked on geologic problems very different than mine. The experience of managing this lab as well as the petrologic lab gave me experience beyond my own work which is invaluable to my CV. I am especially appreciative that the department allowed me to basically take over a room with petrographic equipment and set up a sample prep lab.

My research and working experience would have been far more difficult had it not been for the assistance of Jovani Reaves, Tonya Rufus and Danielle Parenti. It seemed like nearly every week I would contact them with a new problem I was having with the management of the lab and every time they provided me with what I needed. From the beginning of my time at Rutgers I have relied on my office mate Fara Lindsay and Jeremy Delaney for technical assistance. I will always be grateful for their willingness to discuss any given problem I was having.

**Table of Contents** Page

**List of Figures:**

**Chapter 1:**



**Chapter 2:**

**Chapter 4:**

**List of Tables:**

**Chapter 1:**



**Chapter 3:**



**Chapter 4:**

# Chapter 1

## Source Lithology of Curacao

**Abstract:**

The late Cretaceous to early Paleocene (Loewen et al., 2013; Sinton et al., 1998) lavas of Curacao are thought to be some of the earliest magmatism associated with the Galápagos plume (Geldmacher et al., 2003; Hauff et al., 2000; Kerr et al., 1996b). Presented here are olivine data obtained from two Curacao picrites. Petrologic modeling of olivine compositions indicates that the observed trends in Ca, Mn, Fe/Mn and Ni can not be explained by a pyroxenitic component. This differs from the modern Galápagos, which has pyroxenite in its source (Vidito et al., 2013). Results are consistent with the hypothesis that there have been secular changes in the amount of pyroxenite in the Galápagos plume. Additional modeling of magma chamber processes indicates that the geochemical trends observed in the olivine data could not have been caused by assimilation-fractional crystallization or Cpx crystallization alone. A process in which a peridotite source primary magma is allowed to crystallize olivine + Cpx + plagioclase followed by a recharge event best explains these trends. Modeled olivine compositions that crystallize over a range of mixtures of primary magma and evolved derivative magmas are consistent with the data.

### 1. Introduction

Large igneous provinces (LIPs) are formed by large outpourings of magma that may occur over short periods of time (Coffin and Eldholm, 1994). The potential for volcanic activity to affect the atmosphere and hydrosphere indicates that these large

magmatic events may be the cause of the extictions which coincide temporally with them (e.g. Coffin and Eldholm, 1994; Richards et al., 1989; Sinton and Duncan, 1997; Wignall, 2005). Given the profound effect that magmatism can have on the planet it is essential to understand how these magmatic provinces are formed and how they evolve. Many LIPs may form due to the initial melting of a mantle plume head (Coffin and Eldholm, 1994; Hill et al., 1992; Richards et al., 1991; Sleep, 1996). Many hotspot tracks can be traced back to LIPs indicating that there is a genetic link between these different volcanic features (Richards et al., 1989).

Modeled mantle potential temperatures (Tp) of the present day Galápagos archipelago and the Caribbean Large Igneous Province (CLIP) show that over time the Galápagos plume has cooled (Herzberg and Gazel, 2009). The entrainment of dense recycled crust into a mantle plume may have a negative effect on the buoyancy of a mantle plume, thus allowing more heat to dissipate into the ambient mantle (Kumagai et al., 2008). Such a process would result in a decrease in Tp (Herzberg, 2011) and the degree of melting in a mantle plume. Inferences made from trace element olivine compositions of the present day Galápagos archipelago indicates that pyroxenite is present in the sources of most of the volcanoes produced from the tail stage of the plume (Vidito et al., 2013). Chapter 2 of this thesis shows that after the transition from plume head to plume tail at ~ 70 Ma, a clear signal of recycled crust or pyroxenite is seen. It is apparent that the melting of pyroxenite as well as the dynamic effects of pyroxenite entrainment is seen in the earliest preserved hotspot track as well as the present day Galápagos plume. In this study I present olivine analyses from older CLIP picrites from Curacao in order to determine if a recycled crust was present in the source of these CLIP

lavas. However, inferences about source lithology can be compromised by magma chamber processes, as discussed in this chapter.

## 2. Geologic Background

### 2.1. General CLIP

The CLIP consists of large masses of basaltic lavas that overlie and underplate the oceanic crust of the Caribbean plate (Mauffret and Leroy, 1997). A map of the sub-aerial exposures of the CLIP, accreted terranes (both CLIP and hotspot tracks) and the present day hotspot, are presented in Figure 1. Covering ~$0.8 \cdot 10^6$ $km^2$ (Mauffret and Leroy, 1997), the CLIP reaches a maximum thickness of ~20 km at the Beata Ridge and the Nicaragua Rise (Edgar et al., 1971).

The generally accepted model for the timing of magmatism for the CLIP calls for a main pulse at ~90 Ma and that a second, smaller pulse occurred at ~75 Ma (Sinton et al., 1997). The hypothesis of two pulses of magmatism associated with this LIP may not be secure due to new $^{40}Ar/^{39}Ar$ ages from Haiti and Curacao, which indicate prolonged periods of magmatism without significant hiatuses (Loewen et al., 2014).

Establishing a clear link between the CLIP and the Galapagos hotspot is difficult due to the fact that older tracks of the Galápagos hotspot have been subducted in the Central American trench; thus they cannot be directly traced to the plateau. There are two schools of thought regarding tectonic reconstructions of the Galápagos hotspot. Some workers call for a model in which the CLIP was formed in-situ between the South American and North American continents (e.g. Meschede and Frisch, 1998) and thus is not related to the present day plume. Other reconstructions suggest that the plateau

formed on the Farallon plate in the Pacific. In the model of Duncan and Hargraves, 1984 the plateau formed in the present location of the Galápagos hotspot and then migrated eastward with the plate into its present position between the North and South American continents. “Pacific” models such as that of Duncan and Hargraves, 1984, support a genetic relationship between the present day Galápagos plume and the CLIP. Perhaps the strongest evidence against the fixist model comes from radiolaria fauna found in chert of the Bermeja complex on Puerto Rico that was of a Pacific origin and pre-date the opening of the Caribbean (Montgomery et al., 1994).

Apart from tectonic reconstructions, links between the present day Galápagos plume and the CLIP comes from isotopic data. Studies (Geldmacher et al., 2003; Hauff et al., 1997; Hauff et al., 2000; Hoernle et al., 2002; 2004; Lapierre et al., 2000; Sinton et al., 1998b; Thompson et al., 2004) show that exposures of the CLIP have Pb, Nd and Hf isotopic compositions that overlap those of the Galápagos Archipelago. Isotopic variations within the present day archipelago have been organized into isotopic domains (Hoernle et al., 2000) and characterized by a mixture of isotopic endmembers specific to the archipelago (Harpp and White, 2001). Geldmacher et al., 2003 showed that the central and eastern isotopic domains (Hoernle et al., 2000) existed in the main pulse of the CLIP, while the northern domain (Hoernle et al., 2000) persisted as far back as 65 Ma. In the CLIP the southern domain (Hoernle et al., 2000) isotopic signature is absent with the possible exception of of Curacao (Geldmacher et al., 2003). The northern component (Hoernle et al., 2000) is not observed in the Galápagos magmas until the appearance of Quepos at ~65 Ma (Geldmacher et al., 2003). A component of recycled crust in CLIP lavas has been inferred by isotopic data (Geldmacher et al., 2003; Hauff et

al., 2000), however these studies are not able to determine if the recycled crust was present as separate lithological units (Herzberg, 2011).

Arguments for the presence of a LIP on the Caribbean plate are based primarily on the anomalously thick oceanic crust found in much of the region (see above) and trace element analysis. Basalts of the Caribbean Plateau typically have flat rare earth element (REE) patterns (Hauff et al., 1997; Hauff et al., 2000; Kerr et al., 1997), similar to other oceanic plateaus (e.g. Mahoney et al., 1993; Storey et al., 1992). Modeled mantle potential temperatures from the present day Galápagos archipelago and the CLIP, indicate that the mantle plume has cooled over the last 90 Ma (Herzberg and Gazel, 2009). Figure 2 shows that CLIP mantle potential temperatures modeled in PRIMELT2 (Herzberg and Asimow, 2008) are generally higher than those of the Galápagos archipelago. Moreover, the magmas of the present day Galápagos generally have higher $La/Nd_N$ and $Sm/Yb_N$ (Figure 2). Assuming a similar source for the CLIP and Galápagos hotspot, the depletion of more incompatible REEs (i.e. $La/Nd_N$ and $Sm/Yb_N$ ~1) in the CLIP relative to the present day Galapagos Archipelago, may be interpreted as evidence for higher degrees of melting in the Galápagos plume during the Cretaceous. Some workers propose that this high degree of melt was due in part to the plume head being in close proximity to a spreading center (Kerr et al., 1998; Lapierre et al., 2000).

The lower portions of the CLIP are thought to consist primarily of picrites and rare komatiites. More evolved basalts tend to be emplaced at the top of the sequence (Kerr et al., 1997; Kerr et al., 1998; Kerr et al., 1996a; Mauffret and Leroy, 1997). Primitive mafic and ultramafic rocks may be representative of early stage melts that had

erupted prior to the establishment of crustal magma chambers when the crust was still relatively thin. The higher density of these primitive magmas may prevent them from erupting after the crust has thickened and magma chambers have become well established, hence their absence at the top of the observed sequences (Kerr et al., 1997; Kerr et al., 1998).

## 2.2 Curacao

CLIP units found on Curacao consist primarily of a 5km sequence of pillow basalts of picritic to tholeiitic compositions (Beets et al., 1982; Klaver, 1987). The most primitive picrites are found near the base of the formation and lava compositions become increasingly evolved with stratigraphic height (Kerr et al., 1996a). Initial $^{40}Ar/^{39}Ar$ ages from the top and bottom of the formations at Curacao indicated that the lavas were emplaced in a relatively short interval consistent with the main pulse of the CLIP (Sinton et al., 1998a). The position of the emplacement of the units over a short period of time is strengthened by the presence of only a single intercalation of limestone (Kerr et al., 1997). Despite this evidence a more recent study conducted by Loewen et al., 2014 suggests that magmatism occurred over a longer period. The 16 new $^{40}Ar/^{39}Ar$ ages presented in this study shows that magmatism at Curacao occurred from ~63Ma to 92 Ma with few hiatuses (Loewen et al., 2013).

Picrites found at Curacao have major element trends that indicate that olivine was the only crystallizing phase (an olivine control line). Samples with the highest MgO contents are not representative of primary magmas, rather they thought to be cumulates (Kerr et al., 1996a). Rounded and resorbed olivines from the high MgO picrites is

indicative of olivine accumulation (Beets et al., 1982), while other picrites with dendritic olivines appear to have been formed through the rapid cooling of primitive magmas (Kerr et al., 1996a). An early interpretation of the occurrence of basaltic and ultramafic lavas at Curacao suggested that it was formed in the initial stages of a volcanic arc (Beets et al., 1982). However there is a lack of an ARC geochemical signal (e.g. K and Pb enrichment and Nb and Ta depletion). The Curacao lavas generally have flat REEs, similar to most CLIP samples (Beets et al., 1982; Kerr et al., 1996a) however Klaver, 1987 noted that REE abundances increased from the most primitive picrites to the tholeiitic basalts. Trace and major element trends were used in Klaver's thesis to show that the picrites may representative of parental magmas to the more evolved tholeiites (Klaver, 1987). Since REEs are highly incompatible and major element trends indicate that plagioclase and clinopyroxene do not enter the LLD until the MgO contents reach 8-9% MgO, the sub parallel trends in REEs can be explained by the formation of evolved magmas by fractional crystallization of a picritic parental magma (Kerr et al., 1996a). Furthermore, Klaver, 1987 interpreted the chemisty and petrography of the sequence at Curacao to be representative of open and continually replenished magma chambers.

εNd and εHf systematics indicate that most samples from Curacao are similar to the central domain (Hoernle et al., 2000), while a few samples have signatures that indicate a component of the southern domain (Geldmacher et al., 2003). This interpretation is complicated by the fact that none of the Curacao samples have the characteristic signal of radiogenic Pb enrichment associated with the southern domain (Geldmacher et al., 2003). Curacao picrites have a narrower range of εNd, $^{87}Sr/^{86}Sr$ (Kerr et al., 1996a) and Pb isotopic ratios than the basalts (Hergt et al., 1994).

Variations in $^{87}Sr/^{86}Sr$ and Sr concentrations led Kerr et al. to conclude that the basalts of Curacao had assimilated altered oceanic crust during the process of fractional crystallization. The possibility of contamination by a continental component was dismissed on the basis that Curacao is underlain by a basaltic basement (MORB) and that the Sr isotopic anomalies were not followed by a decrease in $^{143}Nd/^{144}Nd$. Repeated leachings of Curacao samples failed to yield analyses with significantly lower $^{87}Sr/^{86}Sr$, thus eliminating the possibility that the anomalous Sr signal was due to the alteration of the Curacao samples (Kerr et al., 1996a).

## 3. Methods

### 3.1 Analytical Methods

Major and minor element compositions were obtained from olivines using a modified version of the high precision EPMA protocol of Sobolev et al., 2007. These samples were analyzed with a focused beam (~1 um) at 20 kV and 300 nA. On peak count times for all analyses are as follows: Si: 50s; Mg: 80s; Fe: 100s; Ni: 150s; Ca: 150s and Mn: 150s. In order to correct for instrumental drift the San Carlos olivine standard was analyzed at regular intervals during each run. A summary of the secondary standards, primary standards and statistics for the olivine analyses are given in Table 1.

### 3.2 Computational Methods

Liquid lines of decent (LLD), in which olivine is the sole crystallizing phase, were calculated using the algorithms of Herzberg, 2011. High pressure Cpx crystallization, occurring concurrently with olivine crystallization was calculated using algorithms of Herzberg et al., 2013. AFC modeling for the Curacao samples was done by

integrating the DePaolo, 1981 model into the algorithms of Herzberg, 2011 and Herzberg et al., 2013. Potential assimilants, which consisted of various lithologies from the oceanic lithosphere, were obtained from http://georoc.mpch-mainz.gwdg.de. R values (mass assimilant/mass crystallizing phases) < 1 were used for most models as it is assumed that latent heat of fusion from crystallization provides the heat required for assimilation (DePaolo, 1981). However, it has been shown that in the early stages of fractionation that R values can exceed 1 (Reiners et al., 1995). Magma mixing modeling was accomplished in 3 separate stages and is similar to the method given in Herzberg et al., 2014. The first stage consisted of LLD modeling in PETROLOG (Danyushevsky and Plechov, 2011). PETROLOG LLD modeling included olivine, clinopyroxene, and plagioclase crystallization at 1 atm. Olivine was modeled with the olivine lquidus temperature calculation from Beattie, 1993 together with the Fe/Mg exchange coefficient of Toplis, 2005. Plagioclase and clinopyroxene compositions were calculated with the models of Danyushevsky, 2001. In the subsequent step Ni, Ca and Mn was re-calculated for olivine using the partition coefficient calculations of Beattie, 1993 for Ni and Herzberg and O'Hara, 2002 for Ca and Mn. Ni was calculated for Cpx using the partition coefficient calculation of Herzberg et al., 2013. Ni, Ca and Mn concentrations in the liquids were also re-calculated at this step. Ranges of mixed magma compositions were then calculated, as were olivines in equilibrium with these mixed magmas.

## 4. Results

The two Curacao olivine populations (Figure 3) trend towards calculated olivine compositions from peridotite source primary magmas (Herzberg, 2011), this suggest that

the source of these Curacao magmas is peridotite. After performing inverse modeling of all of the possible primary magma compositions calculated from whole rock analyses (Kerr et al., 1996b; Klaver, 1987) in PRIMELT2 (Herzberg and Asimow, 2008), the solution for sample 79be028 (Klaver, 1987) was determined to be the most consistent with the olivine data. Nevertheless adjustments had to be made to the composition in order for it to be consistent with the olivine data. The affect of olivine sorting can have a dramatic effect on the Ni contents of whole rock, thus the Ni content of the peridotite source magma was calculated using the equation of Herzberg, 2011 (See Table 3). Additionally, Computed Mn and Ca show inconsistencies with the observed olivines which were corrected (Table 3). Modeled olivine trends which most closely match the measured olivines indicate that 70% to 90% Cpx crystallization with 30% to 10% olivine crystallization is required. This solution is unacceptable as dominant phenocryst phase in these samples is olivine (~50%) and it contradicts geochemical observations (Kerr et al., 1996b; Klaver, 1987). It is also possible that crystallization of olivine and Cpx occurred below the Moho (Herzberg et al., 2013; Geist et al., 1998; Vidito et al., 2014) and that when eruption occurred olivine crystallized, but Cpx did not. In such a case the geochemical signature of extensive Cpx crystallization would be preserved, but the amount of Cpx (if present at all) in the rock would not be proportional to this geochemical signature (e.g. Elthon et al., 1995; Thompson et al., 1980; O'Donnell and Presnall, 1980). Nevertheless, given the requirement of such a large proportion of cpx crystallization relative to olivine, other models are explored below.

The proportion of Cpx crystallization required by the LLD modeling may be reduced by the addition of pyroxenite source primary magma to the initial parental

magma. Of the samples which returned pyroxenite source errors in PRIMELT2 (Herzberg and Asimow, 2008), sample CUR36 (Kerr et al., 1996b) was chosen as a potential pyroxenite source magma. Computed Ni and Ca in olivine in equilibrium with this magma have consistent offsets with olivines of the peridotite primary magma. Mn contents however were much too high and were adjusted (Table 3) to be consistent with the offsets in Ca and Ni. Offsets in Mn, Ca and Ni relative to olivines in equilibrium with peridotite magmas and their derivative magmas has been interpreted as an indicator of a pyroxenite bearing source (Gurenko et al., 2010; Herzberg, 2011; Sobolev et al., 2005; Sobolev et al., 2007). Olivine compositions crystallized from the assumed pure pyroxenite primary magma are too far offset from the two Curacao samples, thus hybrid compositions were tested in subsequent models. Proportions of pyroxenite in the hybrid primary magma compositions were varied in 10% increments. Hybrid LLD models with 10% - 30% pyroxenite melt are shown for Ca and Ni (Figure 4). In all models the proportions of Cpx and olivine were adjusted to provide the optimum fit to the Ca contents of the measured olivines. The proportion of Cpx for the 10% pyroxenite hybrid (60-80%) is still too high for these picrites. The lack of internal consistency between Ca and Ni in these models becomes worse as the proportion of pyroxenite melt is increased. With as little as 30% pyroxenite melt in the hybrid, trends are not only inconsistent in their overlaps, but also in the slope of the modeled Ni trends compared to the slope of the observed Ni trends. It is obvious from these models that these Curacao samples could not have had a significant component of pyroxenite in its source.

Increasing Sr and $^{87}Sr/^{86}Sr$ anomalies with progressive fractionation of the Curacao magmas has been interpreted as the assimilation of altered oceanic crust during

fractional crystallization (Kerr et al., 1996b). The effects of assimilation-fractional crystallization (AFC) on trace and isotopic compositions of magmas have been recognized for decades (e.g. Bohrson and Spera, 2001, DePaolo, 1981 and Reiners et al., 1995). Although the effect of this process on major and minor elements is generally ignored, and the Sr signal of assimilation is absent in the picrites of Curacao (Kerr et al., 1996b), the possibility of AFC causing the unusual trends in olivine was tested. A number of different assimilant compositions consisting of samples crustal MORB and lithospheric mantle below MORB were tried. The only assimilants tested in this study that produced progressive offsets with increasing fractionation that were consistent with the observed data were harzburgites that had partially altered to talc. While these samples came from ODP-209 on the Mid-Atlantic Ridge (Paulick et al., 2006), the modeling is perfectly general for talc as an assimilant. AFC in which olivine was the sole crystallizing phase, could not reproduce the trends in the observed data even when $R > 1$. Only the solutions with AFC and high pressure, sub-Moho Cpx crystallization produced modeled olivine compositions consistent with the observed data (Figure 5).

The AFC model with Cpx crystallization provides an acceptable fit to the Curacao data with a peridotite primary magma and lower proportions of Cpx crystallization (30%-50%). Since the mode of these samples is dominated by olivine, this proportion of Cpx is more consistent with the petrography. However, given that Talc is a significant phase in this assimilant this solution is also unacceptable. Geochemical observations of Kerr et al., 1996b requires the hydrothermal alteration of the wall rock prior to assimilation. Although the harzburgite was indeed altered and high $^{87}Sr/^{86}Sr$ is found in the rocks recovered from ODP-209 (Paulick et al., 2006), the fact that Cpx must crystallize

concurrently with olivine and AFC precludes this model as a solution. In order for Cpx to be stable within the first 5% of fractional crystallization, the initial pressure would have to be $\geq$ 15 Kbars when the Cpx models of Danyushevsky, 2001 or Langmuir, 1992 are applied. Oxygen isotope measurements from the Oman Ophiolites indicate that hydrothermal alteration of oceanic crust is generally no greater than 6 km. Locally this alteration may penetrate deeper into ultramafic lithologies (Gregory and Taylor, 1981). Although ODP-209 is at a facture zone in the Mid-Atlantic Ridge (Bach et al., 2004), it is still extremely unlikely that this alteration could penetrate to the required depth of ~55 km. Moreover, the mineralogical composition of the proposed assimilant could not exist at the required P/T conditions of the country rock. All the geotherm models of MacGregor and Basu, 1984 for oceanic lithosphere estimate a minimum temperature of 800˚C at a pressure of 15 Kbars in the oceanic crust. At such conditions serpentine and talc breaks down and reverts to olivine, orthopyroxene and water vapor (Kitahara et al., 1966).

Herzberg et al., 2014 explained the deviation of olivines compositions from a typical calculated LLD by modeling the geochemical effects of magma recharge and mixing. Modeled olivine compositions with magma recharge and mixing in Figure 6, show excellent consistency with the observed Curacao olivine compositions without any co-crystallization of Cpx required. Mixtures of 60% to 40% primary magma and 60% - 40% evolved magmas with between 6.0% - 7.5% MgO are the best solutions.

The above recharge model suggests that after recharge, mixing within the magma chamber was imperfect and that further fractional crystallization prior to eruption was not

extensive. Variable mixing within the magma chamber is supported by the presence of olivines that individually have narrow forsterite ranges (avg. 1.5% variation core to rim) and normal, reverse and oscillatory zoning is present. Furthermore, if mixing were complete, yielding a homogeneous magma prior to subsequent fractional crystallization, the compositions of the olivines would not be in equilibrium with a range of mixtures as seen in Figure 6.

## 5. Discussion

If the magmas had homogenized and fractional crystallization had proceeded, the chemistry of the olivines would have been much different. Substantial fractional crystallization after recharge and perfect mixing would yield olivine compositions that form trends that would be sub-parallel to the original LLD in Figure 7. The scenario of perfect mixing followed by additional fractional crystallization is shown in Figure 7. Two mixtures (A and B) of the primary magma and a derivative liquid fractionated to 6.0% MgO were allowed to crystallize olivine, Cpx and plagioclase. Olivine compositions crystallized from hybrid sources, as well as the original peridotite source LLD, are included for comparison. The resulting trends of the modeled olivines are nearly parallel to olivines in equilibrium with the original LLD. Although there is a lack of internal consistency, such data could be mistaken for olivines derived from hybrid, pyroxenite bearing sources. Offsets in Ni and Ca for mixture A roughly coincide with hybrids with between 80% - 100% pyroxenite. Fe/Mn for this mixture however nearly overlaps the olivine compositions modeled from a hybrid with only 20% pyroxenite source melt.

The validity of the original LLD (dashed line in Fig 7) may be questionable. Mixing of a primary magma with the original LLD produced from a previous pulse of primary magma (as shown in Figure 6) may only hold true for the second pulse of magma into the magma chamber. If the system has undergone repeated cycles of magma recharge followed by fractional crystallization, then each subsequent recharge event would be followed by mixing of the new primary magma with a fractionated magma formed on an LLD from a mixed magma, not a primary magma. Modeling given in Figure 8 shows the effect of repeated cycles of fractional crystallization followed with magma mixing with 50% derivative liquid and 50% primary magma. With each cycle the the amount of fractional crystallization (olivine only) is kept constant. After the first cycle there is little change in the chemistry of the olivines and liquids. This is an unlikely scenario since in such a system there would be little variation observed in the chemistry of the erupted magmas or the mineral phases. Unlike the model of O'Hara 1977 in which regular batches of primary magma followed by fractional crystallization results in a steady state, the fact that the two samples in this study have different trends in olivine chemistry suggests that the degree of fractional crystallization between recharge events is not consistent.

A second scenario (Figure 9 A-C) in which with each successive cycle of fractionation and recharge, the amount of fractional crystallization increases. A progressive offset in Ca, Mn and Ni is observed in the modeled olivines with each cycle. Only olivine was allowed to crystallize in these models. This scenario is not possible for Curacao since with each cycle the trend in Ca is steeper. The Ca trend observed in the Curacao olivines is nearly horizontal which necessitates the presence of Cpx as a

crystallizing phase. Panels D-F in Figure 9 shows repeated cycles of fractionation and recharge in which olivine, Cpx and plagioclase are crystallizing phases. This model is consistent with the observed Ca, Fe/Mn and Ni trends in the Curacao samples. Models presented in Figure 6 and 9 while consistent with data are not the only possible recharge and mixing scenarios that could be consistent with the data. It is possible that the primary magma fractionated slightly prior to entering the magma chamber. This may be a viable model for sample 94-54 since Ni in these olivines appears to be trending to derivative liquids of a peridotite source. Also not considered are the effects of polybaric fractional crystallization, AFC and variable proportions of primary and derivative liquids in these multi-stage mixing models. Variable proportions of mixing may be supported by field observations near the base of the formation. The stratigraphic section presented in Kerr et al., 1996b shows that picritic lavas are interlain with more evolved tholeiites. If the models presented here apply to this stage in the magmatic history of Curacao, then it is likely that the mixtures of the more evolved liquids contained less primary magma. Nevertheless, different mixing scenerios does not compromise the interpretation of a peridotite source, since olivines crystallized along a mixing line with a primary magma (or derivative magma from a peridotite source) will invariably trend towards olivine compositions that are in equilibrium with the primary magma or their derivative magmas.

Kerr et al, 1996 notes that the eruption of picrites is inhibited by the high density of the magmas, but that a thin spot in the lithosphere (e.g. spreading center) or deep faulting may facilitate their eruption. Magma recharge and mixing may also provide a mechanism if not an additional factor by which the primitive picritic magmas had erupted to the surface. The injection of hot primitive magma into a magma chamber filled with

more evolved magma induces convection (Sparks et al., 1977) and increases the pressure within the magma chamber (Sparks et al., 1977; Blake, 1981). The increase in pressure may produce cracks in the overlying strata which provide pathways for the magma to escape and heat within the magma chamber decreases the viscosity and density of the magma making it easier to extrude to the surface (Sparks et al., 1977). Although the most evolved magmas modeled here are not particularly evolved (basaltic andesite) nor is a high volatile content expected, vesiculation triggered by magma mixing (Sparks et al., 1977) may not be necessary to trigger the eruptions as magma recharge alone may be adequate to produce the pressure increase required (Blake, 1981).

Although no satisfactory model in which AFC occurs was found to explain the olivine chemistry, this does not necessarily preclude the possibility of AFC. Potential assimilants tested included mid-ocean ridge basalt (MORB) samples with a range of compositions. In general it was found that the assimilation of basaltic country rock by a basaltic magma resulted only in subtle changes in the olivine chemistry. Thus assimilation may have occurred concurrently with crystallization, recharge and magma mixing, but the major and minor element chemistry of the assimilant must not have differed significantly from that of the plume derived magma.

## 6. Conclusions

The presence of a peridotite source for the magmas of Curacao supports the hypothesis of peridotite source for the head stage of the Galápagos plume, however much more work on CLIP is needed. The chemistry of the Curacao olivines reflects the mixing history and degree of fractionation of the previous batch of magma, as well as the

lithology of the primary magma. Of all the models tested, recharge and magma mixing in Curacao reproduced the observed olivine trends best. Crystallization of olivine from a range of magma mixtures is required. The variation in the observed trends suggests that this was a system in which the degree of fractionation between recharge events was variable. The lack of a satisfactory AFC model does not preclude the possibility of AFC, as it is likely that a crustal assimilant would have little impact on major and minor chemistry of olivines.

## 7. References

Alvarado, G.E., P. Denyer and C.W. Sinton, (1997), The 89 Ma Tortugal komatiitic suite, Costa Rica: Implications for a common geological origin of the Caribbean and Eastern Pacific region from a mantle plume: Geology, v. 25, no. 5, p. 439-442.

Arndt, N.T., A.C. Kerr and J. Tarney, (1997), Dynamic melting in plume heads: the formation of Gorgona komatiites and basalts: Earth and Planetary Science Letters, v. 146, no. 1-2, p. 289-301.

Bach, W., H. Paulick, C.J. Garrido, B. Ildefonse, W.P. Meurer and S.E. Humphris, (2006), Unraveling the sequence of serpentinization reactions: petrography, mineral chemistry, and petrophysics of serpentinites from MAR 15°N (ODP Leg 209, Site 1274): Geophysical Research Letters, v. 33, no. 13, p. L13306.

Baitis, H. and F. Swanson, (1976), Ocean rise-like basalts within the Galapagos Arcipelago, Nature, v. 256, p. 195-197.

Beattie, P., (1993), Olivine-Melt and Orto-Pyroxene-Melt Equilibria: Contributions to Mineralogy and Petrology, v. 115, no. 1, p. 103-111.

Beets, D.J., G.T. Klaver, F.F. Beunk, C. Kieft and P. Maaskant, (1982), Picrites as Parental Magma of Morb-Type Tholeiites: Nature, v. 296, no. 5855, p. 341-343.

Blake, S. (1981), Volcanism and the dynamics of open magma chambers, Nature, v. 289, no. 5800, p. 783-785.

Bohrson, W.A., and F.J. Spera, (2001), Energy-Constrained Open-System Magmatic Processes II: Application of Energy-Constrained Assimilation–Fractional Crystallization (EC-AFC) Model to Magmatic Systems: Journal of Petrology, v. 42, no. 5, p. 1019-1041.

Bow, C.S., and D.J. Geist, (1992), Geology and petrology of Floreana Island, Galapagos Archipelago, Ecuador: Journal of Volcanology and Geothermal Research, v. 52, no. 1-3, p. 83-105.

Bow, C.S. (1979), Geology and Petrogenesis of lavas from Floreana and Santa Cruz islands, Galapagos Archipelago, Ph.D. Thesis, University of Oregon, Eugene.

Brugmann, G. E., N. T. Arndt, A. W. Hofmann, and H. J. Tobschall, (1987), Noble-Metal Abundances in Komatiite Suites from Alexo, Ontario, and Gorgona-Island, Colombia, Geochimica Cosmochimica Acta, v. 51, no. 8, p. 2159-2169.

Campbell, I.H., R.W. Griffiths and R.I. Hill, (1989), Melting in an Archean Mantle Plume - Heads Its Basalts, Tails Its Komatiites: Nature, v. 339, no. 6227, p. 697-699.

Coffin, M.F., and O. Eldholm, (1994), Large igneous provinces: Crustal structure, dimensions, and external consequences, Reviews in Geophysics, v. 32, no. 1, p. 1-36.

Denyer, P., P.O. Baumgartner and E. Gazel, (2006), Characterization and tectonic implications of Mesozoic-Cenozoic oceanic assemblages of Costa Rica and Western Panama: Geologica Acta, v. 4, no. 1-2, p. 219-235.

Danyushevsky, L. V., (2001), The effect of small amounts of H2O crystallization of mid-ocean ridge and backarc basin magmas: Journal of Volcanology and Geothermal Research, v. 110, no. 3-4, p. 265-280.

Danyushevsky L.V., P. Plechov, (2011), Petrolog3: integrated software for modeling crystallization processes, Geochemistry Geophysics Geosystems, v. 12, Q07021 http://dx.doi.org/10.1029/2011GC003516.

Depaolo, D. J., (1981), Trace-Element and Isotopic Effects of Combined Wallrock Assimilation and Fractional Crystallization: Earth and Planetary Science Letters, v. 53, no. 2, p. 189-202.

Donnelly, T., M. Melson, R. Kay and J. Rogers, (1973), Basalts and dolerites of Late Cretaceous age from the central Caribbean: Initial Rep. Deep Sea Drill. Proj, v. 15, p. 989-1012.

Donovan, J.J., (2012), Probe for EPMA: Acquisition, Automation and Analysis, Enterprise Edition, Probe Software, Inc., Eugene.

Duncan, R.A., and R.B. Hargraves, (1984), Plate Tectonic Evolution of the Caribbean Region in the Mantle Reference Frame, Geological Society of America Memoirs, v. 162, p. 81-93.

Dupre, B., and L.M. Echeverria, (1984), Pb Isotopes of Gorgona Island (Colombia) - Isotopic Variations Correlated with Magma Type: Earth and Planetary Science Letters, v. 67, no. 2, p. 186-190.

Edgar, N.T., J.I. Ewing, and J. Hennion, (1971), Seismic refraction and reflection in Caribbean sea, AAPG Bulletin, v. 55, no. 6, p. 833-870.

Elthon, D., D. K. Ross, and J. K. Meen, (1995), Compositional Variations of Basaltic Glasses from the Mid-Cayman Rise Spreading Center, J Geophysical Research, v. 100, p. 12497-12512.

Escuder-Viruete, J., A. Perez-Estaun, F. Contreras, M. Joubert, D. Weis, T.D. Ullrich and P. Spadea, (2007), Plume mantle source heterogeneity through time: Insights from the Duarte Complex, Hispaniola, northeastern Caribbean: Journal of Geophysical Research-Solid Earth, v. 112, no. B4.

Geist, D.J., D.J. Fornari, M.D. Kurz, K.S. Harpp, S. A. Soule, M.R. Perfit and A.M. Koleszar, (2006), Submarine Fernandina: Magmatism at the leading edge of the Galápagos hot spot: Geochemistry Geophysics Geosystems, v. 7, no. 12, p. Q12007.

Geist, D.J., A.R. Mcbirney and R.A. Duncan, (1986), Geology and Petrogenesis of Lavas from San Cristobal Island, Galapagos Archipelago: Geological Society of America Bulletin, v. 97, no. 5, p. 555-566.

Geldmacher, J., B.B. Hanan, J. Blichert-Toft, K. Harpp, K. Hoernle, F. Hauff, R. Werner and A.C. Kerr (2003), Hafnium isotopic variations in volcanic rocks from the Caribbean Large Igneous Province and Galapagos hot spot tracks: Geochemistry Geophysics Geosystems, v. 4.

Gibson, S.A., and D. Geist (2010), Geochemical and geophysical estimates of lithospheric thickness variation beneath Galápagos: Earth and Planetary Science Letters, v. 300, no. 3-4, p. 275-286.

Gregory, R.T., and H.P. Taylor (1981), An Oxygen Isotope Profile in a Section of Cretaceous Oceanic Crust, Samail Ophiolite, Oman: Evidence for δ18O Buffering of the Oceans by Deep (> 5 km) Seawater-Hydrothermal Circulation at Mid-Ocean Ridges: Journal of Geophysical Research, v. 86, no. B4, p. 2737-2755.

Griffiths, R.W., and I.H. Campbell, (1990), Stirring and structure in mantle starting plumes: Earth and Planetary Science Letters, v. 99, no. 1–2, p. 66-78.

Gurenko, A. A., A. V. Sobolev, K. A. Hoernle, F. Hauff, and H. U. Schmincke, (2009), Enriched, HIMU-type peridotite and depleted recycled pyroxenite in the Canary plume: A mixed-up mantle, Earth and Planetary Science Letters, v. 277, no. 3-4, p. 514-524.

Harpp, K.S., D.J. Fornari, D.J. Geist and M.D. Kurz, (2003), Genovesa Submarine Ridge: A manifestation of plume-ridge interaction in the northern Galapagos Islands: Geochemistry Geophysics Geosystems, v. 4.

Harpp, K.S., D. Geist, A. Koleszar, B. Christensen, J. Lyons, M. Sabga and N. Rollins, (2013), The geology and geochemistry of Isla Floreana, Galápagos: A different type of late-stage ocean island volcanism: The Galápagos: A Natural Laboratory for the Earth Sciences, edited by K. Harpp et al., AGU, Washington, DC.

Harpp, K.S. and W.M. White, (2001), Tracing a mantle plume: Isotopic and trace element variations of Galapagos seamounts: Geochemistry Geophysics Geosystems, v. 2.

Hauff, F., K. Hoernle, H.U. Schmincke and R. Werner, (1997), A Mid Cretaceous origin for the Galapagos hotspot: Volcanological, petrological and geochemical evidence from Costa Rican oceanic crustal segments: Geologische Rundschau, v. 86, no. 1, p. 141-155.

Hauff, F., K. Hoernle, G. Tilton, D.W. Graham and A.C. Kerr, (2000a), Large volume recycling of oceanic lithosphere over short time scales: geochemical constraints from the Caribbean Large Igneous Province: Earth and Planetary Science Letters, v. 174, no. 3-4, p. 247-263.

Hauff, F., K. Hoernle, P. van den Bogaard, G. Alvarado and D. Garbe-Schönberg, (2000b), Age and geochemistry of basaltic complexes in western Costa Rica: Contributions to the geotectonic evolution of Central America: Geochemistry Geophysics Geosystems, v. 1, no. 5, p. 1-41.

Hergt, J., M. Storey, G. Marriner and J. Tarney, (1994), The Curaçao lava formation: samples of the oldest and most primitive magmas from the Galapagos plume: Mineralogical Magazine, v. 58, p. 414-415.

Herzberg, C., (2011), Basalts as temperature probes of Earth's mantle, Geology, v. 39, no. 12, p. 1179-1180.

Herzberg, C., (2011), Identification of Source Lithology in the Hawaiian and Canary Islands: Implications for Origins, Journal of Petrology, v. 52, no. 5, p. 1013-1046.

Herzberg, C., and P.D. Asimow, (2008), Petrology of some oceanic island basalts: PRIMELT2.XLS software for primary magma calculation: Geochemistry Geophysics Geosystems, v. 9.

Herzberg, C., P.D. Asimow, D.A. Ionov, C. Vidito, M.G. Jackson and D. Geist, (2013), Nickel and helium evidence for melt above the core-mantle boundary: Nature, v. 493, no. 7432, p. 393-U134.

Herzberg, C., R.A. Cabral, M.G. Jackson, C. Vidito, J.M.D. Day and E.H. Hauri, (2014), Phantom Archean crust in Mangaia hotspot lavas and the meaning of heterogeneous mantle: Earth and Planetary Science Letters, v. 396, no. 0, p. 97-106.

Herzberg, C. and E. Gazel, E., (2009), Petrological evidence for secular cooling in mantle plumes, Nature, 458, 619-622, doi: 10.1038/nature07857.

Hill, R.I., I. H. Campbell, G. F. Davies, and R. W. Griffiths, (1992), Mantle Plumes and Continental Tectonics, Science, v. 256, no. 5054, p. 186-193.

Hoernle, K., F. Hauff and P. van den Bogaard, (2004), 70 m.y. history (139–69 Ma) for the Caribbean large igneous province: Geology, v. 32, no. 8, p. 697-700.

Hoernle, K., P. van den Bogaard, R. Werner, B. Lissinna, F. Hauff, G. Alvarado and D. Garbe-Schonberg, (2002), Missing history (16-71 Ma) of the Galpapagos hotspot: Implications for the tectonic and biological evolution of the Americas: Geology, v. 30, no. 9, p. 795-798.

Hoernle, K., R. Werner, J.P. Morgan, D. Garbe-Schonberg, J. Bryce and J. Mrazek, (2000), Existence of complex spatial zonation in the Galapagos plume for at least 14 m.y.: Geology, v. 28, no. 5, p. 435-438.

Jarosewich, E., J.A. Nelen, and J.A. Norberg (1980), Reference Samples for Electron Microprobe Analysis*, Geostandards Newsletter, v. 4, no. 1, p. 43-47.

Jarosewich, E., R. Gooley and J. Husler, (1987), Chromium Augite-A New Microprobe Reference Sample, Geostandards Newsletter, v. 11, no. 2, p. 197-198.

Jochum, K. P., N. T. Arndt, and A. W. Hofmann, (1991), Nb-Th-La in Komatiites and Basalts - Constraints on Komatiite Petrogenesis and Mantle Evolution, Earth Planet Science Letters, v. 107, no. 2, p. 272-289.

Jolly, W.T., J.H. Schellekens and A.P. Dickin, (2007), High-Mg andesites and related lavas from southwest Puerto Rico (Greater Antilles Island Arc): Petrogenetic links with emplacement of the late cretaceous Caribbean mantle plume: Lithos, v. 98, no. 1-4, p. 1-26.

Kamenetsky, V. S., A. A. Gurenko, and A. C. Kerr, (2010), Composition and temperature of komatiite melts from Gorgona Island, Colombia, constrained from olivine-hosted melt inclusions, Geology, v. 38, no. 11, p. 1003-1006.

Kerr, A.C., G.F. Marriner, N.T. Arndt, J. Tarney, A. Nivia, A.D. Saunders and R.A. Duncan, (1996a), The petrogenesis of Gorgona komatiites, picrites and basalts: New field, petrographic and geochemical constraints: Lithos, v. 37, no. 2-3, p. 245-260.

Kerr, A.C., G.F. Marriner, J. Tarney, A. Nivia, A.D. Saunders, M.F. Thirlwall and C.W. Sinton, (1997), Cretaceous basaltic terranes in western Colombia: Elemental, chronological and Sr-Nd isotopic constraints on petrogenesis: Journal of Petrology, v. 38, no. 6, p. 677-702.

Kerr, A.C., J. Tarney, P.D. Kempton, P. Spadea, A. Nivia, G.F. Marriner and R.A. Duncan, (2002), Pervasive mantle plume head heterogeneity: Evidence from the late Cretaceous Caribbean-Colombian oceanic plateau: Journal of Geophysical Research-Solid Earth, v. 107, no. B7.

Kerr, A.C., J. Tarney, G.F. Marriner, G.T. Klaver, A.D. Saunders and M.F. Thirlwall, (1996b), The geochemistry and petrogenesis of the late-Cretaceous picrites and basalts of Curacao, Netherlands Antilles: A remnant of an oceanic plateau: Contributions to Mineralogy and Petrology, v. 124, no. 1, p. 29-43.

Kerr, A.C., J. Tarney, G. F. Marriner, A. Nivia, and A. D. Saunders, (1997), The Caribbean-Colombian Cretaceous igneous province: the internal anatomy of an oceanic plateau, Large igneous provinces: Continental, oceanic, and planetary flood volcanism, American Geophysical Union, p. 123-144.

Kerr, A.C., J. Tarney, A. Nivia, G.F. Marriner and A.D. Saunders, (1998), The internal structure of oceanic plateaus: inferences from obducted Cretaceous terranes in western Colombia and the Caribbean: Tectonophysics, v. 292, no. 3-4, p. 173-188.

Klaver, G.T., (1987), The Curaçao Lava Formation: an ophiolitic analogue of the anomalous thick layer 2B of the mid-Cretaceous oceanic plateaus in the western Pacific and central Caribbean, Natuurwetenschappelijke Studiekring voor Suriname en de Nederlandse Antillen, v. 119.

Kurz, M.D. and D. Geist, (1999), Dynamics of the Galapagos hotspot from helium isotope geochemistry, Geochmica et Cosmochimica Acta, v. 63, p. 4139-4156.

Langmuir, C.H., E.M. Klein and T. Plank, (1992), Petrological Systematics of Mid-Ocean Ridge Basalts: Constraints on Melt Generation Beneath Ocean Ridges, Mantle Flow and Melt Generation at Mid-Ocean Ridges, American Geophysical Union, p. 183-280.

Lapierre, H., D. Bosch, V. Depuis, M. Polve, R.C. Maury, J. Hernandez, P. Monie, D. Yeghicheyan, E. Jaillard, M. Tardy, B.M. de Lepinay, M. Mamberti, A. Desmet, F. Keller and F. Senebier, (2000), Multiple plume events in the genesis of the peri-Caribbean Cretaceous oceanic plateau province, Journal of Geophysical Research – Solid Earth, v. 105, no. B4, p. 8403-8421.

Lapierre, H., V. Dupuis, B.M. de Lepinay, D. Bosch, P. Monnie, M. Tardy, R.C. Maury, J. Hernandez, M. Polve, D. Yeghicheyan and J. Cotton, (1999), Late Jurassic oceanic crust and upper cretaceous Caribbean plateau picritic basalts exposed in the Duarte igneous complex, hispaniola: A reply, Journal of Geology, 107(4), 509-512.

Loewen, M.W., R.A. Duncan, A.J.R. Kent and K. Krawl, (2013), Prolonged plume volcanism in the Caribbean Large Igneous Province: New insights from Curacao and Haiti: Geochemistry Geophysics Geosystems, v. 14, no. 10, p. 4241-4259.

MacDonald, W., J. Estrada and G. Humberto, (1997), Paleoplate affiliations of volcanic accretionary terranes of the northern Andes, *in* Proceedings Geological Society of America Abstracts with Programs, Volume 29, p. 245.

MacGregor, I.D., and A.R. Basu, (1974), Thermal Structure of the Lithosphere: A Petrologic Model: Science, v. 185, no. 4156, p. 1007-1011.

Mahoney, J., R. Storey, K. Duncan, K. Spencer, and M. Pringle, (1993), Geochemistry and Age of the Ontong Java Plateau, The Mesozoic Pacific: geology, tectonics, and volcanism, p. 233-261.

Mamberti, M., H. Lapierre, D. Bosch, E. Jaillard, R. Ethien, J. Hernandez and M. Polve, (2003), Accreted fragments of the Late Cretaceous Caribbean- Colombian Plateau in Ecuador: Lithos, v. 66, no. 3-4, p. 173-199.

Mauffret, A., and S. Leroy (1997), Seismic stratigraphy and structure of the Caribbean igneous province, Tectonophysics, v. 283, no. 1-4, p. 61-104.

McDonough, W. F., and S.S. Sun, (1995), THE COMPOSITION OF THE EARTH: Chemical Geology, v. 120, no. 3-4, p. 223-253.

Meschede, M., and W. Frisch, (1994), Geochemical characteristics of basaltic rocks from Central American Ophiolites. In Seyfried, H., and Hellmann, W., eds. Geology of an evolving island arc (Profil, Bd. 7). Stuttgart, Universität Stuttgart, p. 71–85.

Millward, D., G.F. Marriner and A.D. Saunders, (1984), Cretaceous Tholeiitic Volcanic-Rocks from the Western Cordillera of Colombia: Journal of the Geological Society, v. 141, no. Sep, p. 847-860.

Montgomery, H., E.A. Pessagno, J.F. Lewis, and J. Schellekens (1994), Paleogeography of Jurassic Fragments in the Caribbean, Tectonics, v. 13, no. 3, p. 725-732.

Naumann, T., D. Geist and M. Kurz, (2002), Petrology and geochemistry of Volcan Cerro Azul: Petrologic diversity among the western Galapagos volcanoes: Journal of Petrology, v. 43, no. 5, p. 859-883.

O'Donnell, T. H., and D. C. Presnall, (1980), Chemical Variations of the Glass and Mineral Phases in Basalts Dredged from 25-Degrees-30-Degrees-N Along the Mid-Atlantic Ridge, American Journal of Science, v. 280, p. 845-868.

O'Hara, M. J., (1977), Geochemical evolution during fractional crystallisation of a periodically refilled magma chamber, Nature, v. 266, no. 5602, p. 503-507.

Paulick, H., W. Bach, M. Godard, J.C.M. De Hoog, G. Suhr and J. Harvey, (2006), Geochemistry of abyssal peridotites (Mid-Atlantic Ridge, 15°20′N, ODP Leg 209): Implications for fluid/rock interaction in slow spreading environments: Chemical Geology, v. 234, no. 3–4, p. 179-210.

Reiners, P.W., B.K. Nelson and M.S. Ghiorso, (1995), Assimilation of felsic crust by basaltic magma: Thermal limits and extents of crustal contamination of mantle-derived magmas: Geology, v. 23, no. 6, p. 563-566.

Revillon, S., N.T. Arndt, C. Chauvel and E. Hallot, (2000), Geochemical study of ultramafic volcanic and plutonic rocks from Gorgona Island, Colombia: The plumbing system of an oceanic plateau: Journal of Petrology, v. 41, no. 7, p. 1127-1153.

Revillon, S., C. Chauvel, N.T. Arndt, R. Pik, F. Martineau, S. Fourcade and B. Marty, (2002), Heterogeneity of the Caribbean plateau mantle source: Sr, O and He isotopic compositions of olivine and clinopyroxene from Gorgona Island: Earth and Planetary Science Letters, v. 205, no. 1-2, p. 91-106.

Richards, M. A., R. A. Duncan, and V. E. Courtillot (1989), Flood Basalts and Hot-Spot Tracks - Plume Heads and Tails, Science, v. 246, no. 4926, p. 103-107.

Richards, M.A., D.L. Jones, R.A. Duncan, and D.J. Depaolo (1991), A Mantle Plume Initiation Model for the Wrangellia Flood-Basalt and Other Oceanic Plateaus, Science, v. 254, no. 5029, p. 263-267.

Ryan, W.B.F., S.M. Carbotte, J.O. Coplan, S. O'Hara, A. Melkonian, R. Arko, R.A. Weissel, V. Ferrini, A. Goodwillie, F. Nitsche, J. Bonczkowski, and R. Zemsky, (2009), Global Multi-Resolution Topography synthesis, Geochemistry Geophysics Geosystems, v. 10, Q03014, doi:10.1029/2008GC002332.

Saal, A.E., M.D. Kurz, S.R. Hart, J.S. Blusztajn, J. Blichert-Toft, Y. Liang and D.J. Geist, (2007), The role of lithospheric gabbros on the composition of Galapagos lavas: Earth and Planetary Science Letters, v. 257, no. 3-4, p. 391-406.

Sinton, C.W., and R.A. Duncan (1997), Potential links between ocean plateau volcanism and global ocean anoxia at the Cenomanian-Turonian boundary, Economic Geology, v. 92. No. 7-8, p. 836-842.

Sinton, C.W., R.A. Duncan and P. Denyer, (1997), Nicoya Peninsula, Costa Rica: A single suite of Caribbean oceanic plateau magmas: Journal of Geophysical Research-Solid Earth, v. 102, no. B7, p. 15507-15520.

Sinton, C.W., R.A. Duncan, M. Storey, J. Lewis and J.J. Estrada, (1998), An oceanic flood basalt province within the Caribbean plate: Earth and Planetary Science Letters, v. 155, no. 3-4, p. 221-235.

Sleep, N. H. (1996), Lateral flow of hot plume material ponded at sublithospheric depths, Journal of Geophysical Research: Solid Earth (1978–2012), v. 101, no. B12, p. 28065-28083.

Sparks, S. R. J., H. Sigurdsson, and L. Wilson (1977), Magma mixing: a mechanism for triggering acid explosive eruptions, Nature, v. 267, no. 5609, p. 315-318.

Storey, M., R. Kent, A. Saunders, V. Salters, J. Hergt, H. Whitechurch, J. Sevigny, M. Thirlwall, P. Leat, and N. Ghose (1992), Lower Cretaceous volcanic rocks on continental margins and their relationship to the Kerguelen Plateau, paper presented at Proceedings of the Ocean Drilling Program, scientific results.

Teasdale, R., D. Geist, M. Kurz and K. Harpp, (2005), 1998 eruption at Volcan Cerro Azul, Galapagos Islands: I. Syn-eruptive petrogenesis: Bulletin of Volcanology, v. 67, no. 2, p. 170-185.

Thompson, G., W. B. Bryan, and W. G. Melson, (1980), Geological and Geophysical Investigation of the Mid-Cayman-Rise-Spreading-Center - Geochemical Variation and Petrogenesis of Basalt Glasses, The Journal of Geology, v. 88, p. 41-55.

Thompson, P.M.E., P.D. Kempton, R.V. White, A.C. Kerr, J. Tarney, A.D. Saunders, J.G. Fitton and A. McBirney, (2004), Hf-Nd isotope constraints on the origin of the Cretaceous Caribbean plateau and its relationship to the Galapagos plume: Earth and Planetary Science Letters, v. 217, no. 1-2, p. 59-75.

Toplis, M.J., (2005), The thermodynamics of iron and magnesium partitioning between olivine and liquid: criteria for assessing and predicting equilibrium in natural and experimental systems: Contributions to Mineralogy and Petrology, v. 149, no. 1, p. 22-39.

Tournon, J., and J. Azema, (1984), Granophyres and Ferrodolerites from the Nicoya Complex (Costa-Rica) - Possible Example of Magma Immiscibility: Bulletin De La Societe Geologique De France, v. 26, p. 1336-1347.

Vidito, C., C. Herzberg, E. Gazel, D. Geist and K. Harpp, (2013), Lithological structure of the Galapagos Plume: Geochemistry Geophysics Geosystems, v. 14, no. 10, p. 4214-4240.

Villagómez, D., R. Spikings, T. Magna, A. Kammer, W. Winkler, and A. Beltrán, (2011), Geochronology, geochemistry and tectonic evolution of the Western and Central cordilleras of Colombia, Lithos, v. 125, no. 3–4, p. 875-896.

Walker, R.J., L.M. Echeverria, S.B. Shirey and M.F. Horan, (1991), Re-Os Isotopic Constraints on the Origin of Volcanic-Rocks, Gorgona Island, Colombia - Os

Isotopic Evidence for Ancient Heterogeneities in the Mantle: Contributions to Mineralogy and Petrology, v. 107, no. 2, p. 150-162.

White, R.V., J. Tarney, A.C. Kerr, A.D. Saunders, P.D. Kempton, M.S. Pringle and G. Klaver, (1999), Modification of an oceanic plateau, Aruba, Dutch Caribbean: Implications for the generation of continental crust: Lithos, v. 46, no. 1, p. 43-68.

White, W.M., A.R. McBirney and R.A. Duncan, (1993), Petrology and Geochemistry of the Galaapgos Islands - Portrait of a Pathological Mantle Plume: Journal of Geophysical Research-Solid Earth, v. 98, no. B11, p. 19533-19563.

Wignall, P. (2005), The link between large igneous province eruptions and mass extinctions, Elements, v. 1, no. 5, p. 293-297.

## 8. Figure Captions

**Figure 1:** Map of the subareal exposures of Galápagos Hotspot tracks and the Caribbean Large Igneous Province. Locations covered in this study are in bold black letters. This map was produced in GeoMapApp (www.geomappapp.org) using the basemap of Ryan et al., 2009.

**Figure 2:** ITE ratios and Tp from the CLIP (Arndt et al., 1997; Brugmann et al., 1987; Donnelly et al., 1973; Escuder-Viruete et al., 2007; Hauff et al., 2000a; Hauff et al., 2000b; Jochum et al., 1991; Jolly et al., 2007; Kamenetsky et al., 2010; Kerr et al., 1997; Kerr et al., 2002; LaPierre et al., 1999; LaPierre et al., 2000; Mamberti et al., 2003; Millward et al., 1984; Millward et al., 1997; Revillon et al., 2000; Revillion et al., 2002; Sinton et al., 1997; Villagomez et al., 2002; White et al., 1999) and present day Galapagos hotspot (Baitis and Swanson, 1976; Bow, 1979; Bow and Geist, 1992; Geist et al., 1986; Geist et al., 2006; Gibson and Geist, 2010; Harpp et al., 2003; Kurz and Geist, 1999; Naumann et al., 2002; Saal et al., 2007; Teasdale et al., 2005; White et al., 1993). All trace elements have been normalized to primitive mantle (McDonough and Sun, 1995). Mantle potential temperatures (Tp) were modeled in PRIMELT2 (Herzberg and

Asimow, 2008). Tp is generally lower and ITE ratios higher than samples of the CLIP and Gorgona.

**Figure 3:** Peridotite source modeling and the Curacao olivine data. Analyses of Curacao olivine data plotted against olivines in equilibrium with modeled derivative magmas of a peridotite source primary magma. A reasonable match is obtained, however the requirement of a high proportion of Cpx early in the LLD is not supported by the mode of these samples.

**Figure 4:** Curacao Ca and Ni olivine data compared to modeled derivative magmas of various hybrid sources. Pyroxenite primary magma, calculated from sample CUR36 (Kerr et al., 1996b), was added to the original peridotite primary magma from Figure 1 in 10% increments to produce hybrid magmas. In each set of plots the proportion of Cpx/Ol is set such that the optimal fit with the Curacao Ca data is achieved. This illustrates the decrease in internal consistency between the modeled and observed Ca and Ni contents as the proportion of pyroxenite in the source is increased. This eliminates the possibility of a significant pyroxenite component in source of these two Curacao lavas.

**Figure 5:** AFC model compared to the olivine chemistry of Curacao. In addition to olivine and Cpx crystallization, LLDs represented by the blue lines have had an assimilant (1268A-15) added using the AFC model of DePaolo, 1981. These AFC models require less Cpx than the models shown in figure 1. Unfortunately since the assimilant lithology cannot exist in the T/P conditions required, this is not a valid solution for Curacao.

**Figure 6:** Magma mixing models compared to the olivine chemistry of Curacao. Curacao olivine data compared to modeled derivative magmas initially calculated using PETROLOG (Danyushevsky and Plechov, 2011) and then re-calculated following the algorythm of Herzberg et al., 2014. Calculated olivines in equilibrium with variably mixed primary and evolved derivative magmas provide the best fit to the data. The implication of this model is that frationation during a magma recharge event is most likely to be responsible for the compositional trends.

**Figure 7:** LLDs modeled from magma mixtures compared to hybrid models. Olivine compositions modeled from mixtures of magmas from Figure 4, which were allowed to fractionate normally. Also plotted are modeled olivines that crystallized from various hybrid sources. This shows that olivines crystallized from mixed magmas can appear to have trends that are consistent with hybrid sources.

**Figure 8:** Six cycles of magma fractionation followed by recharge in a system approaching a steady state. The degree of fractional crystallization (olivine only) and proportions of derivative and primary magmas in magma mixing are kept relatively constant for all 6 cycles. This example shows that little change is observed in the olivine chemistry (and liquids) after the first cycle (labeled) provided that conditions remain constant.

**Figure 9:** Progressive magma mixing models in which the degree of fractional crystallization is varied. Panels A-C show six cycles of magma fractionation followed by recharge, in which olivine is the only crystallizing mineral phase. Olivine data from Curacao is not plotted in these three diagrams since with each successive cycle the trend

in Ca becomes increasingly steep, which is the opposite of what is observed in the olivine data. As seen in figure 8, there is an increase in the offset of Ni when recharge occurs with progressively fractionated liquids. Panels D-F show six cycles of magma fractionation followed by recharge in which Ol + Cpx + Plagioclase are allowed to crystallize on the LLD. As with all of the mixing models presented, Mn remains relatively insensitive to the effects of magma recharge and mixing. Ni and Ca show progressive offsets with increasing fractionation and with each successive cycle. Consistency between the Curacao data and the modeled mixing lines indicates that this process of continuous fractionation and recharge is also a viable model for these samples.

## 9. Figures

**Figure 1:**

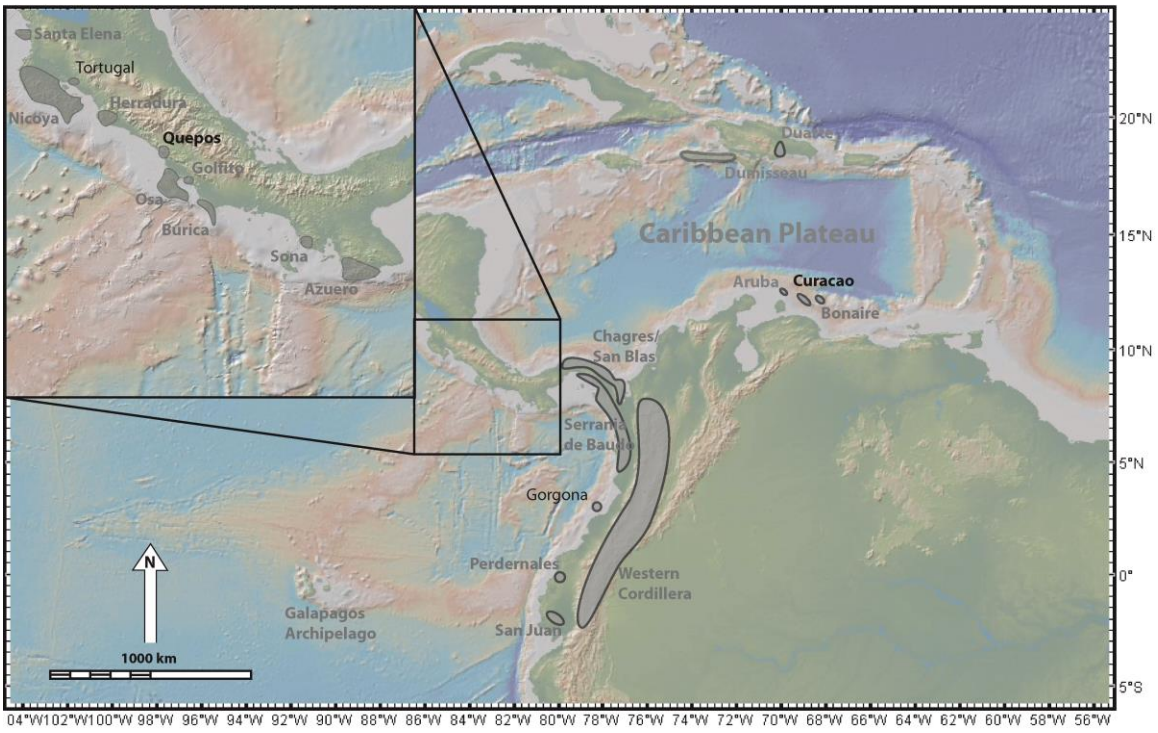

**Figure 2:**

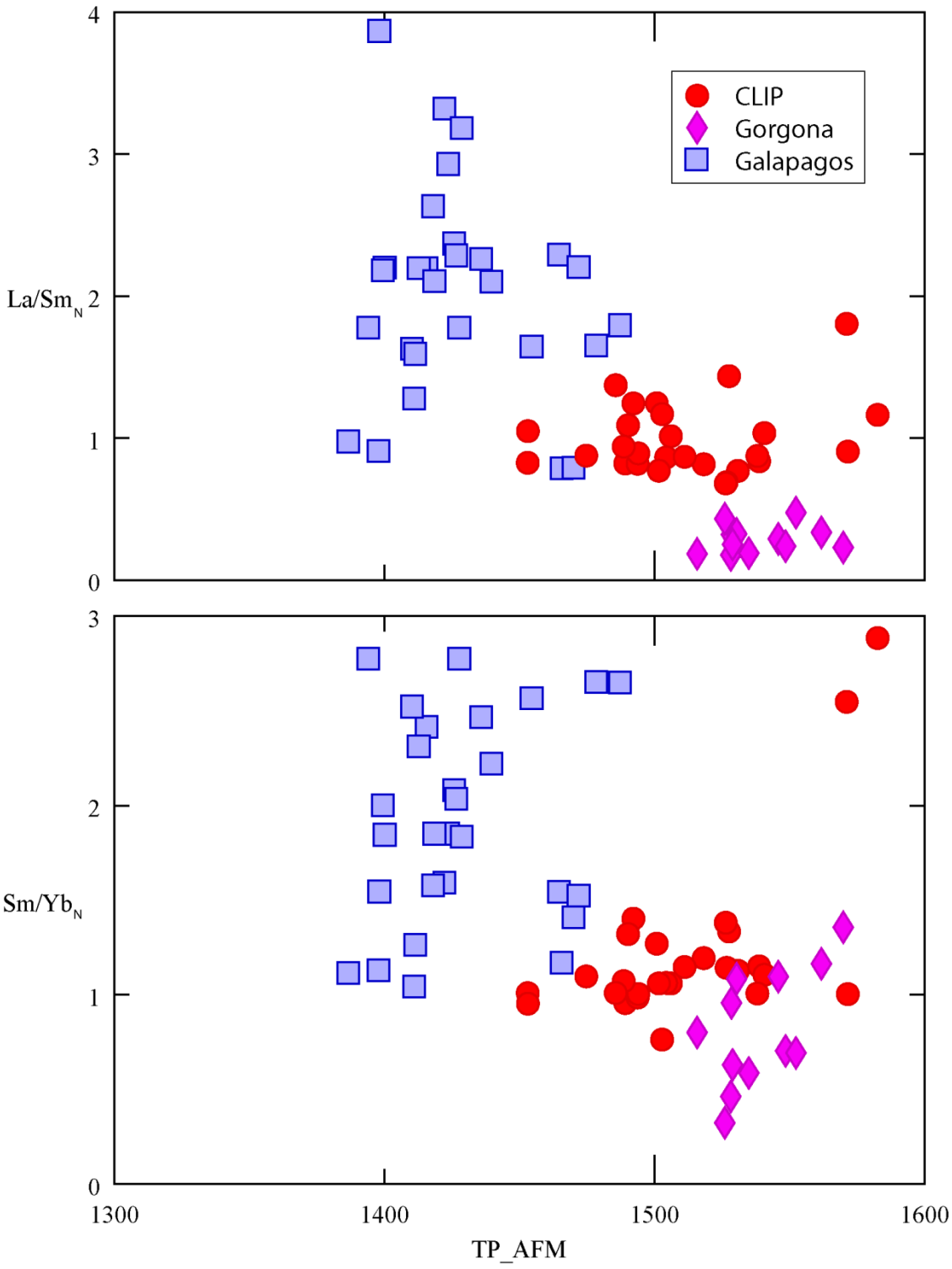
CLIP
Gorgona
Galapagos
La/Sm$_N$
Sm/Yb$_N$
TP_AFM
0
1
2
3
4
1300
1400
1500
1600

**Figure 3:**

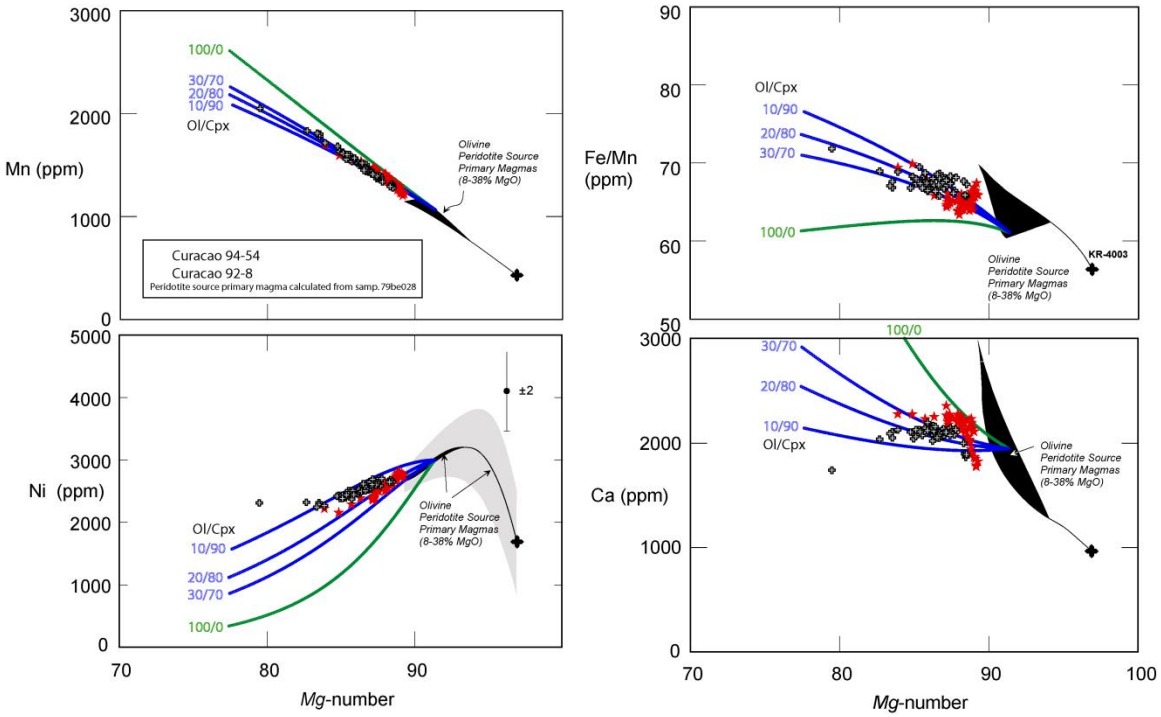
Mn (ppm)
100/0
30/70
20/80
10/90
Ol/Cpx
Olivine Peridotite Source Primary Magmas (8-38% MgO)
Curacao 94-54
Curacao 92-8
Peridotite source primary magma calculated from samp. 79be028
Ni (ppm)
±2
Mg-number
Fe/Mn (ppm)
KR-4003
Ca (ppm)

**Figure 4:**

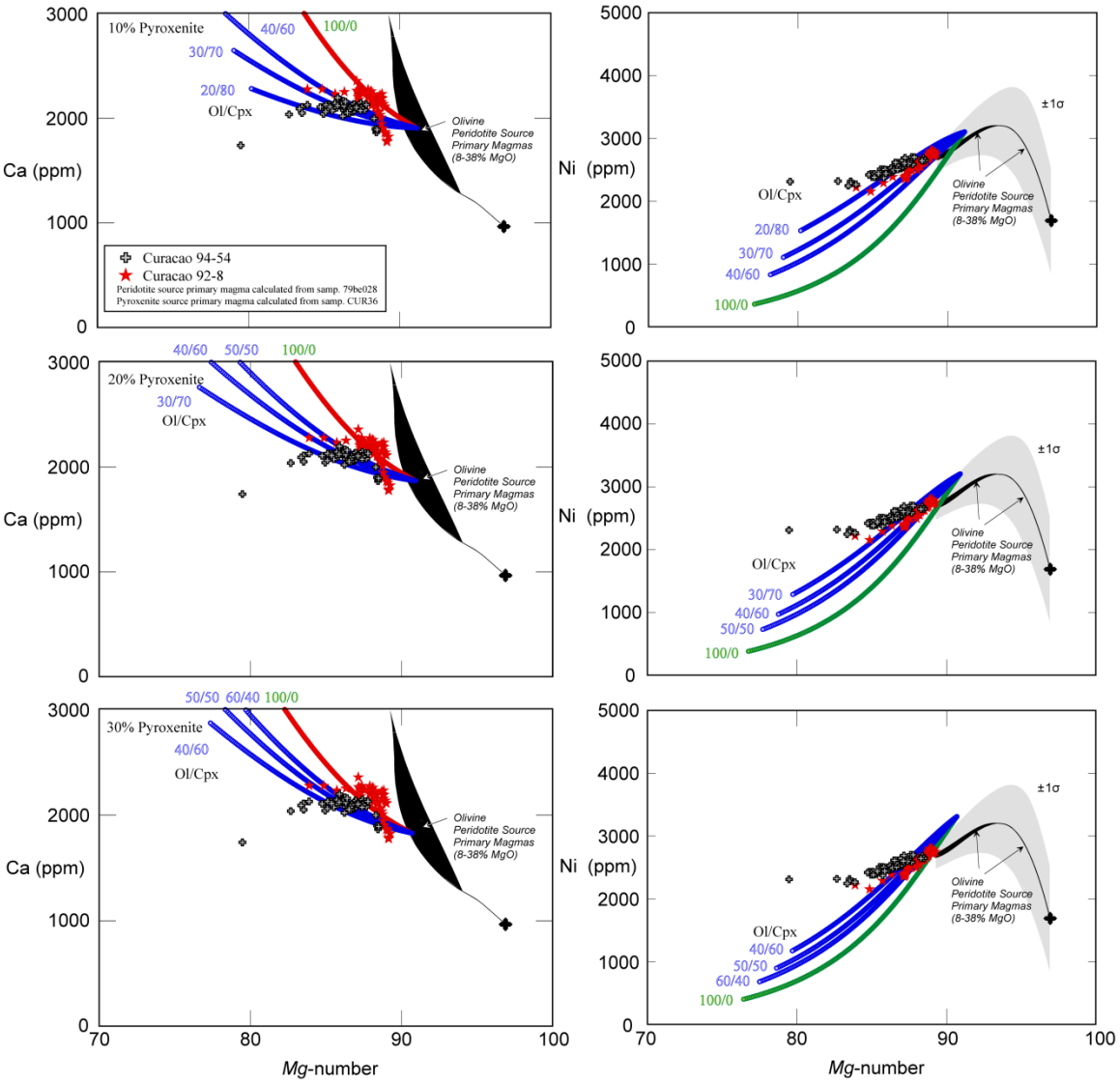
10% Pyroxenite
40/60
100/0
30/70
20/80
Ol/Cpx
Olivine Peridotite Source Primary Magmas (8-38% MgO)
Curacao 94-54
Curacao 92-8
Peridotite source primary magma calculated from samp. 79be028
Pyroxenite source primary magma calculated from samp. CUR36
Ca (ppm)
Ni (ppm)
±1σ
20% Pyroxenite
50/50
30% Pyroxenite
60/40
Mg-number

**Figure 5:**

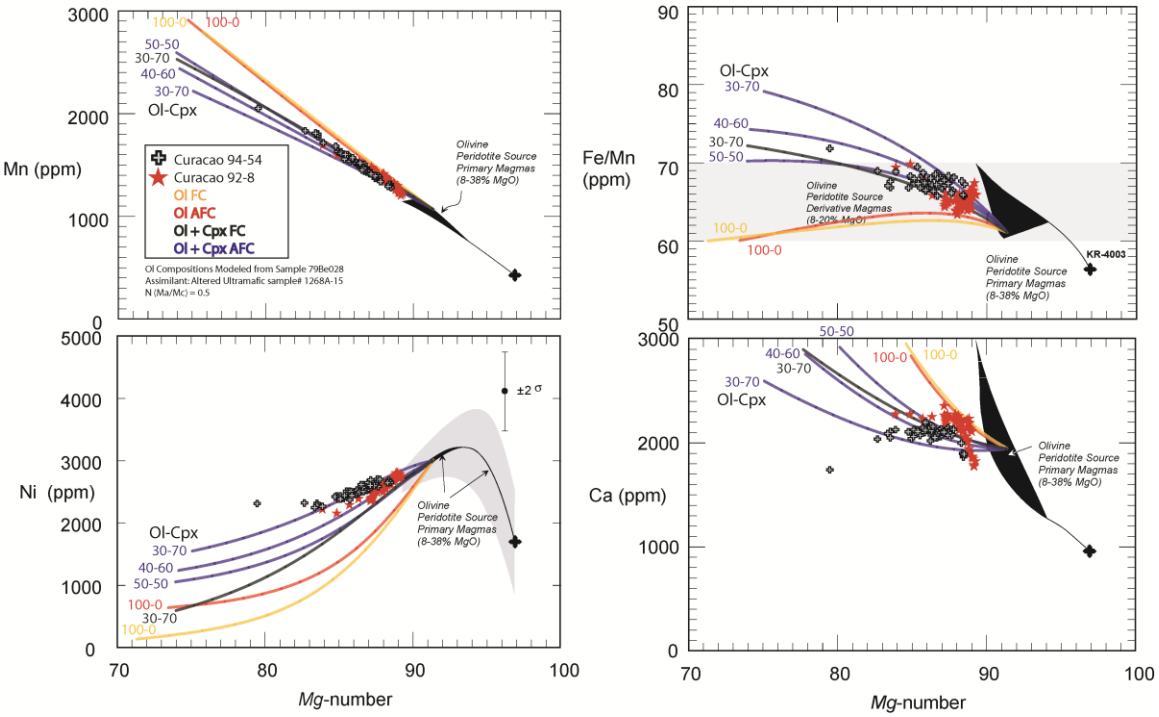


**Figure 6:**

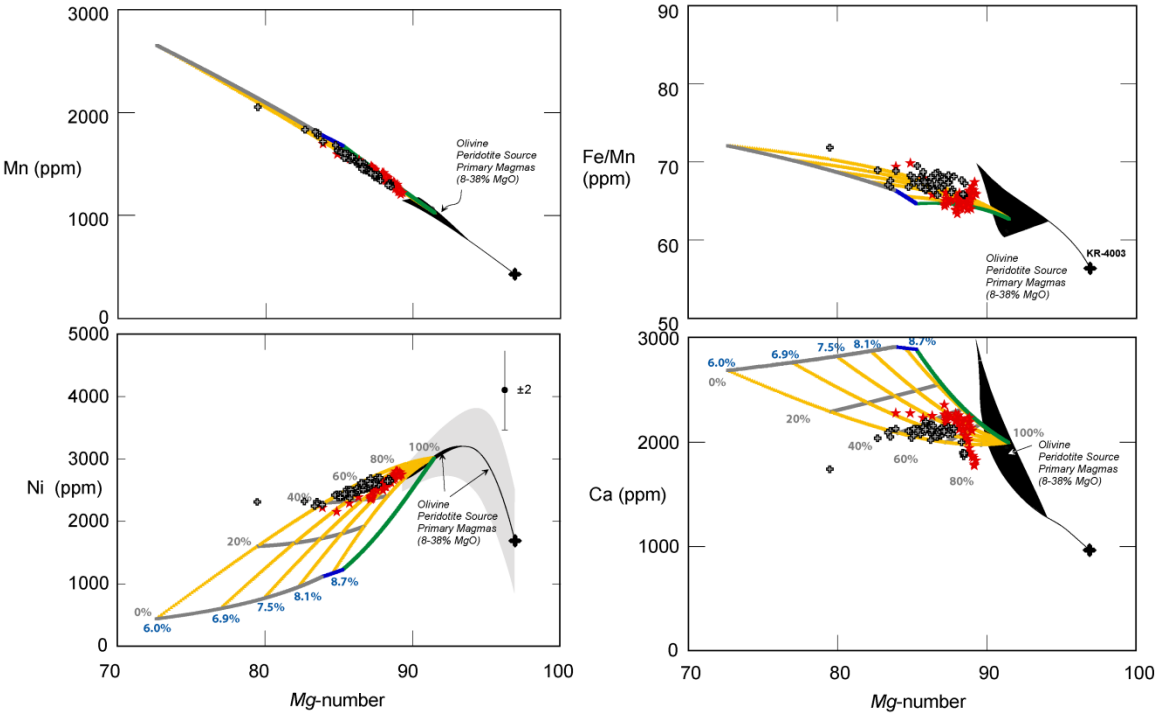

**Figure 7:**

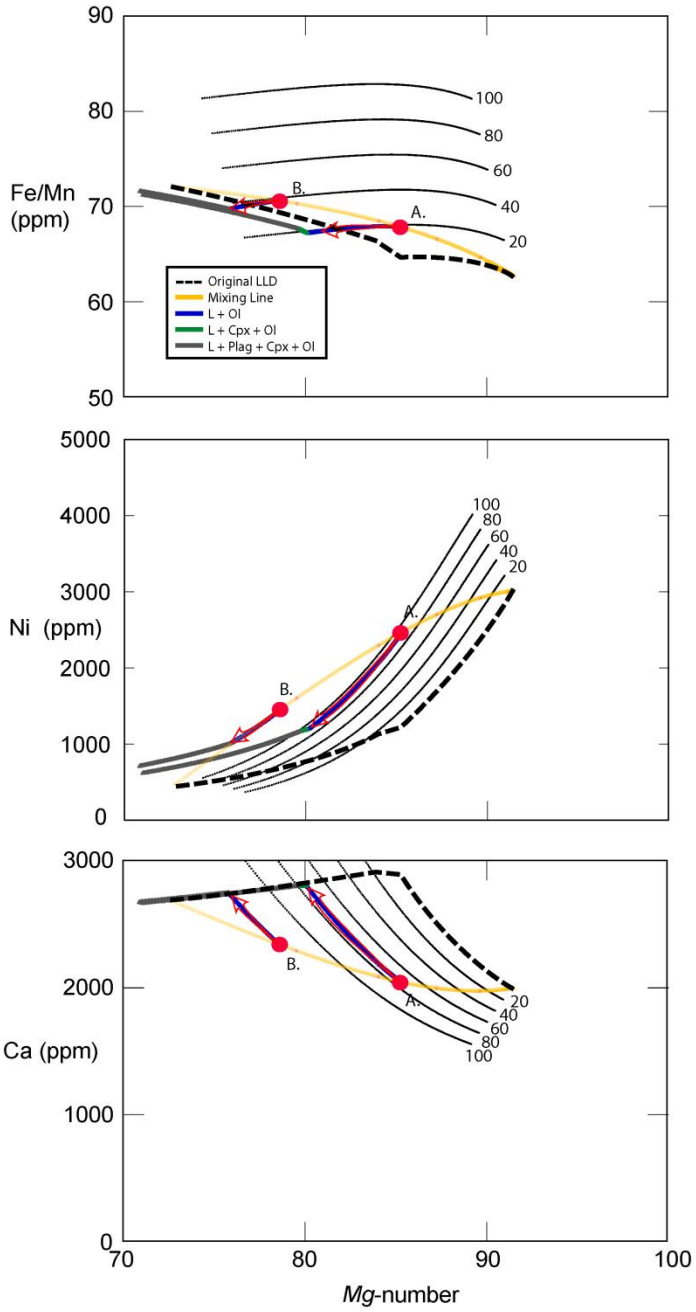
Fe/Mn (ppm)
Ni (ppm)
Ca (ppm)
Mg-number
Original LLD
Mixing Line
L + Ol
L + Cpx + Ol
L + Plag + Cpx + Ol
A.
B.
100
80
60
40
20

**Figure 8:**

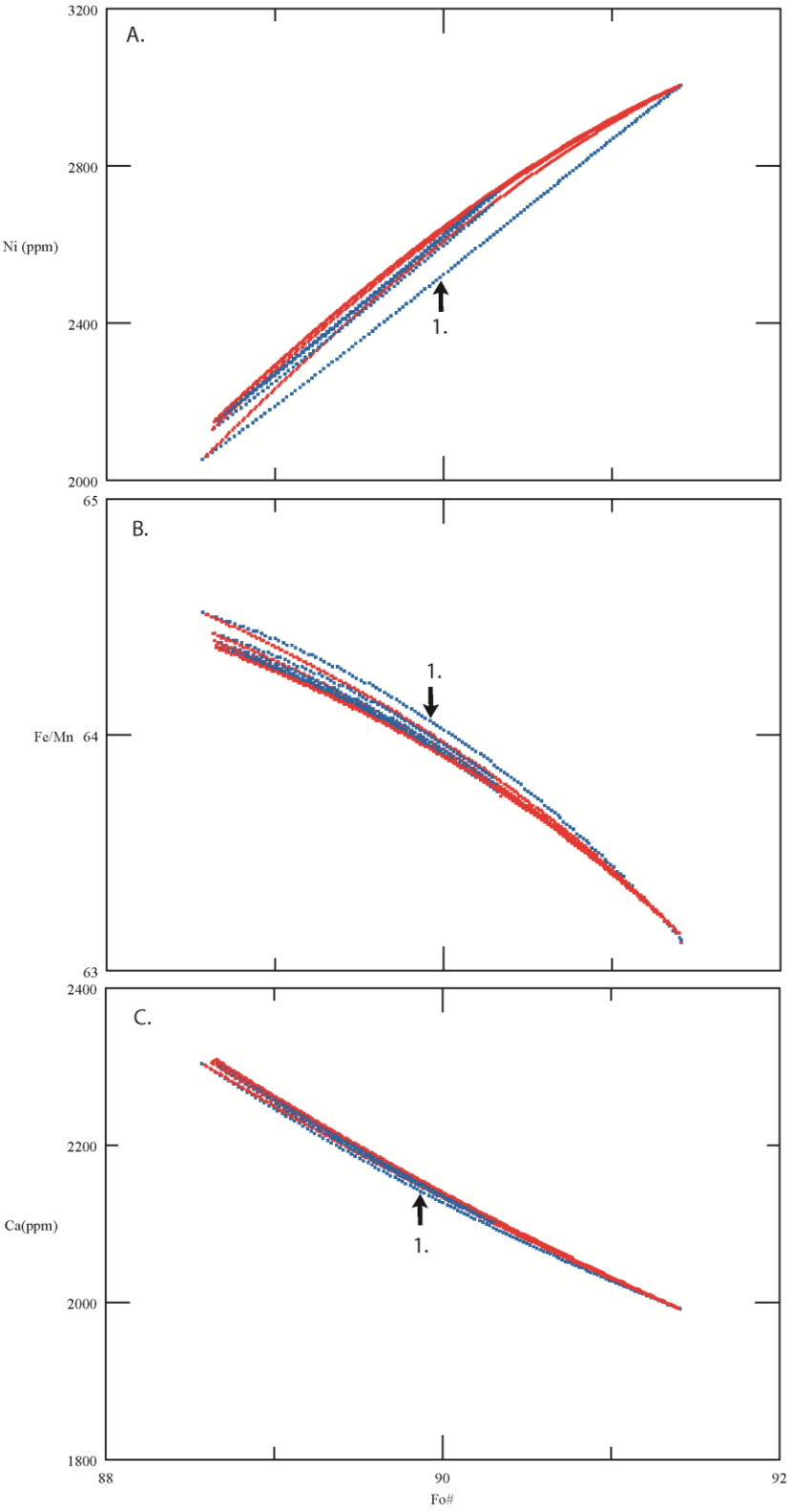
A.
3200
2800
2400
2000
Ni (ppm)
1.
B.
65
64
63
Fe/Mn
1.
C.
2400
2200
2000
1800
Ca(ppm)
1.
88
90
92
Fo#

**Figure 9:**

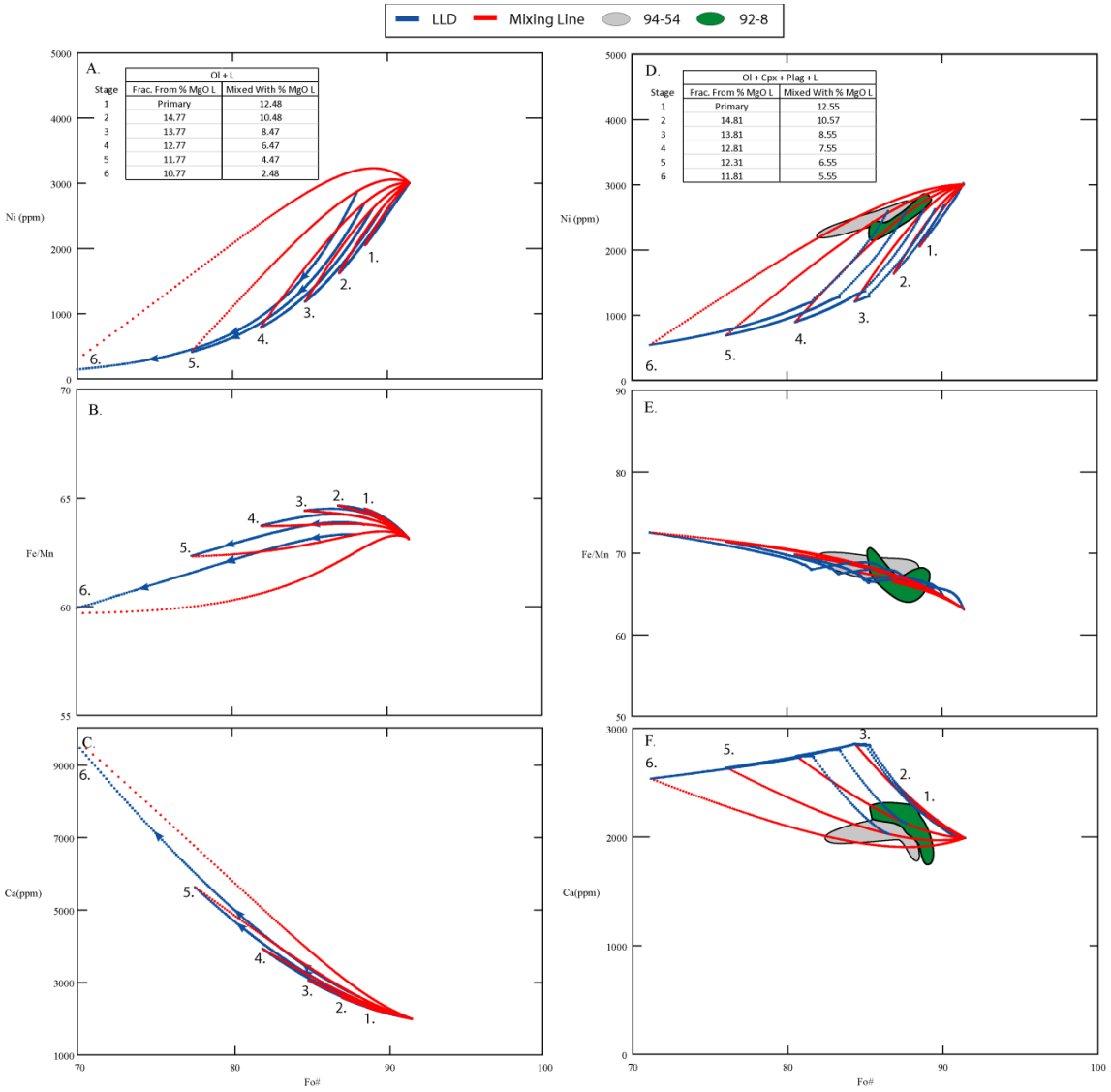
LLD
Mixing Line
94-54
92-8
A.
Ol + L
Stage | Frac. From % MgO L | Mixed With % MgO L
1 | Primary | 12.48
2 | 14.77 | 10.48
3 | 13.77 | 8.47
4 | 12.77 | 6.47
5 | 11.77 | 4.47
6 | 10.77 | 2.48
D.
Ol + Cpx + Plag + L
Stage | Frac. From % MgO L | Mixed With % MgO L
1 | Primary | 12.55
2 | 14.81 | 10.57
3 | 13.81 | 8.55
4 | 12.81 | 7.55
5 | 12.31 | 6.55
6 | 11.81 | 5.55
Ni (ppm)
B.
E.
Fe/Mn
C.
F.
Ca(ppm)
Fo#

## 10. Tables

### Table 1: Secondary Standards, Primary Standards and Statistics

| | San Carlos Olivine, USNM 111312/44 | | | |
|---|---|---|---|---|
| | **Average (N=21)** | **1 Sigma** | **Average** (N=1788)** | **Published*** |
| **SiO2 %** | 40.69 | 0.076 | 40.83 | 40.81 |
| **MgO %** | 49.05 | 0.096 | 48.90 | 49.42 |
| **FeO %** | 9.72 | 0.021 | 9.75 | 9.55 |
| **NiO %** | 0.356 | 0.0022 | 0.358 | 0.37 |
| **MnO %** | 0.132 | 0.0017 | 0.132 | 0.14 |
| **CaO %** | 0.063 | 0.0012 | 0.063 | 0.05 |
| **Fo #** | 90.0 | 0.0 | 89.9 | 90.2 |
| **Fe (ppm)** | 75532 | 160 | 75783 | 74233 |
| **Mn (ppm)** | 1019 | 13 | 1019 | 1084 |
| **Ni (ppm)** | 2798 | 17 | 2816 | 2907 |
| **Ca (ppm)** | 452 | 8 | 450 | 357 |
| **Fe/Mn** | 74.1 | 1 | 74.4 | 68.5 |

*Jarosewich et al., 1980

** All analyses of the RU SCOL standard at high currents and long count times over 4 years

***Jarosewich et al., 1987

| | Chromian Augite, NMNH 164905 (N=3) | | |
|---|---|---|---|
| | **Average** | **1 σ** | **Published*** ** |
| **SiO2** | 50.51 | 0.01 | 50.48 |
| **MgO** | 17.29 | 0.02 | 17.32 |
| **FeO** | 4.71 | 0.00 | 4.69 |
| **NiO2** | 0.046 | 0.004 | n.a. |
| **MnO** | 0.127 | 0.003 | 0.12 |
| **CaO** | ***17.30*** | ***0.01*** | ***17.30*** |

***Ca Standard***

| | Kakanui Pyrope, USNM 143968 (N=3) | | |
|---|---|---|---|
| | **Average** | **1 σ** | **Published*** |
| **SiO2** | 41.62 | 0.47 | 41.46 |
| **MgO** | 19.02 | 0.15 | 18.51 |
| **FeO** | 10.34 | 0.04 | 10.68 |
| **NiO2** | 0.006 | 0.002 | n.a. |
| **MnO** | 0.322 | 0.006 | 0.28 |
| **CaO** | 5.09 | 0.02 | 5.17 |

| | **Primary Standards:** | **Avg. D.L. (3 σ)**** | **Avg. Percent Err. (1 σ)**** |
|---|---|---|---|
| **Si** | Synthetic Fayalite (Takei) | 0.0029 | 0.047 |
| **Mg** | Synthetic Forsterite (Takei) | 0.0041 | 0.076 |
| **Fe** | Synthetic Fayalite (Takei) | 0.0027 | 0.099 |
| **Ni** | Synthetic Ni2SiO4 (Boyd) | 0.0017 | 0.739 |
| **Mn** | Synthetic Tephroite (Takei) | 0.0022 | 1.073 |
| **Ca** | Chromian Augite, NMNH 164905 | 0.0023 | 0.621 |

****Statistics calculated in the Probe for EPMA software (Donovan, 2012)

| | Augite 209 (N=3) | | |
|---|---|---|---|
| | **Average** | **1 σ** | **Published** |
| **SiO2** | 47.67 | 0.18 | 47.90 |
| **MgO** | 12.80 | 0.04 | 12.67 |
| **FeO** | 8.17 | 0.03 | 8.18 |
| **NiO2** | 0.006 | 0.005 | n.a. |
| **MnO** | 0.181 | 0.007 | 0.18 |
| **CaO** | 18.15 | 0.04 | 18.36 |

**Table 2: Curacao Olivine Data**

| Sample | SiO2 % | MgO % | FeO % | NiO % | MnO % | CaO % | Fo# | Fe (ppm) | Mn (ppm) | Ni (ppm) | Ca (ppm) | Fe/Mn |
|---|---|---|---|---|---|---|---|---|---|---|---|---|
| 92_8_Olivine1 | 40.38 | 47.34 | 11.46 | 0.332 | 0.177 | 0.308 | 88.0 | 89060 | 1372 | 2611 | 2204 | 64.9 |
| 92_8_Olivine1 | 40.32 | 47.27 | 11.59 | 0.331 | 0.179 | 0.308 | 87.9 | 90125 | 1383 | 2600 | 2201 | 65.2 |
| 92_8_Olivine1 | 40.00 | 46.17 | 13.02 | 0.304 | 0.198 | 0.315 | 86.3 | 101179 | 1537 | 2386 | 2248 | 65.8 |
| 92_8_Olivine2 | 40.44 | 47.99 | 10.74 | 0.353 | 0.166 | 0.306 | 88.8 | 83494 | 1282 | 2773 | 2186 | 65.1 |
| 92_8_Olivine2 | 40.37 | 48.04 | 10.77 | 0.347 | 0.163 | 0.312 | 88.8 | 83737 | 1262 | 2726 | 2229 | 66.4 |
| 92_8_Olivine2 | 40.35 | 48.00 | 10.82 | 0.349 | 0.166 | 0.307 | 88.8 | 84112 | 1287 | 2746 | 2194 | 65.3 |
| 92_8_Olivine2 | 40.34 | 47.93 | 10.90 | 0.344 | 0.171 | 0.310 | 88.7 | 84726 | 1326 | 2701 | 2217 | 63.9 |
| 92_8_Olivine3 | 40.36 | 48.22 | 10.61 | 0.355 | 0.159 | 0.295 | 89.0 | 82475 | 1233 | 2792 | 2106 | 66.9 |
| 92_8_Olivine3 | 40.44 | 48.12 | 10.63 | 0.356 | 0.162 | 0.295 | 89.0 | 82623 | 1256 | 2794 | 2111 | 65.8 |
| 92_8_Olivine3 | 40.38 | 48.12 | 10.69 | 0.350 | 0.164 | 0.299 | 88.9 | 83069 | 1267 | 2749 | 2134 | 65.6 |
| 92_8_Olivine3 | 40.36 | 48.13 | 10.69 | 0.351 | 0.168 | 0.298 | 88.9 | 83126 | 1299 | 2761 | 2131 | 64.0 |
| 92_8_Olivine3 | 40.37 | 48.01 | 10.80 | 0.350 | 0.167 | 0.301 | 88.8 | 83917 | 1296 | 2747 | 2152 | 64.7 |
| 92_8_Olivine3 | 40.40 | 47.95 | 10.83 | 0.345 | 0.169 | 0.300 | 88.8 | 84199 | 1308 | 2712 | 2146 | 64.4 |
| 92_8_Olivine4 | 40.29 | 47.42 | 11.46 | 0.333 | 0.179 | 0.315 | 88.1 | 89099 | 1389 | 2615 | 2248 | 64.2 |
| 92_8_Olivine4 | 40.27 | 46.87 | 12.04 | 0.319 | 0.186 | 0.315 | 87.4 | 93622 | 1438 | 2507 | 2250 | 65.1 |
| 92_8_Olivine4 | 40.30 | 47.30 | 11.58 | 0.327 | 0.182 | 0.307 | 87.9 | 90025 | 1411 | 2573 | 2195 | 63.8 |
| 92_8_Olivine4 | 40.20 | 46.81 | 12.18 | 0.304 | 0.189 | 0.313 | 87.3 | 94642 | 1463 | 2388 | 2238 | 64.7 |
| 92_8_Olivine5 | 40.20 | 47.47 | 11.53 | 0.318 | 0.183 | 0.309 | 88.0 | 89585 | 1414 | 2497 | 2210 | 63.4 |
| 92_8_Olivine5 | 40.37 | 47.45 | 11.37 | 0.327 | 0.173 | 0.310 | 88.1 | 88411 | 1339 | 2568 | 2216 | 66.0 |
| 92_8_Olivine6 | 40.34 | 47.43 | 11.42 | 0.325 | 0.174 | 0.311 | 88.1 | 88776 | 1350 | 2557 | 2220 | 65.8 |
| 92_8_Olivine6 | 40.25 | 47.51 | 11.42 | 0.331 | 0.179 | 0.315 | 88.1 | 88779 | 1385 | 2597 | 2255 | 64.1 |
| 92_8_Olivine6 | 40.25 | 47.33 | 11.60 | 0.326 | 0.182 | 0.317 | 87.9 | 90158 | 1410 | 2563 | 2269 | 63.9 |
| 92_8_Olivine7 | 40.54 | 48.26 | 10.45 | 0.349 | 0.156 | 0.248 | 89.2 | 81250 | 1205 | 2744 | 1771 | 67.4 |
| 92_8_Olivine7 | 40.49 | 48.27 | 10.48 | 0.354 | 0.159 | 0.250 | 89.1 | 81425 | 1234 | 2783 | 1784 | 66.0 |
| 92_8_Olivine7 | 40.55 | 48.10 | 10.58 | 0.352 | 0.160 | 0.260 | 89.0 | 82267 | 1236 | 2764 | 1859 | 66.6 |
| 92_8_Olivine7 | 40.48 | 48.04 | 10.70 | 0.356 | 0.165 | 0.266 | 88.9 | 83172 | 1277 | 2800 | 1901 | 65.1 |
| 92_8_Olivine7 | 40.41 | 47.97 | 10.83 | 0.345 | 0.169 | 0.280 | 88.8 | 84179 | 1311 | 2710 | 2004 | 64.2 |

| Sample | SiO2 % | MgO % | FeO % | NiO % | MnO % | CaO % | Fo# | Fe (ppm) | Mn (ppm) | Ni (ppm) | Ca (ppm) | Fe/Mn |
|---|---|---|---|---|---|---|---|---|---|---|---|---|
| 92_8_Olivine8 | 40.63 | 48.27 | 10.34 | 0.350 | 0.158 | 0.255 | 89.3 | 80402 | 1220 | 2751 | 1821 | 65.9 |
| 92_8_Olivine8 | 40.57 | 48.16 | 10.50 | 0.348 | 0.159 | 0.258 | 89.1 | 81647 | 1230 | 2731 | 1847 | 66.4 |
| 92_8_Olivine8 | 40.67 | 48.04 | 10.52 | 0.346 | 0.161 | 0.261 | 89.1 | 81759 | 1245 | 2718 | 1867 | 65.7 |
| 92_8_Olivine8 | 40.54 | 47.92 | 10.76 | 0.342 | 0.163 | 0.271 | 88.8 | 83626 | 1261 | 2685 | 1940 | 66.3 |
| 92_8_Olivine8 | 40.53 | 47.67 | 11.00 | 0.334 | 0.170 | 0.287 | 88.5 | 85532 | 1313 | 2622 | 2053 | 65.1 |
| 92_8_Olivine8 | 40.05 | 45.61 | 13.54 | 0.291 | 0.200 | 0.312 | 85.7 | 105231 | 1549 | 2290 | 2228 | 67.9 |
| 92_8_Olivine9 | 40.59 | 47.46 | 11.14 | 0.334 | 0.172 | 0.306 | 88.4 | 86593 | 1331 | 2625 | 2188 | 65.1 |
| 92_8_Olivine9 | 40.42 | 47.46 | 11.30 | 0.335 | 0.177 | 0.305 | 88.2 | 87842 | 1367 | 2635 | 2178 | 64.2 |
| 92_8_Olivine9 | 39.76 | 44.28 | 15.15 | 0.282 | 0.219 | 0.318 | 83.9 | 117742 | 1696 | 2219 | 2274 | 69.4 |
| 92_8_Olivine10 | 40.39 | 47.39 | 11.41 | 0.331 | 0.175 | 0.304 | 88.1 | 88716 | 1358 | 2604 | 2172 | 65.3 |
| 92_8_Olivine10 | 40.48 | 47.48 | 11.23 | 0.333 | 0.172 | 0.305 | 88.3 | 87280 | 1334 | 2615 | 2178 | 65.5 |
| 92_8_Olivine10 | 40.48 | 47.35 | 11.36 | 0.333 | 0.175 | 0.306 | 88.1 | 88272 | 1355 | 2618 | 2186 | 65.1 |
| 92_8_Olivine11 | 40.49 | 47.59 | 11.11 | 0.335 | 0.173 | 0.298 | 88.4 | 86377 | 1339 | 2630 | 2127 | 64.5 |
| 92_8_Olivine11 | 40.51 | 47.57 | 11.12 | 0.337 | 0.172 | 0.294 | 88.4 | 86436 | 1331 | 2650 | 2101 | 64.9 |
| 92_8_Olivine11 | 40.41 | 47.53 | 11.24 | 0.338 | 0.176 | 0.309 | 88.3 | 87334 | 1363 | 2658 | 2211 | 64.1 |
| 92_8_Olivine11 | 40.38 | 47.44 | 11.37 | 0.333 | 0.175 | 0.296 | 88.1 | 88395 | 1358 | 2620 | 2118 | 65.1 |
| 92_8_Olivine11 | 40.29 | 46.73 | 12.18 | 0.316 | 0.187 | 0.308 | 87.2 | 94643 | 1449 | 2483 | 2200 | 65.3 |
| 92_8_Olivine12 | 40.44 | 46.90 | 11.85 | 0.317 | 0.183 | 0.312 | 87.6 | 92106 | 1414 | 2493 | 2230 | 65.1 |
| 92_8_Olivine12 | 40.60 | 47.32 | 11.28 | 0.324 | 0.173 | 0.306 | 88.2 | 87647 | 1342 | 2550 | 2189 | 65.3 |
| 92_8_Olivine12 | 40.38 | 46.65 | 12.17 | 0.301 | 0.185 | 0.315 | 87.2 | 94569 | 1431 | 2367 | 2252 | 66.1 |
| 92_8_Olivine13 | 40.46 | 47.40 | 11.32 | 0.334 | 0.177 | 0.311 | 88.2 | 87969 | 1374 | 2628 | 2223 | 64.0 |
| 92_8_Olivine13 | 40.51 | 47.45 | 11.23 | 0.331 | 0.172 | 0.311 | 88.3 | 87297 | 1330 | 2604 | 2225 | 65.6 |
| 92_8_Olivine13 | 40.27 | 46.84 | 12.06 | 0.322 | 0.187 | 0.318 | 87.4 | 93771 | 1445 | 2529 | 2272 | 64.9 |
| 92_8_Olivine14 | 40.39 | 47.16 | 11.64 | 0.322 | 0.179 | 0.313 | 87.8 | 90473 | 1389 | 2532 | 2238 | 65.1 |
| 92_8_Olivine14 | 40.32 | 46.64 | 12.24 | 0.299 | 0.191 | 0.316 | 87.2 | 95141 | 1478 | 2353 | 2262 | 64.4 |
| 92_8_Olivine14 | 40.34 | 46.59 | 12.25 | 0.303 | 0.190 | 0.329 | 87.1 | 95199 | 1473 | 2384 | 2353 | 64.6 |
| 92_8_Olivine15 | 40.46 | 47.89 | 10.86 | 0.339 | 0.166 | 0.284 | 88.7 | 84421 | 1283 | 2665 | 2030 | 65.8 |
| 92_8_Olivine15 | 40.42 | 47.83 | 10.95 | 0.341 | 0.167 | 0.288 | 88.6 | 85138 | 1292 | 2676 | 2055 | 65.9 |

| Sample | SiO2 % | MgO % | FeO % | NiO % | MnO % | CaO % | Fo# | Fe (ppm) | Mn (ppm) | Ni (ppm) | Ca (ppm) | Fe/Mn |
|---|---|---|---|---|---|---|---|---|---|---|---|---|
| 92_8_Olivine15 | 40.41 | 47.63 | 11.15 | 0.337 | 0.172 | 0.294 | 88.4 | 86678 | 1329 | 2651 | 2101 | 65.2 |
| 92_8_Olivine15 | 40.20 | 46.87 | 12.14 | 0.307 | 0.187 | 0.304 | 87.3 | 94349 | 1452 | 2412 | 2175 | 65.0 |
| 92_8_Olivine15 | 40.15 | 46.81 | 12.25 | 0.306 | 0.189 | 0.300 | 87.2 | 95226 | 1465 | 2404 | 2141 | 65.0 |
| 92_8_Olivine15 | 39.83 | 45.05 | 14.32 | 0.274 | 0.206 | 0.318 | 84.9 | 111325 | 1594 | 2153 | 2273 | 69.9 |
| 95_54_Olivine1 | 39.85 | 45.79 | 13.56 | 0.302 | 0.201 | 0.297 | 85.8 | 105395 | 1558 | 2372 | 2125 | 67.7 |
| 95_54_Olivine1 | 39.03 | 41.21 | 18.96 | 0.294 | 0.265 | 0.243 | 79.5 | 147397 | 2052 | 2310 | 1737 | 71.8 |
| 95_54_Olivine2 | 39.94 | 45.83 | 13.41 | 0.315 | 0.203 | 0.307 | 85.9 | 104240 | 1570 | 2474 | 2193 | 66.4 |
| 95_54_Olivine2 | 39.38 | 43.54 | 16.26 | 0.295 | 0.237 | 0.285 | 82.7 | 126376 | 1833 | 2318 | 2033 | 68.9 |
| 95_54_Olivine3 | 40.39 | 47.74 | 11.11 | 0.338 | 0.170 | 0.260 | 88.5 | 86321 | 1313 | 2656 | 1861 | 65.7 |
| 95_54_Olivine3 | 40.57 | 47.53 | 11.12 | 0.341 | 0.169 | 0.265 | 88.4 | 86473 | 1312 | 2681 | 1895 | 65.9 |
| 95_54_Olivine3 | 40.31 | 47.84 | 11.08 | 0.337 | 0.165 | 0.264 | 88.5 | 86109 | 1280 | 2646 | 1888 | 67.3 |
| 95_54_Olivine3 | 40.26 | 47.70 | 11.26 | 0.336 | 0.167 | 0.279 | 88.3 | 87493 | 1293 | 2642 | 1994 | 67.7 |
| 95_54_Olivine3 | 40.30 | 47.11 | 11.79 | 0.329 | 0.178 | 0.290 | 87.7 | 91642 | 1378 | 2584 | 2075 | 66.5 |
| 95_54_Olivine4 | 39.80 | 45.73 | 13.66 | 0.310 | 0.201 | 0.294 | 85.6 | 106209 | 1555 | 2438 | 2101 | 68.3 |
| 95_54_Olivine4 | 39.86 | 45.61 | 13.71 | 0.312 | 0.206 | 0.297 | 85.6 | 106582 | 1595 | 2456 | 2121 | 66.8 |
| 95_54_Olivine4 | 39.95 | 45.04 | 14.21 | 0.303 | 0.210 | 0.285 | 85.0 | 110477 | 1625 | 2382 | 2037 | 68.0 |
| 95_54_Olivine5 | 39.96 | 46.13 | 13.10 | 0.314 | 0.193 | 0.303 | 86.3 | 101815 | 1498 | 2471 | 2162 | 68.0 |
| 95_54_Olivine5 | 39.91 | 46.01 | 13.27 | 0.318 | 0.198 | 0.299 | 86.1 | 103171 | 1531 | 2499 | 2138 | 67.4 |
| 95_54_Olivine5 | 39.74 | 45.68 | 13.76 | 0.319 | 0.207 | 0.290 | 85.5 | 106975 | 1602 | 2507 | 2069 | 66.8 |
| 95_54_Olivine6 | 40.02 | 45.98 | 13.19 | 0.313 | 0.196 | 0.298 | 86.1 | 102491 | 1520 | 2456 | 2127 | 67.4 |
| 95_54_Olivine6 | 39.68 | 44.03 | 15.47 | 0.294 | 0.230 | 0.295 | 83.5 | 120244 | 1778 | 2313 | 2105 | 67.6 |
| 95_54_Olivine7 | 39.72 | 45.13 | 14.33 | 0.309 | 0.211 | 0.294 | 84.9 | 111427 | 1632 | 2431 | 2101 | 68.3 |
| 95_54_Olivine7 | 39.64 | 45.08 | 14.46 | 0.308 | 0.217 | 0.294 | 84.7 | 112413 | 1683 | 2418 | 2102 | 66.8 |
| 95_54_Olivine7 | 39.58 | 44.12 | 15.49 | 0.290 | 0.233 | 0.286 | 83.5 | 120422 | 1802 | 2281 | 2046 | 66.8 |
| 95_54_Olivine8 | 40.23 | 46.93 | 12.03 | 0.330 | 0.177 | 0.300 | 87.4 | 93543 | 1369 | 2596 | 2141 | 68.3 |
| 95_54_Olivine8 | 40.17 | 46.53 | 12.49 | 0.330 | 0.186 | 0.297 | 86.9 | 97074 | 1439 | 2590 | 2123 | 67.4 |
| 95_54_Olivine8 | 40.08 | 46.09 | 13.03 | 0.320 | 0.196 | 0.290 | 86.3 | 101287 | 1517 | 2511 | 2072 | 66.8 |
| 95_54_Olivine9 | 40.22 | 47.10 | 11.86 | 0.344 | 0.180 | 0.298 | 87.6 | 92180 | 1394 | 2701 | 2126 | 66.1 |

| Sample | SiO2 % | MgO % | FeO % | NiO % | MnO % | CaO % | Fo# | Fe (ppm) | Mn (ppm) | Ni (ppm) | Ca (ppm) | Fe/Mn |
|---|---|---|---|---|---|---|---|---|---|---|---|---|
| 95_54_Olivine9 | 40.20 | 46.56 | 12.43 | 0.337 | 0.187 | 0.298 | 87.0 | 96584 | 1448 | 2647 | 2132 | 66.7 |
| 95_54_Olivine9 | 39.87 | 45.74 | 13.58 | 0.319 | 0.198 | 0.299 | 85.7 | 105555 | 1536 | 2507 | 2138 | 68.7 |
| 95_54_Olivine10 | 40.01 | 46.30 | 12.87 | 0.333 | 0.193 | 0.290 | 86.5 | 100043 | 1495 | 2614 | 2072 | 66.9 |
| 95_54_Olivine10 | 40.24 | 46.24 | 12.71 | 0.332 | 0.190 | 0.292 | 86.6 | 98757 | 1470 | 2611 | 2090 | 67.2 |
| 95_54_Olivine10 | 40.13 | 46.78 | 12.28 | 0.342 | 0.184 | 0.293 | 87.2 | 95418 | 1421 | 2690 | 2092 | 67.1 |
| 95_54_Olivine11 | 40.16 | 47.29 | 11.73 | 0.344 | 0.173 | 0.297 | 87.8 | 91173 | 1338 | 2700 | 2125 | 68.1 |
| 95_54_Olivine11 | 40.16 | 47.02 | 12.02 | 0.334 | 0.179 | 0.293 | 87.5 | 93413 | 1385 | 2623 | 2094 | 67.4 |
| 95_54_Olivine12 | 39.97 | 46.12 | 13.11 | 0.321 | 0.193 | 0.282 | 86.2 | 101937 | 1498 | 2525 | 2016 | 68.0 |
| 95_54_Olivine12 | 39.92 | 45.18 | 14.09 | 0.310 | 0.210 | 0.288 | 85.1 | 109528 | 1627 | 2432 | 2058 | 67.3 |
| 95_54_Olivine13 | 39.57 | 44.42 | 15.20 | 0.288 | 0.222 | 0.297 | 83.9 | 118128 | 1716 | 2265 | 2124 | 68.9 |
| 95_54_Olivine13 | 39.59 | 43.97 | 15.63 | 0.285 | 0.234 | 0.292 | 83.4 | 121513 | 1811 | 2243 | 2087 | 67.1 |
| 95_54_Olivine15 | 39.77 | 45.50 | 13.93 | 0.304 | 0.201 | 0.297 | 85.3 | 108288 | 1558 | 2391 | 2124 | 69.5 |
| 95_54_Olivine15 | 39.78 | 45.30 | 14.12 | 0.303 | 0.208 | 0.297 | 85.1 | 109728 | 1614 | 2381 | 2124 | 68.0 |
| 95_54_Olivine16 | 39.80 | 45.51 | 13.88 | 0.310 | 0.207 | 0.295 | 85.4 | 107907 | 1602 | 2438 | 2105 | 67.3 |
| 95_54_Olivine16 | 39.81 | 45.87 | 13.50 | 0.318 | 0.201 | 0.293 | 85.8 | 104968 | 1557 | 2502 | 2095 | 67.4 |
| 95_54_Olivine17 | 40.05 | 46.75 | 12.40 | 0.323 | 0.183 | 0.294 | 87.0 | 96424 | 1416 | 2535 | 2099 | 68.1 |
| 95_54_Olivine17 | 40.14 | 46.98 | 12.08 | 0.330 | 0.180 | 0.290 | 87.4 | 93881 | 1394 | 2597 | 2070 | 67.3 |
| 95_54_Olivine18 | 40.09 | 46.57 | 12.55 | 0.321 | 0.185 | 0.288 | 86.9 | 97541 | 1432 | 2520 | 2059 | 68.1 |
| 95_54_Olivine18 | 40.01 | 46.66 | 12.54 | 0.321 | 0.187 | 0.288 | 86.9 | 97473 | 1445 | 2522 | 2056 | 67.5 |
| 95_54_Olivine18 | 39.93 | 46.52 | 12.74 | 0.323 | 0.194 | 0.290 | 86.7 | 99054 | 1506 | 2538 | 2075 | 65.8 |
| 95_54_Olivine18 | 39.90 | 46.25 | 13.05 | 0.314 | 0.195 | 0.296 | 86.3 | 101433 | 1510 | 2470 | 2112 | 67.2 |
| 95_54_Olivine18 | 39.92 | 45.85 | 13.42 | 0.311 | 0.203 | 0.296 | 85.9 | 104353 | 1570 | 2441 | 2117 | 66.5 |
| 95_54_Olivine19 | 40.08 | 46.80 | 12.31 | 0.331 | 0.182 | 0.294 | 87.1 | 95700 | 1412 | 2601 | 2100 | 67.8 |
| 95_54_Olivine19 | 40.18 | 46.32 | 12.69 | 0.321 | 0.190 | 0.293 | 86.7 | 98627 | 1473 | 2519 | 2097 | 67.0 |
| 95_54_Olivine19 | 39.94 | 46.27 | 12.97 | 0.317 | 0.196 | 0.301 | 86.4 | 100844 | 1519 | 2494 | 2154 | 66.4 |
| 95_54_Olivine20 | 40.02 | 46.47 | 12.71 | 0.322 | 0.186 | 0.293 | 86.7 | 98776 | 1439 | 2533 | 2093 | 68.7 |
| 95_54_Olivine20 | 40.09 | 46.40 | 12.72 | 0.319 | 0.188 | 0.286 | 86.7 | 98867 | 1453 | 2503 | 2045 | 68.0 |
| 95_54_Olivine20 | 40.30 | 46.19 | 12.70 | 0.327 | 0.190 | 0.290 | 86.6 | 98731 | 1469 | 2571 | 2071 | 67.2 |

| Sample | SiO2 % | MgO % | FeO % | NiO % | MnO % | CaO % | Fo# | Fe (ppm) | Mn (ppm) | Ni (ppm) | Ca (ppm) | Fe/Mn |
|---|---|---|---|---|---|---|---|---|---|---|---|---|
| 95_54_Olivine20 | 40.25 | 46.15 | 12.80 | 0.332 | 0.187 | 0.287 | 86.5 | 99469 | 1451 | 2613 | 2048 | 68.5 |

**Table 3: Curacao Whole Rock and Calculated Primary Magma Compositions**

| Sample | Data | Source | SiO2 | TiO2 | Al2O3 | Cr2O3 | Fe2O3 | FeO | |
|---|---|---|---|---|---|---|---|---|---|
| 79be028 (Klaver 1987) | Whole Rock | | 48.99 | 0.95 | 14.09 | 0 | | 9.44 | |
| Cur36 (Kerr et al., 1996b) | Whole Rock | | 50.69 | 1.2 | 14.28 | 0.02 | 1.36 | 11.04 | |
| 126A-8* (Paullick et al., 2006) | Whole Rock | | 59.27 | 0 | 0.9 | 0.36 | 0.61 | 4.57 | |
| 79be028 | Primary Magma | peridotite | 48.58 | 0.79 | 11.6 | 0 | 0.86 | 9.18 | |
| CUR36 | Primary Magma | pyroxenite | 47.94 | 0.91 | 10.74 | 0.02 | 1.02 | 11.78 | |
| Hybrid(90/10)*** | Primary Magma | hybrid | 48.55 | 0.8 | 11.53 | 0 | 0.88 | 9.45 | |
| Hybrid(80/20)*** | Primary Magma | hybrid | 48.48 | 0.81 | 11.44 | 0 | 0.89 | 9.71 | |
| Hybrid(70/30)*** | Primary Magma | hybrid | 48.42 | 0.82 | 11.35 | 0.01 | 0.91 | 9.97 | |
| Hybrid(60/40)*** | Primary Magma | hybrid | 48.26 | 0.83 | 11.24 | 0.01 | 0.93 | 10.2 | |
| Hybrid(40/20)*** | Primary Magma | hybrid | 48.15 | 0.86 | 11.08 | 0.01 | 0.96 | 10.73 | |
| Hybrid(20/80)*** | Primary Magma | hybrid | 48.05 | 0.88 | 10.91 | 0.01 | 0.99 | 11.25 | |
| Sample | Data | Source | MnO | MgO | CaO | Na2O | K2O | NiO | P2O5 |
| 79be028 (Klaver 1987) | Whole Rock | | 0.18 | 8.82 | 12.68 | 1.36 | 0 | 0.03 | 0.1 |
| Cur36 (Kerr et al., 1996) | Whole Rock | | 0.19 | 7.49 | 11.2 | 2.5 | 0.06 | 0.01 | 0.01 |
| 126A-8* (Paullick et al., 2006) | Whole Rock | | 0.08 | 28.06 | 0.1 | 0.24 | 0.02 | 0.22 | 0.01 |
| 79be028 | Primary Magma | peridotite | 0.178/0.184** | 17.07 | 10.8/10.48** | 1.12 | 0 | 0.0673**** | 0 |
| CUR36 | Primary Magma | pyroxenite | 0.175/0.191** | 16.85 | 8.47 | 1.87 | 0.04 | 0.093 | 0.08 |
| Hybrid(90/10)*** | Primary Magma | hybrid | 0.178 | 17.06 | 10.29 | 1.19 | 0 | 0.0699 | 0.01 |
| Hybrid(80/20)*** | Primary Magma | hybrid | 0.178 | 17.03 | 10.09 | 1.27 | 0.01 | 0.0725 | 0.02 |
| Hybrid(70/30)*** | Primary Magma | hybrid | 0.177 | 17.01 | 9.88 | 1.34 | 0.01 | 0.075 | 0.02 |
| Hybrid(60/40)*** | Primary Magma | hybrid | 0.177 | 16.96 | 9.85 | 1.42 | 0.02 | 0.0775 | 0.03 |
| Hybrid(40/20)*** | Primary Magma | hybrid | 0.176 | 16.92 | 9.39 | 1.57 | 0.03 | 0.0826 | 0.05 |
| Hybrid(20/80)*** | Primary Magma | hybrid | 0.176 | 16.88 | 8.93 | 1.72 | 0.03 | 0.0878 | 0.06 |

*Assimilant for Curacao AFC Modeling

**Original Value/Adjusted Value

*** Peridotite/Pyroxenite

**** Calculated Ni Content using the Equation: Ni (ppm) = $21.6MgO - 0.32MgO^2 + 0.051MgO^3$ (Herzberg, 2011)

## Table 4: PRIMELT2 Primary Magmas and Trace Element Ratios for Figure 3

| LOCATION | Reference | SAMPLE | SiO2 | TiO2 | Al2O3 | Cr2O3 | Fe2O3 | FeO | MnO | MgO | CaO | Na2O | K2O |
|---|---|---|---|---|---|---|---|---|---|---|---|---|---|
| Burica (Galapagos) | Hauff et al., 2000a | BUR4 | 48.32 | 0.74 | 11.77 | 0.00 | 0.86 | 9.16 | 0.16 | 16.86 | 9.87 | 2.12 | 0.09 |
| Cerro Azul (Galapagos) | Teasdale et al., 2005 | 54 | 47.06 | 1.56 | 13.89 | 0.13 | 1.01 | 8.42 | 0.16 | 13.83 | 11.51 | 1.87 | 0.34 |
| Cerro Azul (Galapagos) | Naumann et al., 2002 | CA-46 | 47.38 | 1.69 | 11.68 | 0.16 | 1.16 | 9.17 | 0.17 | 16.13 | 10.10 | 1.84 | 0.29 |
| Cerro Azul (Galapagos) | Teasdale et al., 2005 | 16 | 46.87 | 1.53 | 14.12 | 0.11 | 0.98 | 8.43 | 0.15 | 13.76 | 11.56 | 1.93 | 0.34 |
| Cerro Azul (Galapagos) | Teasdale et al., 2005 | INTRACALDERA SCORIA | 47.06 | 1.61 | 14.07 | 0.15 | 1.04 | 8.26 | 0.16 | 13.30 | 11.73 | 2.04 | 0.36 |
| Cerro Azul (Galapagos) | Teasdale et al., 2005 | 50 | 47.10 | 1.54 | 14.28 | 0.11 | 0.96 | 8.27 | 0.15 | 13.40 | 11.69 | 1.92 | 0.35 |
| Cerro Azul (Galapagos) | Teasdale et al., 2005 | 14 | 46.94 | 1.66 | 13.63 | 0.09 | 0.93 | 8.61 | 0.16 | 14.12 | 11.18 | 2.05 | 0.39 |
| Cerro Azul (Galapagos) | Saal et al., 2007/Kurz and Geist, 1999 | SG93-5 | 46.92 | 1.75 | 12.67 | 0.07 | 0.95 | 9.14 | 0.17 | 15.59 | 10.10 | 2.10 | 0.29 |
| Cerro Azul (Galapagos) | Teasdale et al., 2005 | 42 | 47.34 | 1.60 | 14.46 | 0.13 | 0.94 | 7.97 | 0.15 | 12.68 | 12.03 | 2.11 | 0.37 |
| Espanola (Galapagos) | White et al., 1993 | G86-3 | 46.63 | 1.20 | 14.34 | 0.05 | 1.00 | 8.13 | 0.18 | 12.88 | 10.59 | 2.58 | 1.10 |
| Fernandina (Galapagos) | Geist et al., 2006 | AHA25 A | 47.12 | 1.79 | 15.11 | 0.10 | 0.93 | 8.14 | 0.15 | 13.22 | 10.89 | 2.00 | 0.31 |
| Fernandina (Galapagos) | Geist et al., 2006 | AHA19 A | 47.63 | 1.78 | 13.07 | 0.08 | 1.05 | 8.69 | 0.16 | 14.82 | 9.97 | 2.18 | 0.33 |
| Fernandina (Galapagos) | Geist et al., 2006 | AHA30 A | 47.11 | 1.85 | 12.77 | 0.07 | 0.93 | 9.10 | 0.09 | 15.77 | 9.83 | 1.85 | 0.35 |
| Floreana (Galapagos) | White et al., 1993 | FL-29 | 45.22 | 1.77 | 15.30 | 0.13 | 1.05 | 8.69 | 0.18 | 13.63 | 10.05 | 2.81 | 0.91 |
| Floreana (Galapagos) | Bow, 1979 | FL-78 | 46.50 | 1.52 | 14.16 | 0.00 | 1.06 | 8.68 | 0.19 | 14.26 | 10.62 | 2.24 | 0.53 |
| Floreana (Galapagos) | Bow, 1979 | FL-30 | 46.23 | 1.60 | 14.13 | 0.00 | 1.04 | 8.71 | 0.17 | 13.68 | 10.94 | 2.47 | 0.74 |
| Floreana (Galapagos) | Saal et al., 2007/Kurz and Geist, 1999 | SG93-22 | 46.18 | 1.64 | 14.12 | 0.10 | 1.07 | 8.79 | 0.17 | 13.86 | 10.40 | 2.61 | 0.81 |
| Floreana (Galapagos) | White et al., 1993 | FL-26 | 45.97 | 1.27 | 13.67 | 0.05 | 0.98 | 9.38 | 0.18 | 15.50 | 10.67 | 2.00 | 0.16 |
| Floreana (Galapagos) | White et al., 1993 | FL-25 | 46.01 | 1.33 | 13.56 | 0.05 | 0.97 | 9.32 | 0.19 | 15.22 | 10.77 | 2.14 | 0.23 |
| Floreana (Galapagos) | Saal et al., 2007/Kurz and Geist, 1999 | SG93-19 | 46.55 | 1.73 | 14.05 | 0.12 | 1.05 | 8.52 | 0.18 | 13.79 | 11.16 | 2.15 | 0.48 |
| Floreana (Galapagos) | Saal et al., 2007 | NSK97-260 | 46.71 | 1.76 | 14.39 | 0.12 | 1.02 | 8.15 | 0.17 | 12.86 | 11.75 | 2.30 | 0.54 |
| Floreana (Galapagos) | White et al., 1993 | FL-3 | 46.96 | 1.21 | 14.49 | 0.04 | 1.00 | 8.09 | 0.18 | 12.82 | 10.70 | 2.60 | 1.10 |
| Floreana (Galapagos) | Saal et al., 2007/Kurz and Geist, 1999 | SG93-23 | 47.11 | 1.29 | 14.27 | 0.15 | 1.03 | 8.20 | 0.16 | 12.81 | 10.97 | 2.84 | 0.90 |
| Floreana (Galapagos) | Bow, 1979 | FL-33 | 47.45 | 1.15 | 14.65 | 0.00 | 1.00 | 8.26 | 0.17 | 13.49 | 10.32 | 2.61 | 0.64 |
| San Cristobal (Galapagos) | Geist et al., 1986 | SC-23 | 46.85 | 1.39 | 14.99 | 0.06 | 0.97 | 8.32 | 0.19 | 13.50 | 10.29 | 2.52 | 0.50 |
| San Cristobal (Galapagos) | Saal et al., 2007 | NSK97-126 | 46.64 | 1.07 | 16.12 | 0.06 | 0.95 | 8.21 | 0.16 | 13.26 | 10.68 | 2.34 | 0.32 |
| San Cristobal (Galapagos) | Saal et al., 2007 | NSK97-252 | 46.92 | 0.96 | 16.00 | 0.07 | 0.94 | 8.01 | 0.16 | 12.81 | 11.81 | 2.06 | 0.11 |
| San Cristobal (Galapagos) | White et al., 1993 | SC-75 | 47.20 | 1.05 | 16.46 | 0.08 | 0.93 | 7.79 | 0.17 | 12.44 | 11.56 | 2.01 | 0.18 |
| San Cristobal (Galapagos) | Saal et al., 2007 | NSK97-254 | 47.08 | 0.94 | 15.72 | 0.07 | 0.96 | 8.18 | 0.17 | 13.25 | 11.08 | 2.21 | 0.18 |
| Santa Cruz (Galapagos) | White et al., 1993 | SC-64 | 45.54 | 0.92 | 14.87 | 0.06 | 1.03 | 9.12 | 0.18 | 14.87 | 10.25 | 2.30 | 0.00 |
| Santiago (Galapagos) | Baitis and Swanson, 1976 | JH-86 | 46.07 | 1.12 | 14.19 | 0.00 | 0.99 | 9.22 | 0.18 | 15.42 | 10.64 | 2.02 | 0.05 |
| Santiago (Galapagos) | Gibson and Geist, 2010 | 07DSG74 | 46.15 | 1.08 | 14.49 | 0.04 | 0.94 | 9.14 | 0.17 | 15.26 | 10.55 | 1.98 | 0.06 |
| Gorgona (CLIP) | Revillion et al., 2000 | GOR501 | 45.52 | 0.67 | 11.08 | 0.00 | 1.38 | 10.54 | 0.20 | 19.91 | 9.76 | 0.89 | 0.02 |
| Gorgona (CLIP) | Brugmann et al., 1987/ Jochum et al., 1991 | GOR-159 | 45.33 | 0.66 | 12.09 | 0.46 | 1.30 | 10.26 | 0.18 | 17.94 | 10.35 | 1.26 | 0.03 |
| Gorgona (CLIP) | Kamenetsky et al., 2010 | GOR-94-44 | 46.40 | 0.68 | 11.43 | 0.00 | 1.41 | 10.13 | 0.19 | 19.52 | 9.55 | 0.61 | 0.02 |
| Gorgona (CLIP) | Brugmann et al., 1987/ Jochum et al., 1991 | GOR-160 | 45.55 | 0.66 | 12.01 | 0.22 | 1.28 | 10.25 | 0.18 | 18.03 | 10.29 | 1.32 | 0.06 |

| LOCATION | Reference | SAMPLE | NiO | P2O5 | H2O | %ol add | T | TP AFM | KD | Xfo | F AFM | $La/Sm_N$ | $Sm/Yb_N$ |
|---|---|---|---|---|---|---|---|---|---|---|---|---|---|
| Burica (Galapagos) | Hauff et al., 2000a | BUR4 | 0.00 | 0.06 | 0.00 | 22.85 | 1386.1 | 1504.4 | 0.306 | 0.91 | 0.27 | 0.86 | 1.06 |
| Cerro Azul (Galapagos) | Teasdale et al., 2005 | 54 | 0.05 | 0.16 | 0.00 | 2.75 | 1320.4 | 1427.7 | 0.299 | 0.91 | 0.08 | 1.78 | 2.78 |
| Cerro Azul (Galapagos) | Naumann et al., 2002 | CA-46 | 0.06 | 0.16 | 0.00 | -2.93 | 1370.9 | 1487.2 | 0.303 | 0.91 | 0.18 | 1.80 | 2.65 |
| Cerro Azul (Galapagos) | Teasdale et al., 2005 | 16 | 0.06 | 0.17 | 0.00 | 4.96 | 1318.9 | 1425.8 | 0.297 | 0.91 | 0.07 | 2.37 | 2.08 |
| Cerro Azul (Galapagos) | Teasdale et al., 2005 | INTRACALDERA SCORIA | 0.04 | 0.17 | 0.00 | -1.67 | 1308.4 | 1412.7 | 0.297 | 0.91 | 0.05 | 2.20 | 2.31 |
| Cerro Azul (Galapagos) | Teasdale et al., 2005 | 50 | 0.06 | 0.17 | 0.00 | 5.01 | 1310.7 | 1415.6 | 0.298 | 0.91 | 0.06 | 2.20 | 2.41 |
| Cerro Azul (Galapagos) | Teasdale et al., 2005 | 14 | 0.07 | 0.19 | 0.00 | 11.22 | 1327.0 | 1435.7 | 0.297 | 0.91 | 0.07 | 2.26 | 2.47 |
| Cerro Azul (Galapagos) | Saal et al., 2007/Kurz and Geist, 1999 | SG93-5 | 0.07 | 0.18 | 0.00 | 15.44 | 1359.3 | 1474.0 | 0.299 | 0.91 | 0.12 | 1.76 | 2.50 |
| Cerro Azul (Galapagos) | Teasdale et al., 2005 | 42 | 0.05 | 0.17 | 0.00 | 3.95 | 1293.8 | 1394.0 | 0.297 | 0.91 | 0.04 | 1.78 | 2.78 |
| Espanola (Galapagos) | White et al., 1993 | G86-3 | 0.03 | 0.80 | 0.50 | 0.41 | 1298.5 | 1400.1 | 0.288 | 0.91 | 0.03 | 2.20 | 1.85 |
| Fernandina (Galapagos) | Geist et al., 2006 | AHA25 A | 0.06 | 0.18 | 0.00 | 5.96 | 1306.4 | 1410.2 | 0.298 | 0.91 | 0.08 | 1.63 | 2.52 |
| Fernandina (Galapagos) | Geist et al., 2006 | AHA19 A | 0.06 | 0.18 | 0.00 | 2.53 | 1342.7 | 1454.5 | 0.301 | 0.91 | 0.14 | 1.65 | 2.57 |
| Fernandina (Galapagos) | Geist et al., 2006 | AHA30 A | 0.10 | 0.19 | 0.00 | 16.31 | 1363.2 | 1478.5 | 0.301 | 0.91 | 0.15 | 1.65 | 2.65 |
| Floreana (Galapagos) | White et al., 1993 | FL-29 | 0.05 | 0.22 | 0.00 | 1.66 | 1316.0 | 1422.2 | 0.285 | 0.91 | 0.00 | 3.32 | 1.59 |
| Floreana (Galapagos) | Bow, 1979 | FL-78 | 0.06 | 0.18 | 0.00 | 1.09 | 1330.2 | 1439.6 | 0.295 | 0.91 | 0.07 | 2.10 | 2.22 |
| Floreana (Galapagos) | Bow, 1979 | FL-30 | 0.06 | 0.24 | 0.00 | 2.99 | 1317.1 | 1423.6 | 0.291 | 0.91 | 0.01 | 2.93 | 1.85 |
| Floreana (Galapagos) | Saal et al., 2007/Kurz and Geist, 1999 | SG93-22 | 0.05 | 0.21 | 0.00 | 1.68 | 1321.1 | 1428.5 | 0.290 | 0.91 | 0.01 | 3.18 | 1.84 |
| Floreana (Galapagos) | White et al., 1993 | FL-26 | 0.07 | 0.11 | 0.00 | 15.07 | 1357.6 | 1471.9 | 0.295 | 0.91 | 0.06 | 2.20 | 1.52 |
| Floreana (Galapagos) | White et al., 1993 | FL-25 | 0.08 | 0.13 | 0.00 | 14.70 | 1351.3 | 1464.7 | 0.295 | 0.91 | 0.04 | 2.29 | 1.54 |
| Floreana (Galapagos) | Saal et al., 2007/Kurz and Geist, 1999 | SG93-19 | 0.04 | 0.19 | 0.00 | 0.53 | 1319.6 | 1426.6 | 0.295 | 0.91 | 0.05 | 2.29 | 2.03 |
| Floreana (Galapagos) | Saal et al., 2007 | NSK97-260 | 0.04 | 0.19 | 0.00 | -0.87 | 1298.0 | 1399.4 | 0.293 | 0.91 | 0.02 | 2.18 | 2.00 |
| Floreana (Galapagos) | White et al., 1993 | FL-3 | 0.00 | 0.81 | 0.00 | 0.00 | 1297.1 | 1398.1 | 0.291 | 0.91 | 0.03 | 3.87 | 1.54 |
| Floreana (Galapagos) | Saal et al., 2007/Kurz and Geist, 1999 | SG93-23 | 0.04 | 0.23 | 0.00 | -1.90 | 1296.8 | 1397.9 | 0.290 | 0.91 | 0.01 | 3.87 | 1.81 |
| Floreana (Galapagos) | Bow, 1979 | FL-33 | 0.05 | 0.22 | 0.00 | 2.02 | 1312.6 | 1418.0 | 0.295 | 0.91 | 0.08 | 2.63 | 1.58 |
| San Cristobal (Galapagos) | Geist et al., 1986 | SC-23 | 0.05 | 0.22 | 0.14 | 5.34 | 1313.0 | 1418.5 | 0.294 | 0.91 | 0.07 | 2.11 | 1.85 |
| San Cristobal (Galapagos) | Saal et al., 2007 | NSK97-126 | 0.05 | 0.14 | 0.00 | 5.85 | 1307.4 | 1411.4 | 0.295 | 0.91 | 0.06 | 1.59 | 1.26 |
| San Cristobal (Galapagos) | Saal et al., 2007 | NSK97-252 | 0.04 | 0.10 | 0.00 | 4.55 | 1296.8 | 1397.8 | 0.297 | 0.91 | 0.05 | 0.91 | 1.13 |
| San Cristobal (Galapagos) | White et al., 1993 | SC-75 | 0.04 | 0.10 | 0.00 | 2.30 | 1288.2 | 1386.6 | 0.298 | 0.91 | 0.06 | 0.98 | 1.11 |
| San Cristobal (Galapagos) | Saal et al., 2007 | NSK97-254 | 0.04 | 0.11 | 0.00 | 4.08 | 1307.1 | 1411.1 | 0.298 | 0.91 | 0.07 | 1.28 | 1.04 |
| Santa Cruz (Galapagos) | White et al., 1993 | SC-64 | 0.21 | 0.29 | 0.36 | 8.82 | 1343.8 | 1455.9 | 0.291 | 0.91 | 0.04 | 0.83 | 1.32 |
| Santiago (Galapagos) | Baitis and Swanson, 1976 | JH-86 | 0.00 | 0.09 | 0.00 | 12.94 | 1355.8 | 1469.9 | 0.296 | 0.91 | 0.08 | 0.79 | 1.41 |
| Santiago (Galapagos) | Gibson and Geist, 2010 | 07DSG74 | 0.07 | 0.08 | 0.00 | 15.95 | 1352.2 | 1465.7 | 0.297 | 0.91 | 0.08 | 0.79 | 1.17 |
| Gorgona (CLIP) | Revillion et al., 2000 | GOR501 | 0.00 | 0.03 | 0.00 | -8.10 | 1445.3 | 1569.9 | 0.296 | 0.92 | 0.25 | 0.23 | 1.36 |
| Gorgona (CLIP) | Brugmann et al., 1987/ Jochum et al., 1991 | GOR-159 | 0.10 | 0.04 | 0.00 | -3.59 | 1407.7 | 1528.5 | 0.296 | 0.91 | 0.12 | 0.32 | 0.96 |
| Gorgona (CLIP) | Kamenetsky et al., 2010 | GOR-94-44 | 0.00 | 0.05 | 0.00 | -17.85 | 1438.0 | 1561.8 | 0.302 | 0.92 | 0.30 | 0.33 | 1.16 |
| Gorgona (CLIP) | Brugmann et al., 1987/ Jochum et al., 1991 | GOR-160 | 0.10 | 0.05 | 0.00 | -1.17 | 1409.5 | 1530.4 | 0.296 | 0.91 | 0.13 | 0.33 | 1.09 |

| LOCATION | Reference | SAMPLE | SiO2 | TiO2 | Al2O3 | Cr2O3 | Fe2O3 | FeO | MnO | MgO | CaO | Na2O | K2O |
|---|---|---|---|---|---|---|---|---|---|---|---|---|---|
| Gorgona (CLIP) | Revillion et al., 2000 | GOR514 | 47.34 | 0.40 | 12.23 | 0.00 | 1.33 | 9.52 | 0.19 | 17.93 | 10.08 | 0.75 | 0.20 |
| Gorgona (CLIP) | Revillion et al., 2000 | GOR502 | 45.93 | 0.66 | 11.71 | 0.00 | 1.13 | 10.22 | 0.20 | 18.74 | 10.20 | 1.13 | 0.04 |
| Gorgona (CLIP) | Arndt et al., 1997 | GOR-94-26 | 46.61 | 0.67 | 11.68 | 0.00 | 1.24 | 9.98 | 0.18 | 19.06 | 9.58 | 0.82 | 0.12 |
| Gorgona (CLIP) | Arndt et al., 1997 | GOR-94-35 | 47.73 | 0.42 | 12.06 | 0.00 | 1.31 | 9.59 | 0.18 | 18.23 | 9.60 | 0.63 | 0.22 |
| Gorgona (CLIP) | Arndt et al., 1997 | GOR-94-32 | 47.72 | 0.41 | 12.30 | 0.00 | 1.31 | 9.45 | 0.18 | 17.82 | 10.03 | 0.65 | 0.08 |
| Gorgona (CLIP) | Revillion et al., 2000 | GOR519 | 46.99 | 0.45 | 11.92 | 0.00 | 1.11 | 9.56 | 0.19 | 17.96 | 10.06 | 1.18 | 0.56 |
| Gorgona (CLIP) | Revillion et al., 2000 | GOR520 | 46.79 | 0.43 | 11.44 | 0.00 | 0.91 | 9.93 | 0.19 | 18.88 | 10.08 | 1.30 | 0.03 |
| Gorgona (CLIP) | Arndt et al., 1997/Revillion et al., 2002 | GOR-94-7 | 48.19 | 0.45 | 12.21 | 0.00 | 1.08 | 9.29 | 0.17 | 17.36 | 10.16 | 1.00 | 0.05 |
| Amaime (CLIP) | Villagomez et al., 2011 | DV112 | 48.79 | 0.81 | 11.93 | 0.06 | 0.86 | 8.83 | 0.16 | 16.07 | 10.13 | 2.03 | 0.16 |
| Amaime (CLIP) | Villagomez et al., 2011 | DV111 | 48.56 | 0.69 | 11.79 | 0.06 | 0.86 | 9.08 | 0.18 | 16.79 | 10.49 | 1.27 | 0.07 |
| Aruba (CLIP) | White et al., 1999 | ARU96-21 | 48.32 | 0.80 | 12.11 | 0.00 | 0.93 | 9.15 | 0.18 | 16.93 | 9.93 | 1.50 | 0.09 |
| Central Cordillera (CLIP) | Kerr et al., 2002 | COL536 | 48.73 | 0.81 | 10.97 | 0.00 | 1.15 | 9.44 | 0.17 | 17.90 | 9.85 | 0.85 | 0.05 |
| Central Cordillera (CLIP) | Millward et al., 1997 | GTJ422 | 49.02 | 0.89 | 11.76 | 0.00 | 0.83 | 8.87 | 0.17 | 16.26 | 10.64 | 1.34 | 0.15 |
| Central Cordillera (CLIP) | Kerr et al., 2002 | COL311 | 50.11 | 0.65 | 12.82 | 0.00 | 0.84 | 8.25 | 0.16 | 14.77 | 10.65 | 1.61 | 0.08 |
| Colombia (CLIP) | Villagomez et al., 2011 | DV104 | 46.47 | 0.82 | 11.84 | 0.05 | 0.90 | 9.90 | 0.18 | 17.84 | 10.14 | 1.49 | 0.17 |
| Colombia (CLIP) | Kerr et al., 1997 | COL1 | 48.09 | 0.92 | 12.28 | 0.00 | 0.88 | 9.10 | 0.16 | 16.74 | 10.13 | 1.38 | 0.26 |
| Colombia (CLIP) | Kerr et al., 1997 | BAR7 | 49.68 | 0.75 | 11.76 | 0.00 | 0.84 | 8.86 | 0.16 | 16.34 | 10.19 | 1.30 | 0.06 |
| Colombia (CLIP) | Kerr et al., 1997 | BAR5 | 49.57 | 0.69 | 11.47 | 0.00 | 0.83 | 9.00 | 0.20 | 16.71 | 10.04 | 1.38 | 0.06 |
| Colombia, Quillan | Mamberti et al., 2003 | 97G12 | 47.35 | 0.57 | 10.27 | 0.00 | 0.87 | 10.24 | 0.16 | 20.00 | 9.38 | 1.10 | 0.00 |
| Duarte (CLIP) | Escuder-Viruete et al., 2007 | JE9029 | 44.68 | 1.38 | 7.43 | 0.26 | 1.25 | 11.77 | 0.16 | 24.72 | 7.66 | 0.54 | 0.07 |
| Duarte (CLIP) | LaPierre et al., 2000 | 96VD126* | 46.40 | 1.21 | 8.66 | 0.00 | 1.05 | 10.83 | 0.18 | 19.98 | 9.83 | 1.67 | 0.08 |
| Duarte (CLIP) | Escuder-Viruete et al., 2007 | 5JE37B | 48.33 | 1.97 | 7.15 | 0.19 | 1.20 | 10.29 | 0.16 | 20.55 | 9.35 | 0.59 | 0.05 |
| Duarte (CLIP) | LaPierre et al., 1999 | 97VD09 | 48.93 | 0.71 | 12.34 | 0.00 | 0.87 | 8.84 | 0.17 | 16.21 | 10.06 | 1.46 | 0.33 |
| Herradura (CLIP) | Mamberti et al., 2003 | AH1B | 47.69 | 0.85 | 11.07 | 0.00 | 0.87 | 9.75 | 0.17 | 18.50 | 9.53 | 1.45 | 0.05 |
| Herradura (CLIP) | Hauff et al., 2000a | BH11 | 48.51 | 0.76 | 12.38 | 0.00 | 0.88 | 8.89 | 0.18 | 16.19 | 10.12 | 1.96 | 0.07 |
| Herradura (CLIP) | Mamberti et al., 2003 | AH8 | 48.96 | 0.71 | 12.16 | 0.00 | 0.86 | 8.93 | 0.16 | 16.40 | 9.75 | 1.78 | 0.24 |
| Nicoya (CLIP) | Mamberti et al., 2003 | AN53 | 47.46 | 0.78 | 11.07 | 0.00 | 0.88 | 9.73 | 0.23 | 18.38 | 9.86 | 1.52 | 0.04 |
| Nicoya (CLIP) | Mamberti et al., 2003 | AN76 | 48.66 | 0.64 | 12.12 | 0.00 | 0.85 | 8.94 | 0.16 | 16.41 | 10.31 | 1.57 | 0.29 |
| Nicoya (CLIP) | Hauff et al., 2000a | BN19 | 49.55 | 0.77 | 12.75 | 0.00 | 0.82 | 8.29 | 0.17 | 14.77 | 11.08 | 1.61 | 0.14 |
| Nicoya (CLIP) | Sinton et al., 1997 | NC93-20 | 48.82 | 0.78 | 11.42 | 0.00 | 0.85 | 9.21 | 0.19 | 17.16 | 10.03 | 1.45 | 0.05 |
| Osa (CLIP) | Hauff et al., 2000a | OS9 | 49.63 | 0.81 | 12.29 | 0.00 | 0.91 | 8.60 | 0.16 | 15.62 | 10.03 | 1.79 | 0.09 |
| Pedernales (CLIP) | Mamberti et al., 2003 | 99PE24 | 47.15 | 0.67 | 11.11 | 0.03 | 0.88 | 9.75 | 0.16 | 18.41 | 10.08 | 1.48 | 0.10 |
| Site 146 (CLIP) | Jolly et al., 2007 | CCBP146/43E | 47.26 | 0.89 | 12.16 | 0.00 | 0.93 | 9.43 | 0.16 | 17.47 | 9.81 | 1.73 | 0.07 |
| Venezuelan Basin (CLIP) | Hauff et al., 2000b | 15-146-1 | 47.34 | 0.84 | 11.35 | 0.00 | 0.86 | 9.63 | 0.17 | 18.05 | 10.21 | 1.46 | 0.02 |
| Venezuelan Basin (CLIP) | Donnelly et al., 1973 | 15-146-43R-1(131-143) | 47.62 | 0.85 | 12.15 | 0.00 | 0.85 | 9.52 | 0.16 | 17.85 | 9.68 | 1.20 | 0.06 |

| LOCATION | Reference | SAMPLE | NiO | P2O5 | H2O | %ol add | T | TP AFM | KD | Xfo | F AFM | La/Sm | Sm/Yb |
|---|---|---|---|---|---|---|---|---|---|---|---|---|---|
| Gorgona (CLIP) | Revillion et al., 2000 | GOR514 | 0.00 | 0.04 | 0.00 | -16.39 | 1407.6 | 1528.3 | 0.308 | 0.92 | 0.29 | 0.18 | 0.46 |
| Gorgona (CLIP) | Revillion et al., 2000 | GOR502 | 0.00 | 0.04 | 0.00 | 12.48 | 1423.4 | 1545.8 | 0.298 | 0.92 | 0.21 | 0.29 | 1.10 |
| Gorgona (CLIP) | Arndt et al., 1997 | GOR-94-26 | 0.00 | 0.05 | 0.00 | -1.18 | 1429.5 | 1552.4 | 0.303 | 0.92 | 0.30 | 0.47 | 0.69 |
| Gorgona (CLIP) | Arndt et al., 1997 | GOR-94-35 | 0.00 | 0.03 | 0.00 | -12.61 | 1413.6 | 1535.0 | 0.311 | 0.92 | 0.31 | 0.19 | 0.59 |
| Gorgona (CLIP) | Arndt et al., 1997 | GOR-94-32 | 0.00 | 0.03 | 0.00 | -14.98 | 1405.5 | 1526.0 | 0.311 | 0.92 | 0.30 | 0.43 | 0.32 |
| Gorgona (CLIP) | Revillion et al., 2000 | GOR519 | 0.00 | 0.03 | 0.00 | 6.74 | 1408.1 | 1528.9 | 0.303 | 0.92 | 0.29 | 0.25 | 0.63 |
| Gorgona (CLIP) | Revillion et al., 2000 | GOR520 | 0.00 | 0.03 | 0.00 | 27.53 | 1425.9 | 1548.6 | 0.302 | 0.92 | 0.29 | 0.24 | 0.70 |
| Gorgona (CLIP) | Arndt et al., 1997/Revillion et al., 2002 | GOR-94-7 | 0.00 | 0.04 | 0.00 | 6.22 | 1396.3 | 1515.8 | 0.311 | 0.91 | 0.30 | 0.18 | 0.80 |
| Amaime (CLIP) | Villagomez et al., 2011 | DV112 | 0.09 | 0.08 | 0.00 | 19.62 | 1369.6 | 1485.7 | 0.308 | 0.91 | 0.27 | 1.37 | 1.01 |
| Amaime (CLIP) | Villagomez et al., 2011 | DV111 | 0.09 | 0.06 | 0.00 | 21.94 | 1384.7 | 1502.8 | 0.311 | 0.91 | 0.29 | 1.17 | 0.76 |
| Aruba (CLIP) | White et al., 1999 | ARU96-21 | 0.00 | 0.06 | 0.00 | 17.46 | 1387.6 | 1506.1 | 0.309 | 0.91 | 0.28 | 1.01 | 1.06 |
| Central Cordillera (CLIP) | Kerr et al., 2002 | COL536 | 0.00 | 0.08 | 0.00 | 1.41 | 1407.0 | 1527.6 | 0.315 | 0.91 | 0.31 | 1.44 | 1.33 |
| Central Cordillera (CLIP) | Millward et al., 1997 | GTJ422 | 0.00 | 0.07 | 0.00 | 21.73 | 1373.6 | 1490.2 | 0.313 | 0.91 | 0.28 | 1.09 | 1.32 |
| Central Cordillera (CLIP) | Kerr et al., 2002 | COL311 | 0.00 | 0.05 | 0.00 | 14.92 | 1341.5 | 1453.1 | 0.316 | 0.91 | 0.28 | 1.05 | 0.95 |
| Colombia (CLIP) | Villagomez et al., 2011 | DV104 | 0.13 | 0.07 | 0.00 | 27.33 | 1405.9 | 1526.4 | 0.300 | 0.91 | 0.19 | 0.68 | 1.38 |
| Colombia (CLIP) | Kerr et al., 1997 | COL1 | 0.00 | 0.08 | 0.00 | 20.95 | 1383.6 | 1501.6 | 0.308 | 0.91 | 0.28 | 0.77 | 1.06 |
| Colombia (CLIP) | Kerr et al., 1997 | BAR7 | 0.00 | 0.06 | 0.00 | 21.03 | 1375.2 | 1492.2 | 0.317 | 0.91 | 0.29 | 1.24 | 1.40 |
| Colombia (CLIP) | Kerr et al., 1997 | BAR5 | 0.00 | 0.06 | 0.00 | 23.00 | 1382.9 | 1500.9 | 0.316 | 0.91 | 0.30 | 1.24 | 1.27 |
| Colombia, Quillan | Mamberti et al., 2003 | 97G12 | 0.00 | 0.06 | 0.00 | 34.49 | 1446.9 | 1571.6 | 0.306 | 0.92 | 0.32 | 0.90 | 1.00 |
| Duarte (CLIP) | Escuder-Viruete et al., 2007 | JE9029 | 0.00 | 0.11 | 0.00 | 22.01 | 1524.5 | 1659.6 | 0.288 | 0.93 | 1.03 | 1.31 | 2.48 |
| Duarte (CLIP) | LaPierre et al., 2000 | 96VD126* | 0.00 | 0.12 | 0.00 | 25.81 | 1446.5 | 1571.2 | 0.299 | 0.92 | 0.20 | 1.80 | 2.55 |
| Duarte (CLIP) | Escuder-Viruete et al., 2007 | 5JE37B | 0.00 | 0.15 | 0.00 | 6.70 | 1456.9 | 1582.6 | 0.312 | 0.92 | 0.35 | 1.16 | 2.88 |
| Duarte (CLIP) | LaPierre et al., 1999 | 97VD09 | 0.00 | 0.07 | 0.00 | 19.10 | 1372.6 | 1489.2 | 0.312 | 0.91 | 0.28 | 0.82 | 0.96 |
| Herradura (CLIP) | Mamberti et al., 2003 | AH1B | 0.00 | 0.06 | 0.00 | 28.54 | 1418.8 | 1540.7 | 0.307 | 0.92 | 0.29 | 1.04 | 1.10 |
| Herradura (CLIP) | Hauff et al., 2000a | BH11 | 0.00 | 0.06 | 0.00 | 18.43 | 1372.1 | 1488.6 | 0.307 | 0.91 | 0.27 | 0.94 | 1.07 |
| Herradura (CLIP) | Mamberti et al., 2003 | AH8 | 0.00 | 0.05 | 0.00 | 20.64 | 1376.7 | 1493.7 | 0.310 | 0.91 | 0.28 | 0.82 | 0.99 |
| Nicoya (CLIP) | Mamberti et al., 2003 | AN53 | 0.00 | 0.06 | 0.00 | 28.02 | 1416.5 | 1538.1 | 0.305 | 0.92 | 0.29 | 0.87 | 1.01 |
| Nicoya (CLIP) | Mamberti et al., 2003 | AN76 | 0.00 | 0.04 | 0.00 | 21.11 | 1376.8 | 1494.0 | 0.310 | 0.91 | 0.28 | 0.89 | 1.00 |
| Nicoya (CLIP) | Hauff et al., 2000a | BN19 | 0.00 | 0.06 | 0.00 | 16.59 | 1341.5 | 1453.1 | 0.313 | 0.91 | 0.26 | 0.83 | 1.01 |
| Nicoya (CLIP) | Sinton et al., 1997 | NC93-20 | 0.00 | 0.06 | 0.00 | 24.07 | 1392.1 | 1511.2 | 0.312 | 0.91 | 0.29 | 0.87 | 1.15 |
| Osa (CLIP) | Hauff et al., 2000a | OS9 | 0.00 | 0.06 | 0.00 | 13.10 | 1360.0 | 1474.7 | 0.313 | 0.91 | 0.28 | 0.88 | 1.10 |
| Pedernales (CLIP) | Mamberti et al., 2003 | 99PE24 | 0.12 | 0.05 | 0.00 | 28.31 | 1417.1 | 1538.8 | 0.303 | 0.92 | 0.29 | 0.84 | 1.15 |
| Site 146 (CLIP) | Jolly et al., 2007 | CCBP146/43E | 0.00 | 0.08 | 0.00 | 20.46 | 1398.5 | 1518.3 | 0.303 | 0.92 | 0.27 | 0.81 | 1.19 |
| Venezuelan Basin (CLIP) | Hauff et al., 2000b | 15-146-1 | 0.00 | 0.06 | 0.00 | 28.14 | 1410.0 | 1530.9 | 0.304 | 0.92 | 0.28 | 0.77 | 1.13 |
| Venezuelan Basin (CLIP) | Donnelly et al., 1973 | 15-146-43R-1(131-143) | 0.00 | 0.06 | 0.00 | 27.62 | 1406.1 | 1526.7 | 0.308 | 0.92 | 0.29 | 0.69 | 1.14 |

## Chapter 2

## A pyroxenite source in the Galapagos Plume at 70 Ma: Implications for plume evolution

### Abstract

Plume-related magmas produced in OIB and LIPS and their connecting plume tracks provide evidence on the evolution on mantle temperature, size and composition of heterogeneities, and deep geochemical cycles. Here we provide new $^{40}Ar/^{39}Ar$ ages, radiogenic isotopes, major and trace element data, and high-precision olivine analyses for samples from the Quepos terrane (Costa Rica) to closely examine the critical LIP-OIB transitional phase of the Galapagos Plume. The new ages indicate that Quepos volcanism began at 70 Ma, persisting for 10 Ma. Our results suggest that a dominant pyroxenite (recycled oceanic crust) source lithology appeared in the Galapagos Plume during this transition. The maximum mantle potential temperature of the plume changed from ~1650 to ~1550 °C at 60-70 Ma. This change corresponds to the appearance of this dominant pyroxenite component that also correlates with increments in the high-field strength elements. Radiogenic isotope ratios (Nd-Pb) suggest that the Quepos terrane samples having both enriched (Northern Domain) and intermediate radiogenic signatures (Central Domain). The presence of a dense pyroxenite component may explain the observed decrease in $T_p$ due to its effect on the plume's buoyancy, as well as the isotopic heterogeneity observed in Quepos lavas.

## 1. Introduction

The initial melting of mantle plumes produces unparalleled volumes (5-40 x $10^6$ $km^3$) of lava that form continental and oceanic plateaus, which represent the most significant igneous structures on Earth (e.g., Coffin and Eldholm, 1994; Mahoney and Coffin, 1997; Saunders, 2005; Coffin et al., 2006). This type of intra-plate magmatism originates at a deep boundary layer below the upper mantle, (probably the core-mantle boundary) (e.g., Morgan, 1972; Tolstikhin and Hofmann, 2005; Torvisk et al., 2010; Burke et al., 2011). During ascent, a plume may develop a volumetrically large "head", followed by a narrower conduit or "tail". Geodynamic models suggest that melting of a 500-2000 km wide plume head (Arndt, 2000) forms large igneous provinces (LIPs), characterized by high degrees of partial melting, high mantle potential temperatures ($T_p$), and widespread lava flows (> $10^5$ $km^2$) (Richards et al., 1989; Coffin and Eldholm, 1994, Herzberg and Gazel, 2009). These events are sometimes so large that they effect environmental change leading to catastrophic mass extinctions (e.g., Kerr, 2005). Subsequent melting of a plume conduit will form ocean island basalts (OIBs), which may manifest themselves as linear ocean island hotspot tracks. OIBs are magmatically less productive, formed by lower degrees of partial melting relative to plume heads (Herzberg and Gazel, 2009) of a narrow 100 km wide plume conduit or "tail" (Arndt, 2000).

The Galapagos hotspot provides unparalleled opportunities to reconstruct plume evolution due to the on-land accessibility of LIP terranes in the Caribbean and Costa Rica (Alvarado et al., 1997; Denyer and Gazel, 2009; Loewen et al., 2013) and accreted OIB terranes along the western coasts of Panama and Costa Rica (Hoernle et al., 2002).

Recent petrological studies showed that lavas part of the Caribbean LIP (CLIP) melted more extensively and at higher temperatures than lavas from the modern Galapagos Islands (Herzberg and Gazel, 2009). The $T_p$ of the plume ranged from 1560-1620 °C during the Cretaceous and cooled to 1500 °C at present time (Herzberg and Gazel, 2009) at a rate of ~100 °C/Ma. The wide range in $T_p$ for CLIP lavas depends on whether or not Gorgona komatiites were produced by the Galapagos plume (Herzberg and Gazel, 2009). This secular cooling may reflect either 1) more efficient conductive cooling of plume tails relative to heads (e.g., Nolet et al., 2006) or 2) a change in source lithology leading to a decrease in mantle potential temperatures due to plume buoyancy effects (e.g., Farnetani and Samuel, 2005). A change in source lithology may reflect contributions of a pyroxenite component. Entrained pyroxenite in the plume acts as an "anchor" reducing the vertical transit velocity of a plume, thus diffusing more heat relative to a purely peridotite plume due to longer travel times (Kumagai et al., 2008).

The amount, age, and contribution of this subducted slab reservoir fingerprinted in mantle plume geochemistry stands as a topic of great interest to geoscientists. Although a recycled crust signature has been identified in plumes through the use of radiogenic isotopes and trace-element signatures (Zindler and Hart, 1986; Hofmann, 1997; Chauvel et al., 2008) the exact nature of geochemical exchanges and mixing of pyroxenite with mantle endmembers requires further investigation. Global scale recycling of crustal material undoubtedly plays a key role in the development and evolution of deep geochemical reservoirs as well as affecting the thermodynamic cooling of Earth. Furthermore, when compared with a primitive mantle reference, typical OIB trace

element signatures show positive high field strength element (e.g., Nb and Ta anomalies), suggesting a subducted slab reservoir in the mantle (McDonough, 1991; Rudnick et al., 2000; Kamber and Collerson, 2000). This reservoir could represent the mantle domain component common in all plumes (e.g., C, FOZO) (Zindler and Hart, 1986; Hart et al., 1992; Strake et al, 2005).

Our objective in this study is to clarify the extent of pyroxenite derived melts present in the Quepos terrane, Costa Rica and its affect on $T_p$ during the important CLIP-OIB transition of the plume. Using integrated petrological, isotopic, and olivine geochemical analyses, we show for the first time that a significant decrease in $T_p$ (~100 °C) is evident in Quepos picrobasalts and corresponds to the appearance of a pyroxenite component. Furthermore, previous studies suggested that the age of the Quepos terrane to be 65 Ma (Hauff et al., 2000). However, our new Ar-Ar data indicates that the age of the Quepos terrane is approximately 5 Ma older than previously suggested, at 70 Ma.

**2. Geologic Background**

The formation of the Caribbean Large Igneous Province (CLIP) began circa 95 Ma with the incipient melting of the Galapagos plume head (Duncan and Hargraves, 1984; Richards et al., 1989; Pindel and Barrett, 1990; Kerr, et al., 1996; Hauff et al., 1997; Sinton et al., 1997; Kerr et al., 1997; Hauff et al., 2000a;). The Caribbean plate represents an overthickened section of oceanic crust (~20 km) and is most likely the product of Cretaceous intraplate Galapagos hotspot magmatism (Duncan and Hargraves, 1984; Hauff et al., 1997, 2000a, b; Sinton et al., 1998; Kerr et al., 1996; Hoernle et al., 2002, 2004). The CLIP then migrated northeast with the Farallon Plate where it collided

with the Greater Antilles Arc (e.g., Duncan and Hargraves, 1984; Hauff et al., 2000; Geldmacher et al., 2003). This collision triggered a reversal in subduction polarity, which initiated subduction along the western edge of the CLIP margin (Geldmacher et al., 2003). The reversal in polarity facilitated the migration of the CLIP farther northeast between the converging North and South Americas between Late Cretaceous to Tertiary time (e.g., Duncan and Hargraves, 1984; Hauff et al., 2000a; Hoernle et al., 2002a; Geldmacher et al., 2003).

The exact age of incipient melting of the Galapagos plume still remains contested. Hoernle et al., 2002, 2004 proposed that the CLIP did not form from a single, voluminous pulse of magmatism, but rather through the gradual accretion of igneous structures such hotspot tracks and plateaus. Their $^{40}Ar/^{39}Ar$ age results from the Nicoya Peninsula, Costa Rica extended the CLIP age range of volcanic activity to 70 Ma (139-69 Ma). It is now generally accepted that the main pulse of magmatism occurred at 89 Ma with a second, less voluminous pulse at 75 Ma (Hauff et al., 2000a; Hoernle et al., 2002; Kerr et al., 1996; Revillon et al., 2000; Sinton et al., 1997, 1998).

Petrological and geochemical investigations of the Burica, Osa, and Quepos terranes in western Costa Rica (Figure 1) together with Azuero and Sona terranes in Panama, provide strong evidence that these areas represent accreted Galapagos OIB terranes and aseismic ridges, which resulted from melting of the plume tail post CLIP formation. These terranes are markedly younger than CLIP related lavas (95 Ma) with $^{40}Ar/^{39}Ar$ ages between 65-40 Ma (Sinton et al., 1997; Hauff et al., 2000a; Hoernle et al., 2002a) and represent the oldest Galapagos plume tail segments accreted to Central

America. Around 23 Ma the Farallon Plate broke up to form the Nazca and Cocos plates (e.g., Lonsdale, 2005). During the next 20 Ma the Galapagos hotspot and the Cocos-Nazca ridge experienced a series of complex interactions (Werner et al., 2003). The ridge-hotspot interactions subsequently formed the Cocos and Carnegie aseismic ridges located on the eastward moving Cocos and Nazca Plates respectively.

The present day archipelago is currently divided into four domains, characterized by unique isotopic variations in Nd-Sr-Pb and $^{3}He/^{4}He$ (Harpp and White, 2001; Hoernle et al., 2000) The Eastern Domain represents the most depleted isotopic end-member (Hoernle et al., 2000;Harpp and White, 2001) with compositions resembling those of mid ocean ridge basalt (MORB). The isotope depletion is thought to result from either a) continuous melt depletion as the plume migrates towards the Galapagos Spreading Center (Hoernle et al., 2002) or b) entrainment of asthenospheric material (White and Hofmann, 1978; Geist et al., 1998; White et al., 1993; Harpp and White, 2001). On the opposite end of the spectrum, lavas from the island Floreana define the most isotopically enriched endmember (Southern Domain) with high radiogenic $^{87}Sr/^{88}Sr$ and $^{206}Pb/^{204}Pb$ ratios (Harpp and White, 2001). This characteristic may reflect a HIMU component (Harpp and White, 2001) or hydrously altered oceanic crust (Harpp et al., 2013) present in the plume. Lavas in the Wolf-Darwin Lineament (Northerm Domain) are probably the most enigmatic and the source of this endmember's characteristics remains unknown. These islands typically display small $^{207}Pb$ and $^{208}Pb$ enrichements (Harpp and White, 2001; Vidito et al., 2013) though are depleted in $^{87}Sr/^{88}Sr$ and $^{206}Pb/^{204}Pb$ relative to Floreana lavas (Harpp and White, 2001). Several possibilities exist including contributions of

recycled sediment (Dupré and Allegre, 1983) or subcontinental lithospheric mantle and recycled oceanic crust (Hart, 1984). Lavas from the Quepos terrane (focus of this study) closely resemble the Northern domain in terms of Nd, Hf and $^{206}Pb/^{204}Pb$, yet resemble Central Domain volcanics with respect to $^{207}Pb/^{204}Pb$ and $^{208}Pb/^{204}Pb$ (Hoernle et al., 2000; Geldmacher et al., 2003). Islands in the Central domain, e.g., Fernandina most likely resemble the true "plume" composition and show intermediate enrichments in Sr, Nd, Pb with high $^{3}He/^{4}He$ (Harpp and White, 2001). The northern domain $^{3}He/^{4}He$ ratios typically vary between 8.8-6.9 $R/R_A$, while the central domain $^{3}He/^{4}He$ ratios are as low as 13.7 (Geldmacher et al., 2003) and as high as 30.3 $R/R_A$ (Kurz et al., 2014). Furthermore, Hauff et al. (2000) measured $^{3}He/^{4}He$ ratios on two samples of Quepos olivine separates. Their results show that both samples have high initial $^{3}He/^{4}He$ ratios (11.4 and 11.7 ± 0.3 $R/R_A$). These observed ratios are significantly greater than those measured from MORB ($R/R_A$ = 7-9). It stands important to note that the Sr-Nd-Pb characteristics of the central domain isotopically resemble the C-PHEM-FOZO component common to mantle plumes e.g., Hart et al., 1992; Farley and Craig, 1992; Hanan and Graham, 1996. Olivine phenocrysts from Fernandina (central domain) also record the highest (30.3 $R/R_A$) helium ratios found in the archipelago. These observations suggest that central domain lavas originate from the hot, central part of the plume and indicate the primary magma composition of the source (Graham et al., 1993; Kurz and Geist, 1999; Harpp and White, 2001; Blichert-Toft and White, 2001; Kurz et al., 2014).

The Quepos terrane is one of six fault-bounded oceanic igneous terranes located on the Pacific Costa Rican coast (Figure 1). An intra-plate Galapagos origin is now

generally accepted to explain the formation of Quepos based on petrological (Hauff et al., 1997), field-based observations, and trace element data (Frisch et al., 1992) and represents the oldest accreted segments of the Galapagos OIB stage (Hauff et al., 1997). The lava stratigraphy of Quepos is dominated by a transitional tholeiitic series with incompatible trace element patterns indicative of an OIB source (Hauff et al., 2000).

**3. Methods**

Picrite, diabase, and basalt samples were collected at the Quepos terrane, from in-situ outcrops of fresh-meter size boulders next to outcrops the shoreline to take advantage of fresh surf erosion exposures. Outcrop location can be found in Table S1 in the Supplementary materials.

To obtain the $^{40}Ar/^{39}Ar$ data, groundmass and mineral separates were irradiated for 60 hours at the Oregon State University TRIGA-type reactor in the Cadmium-Lined In-Core Irradiation Tube. At the University of Wisconsin-Madison Rare Gas Geochronology Laboratory, incremental heating experiments were conducted using a 25 Watt $CO_2$ laser. Each step of the experiment included heating at a given laser power, followed by an additional 10 min for gas cleanup. The gas was cleaned with two SAES C50 getters, one of which was operated at ~450 °C and the other at room temperature. Blanks were analyzed after every second laser heating step, and were less than 5 x 10-20 mol/V for $^{36}Ar$ and 2 x $10^{-17}$ mol/V for $^{40}Ar$, respectively. Argon isotope analyses were performed using a MAP 215–50, and the isotope data was reduced using ArArCalc software version 2.5 (http://earthref.org/ArArCALC/). Ages were calculated from the blank-discrimination and decay-corrected Ar isotope data after correction for interfering

isotopes produced from potassium and calcium in the nuclear reactor (Supplementary Materials, Table S2). Ages are reported with 2σ uncertainties (includes the J uncertainty) and are calculated relative to a Fish Canyon standard age of 28.201 ± 0.046 Ma (Kuiper et al., 2008) and a value for $\lambda^{40}K$ of 5.463 ± 0.107 x $10^{-10}$ $yr^{-1}$ (Min et al., 2000) (Supplementary Table 1).

Alteration-free rock chips were selected under microscope and powdered in an alumina mill at the Department of Geosciences at Virginia Tech. From these powders, whole rock major (Figure 2A) and trace element composition (Figure 3) were collected at Washington State University by XRF and ICP-MS (protocols in Johnson et al., 1999) and are reported in Table S1.

Radiogenic isotope ratios for Pb, Nd, and Sr where collected on a Neptune multi collector ICPMS at Center for Elemental Mass Spectrometry (CEMS), University of South Carolina (USC). Pb isotope ratios were determined by the TI-addition technique (White et al., 2000). The NBS-981 was determined at $^{206}Pb/^{204}Pb$ = 16.936 ± 0.001, $^{207}Pb/^{204}Pb$ = 15.490 ± 0.001, $^{208}Pb/^{204}Pb$ = 36.694 ± 0.003 (2 standard deviations, = 13). Isotopic ratios for Nd were normalized to $^{146}Nd/^{144}Nd$ = 0.7219 and the Nd standard $JNd_i$ was measured at $^{143}Nd/^{144}Nd$ = 0.5121 and 0.512112 ± 0.000007 (n=6) at USC. Isotopic ratios for Sr were normalized to $^{86}Sr/^{88}Sr$ = 0.1194 and replicate analyses 0.710320 ± 0.000012. All Sr measurements are reported relative to NBS-987 $^{87}Sr/^{86}Sr$ = 0.710250.

Analyses of olivines from Quepos samples were conducted in Rutgers University's JEOL JXA-8200 Superprobe. A modified version of the protocol of (Sobolev et al., 2007) was utilized to obtain high precision trace-element data. Samples

were analyzed with a focused beam (~1 um) at 20 kV and 300 nA. On peak count times were as follows: Si : 50s; Mg : 80s; Fe : 100s; Ni : 150s; Ca : 150s and Mn : 150s. The San Carlos olivine standard was analyzed at regular intervals during each run in order to correct for instrumental drift. A summary of the primary standards, statistics for the secondary standards and statistics for the olivine analyses are given in Tables 1A-C in Supplementary Materials. We modeled primary magmas to infer pyroxenite source contributions using PRIMELT-II software following method of Herzberg and Asimow, 2008. A detailed description of source magma determination is located in the Supplementary Materials section.

**4. Results**

The matrix of four samples from Quepos (three basalts and one picrite) were dated by $^{40}Ar/^{39}Ar$, and yielding plateau ages of 61.3 ± 0.75, 61.5 ± 1.01, 68.64 ± 0.28, 70.1 ± 2.94, and 70.50 ± 1.36. Supporting data summarizing the $^{40}Ar/^{39}Ar$ age dating results is located in the Supplementary Materials section. Previously published $^{39}Ar/^{40}Ar$ ages of Quepos basalts yielded ages at 60.1 ± 0.7 Ma (Sinton et al., 2007) and 65.0 ± 0.4 (Hoernle et al., 2002). Plagioclase separates from a gabbro yield an age of 59.4 ± 1.8 Ma (Hauff et al., 2000). Our new measurements agree with the ~60 Ma pulse and extend the maximum age of Quepos volcanism to 70 Ma, indicating that the formation of this complex may have occurred over a 10 Ma interval.

New major and trace element results are summarized in Figures 2 and 3. Quepos lavas are both alkaline and sub-alkaline, with $SiO_2$ contents ranging from 44-54 wt% and with $Na_2O+K_2O$ ranging from 2-6 wt% (Figure 2). These lavas are classified as basalts,

basaltic-andesites, trachy-basalts, and one tephrite/basantite (Figure 2). Quepos picrites are markedly lower in $SiO_2$ (43-48 wt%) and $Na_2O+K_2O$ (0.5-2 wt%), but fall well within the picro-basalt/basalt compositional fields (Figure 2). The vast majority of our Quepos samples plot below the peridotite-pyroxenite discrimination line (Figure 2B) defined by Herzberg and Asimow (2008). Primitive mantle normalized spider-diagrams from these samples display broad enrichment in incompatible elements (Figure 3). Quepos lavas show marked positive Ta, Nb, and Ti anomalies as well as depletions in fluid mobile elements (K, Rb, Th, U) relative to elements with similar compatibilities. Additionally, the trace element abundances of our samples closely resemble the incompatible element patterns of both the Cocos and Coiba Ridges (Galapagos tracks) (Figure 3).

High precision analyses of olivines from ten Quepos samples are presented in figure 4 plotted together with analyses from Mauna Kea (Sobolev et al., 2007). Offsets seen in both of these populations from calculated olivine compositions in equilibrium with primary and derivative magmas of a peridotite source (Herzberg, 2011) analyses strongly suggest that both were derived from a mantle source which contained pyroxenite as a separate lithology. Deviation from parallelism in both populations indicates that Cpx fractionation may be contributing to the offset (Herzberg, 2011), however these trends would not extrapolate to peridotite source primary magmas, thus it is impossible for the sources of these magmas to have been a pure peridotite source. Also, given that the offset in the Mauna Kea population is slightly greater, it may be assumed that these magmas were derived from melting of mantle which had more pyroxenite.

Eight new sets of Sr-Nd-Pb isotope ratios are provided in this study (Table X and

Figure 5). The $^{143}Nd/^{144}Nd$ ratios of our samples vary from 0.512934 to 0.512994. The $^{206}Pb/^{204}Pb$ ratios generally range from 18.934 to 19.513. The $^{208}Pb/^{204}Pb$ ratios generally range from 38.690 to 38.928. Theses ratios were age corrected using an average age of 65 Ma, and plotted in Figure 5 compared with modern Galapagos Plume isotopic domains (Hoernle et al. 2000; Harpp and White, 2001).

**5. Discussion**

The new $^{40}Ar/^{39}Ar$ ages presented in this study, suggested that Quepos volcanism lasted for approximately 10 Ma beginning at ~70 Ma and terminating at 60 Ma. Our new data suggest that the initial melting event, which formed this terrane, is ~5 Ma older than previously thought (Hoernle et al., 2002). The trace-element patterns reveal similarity to the current Galapagos hotpsot tracks, Cocos, and Coiba Ridges (Figure 3). Therefore, the Quepos terrane is possibly the oldest accreted Galapagos OIB terrane found in Central America and records the transitional phase between CLIP and OIB type volcanism.

CaO-MgO bulk rock compositions can be used as a first order discrimination between peridotite and pyroxenite source derived melts (Herzberg and Asimow, 2008). Samples from the CLIP plot in the area consistent with a dominant peridotite source composition (Fig. 2B) (Sobolev et al. 2007; Herzberg et al., 2013). Our new samples from Quepos plot below that line in range with Mauna Kea (Hawaii) samples interpreted as derived from a pyroxenitic source (Sobolev et al., 2007; Herzberg, 2010). Meanwhile, modern Galapagos archipelago lavas plot in both areas consistent with presence of both peridotite and pyroxenite sources in the plume, as also confirmed by high-precision olivine data from Vidito et al. (2013).

New high-precision data from olivine phenocrysts from this terrane indicate elevated Ni and Fe/Mn and respectively lower Ca contents indicative of the presence of a pyroxenite component (Figure 4). Detailed petrological modeling of these data can be found in the Supplementary Materials. The olivine compositions are also in good agreement with samples from Mauna Kea, interpreted as deriving from a secondary stage pyroxenite, that resulted form the reaction of recycled eclogite-derived melts and peridotite (Sobolev et al., 2007).

Isotope variations in $^{143}Nd/^{144}Nd$ and $^{208}Pb/^{204}Pb$ and $^{206}Pb/^{204}Pb$ reveal that the Quepos terrane is most similar to the classically defined Northern and Central Domains (Figure 5). In the modern archipelago the Central Domain is by far the most widespread and defines lavas from Fernandina and Isabella (Harpp and White, 2001). This component dominates the center of the archipelago, whereas the other components prevail in the peripheral areas (Harpp and White, 2001). The trace element chemistry, radiogenic isotope ratios, and $^{3}He/^{4}He$ ratios (Graham et al., 1993; Kurz and Geist, 1999) of Fernandina all suggest that lavas erupted in the western reaches of the archipelago represent the most undegassed, primitive part of Galapagos plume (Harpp and White, 2001).

The origin of the Northern Domain is possibly the most enigmatic of the four isotopic end-members. This domain only accounts for 3.3% of the total isotopic variation and is primarily found in the Wolf-Darwin Lineament and in Pinta Island of the present-day archipelago. Hoernle et al., (2000) first documented the existence of the Northern Domain at Quepos in 60-65 Ma. This Domain was later identified as a major part of the

submerged seamounts in the northern section of the Cocos Ridge offshore of Costa Rica (Werner et al., 2003). The Northern Domain stands unique relative to other Galapagos isotopic domains because it is intermediate in $^{87}Sr/^{86}Sr$, εNd, and $^{206}Pb/^{204}Pb$, but elevated in $^{207}Pb/^{204}Pb$ and $^{208}Pb/^{204}Pb$ for a given $^{206}Pb/^{204}Pb$ (Harpp and White, 2001). These high $^{207}Pb/^{204}Pb$ and $^{208}Pb/^{204}Pb$ ratios are also observed in lavas from Kerguelen, Gough, Bouvet, and St. Paul, with compositions running sub-parallel to the MORB array (Dupré and Allégre, 1983; Hart, 1984). However, the high Rb/ Sr, U/Pb, and Th/U indicate that the origin of the anomalous Northern Domain transpired early in Earth's history (Harpp and White, 2001). Some possible mechanisms leading to the formation of this isotopically distinct domain include 1) recycling of entrainment of ancient oceanic crust into the plume (Hart, 1984) 2) recycling of subducted sediment (Dupré and Allégre, 1983) 3) delamination of subcontinental lithosphere (Hart, 1984) and 4) deep mantle heterogeneities related to the formation of continents (Hart, 1984). Based on the new data presented here, we favor the interpretation that recycled oceanic crust is responsible for the unique isotopic variability of the Northern Domain.

Our new $^{40}Ar/^{39}Ar$ ages and geochemical data provide valuable insight into a crucial phase during the life cycle of the Galapagos plume during CLIP-OIB stage transition, thereby elucidating "head-tail plume evolution". A main question that remains is what affect does this pyroxenite contribution have on the evolutionary history of the Galapagos plume? Herzberg and Gazel (2009) proposed that lavas part of the CLIP melted hotter and more extensively than lavas from the 0-15 Ma archipelago and Carnegie and Cocos tracks (Figure 6A). A significant decrease in $T_p$ (100 °C) is also

observed between ~70 Ma Quepos lavas and ~90 Ma CLIP lavas (Herzberg and Gazel, 2009). Interestingly, there is also an increasing trend in high-field strength elements concentration (Nb, Ta, Zr, Hf, etc) from 90 to 15 Ma (Figure 6B). Jackson et al., (2008) reported evidence for a global enriched HFSE reservoir commonly sampled by OIBs with correspondingly high $^{3}He/^{4}He$, and radiogenic $^{187}Os/^{188}Os$ that collectively suggest the existence of a mantle source with a refractory eclogite (pyroxenite) component (Jackson et al., 2008). This result advocates important implications for the development of global mantle geochemical heterogeneity. The high $^{3}He/^{4}He$ ratios of erupted lavas at some hotspots (Galapagos, Hawaii, Samoa, Iceland) are interpreted to originate from a relatively primitive, undegassed mantle reservoir (Kurz et al., 1982; Farley et al., 1992), named PHEM (Farley et al., 1992), FOZO (Hart et al., 1992), or C (Hanan and Graham, 1996). Understanding the nature of FOZO and the development of a nonprimitive (nonchondritic) mantle component is therefore crucial for understanding, the formation of the high HFSE signatures, $^{3}He/^{4}He$ domain frequently sampled by some plumes (Galapagos, Iceland, Hawaii, Samoa), balancing Earth's HFSE budget from subduction to deep recycling., and evaluating large-scale planetary differentiation processes (Jackson et al., 2008).

The results of this study suggest that the appearance of a pyroxenitic component at 70 Ma correlates with a substantial decrease in the Galapagos plume's $T_p$. Geodynamic models suggest that plumes which carry pyroxenite components will upwell at slower vertical velocities relative to purely peridotite plumes (Kumagai et al., 2008) and will diffuse more heat due to longer travel times. Since plumes cool via conductive heat loss

to their surroundings as they move vertically (Farnetani and Samuel, 2005; Nolet et al., 2006; Kumagai et al., 2008), those entraining a dense pyroxenite will cool more efficiently. A main question that remains is whether or not CLIP magmas also carried substantial pyroxenite contributions? It is theoretically possible that the "head" of the Galapagos plume did in fact entrain large amounts of recycled crust, although evidence of this may have been obliterated by high partial melt fractions during CLIP volcanism (Herzberg and Gazel, 2009).

## 6. Conclusions

The new ages constraints presented here indicate LIP-OIB transition occurred about 60-70 Ma in the history of the Galapagos Plume. Our results show that a dominant pyroxenite (recycled oceanic crust) source lithology is observed for the first time ~70 Ma in the record of the Quepos terrane.

The maximum mantle potential temperature of the plume changed from ~1650 to ~1550 °C at ~70 Ma. This change corresponds to the first appearance of the pyroxenite component in the Galapagos plume. Furthermore, there is also an increase in HFSE compositons throughout the evolution of the plume. The presence of a dense pyroxenite component may explain the observed 100 °C decrease in $T_p$ at 70 Ma due to its effect on the plume's buoyancy, as well as the isotopic heterogeneity observed in Quepos lavas.

Radiogenic isotope ratios (Nd-Pb) suggest that the Quepos terrane is sampled both enriched (Northern Domain) and intermediate radiogenic signatures (Central Domain). The enriched compositions are also consistent with a recycled component.

## 7. References

Alvarado, G. E., Denyer, P., and Sinton, C. W., 1997, The 89 Ma Tortugal komatiitic suite, Costa Rica: Implications for a common geological origin of the Caribbean and Eastern Pacific region from a mantle plume: Geology, v. 25, no. 5, p. 439.

Arndt, N., 2000, Hot heads and cold tails: Nature, v. 407, p. 458-461.

Blichert-Toft, J., and White., W. M., 2001, Hf isotope geochemistry of the Galapagos Islands: Geochemistry Geophysics Geosystems, v. 2, no. 1043

Burke, K., 2011, Plate Tectonics, the Wilson Cycle, and Mantle Plumes: Geodynamics from the Top: Annual Review of Earth and Planetary Sciences, v. 39, no. 1, p. 1-29.

Chauvel, C., Lewin, E., Carpentier, M., Arndt, N. T., and Marini, J.-C., 2008, Role of recycled oceanic basalt and sediment in generating the Hf–Nd mantle array: Nature Geoscience, v. 1, no. 1, p. 64-67.

Coffin, M. F., Duncan, R. A., Eldholm, O., Fitton, J. G., Frey, F. A., Larsen, H. C., Mahoney, J. J., Saunders, A. D., Schlich, R., and Wallace, P. J., 2006, Large Igneous Provinces and Scientific Ocean Drilling status quo and a look ahead: Oceanography, v. 19, p. 150-160.

Coffin, M. F., and Eldholm, O., 1994, Large igneous provinces: crustal structure, dimensions, and external consequences: Reviews of Geophysics, v. 32, p. 1-36.

Denyer, P., and Gazel, E., 2009, The Costa Rican Jurassic to Miocene oceanic complexes: Origin, tectonics and relations: Journal of South American Earth Sciences, v. 28, no. 4, p. 429-442.

Duncan, R., and Hargraves, R., 1984, Plate tectonic evolution of the Caribbean region in the mantle reference frame: Geological Society of America Memoirs, v. 162, p. 81-94.

Dupré, B., and Allegre, C. J., 1983, Pb-SR isotope variation in Indian Ocean basalts and mixing phenomena: Nature, v. 303, p. 142-146.

Farley, K. A., and Craig, H., 1992, Mantle Plumes and Mantle Sources: Science, v. 258, no. 5083, p. 821-822.

Farnetani, C. G., and Samuel, H., 2005, Beyond the thermal plume paradigm: Geophysical Research Letters, v. 32, p. 1-4.

Frisch, W., Meschede, M., and Sick, M., 1992, Origin of the Central American ophiolites: Evidence from paleomagnetic results: Geological Society of America Bulletin, v. 104, no. 10, p. 1301-1314.

Geist, D., Naumann, T., and Larson, P., 1998, Evolution of Galápagos magmas: mantle and crustal fractionation without assimilation: Journal of Petrology, v. 39, no. 5, p. 953-971.

Geldmacher, J., Hanan, B. B., Blichert-Toft, J., Harpp, K., Hoernle, K., Hauff, F.,

Werner, R., and Kerr, A. C., 2003, Hafnium isotopic variations in volcanic rocks from the Caribbean Large Igneous Province and Galápagos hot spot tracks: Geochemistry, Geophysics, Geosystems, v. 4, no. 7, p.

Graham, D. W., Christie, D. M., Harpp, K. S., and Lupton, J. E., 1993, Mantle Plume Helium in Submarine Basalts from the Galapagos Platform: Science, v. 262, p. 2023-2026.

Hanan, B. B., and Graham, D. W., 1996, Lead and helium isotope evidence from oceanic basalts for a common deep source of mantle plumes: Science, v. 272, no. 5264, p. 991-995.

Harpp, K. S., and White, W. M., 2001, Tracing a mantle plume: Isotopic and trace element variations of Galapagos seamounts: Geochemistry, Geophysics, Geosystems, v. 2, p. 1525.

Hart, S., Hauri, E., Oschmann, L., and Whitehead, J., 1992, Mantle plumes and Entrainment: isotopic evidence: Science, v. 256, no. 5056, p. 517-520.

Hart, S. R., 1984, A large-scale isotope anomaly in the Southern Hemisphere mantle: Nature, v. 309, p. 753-757.

Hart, S. R., Hauri, E. H., Oschmann, L. A., and Whitehead, J. A., 1992, Mantle Plumes and Entrainment: Isotopic Evidence: Science, v. 256, no. 5056, p. 517-520.

Hauff, F., Hoernle, K., Schmincke, H.-U., and Werner, R., 1997, A Mid Cretaceous origin for the Gala« pagos hotspot: volcanological, petrological and geochemical evidence from Costa Rican oceanic crustal segments: Geologische Rundschaul v. 86, p. 141-155.

Hauff, F., Hoernle, K., Tilton, G., Graham, D. W., and Kerr, A. C., 2000, Large volume recycling of oceanic lithosphere over short time scales: geochemical constraints from the Caribbean Large Igneous Province: Earth and Planetary Science Letters, v. 174, p. 247-263.

Hauff, F., Hoernle, K., van den Bogaard, P., Alvarado, G., and Garbe-Schönberg, D., 2000, Age and geochemistry of basaltic complexes in western Costa Rica: Contributions to the geotectonic evolution of Central America: Geochemistry, Geophysics, Geosystems, v. 1, no. 5, p. 1009.

Herzberg, C., 2011, Basalts as temperature probes of Earth's mantle: Geology, v. 39, o. 12, p. 1179-1180.

Herzberg, C., 2013, Early Earth: Archaean drips: Nature Geoscience, v. 7, no. 1, p. 7-8.

Herzberg, C., and Asimow, P. D., 2008, Petrology of some oceanic island basalts: PRIMELT2.XLS software for primary magma calculation: Geochemistry, Geophysics, Geosystems, v. 9, no. 9, p. 9001

Herzberg, C., and Gazel, E., 2009, Petrological evidence for secular cooling in mantle plumes: Nature, v. 458, p. 619-623.

Hoernle, K., Hauff, F., and Bogaard, P. v. d., 2004, 70 m.y. history (139–69 Ma) for the Caribbean large igneous province: Geology, v. 32, no. 8, p. 697-700.

Hoernle, K., van den Bogaard, P., Werner, R., Lissinna, B., Hauff, F., Alvarado, G., and

Garbe-Schönberg, D., 2002, Missing history (16–71 Ma) of the Galápagos hotspot: Implications for the tectonic and biological evolution of the Americas: Geology, v. 30, no. 9, p. 795.

Hofmann, A. W., 1997, Mantle geochemistry: the message from oceanic volcanism: Nature, v. 385, p. 219-229.

Jackson, M. G., Hart, S. R., Saal, A. E., Shimizu, N., Kurz, M. D., Blusztajn, J. S., and Skovgaard, A. C., 2008, Globally elevated titanium, tantalum, and niobium (TITAN) in ocean island basalts with high 3He/4He: Geochemistry, Geophysics, Geosystems, v. 9,. Q04027,

Johnson, D. M., Hooper, P. R., and Conrey, R. M., 1999, XRF Analysis of rocks and minerals for major and trace elements on a single low dilution Li-tetraborate fused bead: Advances in X-ray Analysis, v. 41, p. 843-867.

Kamber, B., and Collerson, K., 2000, Zr/Nb systematics of ocean island basalts reassessed—the case for binary mixing: Journal of Petrology, v. 41, no. 7, p. 1007-1021.

Kerr, A. C., 2005, Oceanic LIPs: The Kiss of Death: Elements, v. 1, p. 289-292.

Kerr, A. C., Marriner, G. F., Arndt, N., Tarney, J., Nivia, A., Saunders, A. D., and Duncan, R. A., 1996, The petrogenesis of Gorgona komatiites, picrites and basalts: new field, petrographic and geochemical constraints: Lithos, v. 37, p. 245-260.

Kerr, A. C., Tarney, J., Marriner, G. F., Klaver, G. T., Saunders, A. D., and Thirlwall, M. F., 1996, The geochemistry and petrogenesis of the late-Cretaceous picrites and basalts of Curaçao, Netherlands Antilles: a remnant of an oceanic plateau: Contributions to Mineralogy and Petrology, v. 124, no. 1, p. 29-43.

Kumagai, I., Davaille, A., Kurita, K., and Stutzmann, E., 2008, Mantle plumes: Thin, fat, successful, or failing? Constraints to explain hot spot volcanism through time and space: Geophysical Research Letters, v. 35, no. 16.

Kurz, M. D., Jenkins, W. J., and Hart, S. R., 1982, Helium isotopic systematics of oceanic islands and mantle heterogeneity: Nature, v. 297, p. 43-47.

Kurz, M. D., and Geist, D., 1999, Dynamics of the Galapagos hotspot from helium isotope geochemistry: Geochimica et Cosmochimica Acta, v. 63, no. 23/24, p. 4139-4156.

Kurz, M. D., Rowland, S. K., Curtice, J., Saal, A. E., and Naumann, T., 2014, Eruption Rates for Fernandina Volcano, The Galápagos, John Wiley & Sons, Inc, p. 41-54.

Loewen, M. W., Duncan, R. A., Kent, A. J. R., and Krawl, K., 2013, Prolonged plume

volcanism in the Caribbean Large Igneous Province: New insights from Curaçao and Haiti: Geochemistry, Geophysics, Geosystems, v. 14, no. 10, p. 4241-4259.

Lonsdale, P., 2005, Creation of the Cocos and Nazca plates by fission of the Farallon plate: Tectonophysics, v. 404, no. 3-4, p. 237-264.

Mahoney, J. J., and Coffin, F. F., 1997, Large Igneous Provinces: Continental, oceanic, and planetary flood volcanism, Washington, American Geophysical Union Monograph, 100, p. 438.

McDonough, W., 1991, Partial melting of subducted oceanic crust and isolation of its residual eclogitic lithology: Philosophical Transactions of the Royal Society of London. Series A: Physical and Engineering Sciences, v. 335, no. 1638, p. 407-418.

Meschede, M., and Frisch, W., 1994, Gechemical char-acteristics of basaltic rocks from the Central American ophiolites: Profil, v. 7, p. 71-85.

Meschede, M., and Frisch, W., 1998, A plate-tectonic model for the Mesozoic and Early Cenozoic history of the Caribbean plate: Tectonophysics, v. 296, p. 269-291.

Morgan, W. J., 1972, Deep Mantle Convection Plumes and Plate Motion: The American Association of Petroleum Geologists Bulletin, v. 56, no. 2, p. 203-213.

Nolet, G., Karato, S., and Montelli, R., 2006, Plume fluxes from seismic tomography: Earth and Planetary Science Letters, v. 248, no. 3-4, p. 685-699.

O'Connor, J. M., Stoffers, P., Wijbrans, J. R., and Worthington, T. J., 2007, Migration of widespread long-lived volcanism across the Galápagos Volcanic Province: Evidence for a broad hotspot melting anomaly?: Earth and Planetary Science Letters, v. 263, no. 3–4, p. 339-354.

Pindell, J. L., and Barrett, S. F., 1990, Geological evolution of the Caribbean region: a plate tectonic perspective: The Caribbean region: Boulder, Colorado, Geological Society of America, Geology of North America, v. H, p. 405-432.

Revillon, S., Hallot, E., Arndt, N., Chauvel, C., and Duncan, R. A., 2000, A complex history for the Caribbean Plateau: Petrology, geochemistry, and geochronology of the Beata Ridge, South Hispaniola: Journal of Geology, v. 108, p. 641-661.

Richards, M. A., Duncan, R. A., and Courtillot, V. E., 1989, Flood Basalts and Hot-Spot Tracks: Plume Heads and Tails: Science, v. 246, p. 103-107.

Richards, M. A., Duncan, R. A., and Courtillot, V. E., 1989, Flood basalts and hot-spot tracks: Plume heads and tails: Science, v. 246, no. 4926, p. 103-107.

Rudnick, R. L., Barth, M., Horn, I., and McDonough, W. F., 2000, Rutile-bearing refractory eclogites: missing link between continents and depleted mantle: Science, v. 287, no. 5451, p. 278-281.

Saunders, A. D., 2005, Large Igneous Provinces: Origin and Environmental Consequences: Elements, v. 1, p. 259-263.

Sinton, C. W., Duncan, R. A., and Denyer, P., 1997, Nicoya Peninsula, Costa Rica: A single suite of Caribbean oceanic plateau magmas: Journal of Geophysical Research, v. 102, no. B7, p. 15507-15520.

Sinton, C. W., Duncan, R. A., Storey, M., Lewis, J., and Estrada, J. J., 1998, An oceanic flood basalt province within the Caribbean plate: Earth and Planetary Science Letters, v. 155, p. 221-235.

Sobolev, A. V., Hofmann, A. W., Kuzmin, D. V., Yaxley, G. M., Arndt, N. T., Chung, S. L., Danyushevsky, L. V., Elliott, T., Frey, F. A., Garcia, M. O., Gurenko, A. A., Kamenetsky, V. S., Kerr, A. C., Krivolutskaya, N. A., Matvienkov, V. V., Nikogosian, I. K., Rocholl, A., Sigurdsson, I. A., Sushchevskaya, N. M., and Teklay, M., 2007, The amount of recycled crust in sources of mantle-derived melts: Science, v. 316, p. 412-417.

Stolper, E., Sherman, S., Michael, G., Baker, M., and Seaman, C., 2004, Glass in the submarine section of the HSDP2 drill core, Hilo, Hawaii: Geochemistry Geophysics Geosystems, v. 5, no. 7.

Stracke, A., Hofmann, A. W., and Hart, S. R., 2005, FOZO, HIMU, and the rest of the mantle zoo: Geochemistry, Geophysics, Geosystems, v. 6, no. 5, Q05007

Tolstikhin, I., and Hofmann, A. W., 2005, Early crust on top of the Earth's core: Physics of the Earth and Planetary Interiors, v. 148, no. 2-4, p. 109-130.

Torsvik, T. H., Burke, K., Steinberger, B., Webb, S. J., and Ashwal, L. D., 2010, Diamonds sampled by plumes from the core-mantle boundary: Nature, v. 466, no. 7304, p. 352-355.

Vidito, C., Herzberg, C., Gazel, E., Geist, D., and Harpp, K., 2013, Lithological structure of the Galápagos Plume: Geochemistry, Geophysics, Geosystems, v. 14, no. 10, p. 4214-4240.

Werner, R., and Hoernle, K., 2003, New volcanological and volatile data provide strong support for the continuous existence of Galapagos Islands over the past 17 million years: International Journal of Earth Sciences, v. 92, no. 6, p. 904-911.

White, W., and Hofmann, A., 1978, Geochemistry of the Galápagos Islands: implications for mantle dynamics and evolution: Year Book Carnegie Inst. Washington, v. 77, p. 596-606.

White, W. M., Albarede, F., and Telouk, P., 2000, High-precision analysis of Pb isotope ratios by multi-collector ICP-MS: Chemical Geology, v. 167, p. 257-270.

White, W. M., McBirney, A. R., and Duncan, R. A., 1993, Petrology and geochemistry of the Galápagos Islands: Portrait of a pathological mantle plume: Journal of Geophysical Research, v. 98, no. B11, p. 19533.

Zindler, A., and Hart, S., 1986, Chemical Geodynamics: Annual Review of Earth and Planetary Science, v. 14, p. 493-571.

## 8. Figure Captions

**Figure 1:** A) Tectonic location of the study area (modified from Denyer and Gazel, 2009). B) Map of the accreted oceanic complexes along the coast of Costa Rica and Panama (modified from Denyer and Gazel, 2009). C) Geological map of the Quepos terrane showing sample locations, structures, and areas underlain by basalts and picrites from Duran (2013).

**Figure 2:** A) Chemical classification of samples using the total alkali versus silica diagram (TAS). B) CaO-MgO discrimication driagram between peridotite and pyroxenite derived magmas from Herzberg and Asimow (2008). The shaded region represents primary magmas of fertile peridotite produced by accumulated fractional melting. Additional data from Stolper et al. (2004) and the Georoc database (http://georoc.mpch-mainz.gwdg.de/georoc/)

**Figure 3:** Multi-element spider diagram normalized to pyrolite mantle (McDonough and Sun, 1995). Note how the new data from Quepos overlap with the current Galapagos tracks, Cocos, Carnegie and Coiba Ridges. Additional data from Hoernle et al. (2000), Werner et al. (2003) and the Georoc database (http://georoc.mpch-mainz.gwdg.de/georoc/)

**Figure 4:** High-precision olivine composition from picrites of the Quepos terrane plotted in the Herzberg (2010) discrimination diagram. Quepos olivine compositions are not consistent with derivation of a peridotite source. Notice how the new Quepos data is within range of Mauna Kea data from Sobolev et al. (2007) interpreted as olvines that

crystallized from a pyroxenite derived primary magma. The green line shows a possible liquid line of descent from a pyroxenite source primary magma. More detailed modeling in the Supplementary Materials.

**Figure 5:** Age corrected Pb and Nd isotopes of picrite and basalt samples from the Quepos terrane. Most samples fall within the Northern and Central Galapagos Domains.

**Figure 6:** A) Galapagos plume secular cooling curve modified from Herzberg and Gazel, (2009). Note the drastic decrease in $T_p$ at approximately 70-60 Ma. B) Evolution of the Nb contents (in ppm) vs. time (Ma). Notice as the plume cools down the Nb concentrations increased to a max. ~15 Ma.

## 9. Figures

### Figure 1:

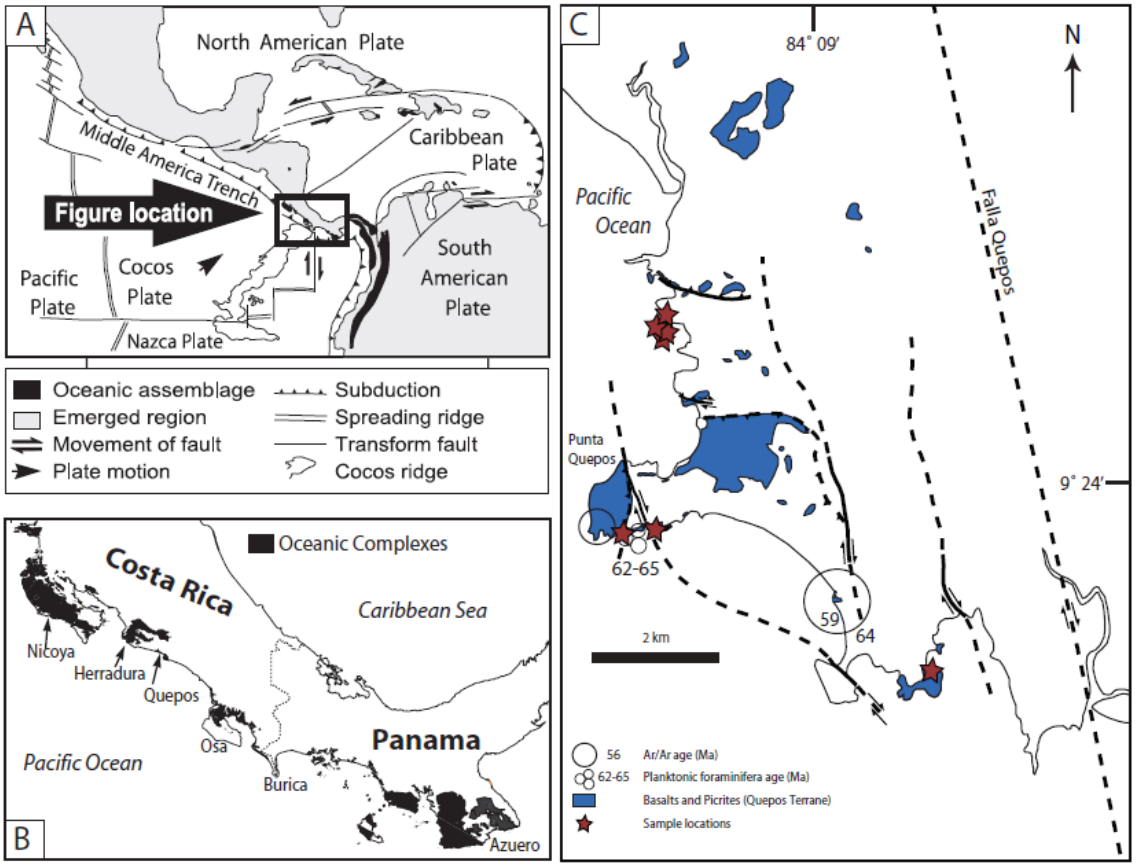

**Figure 2:**

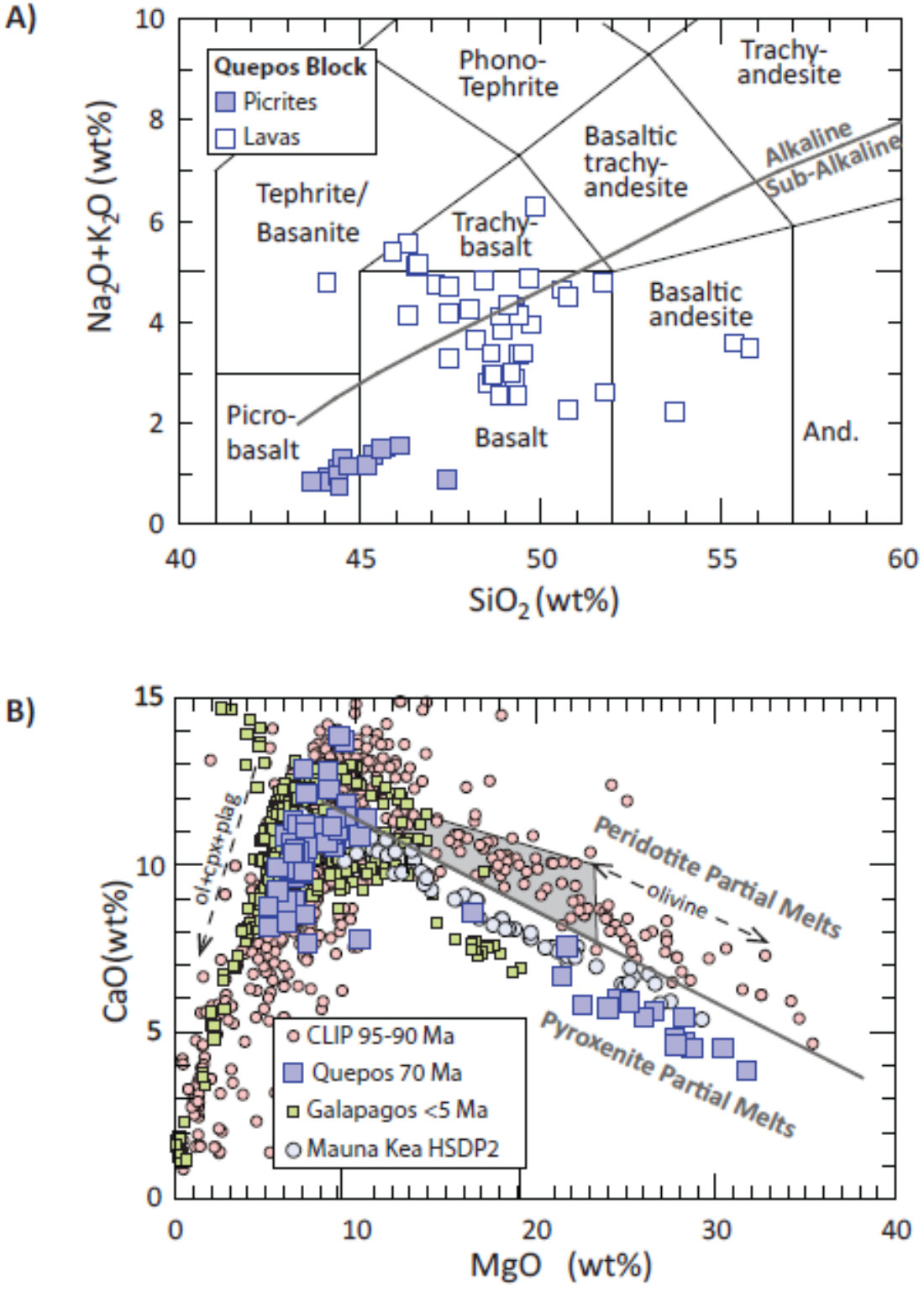
A)
Quepos Block
Picrites
Lavas
Phono-
Tephrite
Trachy-
andesite
Basaltic
trachy-
andesite
Alkaline
Sub-Alkaline
Tephrite/
Basanite
Trachy-
basalt
Basaltic
andesite
Picro-
basalt
Basalt
And.
Na2O+K2O (wt%)
SiO2 (wt%)
B)
ol+cpx+plag
Peridotite Partial Melts
olivine
Pyroxenite Partial Melts
CLIP 95-90 Ma
Quepos 70 Ma
Galapagos <5 Ma
Mauna Kea HSDP2
CaO(wt%)
MgO (wt%)

**Figure 3:**

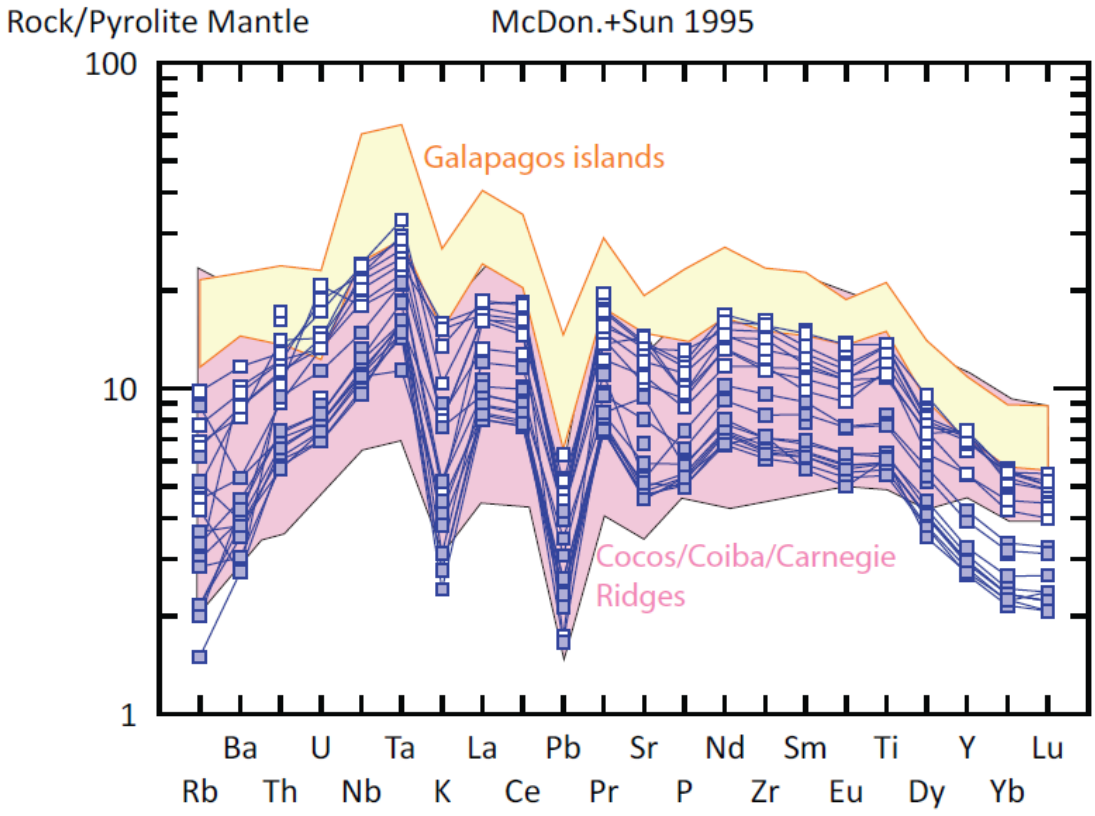
Rock/Pyrolite Mantle
McDon.+Sun 1995
100
10
1
Galapagos islands
Cocos/Coiba/Carnegie
Ridges
Rb Ba Th U Nb Ta K La Ce Pb Pr Sr P Nd Zr Sm Eu Ti Dy Y Yb Lu

**Figure 4:**

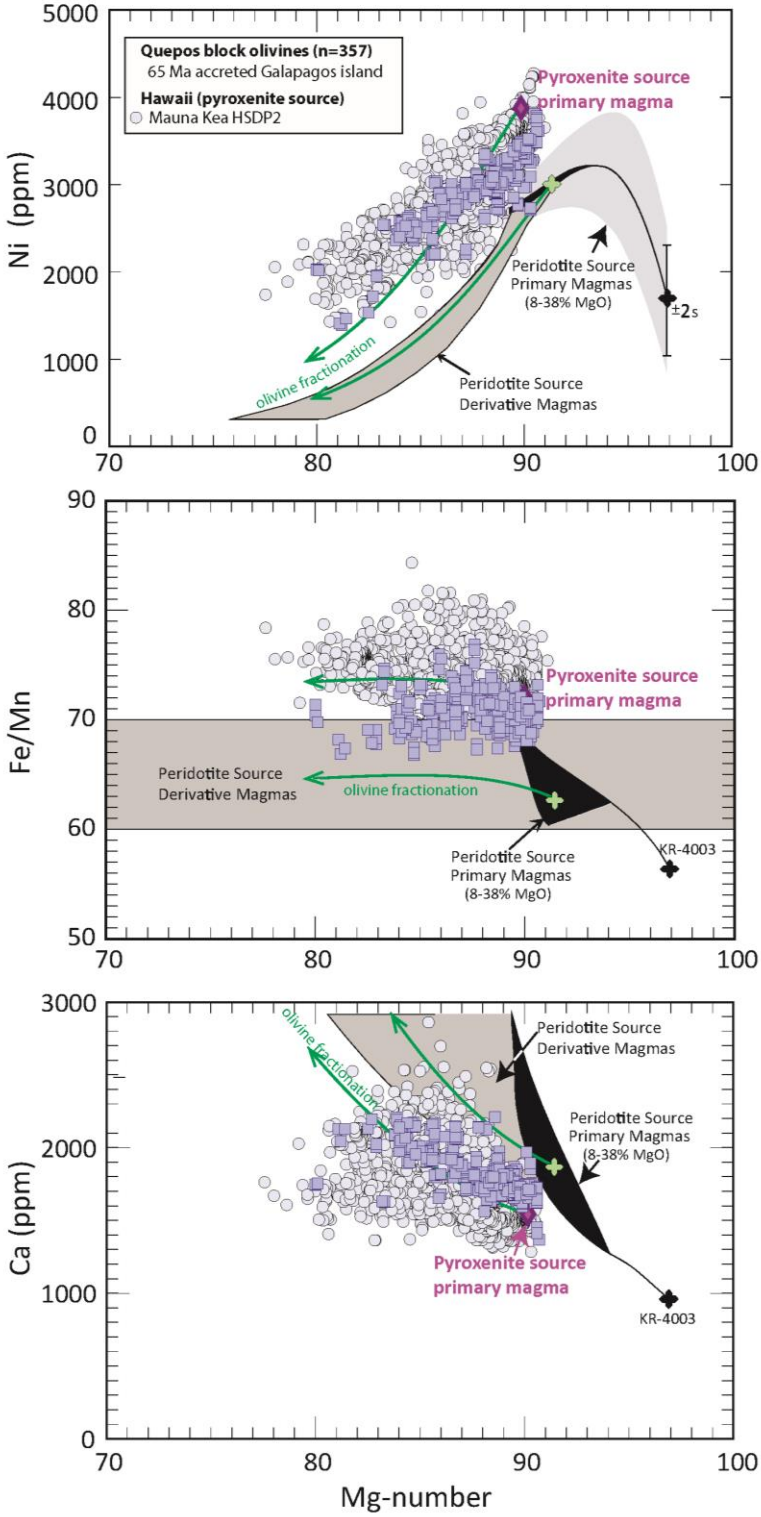
Quepos block olivines (n=357)
65 Ma accreted Galapagos island
Hawaii (pyroxenite source)
Mauna Kea HSDP2
Pyroxenite source primary magma
Peridotite Source Primary Magmas (8-38% MgO)
±2s
olivine fractionation
Peridotite Source Derivative Magmas
Ni (ppm)
Fe/Mn
Ca (ppm)
Mg-number
KR-4003

**Figure 5:**

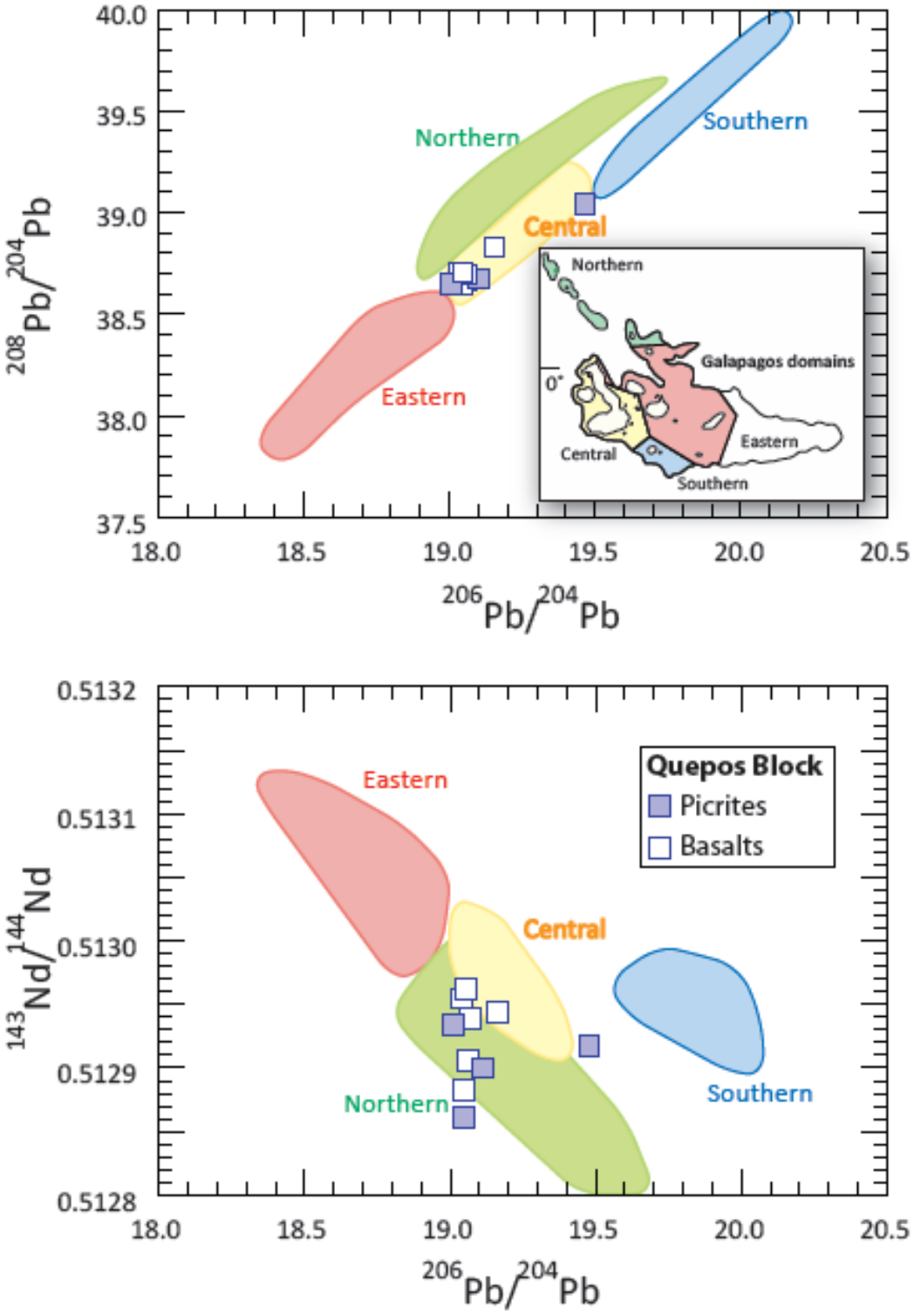
40.0
39.5
39.0
38.5
38.0
37.5
18.0
18.5
19.0
19.5
20.0
20.5
$^{208}Pb/^{204}Pb$
$^{206}Pb/^{204}Pb$
Northern
Southern
Central
Eastern
Northern
Galapagos domains
0°
Central
Eastern
Southern
0.5132
0.5131
0.5130
0.5129
0.5128
$^{143}Nd/^{144}Nd$
Quepos Block
Picrites
Basalts
Eastern
Central
Southern
Northern

**Figure 6:**

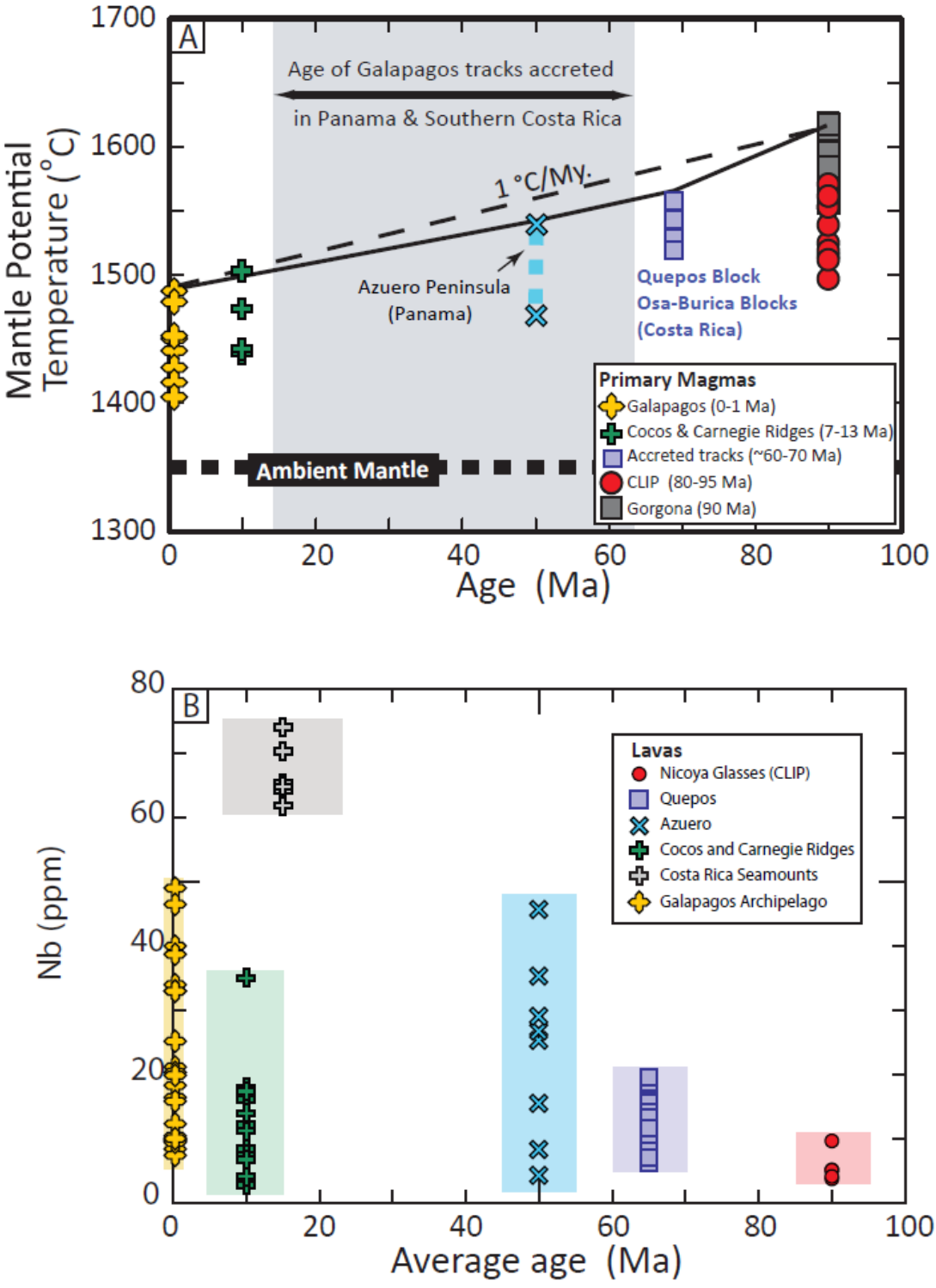
A
Age of Galapagos tracks accreted
in Panama & Southern Costa Rica
1 °C/My
Azuero Peninsula
(Panama)
Quepos Block
Osa-Burica Blocks
(Costa Rica)
Ambient Mantle
Primary Magmas
Galapagos (0-1 Ma)
Cocos & Carnegie Ridges (7-13 Ma)
Accreted tracks (~60-70 Ma)
CLIP (80-95 Ma)
Gorgona (90 Ma)
Mantle Potential Temperature (°C)
1700
1600
1500
1400
1300
0
20
40
60
80
100
Age (Ma)
B
Lavas
Nicoya Glasses (CLIP)
Quepos
Azuero
Cocos and Carnegie Ridges
Costa Rica Seamounts
Galapagos Archipelago
Nb (ppm)
80
60
40
20
0
0
20
40
60
80
100
Average age (Ma)

## S.1. Supplimental Materials

### S.1.1. Modeling

Fields representing olivine compositions of peridotite source magmas (Pacific Ocean and Indian Ocean MORB (Sobolev et al., 2007)) and pyroxenite source magmas (Mauna Kea (Sobolev et al., 2007)) are presented in Figure 1B along with measures olivine compositions from Quepos sample QP-121311-13. The measured olivine compositions from this study overlaps both fields, thus initially the source of Quepos is ambiguous without modeling. The presence of pyroxenite in the source of Quepos is suggested in the whole rock data of Quepos (Appel, 1990; Kussmaul et al., 1982; Tournon and Azema, 1984; Wildberg, 1984; Meschede and Frisch, 1994; Sinton et al., 1997; Hauff et al., 2000 and this study) plotted in Figure 1A along with the discrimination line of Herzberg and Asimow, 2008.

We infer the source lithology of Quepos through the comparison of Mn, Fe/Mn Ni and Ca measured in olivine phenocrysts against modeled olivine compositions. Figure 1 below provides a visual example of the modeling procedure. Such modeling, first presented in Herzberg, 2011, starts with the calculation of primary magmas. A peridotite source primary magma was calculated from CR372T92 (Tournon and Azema, 1984) in PRIMELT2 (Herzberg and Asimow, 2008). In this first step, olivine is added (blue symbols) and subtracted (red symbols) from the starting composition (yellow cross) incrementally. The peridotite source primary magma (Herzberg and Gazel, 2009), represented by the red star, is obtained when ~26.5% olivine is added to the whole rock analysis. The criteria used for the determination of the primary magma were given in

(Herzberg and Asimow, 2008) and will not be repeated here. Since the Ni content of a magma is easily modified by olivine sorting (Herzberg, 2011), the Ni content of the peridotite primary magma solution is calculated with the following equation from Herzberg 2011:

$$\text{Ni (ppm)} = 21.6\text{MgO} - 0.32\text{MgO}^2 + 0.051\text{MgO}^3$$

Computed Mn of the olivine in equilibrium with this peridotite source primary magma was too high, thus the Mn concentration of the primary magma was adjusted. The array of olivine compositions computed in PRIMELT2 (Herzberg and Asimow, 2008) forms a trend that is sub-parallel to the measured olivine crystals therefore it is improbable that the crystals of QP-121311-13 crystallized from a pure, peridotite source magma.

When observed olivine phenocryst compositions are higher in Ni and Fe/Mn and lower in Ca and Mn than phenocrysts crystallized from a peridotite source primary magma a pyroxenite-bearing source is inferred (Herzberg, 2011; Sobolev et al., 2007). A whole rock analysis of QP-121311-13 was the starting composition for the modeling of a pyroxenite source primary magma. As with PRIMELT2 (Herzberg and Asimow, 2008) olivine is added and subtracted incrementally, however in this calculation the composition of the primary magma is determined when the composition of the liquid reaches the pyroxenite cotectic (Herzberg, 2011). The first LLD calculated from the primary magma of QP-121311-13 (green star) only consists of Ol + L (black line). While

the Ca concentrations of the resulting modeled trend is much more consistent with the observed olivine compositions, the slope of the trend does not match the trend in the observed olivine well. The crystallization of Cpx in addition to olivine causes the Ca content of a magmatic liquid to be lower than if olivine crystallized alone. This results in olivines that are progressively lower in Ca. Cpx compositions were computed using equations for partition coefficients presented in (Herzberg et al., 2013). LLDs in which fixed amounts of Cpx relative to Ol crystallize (green lines), produces trends consistent with the observed olivine crystals of QP-121311-13. A successful solution is when there is a reasonable degree of agreement between the modeled Mn, Fe/Mn, Ni and Ca olivine contents and the measured olivine crystals.

S.1.2. Results

LLDs calculated from the hybrid primary magma of QP-121311-13 plots on top of olivine compositions measured from all 10 Quepos samples (Figure 2). This suggests that this primary magma composition may be representative of the primary magma of these samples and perhaps Quepos in general. Trends in Ni and Ca require high pressure, sub-moho Cpx crystallization that occurred concurrently with olivine crystallization (Herzberg et al., 2013). Modeled Ni and Ca however do not produce trends consistent with the observed olivines that have the same proportions of Olivine/Cpx. The best fit between the observed trend in Ca and the calculated LLDs suggests a ratio of Ol/Cpx of 50/50 in the crystallizing assemblage. Ni on the other hand produces a trend that indicates a higher proportion of Cpx relative to Ol is required in the LLD (Figure 2).

Determining the proportion of pyroxenite in Quepos is not a simple matter. Unfortunately, no isotopic data exists for MS90 (Meschede and Frisch, 1994) so any modeling of source endmembers for Quepos is based entirely on major and minor elements. Petrologic modeling of the endmember proportions is made more complicated by the fact that the amount of Ni and Ca in MS90 appears to be much too high (Figure S3). Also, the proportions of peridotite and pyroxenite in the hybrid primary magmas required to reproduce the Mn trend in the olivines, differ from the proportions required to reproduce the Ca trend in the olivines. The calculated proportion of pyroxenitic melt in the source of Quepos, based on Mn alone, is 24%. If Ca is used 64%, pyroxenitic melt is required.

In order to address the inconsistensies between Ca, Mn and Ni, mixtures of variably fractionated peridotite and pyroxenite source primary magmas was tested. The degree of olivine crystallization for either component is limited by the requirement that the resulting mixture has to be in equilibrium with olivine that has a forsterite content no lower than 90%. LLDs produced from the modeled mixtures, which included only olivine addition and subtraction, were plotted against the olivine composition that is in equilibrium with the hybrid primary magma (QP-121311-13). If olivine is allowed to crystallize from the peridotite source primary magma prior to mixing, the resulting hybrid magmas have higher Ni contents. This is the opposite of what is required. When both endmember primary magmas are allowed to crystallize equal proportions olivine prior to mixing, the difference between the resulting LLDs from the mixture of evolved liquids and the LLD of original mixture of the primary magma endmembers is negligible if the

proportions of the components are equal. The best solution is obtained when the peridotite endmember magma is left as primary and the pyroxenite endmember is allowed to crystallize olivine until the magma has reached ~11.5% MgO. Under these conditions, a mixture of 30% derivative pyroxenitic magma and 70% peridotite primary magma closely approximates the hybrid calculated from QP-121311-13.

The main difficulty with the modeling in figure 3 is how to explain the fractionation of only one magmatic endmember component, given that it is assumed that both endmember primary magmas were produced in the same source region. It may be that extreme composition of MS90 does not accurately represent the true pyroxenite endmember. Instead, this sample may be representative of a different pyroxenite body within the Galapagos plume at ~65 Ma. The disproportionately high Ca content and low Mn in the primary magma of MS90 may point to a pyroxenite source that had a lower modal concentration of Cpx and a higher modal concentration of garnet, than the actual pyroxenitic component in the hybrid magmas. Another possibility is that the relatively low Ni content of the hybrid pyroxenite primary magma is a result of a pyroxenitic component that is not completely free of olivine.

**S.2. References**

Appel. H. (1990), Geochemie und K/Ar - Datierung an Magmatiten in Costa Rica. Zentralamerika. Unpublished Diplomarbeit. University of Mainz. 149 pp.

Donovan, J. J. (2012), Probe for EPMA: Acquisition, Automation and Analysis edited, Enterprise Edition Probe Software, Inc., Eugene

Hauff, F., K. Hoernle, P. van den Bogaard, G. Alvarado, and D. Garbe-Schönberg (2000), Age and geochemistry of basaltic complexes in western Costa Rica: Contributions to the geotectonic evolution of Central America, Geochem. Geophys. Geosyst., 1(5), 1-41.

Herzberg, C. (2011), Identification of Source Lithology in the Hawaiian and Canary Islands: Implications for Origins (vol 52, pg 113, 2011), Journal of Petrology, 52(5), 1047-1047.

Herzberg, C., and P. D. Asimow (2008), Petrology of some oceanic island basalts: PRIMELT2.XLS software for primary magma calculation, Geochem Geophy Geosy, 9.

Herzberg, C., and E. Gazel (2009), Petrological evidence for secular cooling in mantle plumes, Nature, 458(7238), 619-U683.

Herzberg, C., P. D. Asimow, D. A. Ionov, C. Vidito, M. G. Jackson, and D. Geist (2013), Nickel and helium evidence for melt above the core-mantle boundary, Nature, 493, 393-398, DOI: 10.1038/nature11771.

Jarosewich, E., R. Gooley and J. Husler (1987), Chromian Augite – A New Microprobe Reference Sample, Geostand Geoanal Res, 11(2), 197-198.

Jarosewich, E., J. A. Nelen, and J. A. Norberg (1980), Reference Samples for Electron Microprobe Analysis*, Geostand Geoanal Res, 4(1), 43-47.

Kussmaul, S., Paniagua, S., Gainza, J., 1982. Recopilación, clasifica-ción e interpretación petroquímica de las rocas ígneas de Costa Rica. Inf. Semest.-Inst. Geogr. Nac. 28, 17 – 79 (Julio – Diciembre)

Meschede, M., and W. Frisch (1994), Geochemical characteristics of basaltic rocks from the Central American ophiolites, Profil, 7, 71-85.

Sinton, C. W., R. A. Duncan, and P. Denyer (1997), Nicoya Peninsula, Costa Rica: A single suite of Caribbean oceanic plateau magmas, J Geophys Res-Sol Ea, 102(B7), 15507-15520.

Sobolev, A. V., et al. (2007), The amount of recycled crust in sources of mantle-derived melts, Science, 316(5823), 412-417.

Tournon, J., and J. Azema (1984), Granophyres and Ferrodolerites from the Nicoya Complex (Costa-Rica) - Possible Example of Magma Immiscibility, B Soc Geol Fr, 26(6), 1336-1347.

Wildberg, H.G.H., 1984, Der Nicoya-Komplex, Costa Rica, Zentralamerika: Magmatismus und Genese eines polymagmatischen Ophiolith-Komplexes: Münstersche Forschungen zur Geologie und Paläontologie, v. 62, 123 p.

## S.3. Figure Captions

**Figure S1:** Modeled olivine and derivative liquid compositions for Quepos. Pacific Ocean and Indian Ocean MORB (Sobolev et al., 2007) are included as examples of peridotite source magmas, while Mauna Kea (Sobolev et al., 2007) is included as an example of a pyroxenite source primary magma. The modeling of the peridotite source primary magma (red star) is done by olivine addition (blue circles) and subtraction (red circles) from the whole rock composition (yellow cross) in PRIMELT2 (Herzberg and Asimow, 2008). Since the trend in the measured olivines (orange circles) are sub-parallel to the olivines modeled in PRIMELT2 (Herzberg and Asimow, 2008) a different primary magma (blue star) is computed by subtracting olivine from the whole rock analysis of QP-121311-13. An LLD of Ol + L is calculated from this primary magma as well as Ol + Cpx + L. The consistency with this second model suggests that these olivines crystallized from a pyroxenite-bearing source.

**Figure S2:** Olivine compositions of ten lavas from Quepos compared to modeled peridotite and pyroxenite source magmas. Modeled olivine compositions from derivative magmas of a peridotite source are sub-parallel to measured olivine compositions in all 4 plots. Good internal consistency between modeled olivine compositions of QP-121311-13 and measured olivines, suggest that this primary magma is representative of the source of these magmas. The largest observed offset of any primary magma from the expected peridotite source compositions indicates that this magma may have been derived from a relatively pure pyroxenite source.

**Figure S3:** Modeling of mixtures of the peridotite and pyroxenite endmembers to estimate the proportion of pyroxenite in the source of Quepos. These plots show the LLD of a hybrid magma composition consisting of a mixture of 70% peridotite primary magma and 30% of a derivative magma obtained from a pyroxenite primary magma which has crystallized olivine until the MgO content reached ~11.4%. A solution for a mixture of the pure pyroxenite endmember was not possible do to the extremely high Ni content of this primary magma.

## S.4. Figures

**Figure 1:**

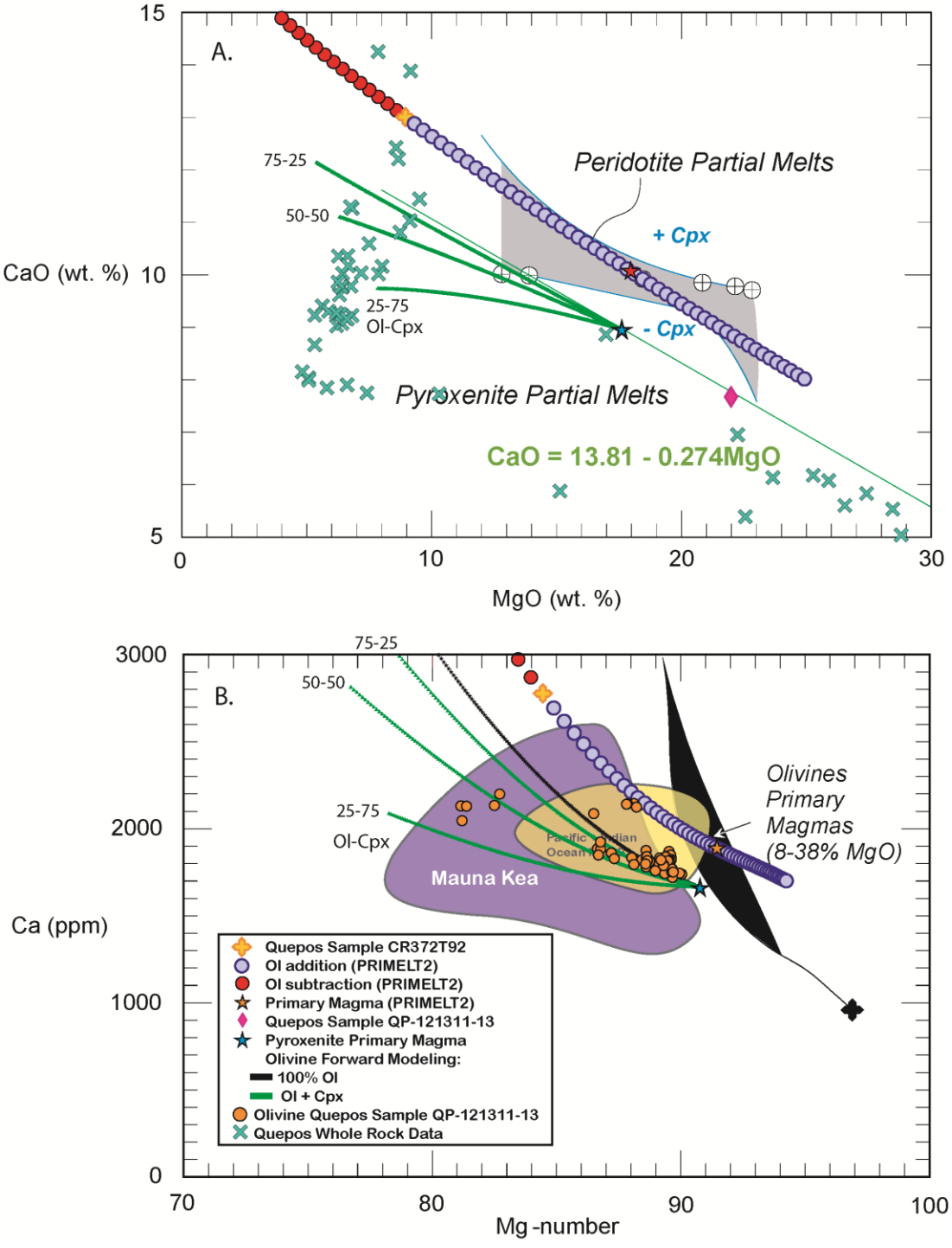

**Figure 2:**

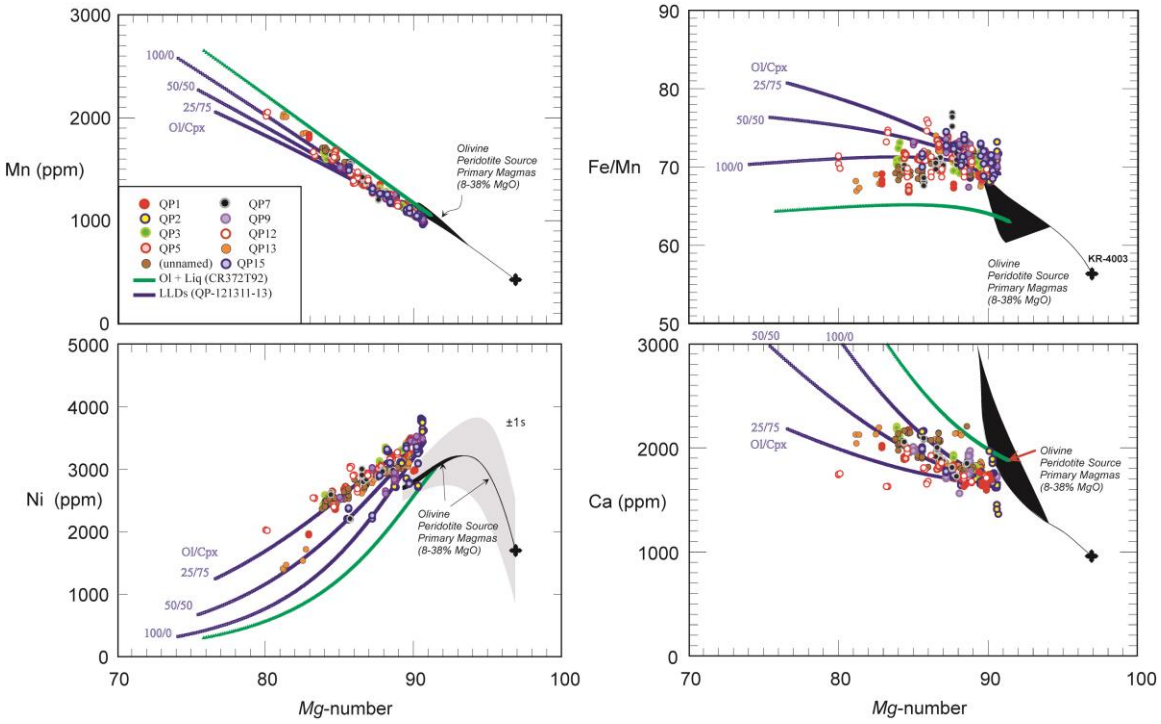
Mn (ppm)
Ni (ppm)
Fe/Mn
Ca (ppm)
Mg-number
100/0
50/50
25/75
Ol/Cpx
Olivine Peridotite Source Primary Magmas (8-38% MgO)
QP1
QP2
QP3
QP5
(unnamed)
QP7
QP9
QP12
QP13
QP15
Ol + Liq (CR372T92)
LLDs (QP-121311-13)
±1s
KR-4003

**Figure 3:**

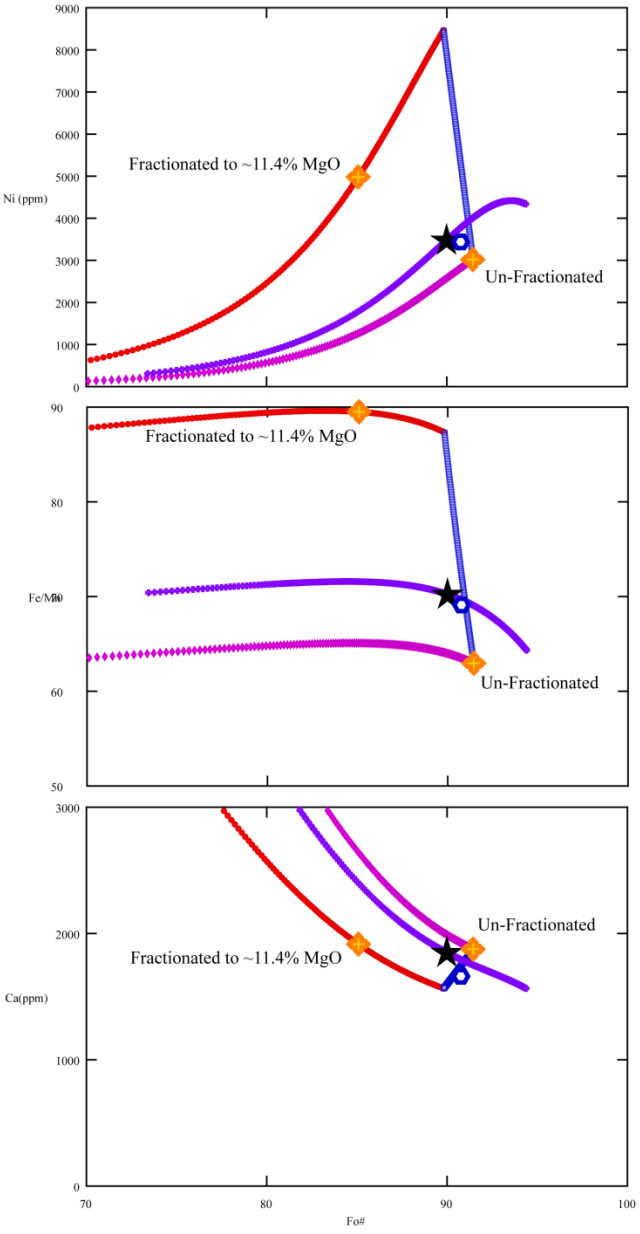
Fractionated to ~11.4% MgO
Un-Fractionated
Ni (ppm)
Fractionated to ~11.4% MgO
Un-Fractionated
Fe/Mn
Un-Fractionated
Fractionated to ~11.4% MgO
Ca(ppm)
Fo#

## Chapter 3

## Phantom Archean crust in Mangaia hotspot lavas and the meaning of heterogeneous mantle

### Abstract

Lavas from Mangaia in the Cook-Austral island chain, Polynesia, define a HIMU (or high μ, where $\mu = {}^{238}U/{}^{204}Pb$) global isotopic end-member among ocean island basalts (OIB) with the highest ${}^{206,207,208}Pb/{}^{204}Pb$. This geochemical signature is interpreted to reflect a recycled oceanic crust component in the mantle source. Mass independently fractionated (MIF) sulfur isotopes indicate that Mangaia lavas sampled recycled Archean material that was once at the Earth's surface, likely hydrothermally-modified oceanic crust. Recent models have proposed that crust that is subducted and then returned in a mantle plume is expected to transform to pyroxenite/eclogite during transit through the mantle. Here we examine this hypothesis for Mangaia using high-precision electron microprobe analysis on olivine phenocrysts. Contrary to expectations of a crustal component and, hence pyroxenite, results show a mixed peridotite and pyroxenite source, with peridotite dominating. If the isotopic compositions were inherited from subduction of recycled oceanic crust, our work shows that this source has phantom-like properties in that it can have its lithological identity destroyed while its isotope ratios are preserved. This may occur by partial melting of the pyroxenite and injection of its silicic melts into the surrounding mantle peridotite, yielding a refertilized peridotite. Evidence from one sample reveals that not all pyroxenite in the melting region was destroyed. Identification of source lithology using olivine phenocryst chemistry can be further compromised by

magma chamber fractional crystallization, recharge, and mixing. We conclude that the commonly used terms mantle "heterogeneities" and "streaks" are ambiguous, and distinction should be made of its lithological and isotopic properties.

## 1. Introduction

Oceanic plates, including crust and mantle lithosphere, enter the mantle at subduction zones. Integrated over geologic time, subduction of oceanic crust has generated a large reservoir of crustal material that must now reside in the Earth's mantle. Regions of buoyantly upwelling mantle, called mantle plumes, are thought to return some of the crustal material to the shallow mantle, where it melts and is erupted at hotspots (Morgan, 1971; Hofmann and White, 1982; White and Hofmann, 1982). In order to evaluate this hypothesis for deep recycling, it is important to detect petrological and geochemical signatures of ancient subducted materials in hotspot lavas.

Lavas from the island of Mangaia, located in the Cook Islands, have the most radiogenic Pb isotope compositions amongst both the HIMU end-member and OIB globally (Woodhead, 1982; Chauvel et al., 1997). This isotopic signature, together with trace element compositions, has been interpreted to reflect a recycled oceanic crust component in the mantle source of Mangaia lavas (Zindler and Hart, 1986; Chauvel et al., 1992; 1995; Hauri and Hart, 1993; Hofmann, 1997; Weaver, 1991; Willbold and Stracke, 2006). Supporting this hypothesis, MIF sulfur isotope signatures, which were uniquely generated in the Earth's atmosphere in the Archean, were recently discovered in olivine-hosted sulfide inclusions from Mangaia lavas (Cabral et al., 2013). This signature provides the strongest evidence yet for deep recycling of surface materials into the mantle

source of hotspot lavas. Armed with this evidence for deep recycling—from subduction zones to mantle plumes—it is important to characterize the present-day mantle that sourced Mangaia lavas.

The Pb isotope ratios that characterize the HIMU component in OIB must involve a process that strongly fractionates U/Pb and Th/Pb. Loss of Pb during subduction-driven dewatering of the oceanic crust is one such process (Chauvel et al., 1992; 1995; Hofmann, 1997). OIB that sample a region of the mantle with subducted crust, preserved as pyroxenite/eclogite, are expected to crystallize olivine with high Ni, low Ca, low Mn and high Fe/Mn compared to melts of peridotite (Sobolev et al., 2005; 2007; Gurenko et al., 2009; 2010; Herzberg, 2011), and may also be expressed in terms of distinctive trace-element and isotope systematics (Gurenko et al., 2009; Day et al., 2009; 2010; Day and Hilton, 2011). An important question, therefore, is whether HIMU lavas, which sample recycled oceanic crust, crystallize olivine that implicates a pyroxenite protolith.

While recycled crust may contribute to the HIMU component in OIB, it may not be expressed as a distinct pyroxenite lithology. Recycled crust that is mixed into its host peridotite during convective stirring might produce a fertilized peridotite (Jackson et al., 2008; Gurenko et al., 2009; Parai et al., 2009). Understanding the source lithology of HIMU magmas can therefore place constraints on the long-term involvement of recycled crust, whether it is direct in the form of pyroxenite melting beneath a hotspot or indirect in the form of peridotite melting. Inferences about source lithology are now a tractable problem using the composition of olivine phenocrysts as a tracer. Using olivine phenocryst compositions, we draw first-order conclusions about the source lithology of

the HIMU isotopic reservoir using samples from Mangaia, the HIMU type locality, and we discuss implications for the preservation of recycled crust as a pyroxenite lithology in the mantle.

## 2. Samples, Analytical Methods and Results

Five lavas from the island of Mangaia were examined in this study, and they are all porphyritic olivine- and clinopyroxene-bearing alkali basalts. Two of the lavas, MGA-B-25 and MGA-B-47, were collected in the 1990 field season and were previously characterized geochemically by Hauri and Hart (1993; 1997), and both host MIF sulfur anomalies (Cabral et al., 2013). Point counting of phenocrysts in petrographic thin sections reveals 20% olivine and 20% clinopyroxene in MGA-B-25, and 60% olivine and 10% clinopyroxene in MGA-B-47. New samples were collected during a field campaign in 2010, and they have the following phenocryst modes: MG-1001 (40% olivine and 10% clinopyroxene), MG-1002 (20% olivine and 30% clinopyroxene), and MG-1006 (20% olivine and 10% clinopyroxene). Additionally, all samples contain opaque phases, most likely as chrome-rich spinels as revealed in positive correlations of whole rock MgO-$Cr_2O_3$.

Major and select trace element (Sc, V, Cr, Co, Ni, Cu, Zn, Ga, Rb, Sr, Y, Zr, Nb, Ba, La, Ce, Pb, U, and Th) compositions for samples MG-1001, MG-1002, and MG01006 were measured by XRF at Franklin and Marshall College using a *PW 2404 PANalytical XRF* vacuum spectrometer following the procedures outlined in Boyd and Mertzmann (1987). Briefly, major element analyses by XRF involved standard lithium tetraborate fusion techniques using 3.6:0.4 g $LiBO_4$:sample powder. Ferrous iron

concentrations were determined by titration with potassium dichromate. Trace element analyses involved standard copolywax preparation (7 g powder: 1.4 g copolywax). Additional details of analytical methods are given at http://www.fandm.edu/earth-and-environment/major-element-technique. Whole rock data for MG-B-47 and MG-B-25 were given in Hauri and Hart (1997; 1993).

We analyzed olivine phenocrysts in 7 samples from Mangaia. A total of 316 high precision analyses were obtained from olivine phenocrysts of varying sizes and forsterite contents. Single core analyses were taken from olivine phenocrysts identified as homogeneous from backscatter images. Traverses were taken from olivines that exhibited zoning.

Olivine, major element, and trace element data were obtained using a slightly modified method of Sobolev et al. (2007). Analyses were conducted on the Jeol JXA-8200 electron microprobe at Rutgers University. A current of 300 nA and an accelerating voltage of 20 kV were used for all analyses. Count times on the elements are as follows: 50 s for Si, 80 s for Mg, 100 s for Fe, and 150 s for Mn, Ni, and Ca. We calibrated on synthetic fayalite or tephroite for Si; synthetic forsterite for Mg; synthetic fayalite for Fe; synthetic tephroite for Mn; synthetic $Ni_2SiO_2$ or SRM 126c (36% Ni) for Ni and Kakanui Augite (USNM 122142) for Ca. We used a San Carlos olivine standard only for drift correction, and it was analyzed at regular intervals throughout every run. Detection limits at a 3σ (99%) confidence level and errors (2σ) were obtained from the Probe for EPMA program (Donovan, 2012). Average detection limits for Si, Mg, and Fe are 30, 22 and 32 ppm, respectively. Average detection limits for trace elements Ni, Mn,

and Ca are 23, 22, and 19 ppm, respectively. Analyses of major elements Si, Mg, and Fe have an average relative 2σ error of ~0.09%, ~0.09%, and ~0.18% respectively. Average 2σ errors for trace elements Ni, Mn, and Ca are 25 ppm, 31 ppm, and 33 ppm respectively. 2 standard deviations of Ni, Mn, Ca and Fo# for the San Carlos olivine analyses (n=97) in our study are 57 ppm, 31 ppm, 19 ppm and 0.1% respectively. Analyses with oxide totals greater than ±2% deviation from 100% were excluded. Chemical formulas were calculated for all analyses. Analyses with deviations in stoichiometry greater than ±1% were excluded.

Olivine compositions are shown in Fig. 1 for MG-1001, MG-1002, MGA-B-25 and MGA-B-47; they are homogeneous or they display modest normal zoning, with Mg-numbers decreasing from the cores to rims. Results for MG-1006 differ and they will be discussed separately.

## 3. Petrological Modeling

Our goal is to use high precision olivine data shown in Fig. 1 to infer the lithology of the source that melted to produce the Mangaia lavas. When olivine Mg-numbers are greater than 90, pyroxenite sources are often revealed in olivine phenocrysts with high Ni, low Ca, low Mn and high Fe/Mn compared to olivines that crystallize from melts of peridotite (Sobolev et al., 2005; 2007; Gurenko et al., 2009; 2010; Herzberg, 2011). For example, olivine in mantle peridotite from a wide range of tectonic environments typically contain ~ 3000 ppm Ni (Herzberg et al., 2013); these are similar to olivine in primitive MORB from the East Pacific Rise and olivines that have been inferred to have crystallized from primary magmas of Archean komatiites (Herzberg, 2011; Herzberg et

al., 2013). The inference of source lithology becomes more challenging when interpreting olivine phenocrysts with Mg numbers < 90, like those from Mangaia (i.e., 79-86; Fig. 1). For example, extraction of heat from a peridotite-source primary magma can be accomplished by fractional crystallization of both olivine and clinopyroxene. When clinopyroxene participates, the derivative magma will be relatively enriched in Ni and depleted in Ca and Mn (Herzberg et al., 2013; Vidito et al., 2013). Olivines that crystallize from such derivative magmas will also be relatively enriched in Ni and depleted in Ca and Mn, a signal that might be confused with a pyroxene-rich source. For Mangaia, the case for clinopyroxene crystallization is obvious in their observed phenocrysts. We assume that clinopyroxene crystallized in a shallow magma chamber below Mangaia, but acknowledge that in other cases it can occur in the mantle (O'Hara, 1968; Albarède et al., 1997; Geist et al., 1998; Herzberg and Asimow, 2008; Herzberg et al., 2013; Vidito et al., 2013). The effects of fractional crystallization must be evaluated in order to draw conclusions about the mantle source (O'Hara, 1968), and this involves petrological modeling.

A detailed description of the method we adopt for petrological modeling (Herzberg, 2011; Herzberg et al., 2013), and is given again in a somewhat abbreviated form. The petrological model has the following components: 1) identification of a primary magma composition, 2) calculation of a liquid line of descent after variable proportions of olivine and clinopyroxene have been subtracted, 3) calculation of the compositions of olivine that crystallize from these derivative magmas, 4) comparison of model and observed olivine compositions.

### 3.1. Mangaia Primary Magma Composition

Primary magma compositions for peridotite-sources have been computed from primitive lava compositions using PRIMELT2 (Herzberg and Asimow, 2008) and results for lavas from the Cook-Austral Islands were reported earlier (Herzberg and Asimow, 2008; Herzberg and Gazel, 2009). However, successful solutions for Mangaia could not be obtained because the published lava database is limited. Furthermore, implementation of PRIMELT2 inverts the effects of fractional crystallization of olivine in order to restore primary magma composition (Herzberg and O'Hara, 2002), and the method is restricted to primitive lavas and glasses that gained or lost only olivine. This excludes Mangaia lavas because of their substantial content of clinopyroxene phenocrysts, and we know of no method that reliably inverts clinopyroxene crystallization because crystal sorting can yield considerable variation in phenocryst mode. Furthermore, we will show that the olivine phenocryst compositions are consistent with magma chamber dynamics that include fractional crystallization, recharge and mixing, processes that rule out the possibility of properly restoring primary magma composition.

Given that an inverse model is not tractable for Mangaia, a forward model strategy is adopted that assumes a peridotite-source primary magma composition. We begin by identifying a glass produced in experiment 40.06 by Walter (1998) on fertile peridotite KR-4003 as our assumed Mangaia peridotite-source primary magma composition. The experiment was run at 4 GPa and 1590°C, the residuum mineralogy is olivine + clinopyroxene + garnet, the glass contains 18.58 % MgO and it was produced by 9.2% equilibrium melting of peridotite (Walter, 1998). It is understood that the exact

matching of Mangaia's primary magma with any experimental melt is unlikely for many reasons. We will show that Walter's melt composition is slightly low in CaO; $TiO_2$ is also too low most, likely because it does not capture contributions from recycled crust (Prytulak and Elliott, 2007). Walter did not report Ni in his experiments, so we assumed the Ni content using Ni (ppm) = $21.6MgO - 0.32MgO^2 + 0.051MgO^3$ for a peridotite source (Herzberg, 2011). However, Walter's melt 40.06 is very similar in composition to a successful PRIMELT2 solution listed in Herzberg and Gazel (2009) for basalt sample RRT-B-21 from Rurutu in the Cook-Austral chain (Hauri and Hart, 1997), which is similarly high in MgO (18.8%) and exhibits a strong HIMU flavor. A successful PRIMELT2 solution was also obtained for one sample from Tubuaii which is located closer to Mangaia and for which 16.4% MgO was obtained for the primary magma; however, this solution yielded model olivine compositions that were much lower in Ni and higher in Fe/Mn than observed Mangaia olivines.

### 3.2. Liquid Line of Descent (LLD)

We assumed that fractional crystallization of our primary magma occurred strictly in a shallow magma chamber at 0.2 GPa, and computed the liquid line of descent using PETROLOG (Danyushevsky and Plechov, 2011). To keep the LLD geochemically faithful to Walter's experimental melt composition, we assumed that crystallization was anhydrous and with all iron as FeO. Olivine is the liquidus phase, and it is followed by clinopyroxene and plagioclase, a result that is also obtained using pMELTS (Ghiorso et al., 2002). Clinopyroxene dominates over olivine when it begins to crystallize, and this is revealed by a break in the LLD for CaO and Ni (Fig. 2). PETROLOG permits the user to

input the olivine/melt distribution coefficients for Ni ($D_{Ni}$), and we have chosen the Beattie-Jones model (Jones, 1984; Beattie et al., 1991) because it provides consistency with previous work (Herzberg, 2011; 2013). There are other olivine/liquid distribution models, and all are parameterizations of experimental data. But the Beattie-Jones model has the minimum root mean square error (Table 1), and it is the most accurate. For clinopyroxene and liquid, we assumed $D_{Ni}$ varies with the composition of the liquid (Herzberg et al., 2013; Supplementary Information), yielding D values that are in good agreement with experimental measurements of LeRoux et al. (2011).

### 3.3. Olivines on the Liquid Line of Descent (OLLD)

The compositions of olivine that crystallizes along the liquid line of descent (OLLD) were calculated for Ni using the Beattie-Jones model and for Ca and Mn using distribution coefficients reported in Herzberg and O'Hara (2002).

### 3.4. Comparison of model and observed olivine compositions

Model olivine compositions on the liquid line of descent are now compared with observed olivine compositions for MG-1001, MG-1002, MGA-B-25 and MGA-B-47. As mention above, results for MG-1006 differ and they will be discussed separately.

## 4. Model Results and Evidence for Peridotite in the Mantle Source for Mangaia

Fig. 1 illustrates that, within the precision of measurement, Fe/Mn in observed olivines are well-matched with model olivines as well as those from East Pacific Rise MORB for which a peridotite source has been inferred (Sobolev et al., 2007; Herzberg, 2011). However, observed olivines differ from model olivines on the liquid line of

descent in having higher Ni and lower Ca at any given Mg-number. And like Mangaia, work on mid ocean ridge basalts reveals that their geochemistry also cannot be explained solely by fractional crystallization, but must include recharge of the magma chamber with primary magma and subsequent mixing with liquid on the LLD (O'Hara, 1077; O'Neill and Jenner, 2013). We now include magma chamber recharge of our primary magma and mixing with liquids on the LLD (Fig. 2), and calculate the olivine compositions that would crystallize from these new liquid compositions (Fig. 1). Results show that this process yields a field of mixed magmas that would crystallize olivines that are a good match to observed olivines when we used a derivative liquid having 6% MgO. While the calculation was made to produce an optimum match, it may be no coincidence that lavas from the Cook-Austral chain also have maximum FeO contents at around 6% MgO, dropping at lower MgO contents owing to magnetite fractionation. Application of PETROLOG to our primary magma, modified for an oxygen fugacity at the QFM buffer, and calculation of magma density (Lang and Carmichael, 1987) along the LLD reveals the production of FeO-rich liquids with maximum densities at around 6% MgO. Such derivative liquids may have settled to the magma chamber floor where they were exposed to and mix with subsequent batches of primary melt.

The Ca contents of observed olivines are generally higher than model olivines that crystallize from either the LLD or mixed magmas (Fig. 1). This misfit likely arises because the CaO content of our assumed Mangaia primary magma is too low. A better result is obtained by increasing CaO in Walter's experimental composition a small amount, from 10.31 to 11.31% (Figs. 1, 2). It is possible that a carbonated peridotite

might be a better source because its partial melts are higher in CaO that volatile-free peridotite (Dasgupta et al., 2007). Primitive high-Mg lavas from the Cook-Austral chain consist of a continuum of compositions from basalts having ~ 48% $SiO_2$ to nephelinites with 38% $SiO_2$. The lavas display negative $SiO_2$-CaO correlations, indicating they are related by partial melting of a carbonated peridotite source (Dasgupta et al., 2007). However, the lavas have higher alkalis than the experimental melts of Dasgupta et al. (2007) and negative $SiO_2$-La/Yb correlations, a difference that might be attributed to refertilization or metasomatism of a peridotite source from recycled crust (Jackson and Dasgupta, 2008).

The most important conclusion drawn from petrological modeling is that the Mangaia lavas are reasonably well-described by a model that involves a peridotite source, and one that was likely carbonated. Fractional crystallization of the Mangaia primary magma occurred in a shallow magma chamber which was replenished by subsequent batches of primary magma. A model of magma mixing and crystallization yields olivines that are a good match with observed olivine compositions. We now evaluate whether this peridotite source model is unique.

## 5. Evidence for Refertilized Peridotite in the Mantle Source for Mangaia

The evidence from olivine of a peridotite source for Mangaia appears to be at odds with isotopic evidence for a role played by recycled crust. We now seek a resolution to this paradox by examining prior hypotheses for the origin of a peridotite source for HIMU lavas from the Canary Islands (Gurenko et al., 2009; 2010; Day et al., 2009; 2010). While there is no compelling reason to assume the sources of Mangaia and

the Canary Islands were identical, it is worth noting that the models for the later differ in details that may be relevant to the present discussion.

Gurenko et al. (2009; 2010) form HIMU peridotite by mixing of recycled crust into peridotite, similar to that proposed by Parai et al. (2009) for the Cook-Austral Islands. Based on Pb-Os isotope systematics Hauri and Hart (1993) estimated a HIMU Mangaia source as a basalt-peridotite mixture, the proportions of which depend on the age of the crust (~20% for ancient basaltic crust). Day et al. (2009; 2010) and Hanyu et al. (2011) propose a mixed peridotite-pyroxenite source, partial melting of the recycled crust, and metasomatic injection and reaction of the melts into the host peridotite in order to comply with the severe constraints on total crustal source material imposed by Os isotopes. This model was originally proposed by Yaxley and Green (1998) who showed that recycled basaltic crust can partially melt at 3 GPa to yield dacite, an experimental observation that has been reproduced (Pertermann and Hirschmann, 2003; Spandler et al., 2008). At 3 GPa, $SiO_2$-rich melts of quartz eclogite have been observed to react with the peridotite host to produce orthopyroxene-rich layers (Yaxley and Green, 1998); if such melts percolate into the peridotite, they may react out of existence, forming a solid refertilized peridotite enriched in orthopyroxene, clinopyroxene and garnet (Yaxley and Green, 1989). This process was examined experimentally by Mallik and Dasgupta (2012; 2013) who showed that the infiltrated melts can evolve to silica-deficient compositions. In nature, whether dacitic melts produce layers of pyroxenite or refertilized peridotite will likely depend on the mode of melt transport; porous flow is expected to yield refertilized peridotite whereas pyroxenite is likely to be produced by channel flow. Evidence for

production of pyroxenite veins by peridotite-dacite melt has been documented in mantle xenoliths (Liu et al., 2005). Prytulak and Elliott (2009) suggested that peridotite refertilized by dacitic melts might be an ideal way to reconcile the low melt productivity of Pico Island in the Azores as inferred from $^{238}U$-$^{230}Th$ and $^{235}U$-$^{231}Pa$ disequilibria with the geochemical evidence for involvement of recycled crust. And evidence for peridotite refertilization by melts of pyroxenite have been documented in orogenic peridotite (Marchesi et al., 2013). The essential question is whether olivine phenocryst compositions can be used to distinguish partial melts of fertilized peridotite or pyroxenite. Sobolev et al. (2005; 2007) and later Herzberg (2011) proposed that partial melts olivine-free pyroxenites will crystallize olivines in Hawaii and other occurrences with elevated Ni and low Ca and Mn. But how do such olivines compare with those that crystallize from partial melts of refertilized peridotite? We now examine this model computationally because there presently exist no high precision olivine data on experimental melts of fertilized peridotite appropriate to Mangaia.

The model setup is similar to that which was described previously (Herzberg and O'Hara, 2002; Herzberg, 2013), and consists of the following components: 1) a dacite melt composition A200K from Pertermann and Hirschmann (2003) is mixed with peridotite KR-4003 in 10 weight % increments to yield a variety of source compositions that range from refertilized peridotite to pyroxenite; Ni contents were not measured, so we calculated it assuming the dacite is in equilibrium with mantle olivine having 0.36%, similar to that described by Wang and Gaetani (2008); 2) the compositions of liquids extracted from residues of olivine and olivine + orthopyroxene were computed by mass

balance solutions to the equation for accumulated fractional melting using bulk distribution coefficients derived from distribution coefficients of olivine and orthopyroxene weighted in variable proportions in the peridotite-dacite mixes; 3) olivine phenocryst compositions are computed as described above for olivines that crystallize along a liquid line of descent at 0.2 GPa. We emphasize that the model has its limitations because residual clinopyroxene and garnet have not been included owing to the added computational complexity; nevertheless, it provides a bound on the possible olivine compositions and the effects of residual clinopyroxene and garnet can be estimated qualitatively. Results are shown in Fig. 3.

When increasing amounts of dacite are added to peridotite, the partial melts crystallize olivines with increasing Ni, decreasing Ca, and increasing Fe/Mn (Fig. 3). For Ni, the effect is similar to that explored by Kelemen et al. (1998) wherein Ni-rich melts in equilibrium with orthopyroxene are produced by the reaction of a silica – rich melt with olivine in peridotite. Fe/Mn in olivine is high because Mn is low owing to preferential partitioning into orthopyroxene. Ca decreases because the dacite composition and the variable mixtures are low in Ca. When the amount of dacite added to peridotite reaches about 40%, the mixture becomes nearly olivine-free pyroxenite and the olivines that crystallize from their partial melts become similar in composition to many olivine phenocrysts from Koolau volcano in Hawaii and El Hierro in the Canary Islands (Fig. 3; Sobolev et al., 2007; Gurenko et al., 2009; Herzberg, 2011). The effect of including clinopyroxene and garnet would be to further increase Ni and Fe/Mn and decrease Ca, based on partition coefficients given in Herzberg et al. (2013).

A role for pyroxenite melting has been recognized for Koolau and El Hiero using a wide variety of geochemical, isotopic, and petrological approaches (Sobolev et al., 2007; Gurenko et al., 2009; Herzberg, 2011; Day et al., 2009; 2010; Hauri, 1996; Lassiter and Hauri, 1998; Blichert-Toft et al., 1999; Huang and Frey, 2005; Jackson et al., 2012). Melts of pyroxenite can be $SiO_2$–rich like Koolau and $SiO_2$–poor like El Hierro and Mangaia (Herzberg, 2011), and it is important to understand how they can be related. At high pressures the pyroxene-garnet plane is a thermal divide that separates $SiO_2$–rich and –poor pyroxenite, and it is not possible to derive a partial melt of one from the other. A typical basalt, for example, is $SiO_2$–rich and will consist of quartz or coesite eclogite which, when melted can produce dacitic $SiO_2$–rich melts. The following are different petrological pathways that can yield El Hierro or Koolau type basalts: 1) dacitic melts can react with peridotite to make a second stage pyroxenite consisting of Cpx+Gt+Opx+Qz(Cs); partial melts are MgO- and $SiO_2$–rich basalts similar to Koolau primary magmas; they plot to the $SiO_2$–rich side of the pyroxene-garnet plane, or within the plane (Herzberg, 2011); olivine phenocrysts from such melts will have maximum Ni contents (Fig. 3). 2) the infiltration of low degree $SiO_2$–rich melts or advanced melts into surrounding peridotite will react with it, producing a refertilized peridotite which, when melted, can yield an $SiO_2$–poor alkali melt (Yaxley and Green, 1978;); addition of $CO_2$ is expected to further lower $SiO_2$ (Dasgupta et al., 2007) and will likely contribute to the wide range of silica deficient rock types in the Canary and Cook-Austral Islands. 3) bimineralic eclogite residues of advanced melts of the basalt protolith will be in spatial contact with peridotite, producing a local region of olivine-poor pyroxenite which will

can also yield $SiO_2$–poor melts (Mallik and Dasgupta, 2012; 2013). Olivine phenocrysts of refertilized peridotite can have high Ni, depending on the mass fraction of infiltrated $SiO_2$–rich melt (Fig. 3).

Mangaia lavas share the alkalic properties of El Hierro, and both have olivines with overlapping Ni at Mg-numbers in the 79-83 range. As discussed below, this might be evidence for a pyroxenite source origin for Mangaia. However, the evidence is contradictory in that Mangaia olivines exhibit a Ni trend towards those expected of a peridotite source. Mangaia Ca contents are similar to some olivines from El Hierro and fertilized peridotite, but others have much higher Ca contents and Mg-numbers (Fig. 3). Mangaia olivines have lower Fe/Mn than those expected of fertilized peridotite (Fig. 3), but this may be an artifact of spinel crystallization. The drop in Fe/Mn in El Hierro and Koolau is likely the result of spinel fractionation because spinel contains no Mn; its fractionation will drop Fe/Mn in the derivative magmas and the olivines from which they crystallize. For Mangaia, while the variation in Fe/Mn is within the precision of measurement, there is a hint of a refertilized peridotite source as seen by the distinct positive trend towards ~ 10% dacite addition (Fig. 3); the positive trend in Fe/Mn may be accounted for by some combination of olivine and spinel fractionation.

Olivine compositions for the Canary Islands (Gurenko et al., 2009) shown in Fig. 4 are good examples of olivine crystallization from a refertilized peridotite source provenance. They are particularly helpful because the olivines extend to higher Mg-numbers than those from Mangaia, and provide a more secure inference about source lithology. For purposes of preserving clarity, we restrict this analysis to olivine

populations with well-separated compositions; we have also excluded Mangaia samples MG-1001, MG-1002, MGA-B-25 and MGA-B-47, but the reader can readily draw comparisons with Fig. 1. Many olivines from La Gomera have high Ca contents and Mg-numbers that are similar to Mangaia, and trend in a direction that is consistent with a peridotite that has been refertilized by about 10-20% dacite. Peridotite melting is most pronounced and yet, relative to other volcanoes in the Canary Islands, the lavas from La Gomera have the most radiogenic Nd, Sr, and Pb isotopic compositions (Gurenko et al., 2009).

## 6. Evidence for Pyroxenite in the Mantle Source for Mangaia

Mangaia sample MG-1006 stands out as different from all others (Fig. 5). It is complex in that its olivines are both normally and inversely zoned in terms of Mg-number, it contains skeletal olivines, and large clinopyroxene phenocrysts that are spongy and embayed. Zoning is most pronounced near phenocryst edges and zoning profiles were obtained on 4 to 5 individual core-rim analyses. Reversely zoned olivines are generally larger than normally zoned olivines, and many are clearly separated from the normally zoned olivines in having anomalously low Ca and Mg-number. However, some of the reversely zoned grains trend towards the normally zoned population from core to rim, and develop high Ca contents characteristic of normally zoned olivines. A similar core-rim pattern is revealed in Fe/Mn (Fig. 5). Normally zoned olivines show a trend where Fe/Mn is positively correlated with Mg-number, reversely zoned olivines show a negative trend, and the two olivine populations converge at an Mg-number of about 80. We interpret these trends as olivines that crystallized from separate batches of magma

that mixed; the reversely zoned olivines have compositions that are similar to many olivines from El Hierro. The normally zoned olivines have attributes of both peridotite and pyroxenite sources; the highest Ca contents and lowest Fe/Mn are similar to those of a peridotite source; however, in detail they define trends in the direction of olivines from Koolau volcano, and there is some overlap with olivines from El Hierro (Fig. 5). It is possible that the entire olivine population in MG-1006 originated from the mixing of separate batches of pyroxenite-source magmas. To relate them, it is likely that the early batch crystallized olivines with the lowest Mg-numbers settled as anticrysts in the next batch of magma, and partial reequilibration was expressed as reversed zoning along the rims.

The signal of recycled crust in sample MG-1006 as a pyroxenite lithology is consistent with isotopic and trace element evidence presented by many workers and reviewed above. It also point to deficiencies in our use of Walter's (1998) model peridotite source primary magma for Mangaia samples MG-1001, MG-1002, MGA-B-25 and MGA-B-47. Our primary magma would predict basaltic compositions that are significantly lower in $TiO_2$ than observed, a misfit that also points to a role played by recycled crust (Prytulak and Elliott, 2007). A carbonated peridotite source is more likely, with $CO_2$ originating from recycled carbonate associated with recycled crust (Jackson and Dasgupta, 2008; Dasgupta et al., 2007; Dasgupta and Hirschmann, 2010).

## 7. Phantom, Fugitive and Possibly Stealth Recycled Crust as Recorded in Olivine Chemistry

Fig. 6 captures the similarities and differences in olivine Ca contents for all Mangaia samples that were studied. Olivines from Mangaia samples MG-1001, MG-1002, MGA-B-25 and MGA-B-47 have Ca contents that are high and trend to high Mg-numbers characteristic of crystallization from derivative melts of peridotite or refertilized peridotite. If the isotopic compositions were inherited from subduction of recycled oceanic crust, then this crust can be considered phantom because its lithological identity has been destroyed. A mechanism for partial crust destruction that is compatible with the olivine chemistry has partial melting of recycled crust and metasomatic injection of silicic melts into the surrounding peridotite (Yaxley and Green, 1998; Spandler et al., 2008; Prytulak and Elliott, 2009; Day et al., 2009; 2010; Hanyu et al., 2011; Mallik and Dasgupta, 2012; 2013). For Mangaia, direct evidence for a role played by recycled crust is in olivine chemistry of sample MG-1006. Olivines in this sample can have lower Ca contents, and trend in directions that are consistent with a pyroxenite source. Given that the crustal lithological identity had successfully escaped destruction by partial melting, we refer to this as "fugitive" recycled crust.

For the entire olivine database with normal zoning, there is converge to a common Ca content and Mg-number of ~ 80 (Fig. 6); they are also similar in Fe/Mn and Ni (Figs. 1, 4). Clearly, no inferences about source lithology would be secure from this population of data having a restricted composition. It is consistent with magma chamber fractional crystallization, recharge, and mixing of magmas of a variably fertilized peridotite source (Fig. 1, 3). But it may also be consistent with pyroxenite melts that undergo similar magma chamber processes; unfortunately, we cannot identify an appropriate lava

composition for which a liquid line of decent can be computed. It is further conjectured that the convergent olivines may have crystallized from the mixing of peridotite- and pyroxenite-sources that fractionated to a common LLD. Whatever the correct explanation may be, it is clear that information concerning the source lithologies of primary magmas can be destroyed by both magma chamber and deep partial melting processes. If the details in our analysis of the problem seem unsatisfactory, they are given in the spirit of trying to give substance and definition to a phantom.

This analysis has been restricted to the formation of stage 2 pyroxenite and refertilized peridotite by dacitic melt production from recycled basalt. It is a successful way of explaining many petrological and geochemical features, but it may not be unique. Advanced or total melts of a pyroxenite protolith with a basaltic composition must necessarily yield basaltic compositions, not dacite (Pertermann and Hirschmann, 2003; Spandler et al., 2008). Stage 2 pyroxenite that forms by reaction of basalt with peridotite will have lower Ni and higher Ca contents and higher Fe/Mn, as will their partial melts and crystallizing olivines (Herzberg, 2011). We term this class of pyroxenite as "stealth pyroxenite" in that it may melt and crystallize olivine phenocrysts with compositions similar to those of melts from mantle peridotite. And, it is expected to be similar to phantom pyroxenite in that it has the isotopic and geochemical characteristics of recycled crust, but olivine compositions that are confused with a peridotite provenance. The possible formation of stealth pyroxenite requires further study from both a computational and experimental point of view. If verified, it will be place important restrictions on the use of olivine chemistry to infer source lithology.

## 8. Conclusions

Inferences have been drawn about possible mantle source lithologies that melted to yield lavas from Mangaia in the Cook-Austral island chain, Polynesia. The method involves a comparison of olivine phenocryst chemistry with forward calculations of olivine compositions that are expected to crystallize from primary magmas of peridotite that has been variably fertilized by a dacite melt produced by partial melting of pyroxenite. Olivine phenocrysts have Mg-numbers that are too low to have been direct precipitates from primary magmas, and inferences about source lithology require an evaluation of the effects of magma chamber fractional crystallization, recharge, and mixing. Results show that most olivine phenocrysts from Mangaia have Ni and Ca contents and Fe/Mn ratios that are consistent with crystallization of magmas that originated from a peridotite or fertilized peridotite source.

If the isotopic compositions were inherited from subduction of recycled oceanic crust, then its lithological identity has been destroyed. A mechanism for partial crust destruction that is compatible with the olivine chemistry has partial melting of recycled crust and metasomatic injection of silicic melts into the surrounding peridotite (Yaxley and Green, 1998; Spandler et al., 2008; Prytulak and Elliott, 2009; Day et al., 2009; 2010; Hanyu et al., 2011). Direct evidence in support of this model has been found in olivines from one Mangaia sample that have preserved the chemical signature of pyroxenite. We conclude that the commonly used terms mantle “heterogeneities” and “streaks” are ambiguous, and distinction should be made of its lithological and isotopic properties.

## 9. Acknowledgments

We are grateful to anonymous reviewers and to Tim Elliott for comments. CH thanks Paul Asimow for help with pMELTS. MGJ acknowledges funding from OCE-1061134 and EAR-1145202. JMDD acknowledges support from NSF EAR-1116089 and the National Geographic Society (GEFNE28-11).

## 10. References

Albarède, F., B. Luais, G. Fitton, M. Semet, E. Kaminski, B.G.J. Upton, P. Bachèlery and J.L. Cheminée, (1997), The geochemical regimes of Piton de la Fournaise volcano (Réunion) during the last 530000 years. Journal of Petrology, v. 38, p. 171-201.

Beattie, P., C. Ford, and D. Russell, (1991), Partition coefficients for olivine-melt and orthopyroxene-melt systems. Contributions to Mineralearalogy and Petrology, v. 109, p. 212-224.

Blichert-Toft, J., F.A. Frey and F. Albarède, (1999), Hf isotope evidence for pelagic sediments in the source of Hawaiian basalts. Science, v. 285, p. 879-882.

Boyd F.R. and S.A. Mertzman, (1987), Composition and structure of the Kaapvaal lithosphere, southern Africa. In: Mysen, B.O. (Ed.), Magmatic Processes: Physicochemical Principles, The Geochimical Society Special Publication 1, p. 13-24.

Cabral, R., M.G. Jackson, E.F. Rose-Koga, K.T. Koga, M.J. Whitehouse, M.A. Antonelli, J. Farquhar, J.M.D. Day and E.H. Hauri, (2013), Anomalous sulphur isotopes in plume lavas reveal deep mantle storage of Archaean crust. Nature, v. 496, p. 490-493.

Chauvel, C., A. Hofmann and P. Vidal, (1992), HIMU-EM: The French Polynesian connection. Earth Planetary Science Letters, v. 110, p. 99-119.

Chauvel, C., S.L. Goldstein and A.W. Hofmann, (1995), Hydration and dehydration of oceanic crust controls Pb evolution in the mantle. Chemical Geology, v. 126, p. 65-75.

Chauvel, C., W. McDonough, G. Guille, R. Maury and R. Duncan, (1997), Contrasting old and young volcanism in Rurutu Island, Austral chain. Chemical Geology, v. 139, p. 125-143.

Danyushevsky, L.V. and P. Plechov, (2011), Petrolog3: Integrated software for modeling crystallization processes. Geochemistry Geophysics Geosystems, 12, Q07021, doi:10.1029/2011GC003516.

Dasgupta, R., M.M. Hirschmann and N.D. Smith, (2007), Partial melting experiments of peridotite $CO_2$ at 3 GPa and genesis of alkalic ocean island basalts. Journal of Petrology, v. 48, p. 2093-2124.

Dasgupta, R. and M.M. Hirschmann, (2009), The deep carbon cycle and melting in Earth's interior. Earth and Planetary Science Letters, v. 298, p. 1-13.

Day, J.M.D., D.G. Pearson, C.G. Macpherson, D. Lowry and J.C. Carracedo, (2009), Pyroxenite-rich mantle formed by recycled oceanic lithosphere: Oxygen-osmium isotope evidence from Canary Island lavas. Geology, v. 37, p. 555-558.

Day, J.M.D., D.G. Pearson, C.G. Macpherson, D. Lowry and J.C. Carracedo, (2010), Evidence for distinct proportions of subducted oceanic crust and lithosphere in HIMU-type mantle beneath El Hierro and La Palma, Canary Islands. Geochimica et Cosmochimica Acta, v. 74, p. 6565-6589.

Day, J.M.D. and D.R. Hilton, (2011), Origin of $^{3}He/^{4}He$ ratios in HIMU-type basalts constrained from Canary Island lavas. Earth Planetary Science Letters, v. 305, p. 226-234.

Donovan, J.J., (2012), Probe for EPMA: Acquisition, Automation and Analysis, Enterprise Edition, Probe Software, Inc., Eugene.

Dupuy, C., H.G. Barsczus, J. Dostal, P. Vidal and J.M. Liotard, (1989), Subducted and recycled lithosphere as the mantle sources of ocean island basalts from Southern Polynesia, Central Pacific, Chemical Geology, v. 77, p. 1-18.

Fodor, R.V., G.R. Bauer and K. Keil, (1982), Ultramafic inclusions and megacrysts in olivine nephelinite, Aitutaki Island, Cook Islands. New Zealand Journal of Geology and Geophysics, v. 25, p. 67-76.

Geist, D., T. Naumann, and P. Larson, (1998), Evolution of Galapagos magmas: mantle and crustal fractionation without assimilation. Journal of Petrology, v. 39, p. 953-971.

Ghiorso, M.S., M.M. Hirschmann, P.W. Reiners and V.C. Kress, (2002), "The pMELTS: A revision of MELTS for improved calculation of phase relations and major element partitioning related to partial melting of the mantle to 3 GPa", Geochemistry Geophysics Geosystems 3, 10.1029/2001GC000217.

Gurenko, A., A.V. Sobolev, K.A. Hoernle, F. Hauff and H.U. Schmincke, (2009), Enriched, HIMU-type peridotite and depleted recycled pyroxenite in the Canary plume: A mixed-up mantle. Earth Planetary Science Letters, v. 277, p. 514-524.

Gurenko, A., K.A. Hoernle, A.V. Sobolev, F. Hauff and H.U. Schmincke, (2010), Source components of the Gran Canaria (Canary Islands) shield stage magmas: evidence from olivine composition and Sr-Nd-Pb isotopes. Contributions to Mineralogy and Petrology, v. 159, p. 689-702.

Hanyu, T., Y. Tatsumi, R. Senda, T. Miyazaki, Q. Chang, Y. Hirahara, T. Takahashi, H. Kawabata, K. Suzuki and J.I. Kimuria, (2011), Geochemical characteristics and

origin of the HIMU reservoir: a possible mantle plume source in the lower mantle. Geochemistry Geophysics Geosystems, v. 12, Q0AC09, doi:10.1029/2010GC003252.

Hart, S.R., K.E. Davis, (1978), Nickel partitioning between olivine and silicate melt. Earth and Planetary Science Letters, v. 40, p. 203-219.

Hauri, E. H., (1996), Major-element variability in the Hawaiian mantle plume. Nature, v. 382, p. 415-419.

Hauri, E. and S.R. Hart, (1993), Re-Os isotope systematic of HIMU and EMII oceanic island basalts from the south Pacific Ocean. Earth and Planetary Science Letters, v. 114, p. 353-371.

Hauri, E. and S.R. Hart, (1997), Rhenium abundances and systematic in oceanic basalts. Chem. Geol., v. 139, p. 185-205.

Herzberg, C., (2011), Identification of Source Lithology in the Hawaiian and Canary Islands: Implications for Origins. Journal of Petrology, v. 52, p. 113-146.

Herzberg, C. and P.D. Asimow, (2008), Petrology of some oceanic island basalts: PRIMELT2.XLS software for primary magma calculation. Geochemistry Geophysics Geosystems, v. 8, Q09001, doi:10.1029/2008GC002057.

Herzberg, C. and E. Gazel, (2009), Petrological Evidence for Secular Cooling in Mantle Plumes, Nature, v. 458, p. 619-622.

Herzberg, C., P. Asimow, D. Ionov, C. Vidito, M.G. Jackson, D. Geist, (2013), Nickel and helium evidence for melt above the core-mantle boundary. Nature, v. 493, p. 393-397.

Hofmann, A.W., (1997), Mantle geochemistry: the message from oceanic volcanism. Nature, v. 385, p. 219-229.

Hofmann, A.W. and W.M. White, (1982), Mantle plumes from ancient oceanic crust. Earth and Planetary Science Letters, v. 57, p. 421-436.

Huang, S., F.A. Frey, (2005), Recycled oceanic crust in the Hawaiian plume: evidence from temporal geochemical variations within the Koolau shield. Contributions to Mineralogy and Petrology, v. 149, p. 556-575.

Jackson, M.G., S.R. Hart, A.E. Saal, N. Shimizu, M.D. Kurz, J. Blusztajn and A. Skovgaard, (2008), Globally elevated titanium, tantalum, and niobium (TITAN) in ocean island basalts with high $^{3}He/^{4}He$. Geochemistry Geophysics Geosystems, v. 9, doi:10.1029/2007GC001876.

Jackson, M.G. and R. Dasgupta, (2008), Compositions of HIMU, EM1, and EM2 from global trends between radiogenic isotopes and major elements in ocean island basalts. Earth and Planetary Science Letters, p. 276, v. 175-186.

Jackson, M.G., D. Weis and S. Huang, (2012), Major element variations in Hawaiian shield lavas: source features and perspectives from global ocean island basalt

(OIB) systematics. Geochemistry Geophysics, Geosystems, v. 13, Q09009, doi:10.1029/2012GC004268.

Jones, J.H., (1984), Temperature and pressure- independent correlations of olivine-liquid partition coefficients and their application to trace element partitioning. Contributions to Mineralogy and Petrology, v. 88, p. 126-132.

Kelemen, P.B., S.R. Hart and S. Bernstein, (1998), Silica enrichment in the continental upper mantle via melt/rock reaction. Earth and Planetary Science Letters, v. 164, p. 387-406.

Kogiso, T., Y. Tatsumi, G. Shimoda and H.G. Barsczus, (1997), High μ (HIMU) ocean island basalts in southern Polynesia: New evidence for whole mantle scale recycling of subducted oceanic crust. Journal of Geophysical Research, v. 102, p. 8085–8103.

Lange, R.A. and I.S.E. Carmichael, (1987), Densities of $Na_2O$–$K_2O$–CaO–MgO–FeO–$Fe_2O_3$–$Al_2O_3$–$TiO_2$–$SiO_2$ liquids: new measurements and derived partial molar properties. Geochimica et Cosmochimica Acta, v. 51, p. 2931–2946.

Lassiter, J.C. and H. Hauri, (1998), Osmium-isotope variations in Hawaiian lavas: evidence for recycled oceanic lithosphere in the Hawaiian plume. Earth and Planetary Science Letters, v. 164, p. 483-496.

Le Roux, V., R. Dasgupta and C.-T.A. Lee, (2011), Mineralogical heterogeneities in the Earth's mantle: Constraints from Mn, Co, Ni and Zn partitioning during partial melting. Earth and Planetary Science Letters, v. 307, p. 395-408.

Li, C. and E.M. Ripley, (2010), The relative effects of composition and temperature on olivine-liquid Ni partitioning: Statistical deconvolution and implications for petrologic modeling. Chemical Geology, v. 275, p. 99-104.

Liu, Y., S. Gao, C.T. Lee, S. Hu, X. Liu and H. Yuan, (2005), Melt–peridotite interactions: Links between garnet pyroxenite and high-Mg# signature of continental crust. Earth and Planetary Science Letters, v. 234, p. 39-57.

Mallik, A. and R. Dasgupta, (2012), Reaction between MORB-eclogite derived melts and fertile peridotite and generation of ocean island basalts. Earth and Planetary Science Letters, v. 329-330, p. 97-108.

Mallik, A, and R. Dasgupta, (2013), Reactive Infiltration of MORB-Eclogite-Derived Carbonated Silicate Melt into Fertile Peridotite at 3 GPa and Genesis of Alkalic Magmas. Journal of Petrology, v. 54, p. 2267-2300.

Marchesi, C., C.J. Garrido, D. Bosch, J.L. Bodinier, F. Gervilla and K. Hidas, (2013), Mantle refertilization by melts of crustal-derived garnet pyroxenite: evidence from the Ronda peridotite massif, southern Spain. Earth and Planetary Science Letters, v. 362, p. 66-75.

Matzen, A.K., M.B. Baker, J.R. Beckett and E.M. Stolper, (2013), The temperature and pressure dependence of nickel partitioning between olivine and silicate melt. Journal of Petrology, v. 54, p. 2521-2545.

Morgan W. J., (1971), Convection plumes in the lower mantle. Nature, v. 230, p. 42–43.

Niu, Y., M. Wilson, E.R. Humphreys and M.J. O'Hara, (2011), The origin of intra-plate ocean island basalts (OI B): the lid effect and its geodynamic implications. Journal of Petrology, v. 52, p. 1443-1468.

O'Hara, M.J., (1968), The bearing of phase equilibria studies in synthetic and natural systems on the origin of basic and ultrabasic rocks. Earth Science Reviews, v. 4, p. 69-133.

O'Hara, M.J., (1977), Geochemical evolution during fractional crystallization of a periodically refilled magma chamber. Nature, v. 266, p. 503-507.

O'Neill, H.S.C. and F. Jenner, (2012), The global pattern of trace-element distributions in ocean floor basalts. Nature, v. 491, p. 698-704.

Parai, R., S. Mukhopadhyay and J. Lassiter, (2009), New constraints on the HIMU mantle from neon and helium isotopic compositions of basalts from the Cook-Austral Islands. Earth and Planetary Science Letters, v. 277, p.253-261.

Pertermann, M. and M.M. Hirschmann, (2003), Anhydrous partial melting experiments on MORB-like eclogite: phase relations, phase compositions and mineral-melt partitioning of major elements at 2-3 GPa. Journal of Petrology, v. 44, p. 2173-2201.

Prytulak, J. and T. Elliott, (2007), $TiO_2$ enrichment in ocean island basalts. Earth and Planetary Science Letters, v. 263, p. 388-403.

Prytulak, J. and T. Elliott, (2009), Determining melt productivity of mantle source from $^{238}U$-$^{230}Th$ and $^{235}U$-$^{231}Pa$ disequilibria: an example from Pico Island, Azores. Geochimica et Cosmochimica Acta, v. 73, p. 2103-2122.

Putirka, K.D., F.J. Ryerson, M. Perfit and W.I. Ridley, (2011), Mineralogy and composition of oceanic mantle. Journal of Petrology 52, 279-313.

Sobolev, A.V., A.W. Hofmann, S.V. Sobolev and I.K. Nikogosian (2005), An olivine-free mantle source of Hawaiian shield basalts. Nature, v. 434, p. 590-597.

Sobolev, A.V., A.W. Hofmann, D.V. Kuzmin, G.M. Yaxley, N.T. Arndt, S.-L. Chung, L.V. Danyushevsky, T. Elliott, F.A. Frey, M.O. Garcia, A.A. Gurenko, V.S. Kamenetsky, A.C. Kerr, N.A. Krivolutskaya, V.V. Matvienkov, I.K. Nikogosian, A. Rocholl, I.A. Sigurdsson, N.M. Sushchevskaya and M. Teklay, (2007), The amount of recycled crust in sources of mantle-derived melts. Science, v. 316, p. 412-417.

Spandler, C., G. Yaxley, D.H. Green and A. Rosenthal, (2008), Phase relations and melting of anhydrous K-bearing eclogite from 1200 to 1600°C and 3 to 5 GPa. Journal of Petrology, v. 49, p. 771-795.

Vidito, C., C. Herzberg, E. Gazel, D. Geist and K. Harpp, (2013), Lithological structure of the Galápagos Plume. Geochemistry Geophysics Geosystems, v. 14, doi:10.1002/ggge.20270.

Walter, M.J., (1998), Melting of garnet peridotite and the origin of komatiite and depleted lithosphere. Journal of Petrology 39, 29-60.

Wang, Z.. and G.A. Gaetani, (2008), Partitioning of Ni between olivine and siliceous eclogite partial melt: experimental constraints on the mantle source of Hawaiian basalts. Contributions to Mineralogy and Petrology, v. 156, p. 661-678.

Weaver, B., (1991), The origin of ocean island basalt end-member compositions: trace element and isotopic constraints. Earth Planetary Science Letters, v. 104, p. 381-397.

White, W.M. and A.W. Hofmann, (1982), Sr and Nd isotope geochemistry of oceanic basalts and mantle evolution. Nature, v. 296, p. 821–825.

Willbold, M., and A. Stracke, (2006), Trace element composition of mantle end-members: Implications for recycling of oceanic and upper and lower continental crust. Geochemistry Geophysics Geosystems 7, Q04004, doi:10.1029/2005GC001005.

Wood, C.P., (1978), Petrology of Atiu and Mangaia, Cook Islands (Note), New Zealand Journal of Geology and Geophysics, v. 21, p. 767-771.

Woodhead, J.D., (1996), Extreme HIMU in an oceanic setting: the geochemistry of Mangaia Island (Polynesia), and temporal evolution of the Cook-Austral hotspot. Journal of Volcanology Geothermal Research, v. 72, p. 1-19.

Yaxley, G.M., and D.H. Green, (1998), Reactions between eclogite and peridotite: mantle refertilisation by subduction of oceanic crust. Schweizerische Mineralogische Petrographische Mitteilungen, v. 78, p. 243-255.

Zindler, A., and S. Hart, (1986), Chemical geodynamics, v. 14, p. 493-571.

## 11. Figure Captions:

**Figure 1:** Mg-numbers versus Ni and Ca contents and Fe/Mn for calculated (Herzberg, 2011) and observed olivine. An Mg-number is defined as 100MgO/(MgO + FeO) in mole per cent. Black forms = calculated Ni and Ca in olivines that crystallize from all primary melts derived from a fertile peridotite source having 1960 ppm Ni, 3.45% CaO and 0.13% MnO (Herzberg, 2011); the ±1σ uncertainty for Ni is discussed in Herzberg et al.

(2013). The gray lines are olivine compositions that crystallize from an assumed Mangaia primary magma that subsequently fractionated olivine, clinopyroxene and plagioclase at 0.2 GPa, an olivine liquid line of descent (OLLD). The fields bounded by the broken lines and OLLD simulate the range of olivine compositions that would crystallize by magma chamber fractional crystallization, recharge, and mixing. Mangaia olivines are from samples MGA-B-25, MGA-B-47, MG-1001, MG-1002, normalized to 100%. Precision in Ca and Ni is about the size of the symbols. Small variations in Mn propagate to significant variations in Fe/Mn as represented by the bracket. Olivines from the East Pacific Rise MORB are from Sobolev et al., (2007).

**Figure 2:** A model for fractional crystallization of a Mangaia primary magma, recharge and mixing in a magma chamber at 0.2 GPa. Black lines are computed liquid lines of descent (LLD) using PETROLOG (Danyushevsky and Plechov, 2011) on a Mangaia primary magma that is assumed to have the compositions of Walter's (1998) 40.06 experimental composition, modified also by 1% CaO addition. Walter's melt composition was performed on fertile peridotite KR-4003. Broken lines are mixed end-members that, together with the LLD, provide bounds on the fields of mixed magmas. Whole rock analyses for lavas from Managaia: open circles are compiled whole rock compositions (Wood, 1997; Woodhead, 1996; Dupuy et al., 1989; Kogiso et al., 1997; Hauri and Hart (1993; 1997). Black squares are new whole rock data for MG-1001, -1002, and -1006 reported in this paper (Table A1) and MGA-B-47 reported by Hauri and Hart (1997); analysis MGA-B-25 (Hauri and Hart (1993) plots off scale and is unreliable owing to extensive alteration.

**Figure 3:** A model of olivine compositions that crystallize from primary magmas of peridotite that has been fertilized by variable addition of a dacite melt, and olivines that crystallize along a liquid line of descent (OLLD) at 0.2 GPa. Model olivines are compared with observed Mangaia olivines from samples MGA-B-25, MGA-B-47, MG-1001, MG-1002 and those from Koolau and El Hierro (Sobolev et al., 2007; Gurenko et al., 2009).

**Figure 4:** A model of olivine compositions that crystallize from primary magmas of peridotite that has been fertilized by variable addition of a dacite melt, from Fig. 3, compared with selected observed olivines from the Canary Islands (Gurenko et al., 2009). Note the general compatibility between observed olivines from La Gomera and La Palma with model olivines of a peridotite source that has been fertilized with ~ 10-20% dacite melt. This is supporting evidence that Mangaia olivines having the highest Ca contents and Mg-numbers (Fig. 3) crystallized from a fertilized peridotite source, not pyroxenite.

**Figure 5:** Olivines from Mangaia sample MG-1006 compared with model olivines of a peridotite source, from Fig. 1. Core compositions of reversely zoned olivines, indicated by the white crosses, are similar to those from Koolau and El Hierro, for which a pyroxenite source was inferred (Sobolev et al., 2007; Gurenko et al., 2009). Rim compositions of reversely zoned olivines are similar to those of normally zoned olivines. Ca contents and Mg-numbers of normally zoned olivines, indicated by the black squares, trend in a direction towards olivines of a pyroxenite source provenance.

**Figure 6:** Summary of Ca contents and Mg-numbers for all measured Mangaia olivine phenocrysts compared with olivines expected to crystallize from primary magmas of a

peridotite source that had variable amounts of dacite added, from Fig. 3. Ca contents of observed olivine phenocrysts trend in directions that point towards fertilized peridotite and pyroxenite sources.

## 12. Figures:

### Figure 1:

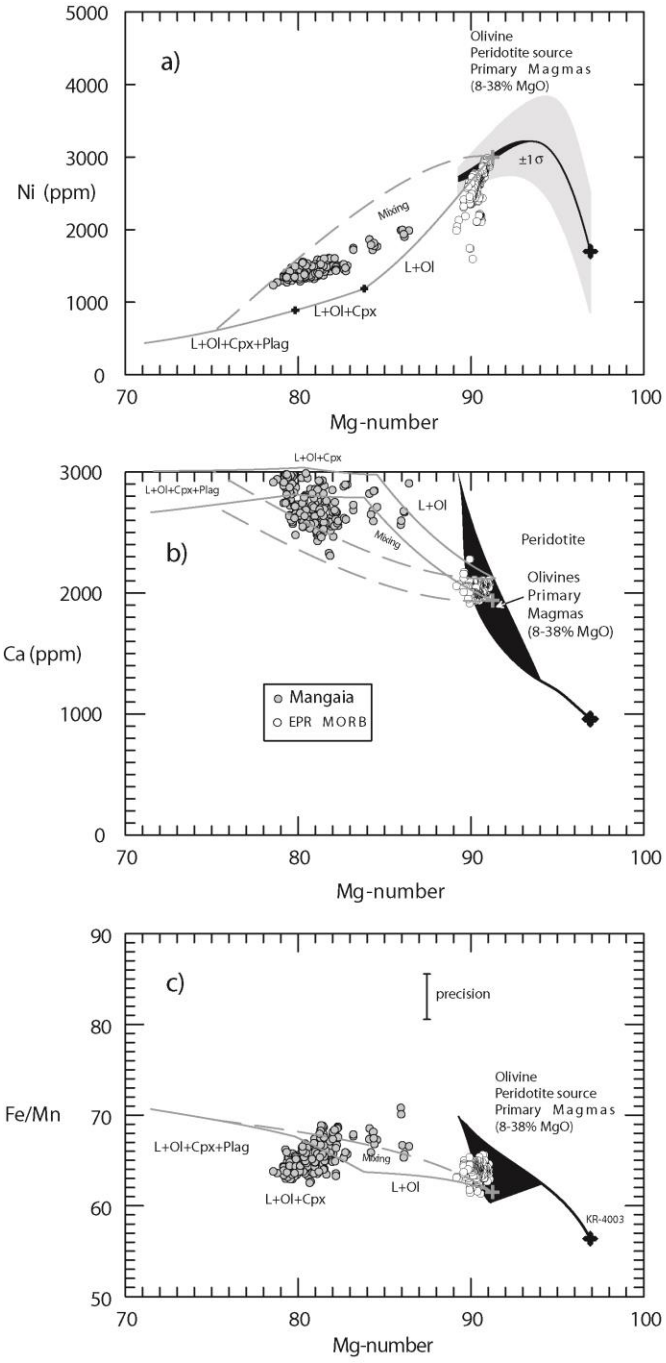


Figure 1

**Figure 2:**

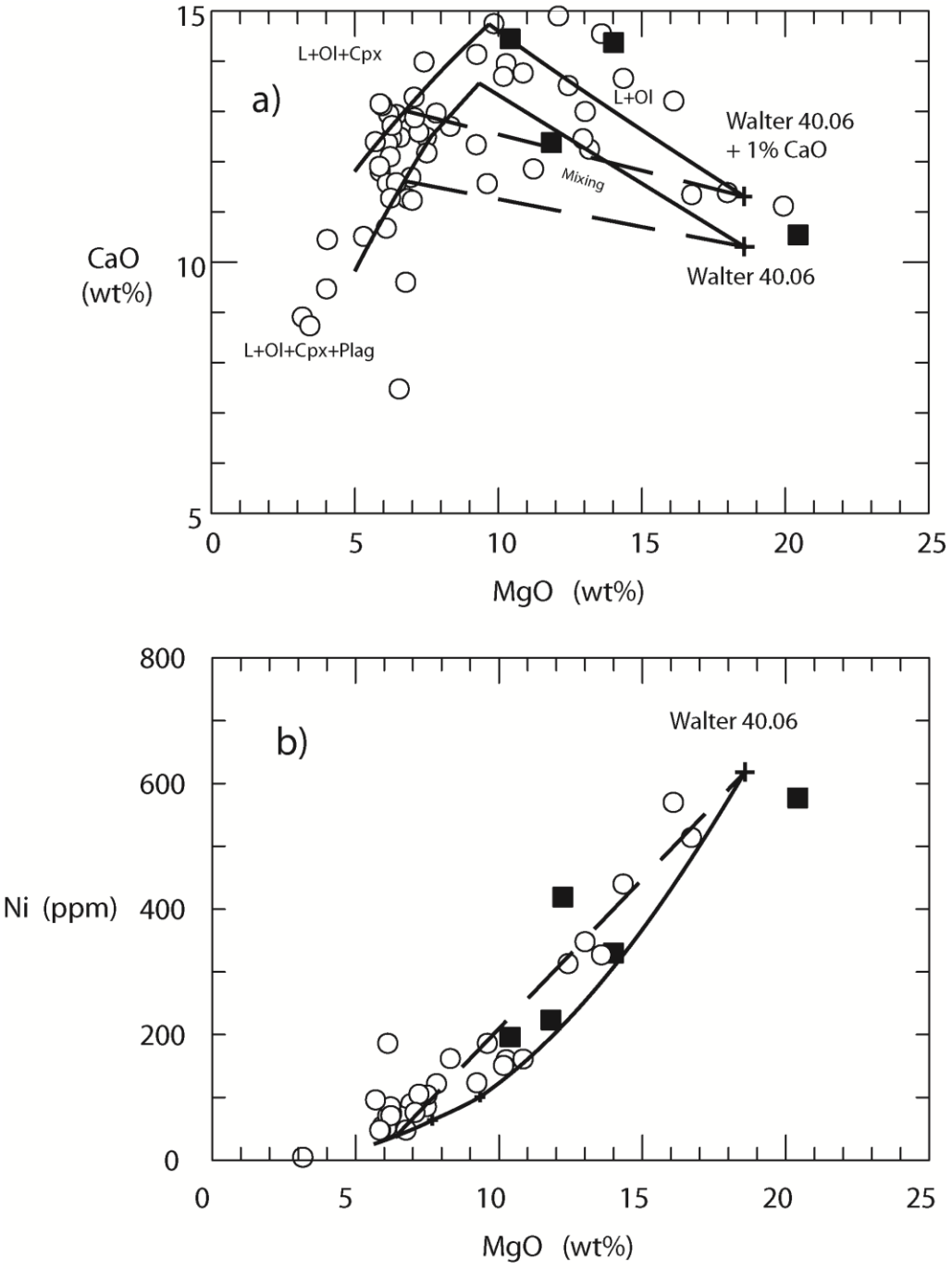


Figure 2

**Figure 3:**

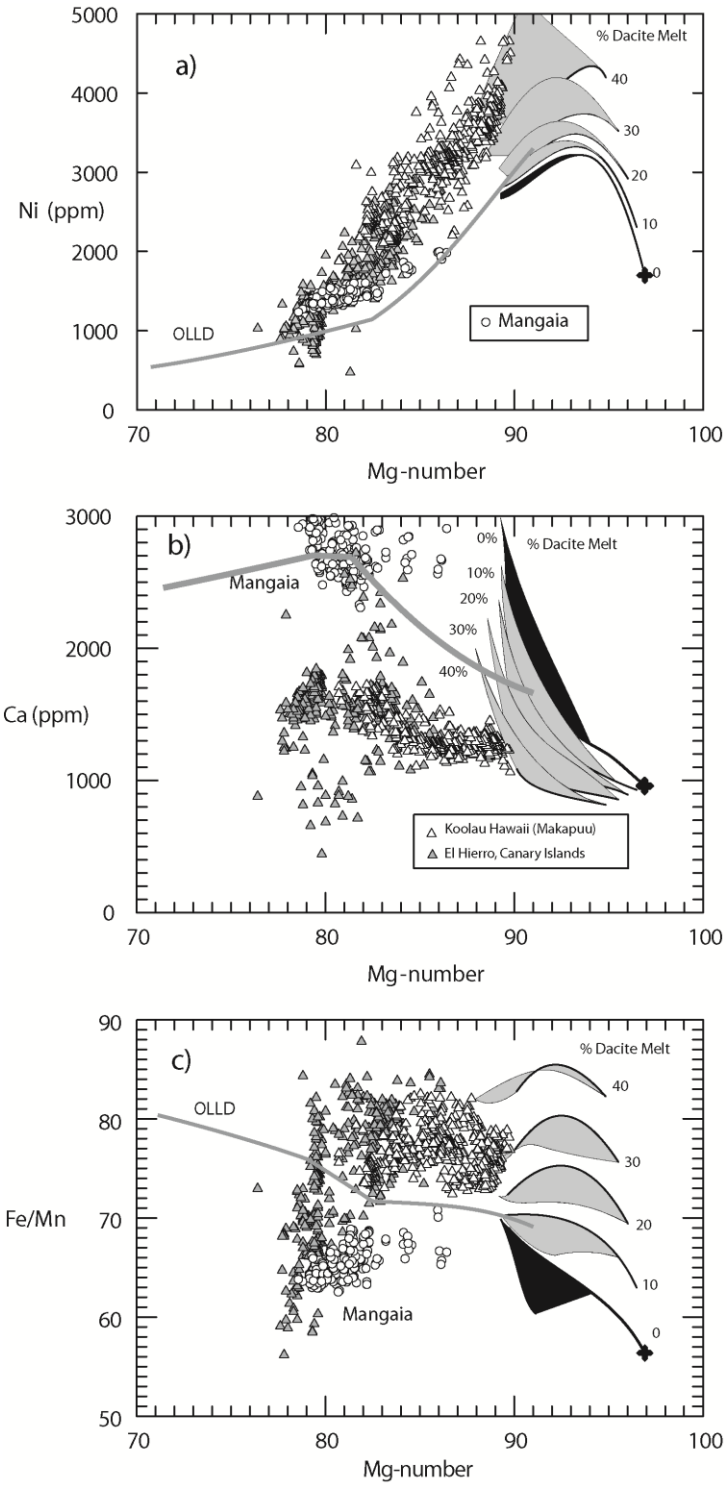


Figure 3

**Figure 4:**

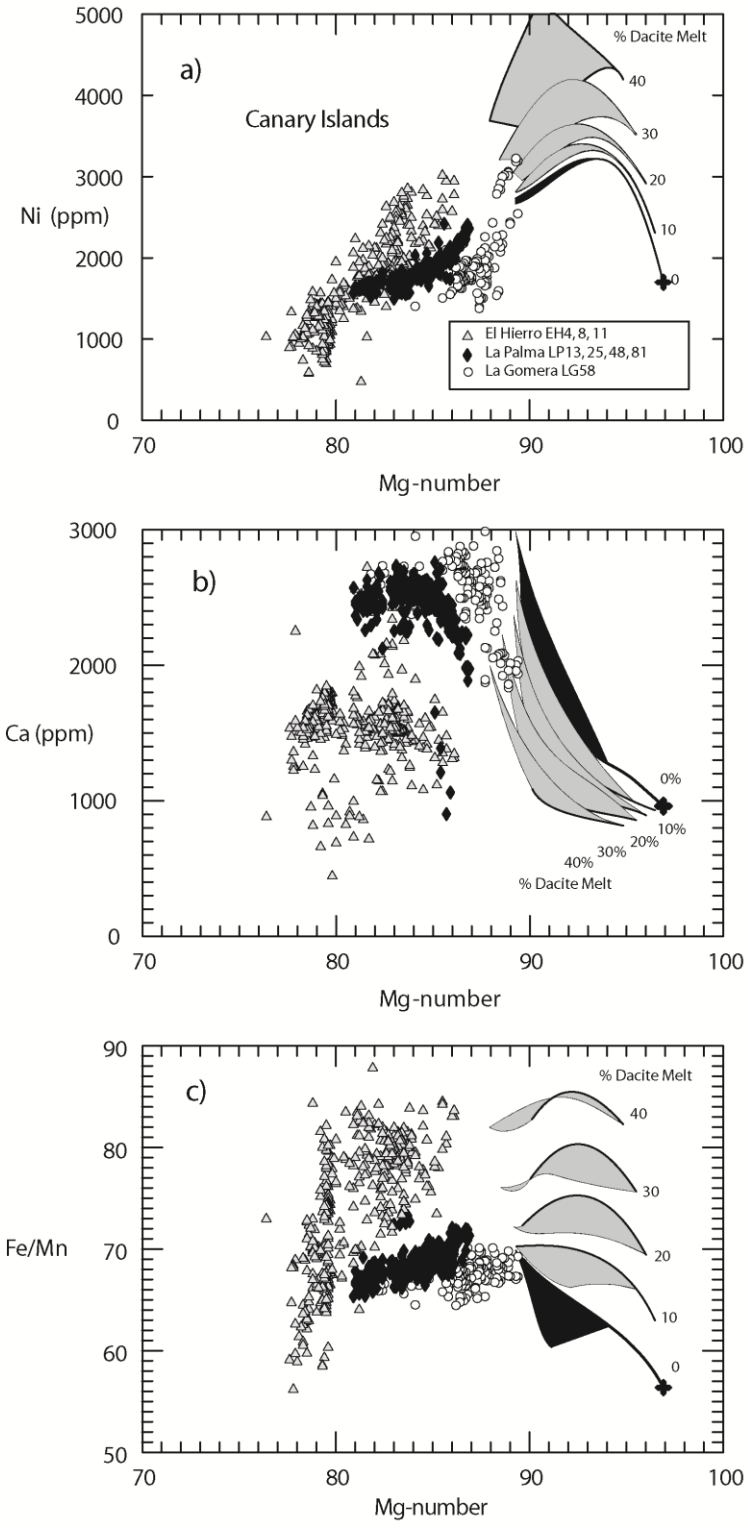


Figure 4

**Figure 5:**

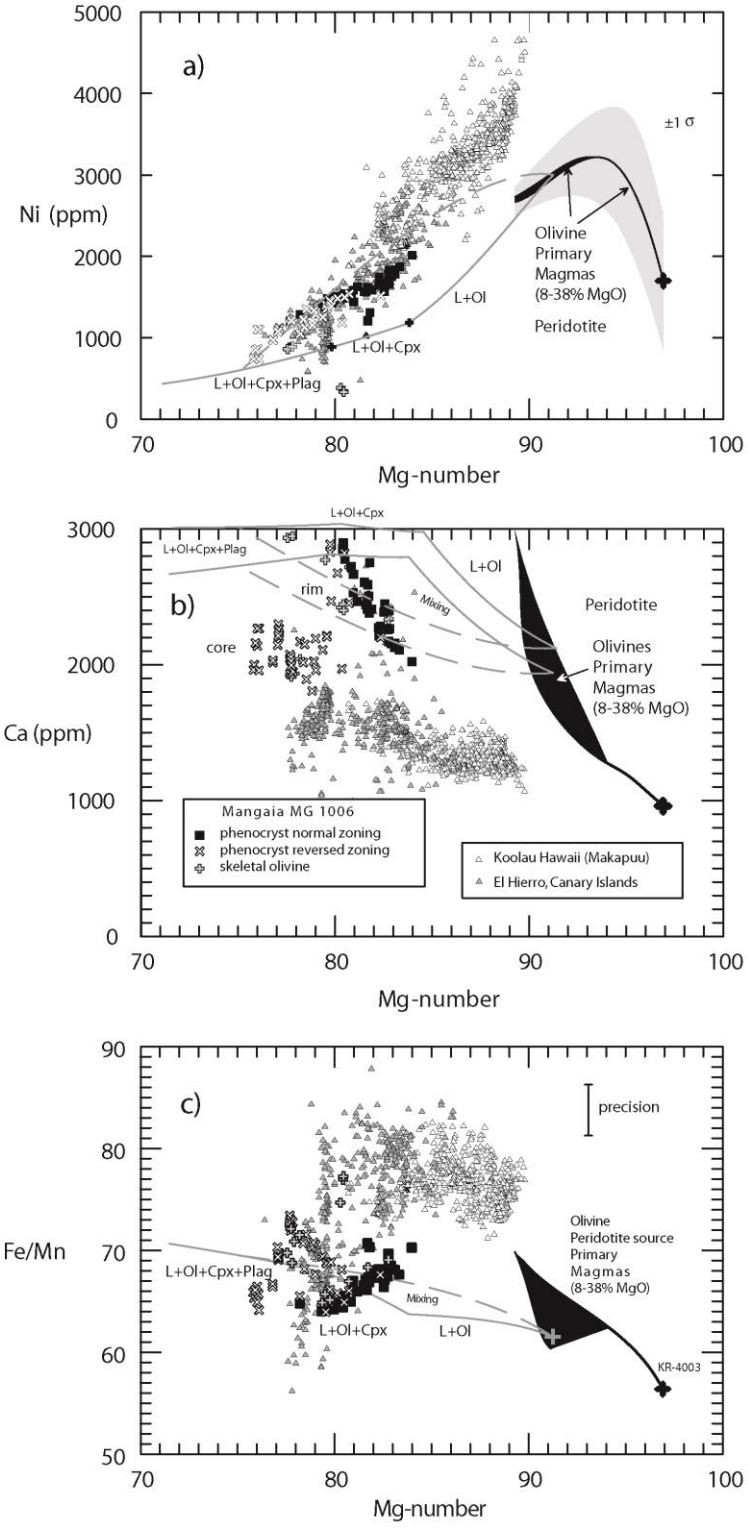


Figure 5

**Figure 6:**

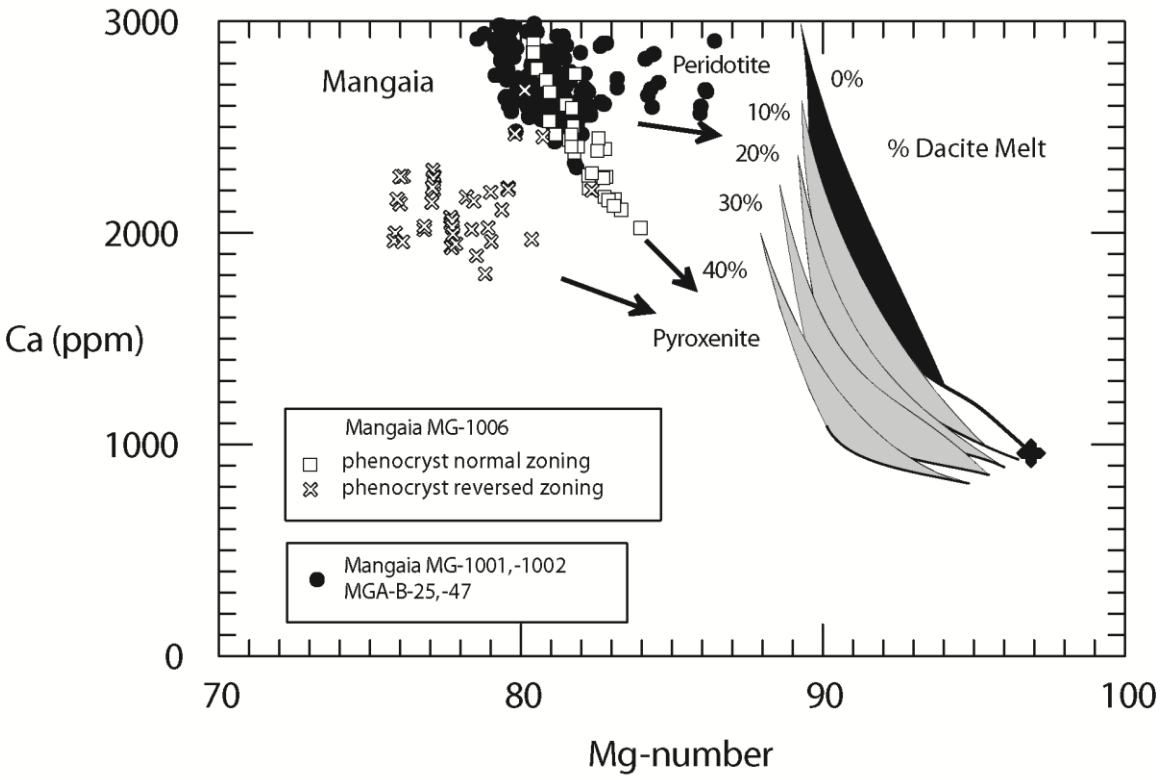


Figure 6

**13. Tables:**

**Table 1: Olivine/Liquid Ni Partition (D) Models & Their Uncertainties**

| Model | RMSE |
|---|---|
| Beattie et al. (1993) | 1.1 |
| Li and Ripley (2010) | 1.4 |
| Putirka et al. (2011; equation 2a) | 2.7 |
| Putirka et al. (2011; equation 2b) | 2.0 |
| Putirka et al. (2011; equation 2c) | 2.9 |
| Matzen et al. (2013) | 2.5 |
| Hart and Davis (1978) | 4.2 |
| Niu et al. (2011)* | 2.1 |

RMSE = Root Mean Square Error

1 RMSE = $(\Sigma(\text{model D Ni - experimental D Ni})^2/N)^{0.5}$

N = 271 experiments listed in Herzberg et al. (2013)
together with 13 experiments in Matzen et al. (2013)

* does not include data at 1 atmosphere

S.1.Supplimentary Information:

**Table A1: Major and trace elements for Mangaia lavas hosting olivine phenocrysts**

| **Specimen** | MG1001 | MG1002 | MG1006 | MGA-B-47 | MGA-B-25 |
|---|---|---|---|---|---|
| **$SiO_2$** | 43.57 | 43.35 | 43.23 | 44.5 | 44.23 |
| **$TiO_2$** | 2.22 | 2.61 | 2.92 | 1.74 | 2.13 |
| **$Al_2O_3$** | 9.50 | 11.57 | 11.76 | 7.99 | 8.54 |
| **$Fe_2O_3T$** | 13.73 | 14.40 | 14.8 | 14.29 | 14.2 |
| **MnO** | 0.19 | 0.22 | 0.2 | 0.19 | 0.21 |
| **MgO** | 13.81 | 10.26 | 11.7 | 20.67 | 12.26 |
| **CaO** | 14.15 | 14.24 | 12.22 | 10.65 | 17.92 |
| **$Na_2O$** | 1.86 | 2.29 | 2.23 | 1.68 | 1.32 |
| **$K_2O$** | 0.52 | 0.68 | 0.71 | 0.48 | 0.35 |
| **$P_2O_5$** | **0.28** | **0.37** | 0.41 | 0.23 | |
| **Total** | 99.83 | 99.99 | 100.18 | 102.42 | |
| **LOI** | 8.80 | 6.78 | 2.29 | | |
| **FeO** | 7.96 | 8.89 | 8.94 | | |
| **$Fe_2O_3$** | 4.88 | 4.52 | 4.86 | | |
| **Rb** | 6 | 10 | 12 | 11 | |
| **Sr** | 377.0 | 659.0 | 483 | 270 | |
| **Y** | 23 | 27 | 28.8 | 16 | |
| **Zr** | 133 | 177 | 204 | 112 | |
| **V** | 266 | 285 | 308 | 211 | |
| **Ni** | 320 | 190 | 217 | 574 | |
| **Cr** | 1125.0 | 512.0 | 559 | 1499 | |
| **Nb** | 27.8 | 43.7 | 50.6 | 30 | |
| **Ga** | 12 | 14 | 15.2 | 11 | |
| **Cu** | 103 | 107 | 148 | 106 | |
| **Zn** | 127 | 179 | 101 | 89 | |
| **Co** | 71 | 60 | 67 | | |
| **Ba** | 163 | 247 | 235 | 108 | |
| **La** | 12 | 16 | 17 | 18.8 | |
| **Ce** | 43.0 | 42.0 | 40 | 37.1 | |
| **U** | <0.5 | <0.5 | 1.6 | 0.52 | |
| **Th** | 2 | <0.5 | 7 | 1.96 | |
| **Sc** | 40 | 36 | 36 | 38 | |
| **Pb** | 5 | <1 | 5 | 1.82 | |

MGA-B-47 is from Hauri and Hart (1997)

Sample MGA-B-25 is from Hauri and Hart (1993). Analysis is unreliable as it is heavily altered

**Table S2: High precision Mangaia olivine phenocryst analyses.**

| Sample | SiO2 | MgO | FeO | CaO | MnO | NiO | Cr2O3 | Al2O3 | Total | OL Mg# | Ni ppm | Mn ppm | Ca ppm | Fe ppm |
|---|---|---|---|---|---|---|---|---|---|---|---|---|---|---|
| MG-1001 | 39.1 | 40.93 | 18.92 | 0.4 | 0.291 | 0.172 | 0.017 | 0.027 | 99.86 | 79.41 | 1351 | 2254 | 2859 | 147123 |
| MG-1001 | 39.11 | 40.63 | 18.85 | 0.406 | 0.292 | 0.176 | 0.013 | 0.024 | 99.5 | 79.35 | 1383 | 2262 | 2902 | 146579 |
| MG-1001 | 39.12 | 40.91 | 18.96 | 0.397 | 0.297 | 0.174 | 0.012 | 0.028 | 99.9 | 79.36 | 1367 | 2301 | 2838 | 147434 |
| MG-1001 | 39.11 | 41.17 | 18.64 | 0.416 | 0.292 | 0.171 | 0.012 | 0.024 | 99.84 | 79.74 | 1343 | 2262 | 2974 | 144946 |
| MG-1001 | 39.21 | 41.2 | 18.75 | 0.414 | 0.299 | 0.172 | 0.014 | 0.025 | 100.08 | 79.66 | 1351 | 2316 | 2959 | 145801 |
| MG-1001 | 39.09 | 41.06 | 18.84 | 0.411 | 0.3 | 0.169 | 0.021 | 0.027 | 99.92 | 79.53 | 1328 | 2324 | 2938 | 146501 |
| MG-1001 | 39.08 | 40.88 | 18.77 | 0.407 | 0.295 | 0.171 | 0.015 | 0.029 | 99.64 | 79.52 | 1343 | 2285 | 2909 | 145956 |
| MG-1001 | 39.21 | 40.94 | 18.74 | 0.416 | 0.297 | 0.176 | 0.011 | 0.027 | 99.82 | 79.57 | 1383 | 2301 | 2974 | 145723 |
| MG-1001 | 39.29 | 41.26 | 18.93 | 0.381 | 0.296 | 0.173 | 0.011 | 0.018 | 100.36 | 79.53 | 1359 | 2293 | 2723 | 147201 |
| MG-1001 | 39.23 | 41.41 | 18.66 | 0.427 | 0.288 | 0.172 | 0.016 | 0.026 | 100.23 | 79.82 | 1351 | 2231 | 3052 | 145101 |
| MG-1001 | 39.11 | 41.08 | 19.14 | 0.417 | 0.305 | 0.166 | 0.01 | 0.027 | 100.26 | 79.28 | 1304 | 2363 | 2981 | 148834 |
| MG-1001 | 39.2 | 41.22 | 19.1 | 0.397 | 0.298 | 0.172 | 0.014 | 0.029 | 100.43 | 79.37 | 1351 | 2308 | 2838 | 148523 |
| MG-1001 | 39.05 | 40.8 | 19.09 | 0.403 | 0.298 | 0.168 | 0.017 | 0.033 | 99.86 | 79.21 | 1320 | 2308 | 2881 | 148445 |
| MG-1001 | 38.97 | 40.64 | 19.1 | 0.407 | 0.298 | 0.165 | 0.015 | 0.032 | 99.63 | 79.13 | 1296 | 2308 | 2909 | 148523 |
| MG-1001 | 39.22 | 40.89 | 18.96 | 0.457 | 0.299 | 0.162 | 0.009 | 0.024 | 100.03 | 79.35 | 1273 | 2316 | 3267 | 147434 |
| MG-1001 | 39.46 | 42.21 | 17.3 | 0.383 | 0.266 | 0.188 | 0.023 | 0.031 | 99.86 | 81.3 | 1477 | 2060 | 2738 | 134526 |
| MG-1001 | 39.36 | 42.39 | 17.21 | 0.382 | 0.261 | 0.189 | 0.018 | 0.033 | 99.85 | 81.45 | 1485 | 2022 | 2731 | 133826 |
| MG-1001 | 39.35 | 42.41 | 17.02 | 0.38 | 0.262 | 0.189 | 0.021 | 0.031 | 99.66 | 81.62 | 1485 | 2029 | 2716 | 132348 |
| MG-1001 | 39.21 | 41.5 | 18.26 | 0.413 | 0.281 | 0.177 | 0.021 | 0.028 | 99.89 | 80.2 | 1390 | 2177 | 2952 | 141991 |
| MG-1001 | 38.95 | 41.06 | 18.54 | 0.403 | 0.284 | 0.172 | 0.016 | 0.027 | 99.45 | 79.79 | 1351 | 2200 | 2881 | 144168 |
| MG-1001 | 39.03 | 41.3 | 18.71 | 0.397 | 0.288 | 0.176 | 0.016 | 0.026 | 99.95 | 79.73 | 1383 | 2231 | 2838 | 145490 |
| MG-1001 | 38.92 | 40.93 | 18.86 | 0.394 | 0.29 | 0.174 | 0.016 | 0.039 | 99.63 | 79.46 | 1367 | 2246 | 2816 | 146656 |
| MG-1001 | 38.93 | 40.83 | 18.85 | 0.403 | 0.294 | 0.17 | 0.012 | 0.025 | 99.51 | 79.43 | 1335 | 2277 | 2881 | 146579 |
| MG-1001 | 39.26 | 41.07 | 19.17 | 0.402 | 0.304 | 0.173 | 0.009 | 0.025 | 100.41 | 79.25 | 1359 | 2355 | 2873 | 149067 |
| MG-1001 | 39.11 | 40.98 | 19.01 | 0.398 | 0.298 | 0.171 | 0.017 | 0.04 | 100.02 | 79.35 | 1343 | 2308 | 2845 | 147823 |
| MG-1001 | 39.22 | 41.29 | 19.12 | 0.402 | 0.3 | 0.172 | 0.015 | 0.021 | 100.54 | 79.38 | 1351 | 2324 | 2873 | 148678 |
| MG-1001 | 39.16 | 41.29 | 18.84 | 0.425 | 0.295 | 0.165 | 0.012 | 0.027 | 100.22 | 79.62 | 1296 | 2285 | 3038 | 146501 |

| Sample | SiO2 | MgO | FeO | CaO | MnO | NiO | Cr2O3 | Al2O3 | Total | OL Mg# | Ni ppm | Mn ppm | Ca ppm | Fe ppm |
|---|---|---|---|---|---|---|---|---|---|---|---|---|---|---|
| MG-1001 | 39.05 | 40.82 | 18.74 | 0.37 | 0.286 | 0.178 | 0.014 | 0.03 | 99.49 | 79.52 | 1398 | 2215 | 2645 | 145723 |
| MG-1001 | 39.17 | 41.2 | 18.73 | 0.36 | 0.286 | 0.18 | 0.02 | 0.029 | 99.99 | 79.68 | 1414 | 2215 | 2573 | 145645 |
| MG-1001 | 39.05 | 41.1 | 18.7 | 0.362 | 0.291 | 0.179 | 0.016 | 0.03 | 99.73 | 79.66 | 1406 | 2254 | 2588 | 145412 |
| MG-1001 | 39.12 | 41.27 | 18.69 | 0.368 | 0.295 | 0.177 | 0.013 | 0.027 | 99.96 | 79.74 | 1390 | 2285 | 2630 | 145334 |
| MG-1001 | 39.14 | 41.46 | 18.63 | 0.402 | 0.288 | 0.173 | 0.017 | 0.029 | 100.13 | 79.86 | 1359 | 2231 | 2873 | 144868 |
| MG-1001 | 39.41 | 41.55 | 18.26 | 0.363 | 0.276 | 0.196 | 0.017 | 0.034 | 100.1 | 80.22 | 1540 | 2138 | 2595 | 141991 |
| MG-1001 | 39.22 | 41.71 | 18.12 | 0.357 | 0.272 | 0.192 | 0.019 | 0.037 | 99.94 | 80.4 | 1508 | 2107 | 2552 | 140902 |
| MG-1001 | 39.38 | 41.65 | 18.45 | 0.375 | 0.282 | 0.185 | 0.016 | 0.026 | 100.36 | 80.09 | 1453 | 2184 | 2680 | 143468 |
| MG-1001 | 39.33 | 42.1 | 18.1 | 0.369 | 0.287 | 0.178 | 0.017 | 0.034 | 100.41 | 80.57 | 1398 | 2223 | 2638 | 140747 |
| MG-1001 | 39.28 | 41.66 | 18.03 | 0.374 | 0.277 | 0.182 | 0.016 | 0.033 | 99.84 | 80.46 | 1430 | 2146 | 2673 | 140202 |
| MG-1001 | 39.27 | 41.71 | 17.95 | 0.369 | 0.28 | 0.183 | 0.018 | 0.031 | 99.81 | 80.55 | 1438 | 2169 | 2638 | 139580 |
| MG-1001 | 39.23 | 41.8 | 18.23 | 0.386 | 0.279 | 0.178 | 0.017 | 0.031 | 100.15 | 80.34 | 1398 | 2161 | 2759 | 141757 |
| MG-1001 | 39.37 | 41.36 | 18.57 | 0.376 | 0.287 | 0.172 | 0.011 | 0.029 | 100.18 | 79.88 | 1351 | 2223 | 2688 | 144401 |
| MG-1001 | 39.35 | 41.92 | 18.69 | 0.374 | 0.295 | 0.179 | 0.019 | 0.028 | 100.86 | 79.99 | 1406 | 2285 | 2673 | 145334 |
| MG-1001 | 39.37 | 41.84 | 18.76 | 0.382 | 0.297 | 0.173 | 0.014 | 0.031 | 100.86 | 79.9 | 1359 | 2301 | 2731 | 145879 |
| MG-1001 | 39.28 | 41.59 | 18.81 | 0.396 | 0.296 | 0.174 | 0.013 | 0.032 | 100.59 | 79.76 | 1367 | 2293 | 2831 | 146267 |
| MG-1001 | 39.27 | 41.52 | 18.77 | 0.381 | 0.298 | 0.174 | 0.018 | 0.029 | 100.47 | 79.77 | 1367 | 2308 | 2723 | 145956 |
| MG-1001 | 39.27 | 41.29 | 18.58 | 0.347 | 0.286 | 0.172 | 0.019 | 0.03 | 99.99 | 79.84 | 1351 | 2215 | 2480 | 144479 |
| MG-1001 | 39.51 | 42.73 | 16.58 | 0.385 | 0.247 | 0.188 | 0.022 | 0.029 | 99.69 | 82.12 | 1477 | 1913 | 2752 | 128927 |
| MG-1001 | 39.44 | 42.77 | 16.7 | 0.345 | 0.255 | 0.194 | 0.023 | 0.035 | 99.76 | 82.03 | 1524 | 1975 | 2466 | 129860 |
| MG-1001 | 39.13 | 42.5 | 16.77 | 0.352 | 0.256 | 0.191 | 0.029 | 0.048 | 99.27 | 81.87 | 1500 | 1983 | 2516 | 130404 |
| MG-1001 | 39.52 | 42.9 | 16.9 | 0.357 | 0.261 | 0.196 | 0.023 | 0.033 | 100.19 | 81.9 | 1540 | 2022 | 2552 | 131415 |
| MG-1001 | 39.39 | 42.4 | 17.36 | 0.353 | 0.268 | 0.197 | 0.02 | 0.032 | 100.01 | 81.32 | 1548 | 2076 | 2523 | 134992 |
| MG-1001 | 39.01 | 40.95 | 18.75 | 0.388 | 0.299 | 0.176 | 0.015 | 0.029 | 99.62 | 79.56 | 1383 | 2316 | 2773 | 145801 |
| MG-1001 | 39.32 | 42.56 | 17.43 | 0.377 | 0.263 | 0.19 | 0.024 | 0.029 | 100.2 | 81.32 | 1493 | 2037 | 2695 | 135537 |
| MG-1001 | 39.44 | 42.8 | 17.62 | 0.375 | 0.272 | 0.194 | 0.021 | 0.031 | 100.76 | 81.24 | 1524 | 2107 | 2680 | 137014 |
| MG-1001 | 39.57 | 42.65 | 17.71 | 0.392 | 0.266 | 0.192 | 0.026 | 0.027 | 100.84 | 81.1 | 1508 | 2060 | 2802 | 137714 |
| MG-1001 | 39.48 | 42.88 | 17.4 | 0.395 | 0.257 | 0.197 | 0.034 | 0.041 | 100.69 | 81.45 | 1548 | 1991 | 2823 | 135303 |

| Sample | SiO2 | MgO | FeO | CaO | MnO | NiO | Cr2O3 | Al2O3 | Total | OL Mg# | Ni ppm | Mn ppm | Ca ppm | Fe ppm |
|---|---|---|---|---|---|---|---|---|---|---|---|---|---|---|
| MG-1001 | 39.5 | 42.44 | 17.44 | 0.385 | 0.259 | 0.198 | 0.031 | 0.032 | 100.28 | 81.26 | 1555 | 2006 | 2752 | 135614 |
| MG-1001 | 39.16 | 41.74 | 18.21 | 0.38 | 0.281 | 0.185 | 0.027 | 0.05 | 100.03 | 80.34 | 1453 | 2177 | 2716 | 141602 |
| MG-1001 | 39.51 | 42.37 | 17.94 | 0.377 | 0.273 | 0.186 | 0.02 | 0.035 | 100.71 | 80.8 | 1461 | 2115 | 2695 | 139502 |
| MG-1001 | 39.52 | 42.6 | 17.67 | 0.34 | 0.268 | 0.202 | 0.034 | 0.038 | 100.67 | 81.12 | 1587 | 2076 | 2430 | 137403 |
| MG-1001 | 39.36 | 42.35 | 17.59 | 0.347 | 0.269 | 0.194 | 0.03 | 0.038 | 100.18 | 81.1 | 1524 | 2084 | 2480 | 136781 |
| MG-1001 | 39.39 | 42.48 | 17.38 | 0.379 | 0.271 | 0.189 | 0.028 | 0.034 | 100.15 | 81.33 | 1485 | 2099 | 2709 | 135148 |
| MG-1001 | 39.23 | 41.4 | 19.14 | 0.414 | 0.304 | 0.167 | 0.014 | 0.032 | 100.7 | 79.4 | 1312 | 2355 | 2959 | 148834 |
| MG-1001 | 39.33 | 41.61 | 19.05 | 0.433 | 0.298 | 0.173 | 0.015 | 0.03 | 100.94 | 79.56 | 1359 | 2308 | 3095 | 148134 |
| MG-1001 | 39.37 | 41.59 | 19.01 | 0.394 | 0.297 | 0.174 | 0.018 | 0.03 | 100.88 | 79.59 | 1367 | 2301 | 2816 | 147823 |
| MG-1001 | 39.25 | 41.51 | 18.9 | 0.406 | 0.299 | 0.173 | 0.016 | 0.03 | 100.59 | 79.65 | 1359 | 2316 | 2902 | 146967 |
| MG-1001 | 39.15 | 41.49 | 18.96 | 0.364 | 0.298 | 0.188 | 0.02 | 0.032 | 100.49 | 79.59 | 1477 | 2308 | 2602 | 147434 |
| MG-1001 | 39.24 | 41.6 | 19 | 0.364 | 0.297 | 0.182 | 0.022 | 0.045 | 100.74 | 79.6 | 1430 | 2301 | 2602 | 147745 |
| MG-1001 | 39.2 | 41.04 | 19.08 | 0.385 | 0.299 | 0.179 | 0.021 | 0.028 | 100.23 | 79.31 | 1406 | 2316 | 2752 | 148367 |
| MG-1001 | 39.08 | 40.93 | 19.2 | 0.404 | 0.3 | 0.174 | 0.019 | 0.028 | 100.14 | 79.16 | 1367 | 2324 | 2888 | 149300 |
| MG-1001 | 39.27 | 40.95 | 19.2 | 0.408 | 0.304 | 0.171 | 0.011 | 0.028 | 100.34 | 79.17 | 1343 | 2355 | 2916 | 149300 |
| MG-1001 | 39.02 | 42.03 | 17.03 | 0.379 | 0.259 | 0.191 | 0.023 | 0.03 | 98.97 | 81.48 | 1500 | 2006 | 2709 | 132426 |
| MG-1001 | 39.74 | 43.13 | 16.99 | 0.367 | 0.258 | 0.194 | 0.028 | 0.033 | 100.74 | 81.9 | 1524 | 1998 | 2623 | 132115 |
| MG-1001 | 39.42 | 42.74 | 17.02 | 0.363 | 0.259 | 0.195 | 0.025 | 0.035 | 100.06 | 81.74 | 1532 | 2006 | 2595 | 132348 |
| MG-1001 | 39.93 | 42.99 | 16.55 | 0.373 | 0.249 | 0.191 | 0.027 | 0.036 | 100.35 | 82.24 | 1500 | 1929 | 2666 | 128694 |
| MG-1001 | 39.46 | 42.88 | 16.8 | 0.399 | 0.26 | 0.197 | 0.032 | 0.028 | 100.05 | 81.98 | 1548 | 2014 | 2852 | 130638 |
| MG-1001 | 38.97 | 41.09 | 18.91 | 0.369 | 0.295 | 0.174 | 0.015 | 0.031 | 99.86 | 79.48 | 1367 | 2285 | 2638 | 147045 |
| MG-1001 | 38.89 | 40.63 | 18.66 | 0.397 | 0.289 | 0.181 | 0.014 | 0.026 | 99.1 | 79.51 | 1422 | 2239 | 2838 | 145101 |
| MG-1001 | 39.2 | 41.81 | 18.19 | 0.376 | 0.282 | 0.184 | 0.015 | 0.028 | 100.09 | 80.38 | 1445 | 2184 | 2688 | 141446 |
| MG-1001 | 39.12 | 41.22 | 18.23 | 0.38 | 0.28 | 0.184 | 0.017 | 0.023 | 99.46 | 80.12 | 1445 | 2169 | 2716 | 141757 |
| MG-1001 | 39.08 | 40.69 | 19.1 | 0.384 | 0.3 | 0.172 | 0.01 | 0.029 | 99.77 | 79.15 | 1351 | 2324 | 2745 | 148523 |
| MG-1001 | 39.93 | 44.33 | 14.72 | 0.375 | 0.218 | 0.219 | 0.04 | 0.032 | 99.86 | 84.3 | 1720 | 1689 | 2680 | 114463 |
| MG-1001 | 39.46 | 42.04 | 17.92 | 0.4 | 0.275 | 0.19 | 0.014 | 0.029 | 100.34 | 80.7 | 1493 | 2130 | 2859 | 139347 |
| MG-1001 | 39.05 | 41.18 | 19.1 | 0.417 | 0.301 | 0.171 | 0.012 | 0.027 | 100.26 | 79.35 | 1343 | 2332 | 2981 | 148523 |

| Sample | SiO2 | MgO | FeO | CaO | MnO | NiO | Cr2O3 | Al2O3 | Total | OL Mg# | Ni ppm | Mn ppm | Ca ppm | Fe ppm |
|---|---|---|---|---|---|---|---|---|---|---|---|---|---|---|
| MG-1001 | 39.02 | 41.18 | 18.93 | 0.402 | 0.295 | 0.17 | 0.015 | 0.028 | 100.03 | 79.5 | 1335 | 2285 | 2873 | 147201 |
| MG-1001 | 39.35 | 42.6 | 17.16 | 0.383 | 0.265 | 0.196 | 0.021 | 0.031 | 100.01 | 81.57 | 1540 | 2053 | 2738 | 133437 |
| MG-1001 | 39.38 | 41.98 | 17.58 | 0.383 | 0.267 | 0.194 | 0.021 | 0.03 | 99.83 | 80.97 | 1524 | 2068 | 2738 | 136703 |
| MG-1001 | 40.77 | 40.63 | 17.04 | 0.363 | 0.254 | 0.187 | 0.017 | 0.057 | 99.32 | 80.95 | 1469 | 1967 | 2595 | 132504 |
| MG-1001 | 39.37 | 41.81 | 18.26 | 0.374 | 0.276 | 0.195 | 0.017 | 0.028 | 100.33 | 80.32 | 1532 | 2138 | 2673 | 141991 |
| MG-1001 | 39.29 | 41.15 | 18.54 | 0.38 | 0.284 | 0.19 | 0.015 | 0.024 | 99.87 | 79.82 | 1493 | 2200 | 2716 | 144168 |
| MG-1001 | 39.31 | 41.88 | 18.14 | 0.376 | 0.277 | 0.182 | 0.016 | 0.028 | 100.21 | 80.45 | 1430 | 2146 | 2688 | 141058 |
| MG-1001 | 39.21 | 42.23 | 17.37 | 0.367 | 0.264 | 0.184 |  |  | 99.62 | 81.25 | 1445 | 2045 | 2623 | 135070 |
| MG-1001 | 39.19 | 42.22 | 17.45 | 0.372 | 0.265 | 0.183 |  |  | 99.68 | 81.18 | 1438 | 2053 | 2659 | 135692 |
| MG-1001 | 39.06 | 42.29 | 17.15 | 0.357 | 0.263 | 0.18 |  |  | 99.3 | 81.46 | 1414 | 2037 | 2552 | 133359 |
| MG-1001 | 39.01 | 42.71 | 17.13 | 0.359 | 0.256 | 0.181 |  |  | 99.64 | 81.63 | 1422 | 1983 | 2566 | 133204 |
| MG-1001 | 39.2 | 42.33 | 17.41 | 0.364 | 0.267 | 0.182 |  |  | 99.75 | 81.25 | 1430 | 2068 | 2602 | 135381 |
| MG-1001 | 39.16 | 42.35 | 17.53 | 0.371 | 0.268 | 0.178 |  |  | 99.85 | 81.15 | 1398 | 2076 | 2652 | 136314 |
| MG-1001 | 39.29 | 42.69 | 16.95 | 0.326 | 0.256 | 0.205 |  |  | 99.71 | 81.78 | 1610 | 1983 | 2330 | 131804 |
| MG-1001 | 39.41 | 42.8 | 16.92 | 0.323 | 0.258 | 0.204 |  |  | 99.92 | 81.85 | 1603 | 1998 | 2309 | 131571 |
| MG-1001 | 39.13 | 41.97 | 18.02 | 0.359 | 0.278 | 0.172 |  |  | 99.93 | 80.59 | 1351 | 2153 | 2566 | 140124 |
| MG-1001 | 39.12 | 42.11 | 18.07 | 0.36 | 0.276 | 0.175 |  |  | 100.11 | 80.6 | 1375 | 2138 | 2573 | 140513 |
| MG-1001 | 39.41 | 42.54 | 17.66 | 0.349 | 0.279 | 0.173 |  |  | 100.41 | 81.11 | 1359 | 2161 | 2495 | 137325 |
| MG-1001 | 39.3 | 42.65 | 17.36 | 0.364 | 0.272 | 0.178 |  |  | 100.13 | 81.41 | 1398 | 2107 | 2602 | 134992 |
| MG-1001 | 39.25 | 41.98 | 18.24 | 0.362 | 0.288 | 0.169 |  |  | 100.28 | 80.4 | 1328 | 2231 | 2588 | 141835 |
| MG-1001 | 39.06 | 41.72 | 18.24 | 0.362 | 0.287 | 0.17 |  |  | 99.83 | 80.3 | 1335 | 2223 | 2588 | 141835 |
| MG-1001 | 39.18 | 42.49 | 17.28 | 0.35 | 0.267 | 0.183 |  |  | 99.76 | 81.42 | 1438 | 2068 | 2502 | 134370 |
| MG-1001 | 39.24 | 42.42 | 17.27 | 0.349 | 0.266 | 0.184 |  |  | 99.73 | 81.41 | 1445 | 2060 | 2495 | 134292 |
| MG-1001 | 39.17 | 42.13 | 17.82 | 0.381 | 0.281 | 0.171 |  |  | 99.96 | 80.82 | 1343 | 2177 | 2723 | 138569 |
| MG-1001 | 39.49 | 42.33 | 17.8 | 0.379 | 0.281 | 0.168 |  |  | 100.45 | 80.91 | 1320 | 2177 | 2709 | 138414 |
| MG-1001 | 39.35 | 42.45 | 17.41 | 0.37 | 0.264 | 0.176 |  |  | 100.03 | 81.29 | 1379 | 2043 | 2646 | 135381 |
| MG-1001 | 39.46 | 42.55 | 17.51 | 0.373 | 0.266 | 0.18 |  |  | 100.33 | 81.24 | 1412 | 2061 | 2668 | 136159 |
| MG-1001 | 39.41 | 42.28 | 17.33 | 0.361 | 0.264 | 0.177 |  |  | 99.82 | 81.3 | 1387 | 2043 | 2579 | 134759 |

| Sample | SiO2 | MgO | FeO | CaO | MnO | NiO | Cr2O3 | Al2O3 | Total | OL Mg# | Ni ppm | Mn ppm | Ca ppm | Fe ppm |
|---|---|---|---|---|---|---|---|---|---|---|---|---|---|---|
| MG-1001 | 39.36 | 41.77 | 17.98 | 0.365 | 0.274 | 0.175 | | | 99.92 | 80.55 | 1378 | 2122 | 2608 | 139813 |
| MG-1001 | 39.45 | 41.93 | 17.9 | 0.364 | 0.273 | 0.17 | | | 100.09 | 80.68 | 1333 | 2115 | 2603 | 139191 |
| MG-1001 | 38.65 | 40.82 | 18.35 | 0.368 | 0.286 | 0.169 | | | 98.64 | 79.86 | 1328 | 2217 | 2631 | 142691 |
| MG-1001 | 38.58 | 40.94 | 18.4 | 0.372 | 0.283 | 0.171 | | | 98.75 | 79.86 | 1340 | 2189 | 2656 | 143079 |
| MG-1001 | 38.65 | 40.99 | 18.41 | 0.368 | 0.284 | 0.171 | | | 98.88 | 79.87 | 1343 | 2197 | 2628 | 143157 |
| MG-1001 | 38.6 | 41.05 | 18.17 | 0.372 | 0.284 | 0.164 | | | 98.65 | 80.11 | 1287 | 2201 | 2662 | 141291 |
| MG-1001 | 38.59 | 40.9 | 18.12 | 0.37 | 0.285 | 0.168 | | | 98.44 | 80.09 | 1317 | 2208 | 2641 | 140902 |
| MG-1001 | 38.54 | 41.03 | 18.15 | 0.373 | 0.283 | 0.171 | | | 98.55 | 80.12 | 1344 | 2191 | 2663 | 141135 |
| MG-1001 | 39.39 | 42.87 | 16.78 | 0.359 | 0.248 | 0.19 | | | 99.84 | 81.99 | 1495 | 1924 | 2568 | 130482 |
| MG-1001 | 39.54 | 43.08 | 16.73 | 0.361 | 0.246 | 0.192 | | | 100.15 | 82.11 | 1511 | 1905 | 2577 | 130093 |
| MG-1001 | 39.72 | 42.78 | 17.83 | 0.351 | 0.272 | 0.174 | | | 101.14 | 81.05 | 1368 | 2105 | 2511 | 138647 |
| MG-1001 | 39.83 | 42.85 | 17.76 | 0.353 | 0.272 | 0.176 | | | 101.24 | 81.13 | 1379 | 2105 | 2523 | 138103 |
| MG-1001 | 39.61 | 42.6 | 17.79 | 0.355 | 0.274 | 0.176 | | | 100.81 | 81.02 | 1383 | 2125 | 2539 | 138336 |
| MG-1001 | 39.75 | 42.82 | 17.82 | 0.352 | 0.272 | 0.178 | | | 101.2 | 81.07 | 1397 | 2104 | 2513 | 138569 |
| MG-1001 | 39.45 | 42.52 | 17.55 | 0.367 | 0.274 | 0.177 | | | 100.34 | 81.2 | 1390 | 2119 | 2626 | 136470 |
| MG-1001 | 39.48 | 42.59 | 17.45 | 0.373 | 0.27 | 0.176 | | | 100.33 | 81.31 | 1381 | 2093 | 2665 | 135692 |
| MG-1001 | 39.05 | 42.27 | 17.13 | 0.36 | 0.25 | 0.177 | | | 99.24 | 81.47 | 1391 | 1940 | 2570 | 133204 |
| MG-1001 | 38.98 | 42.06 | 17.1 | 0.353 | 0.25 | 0.179 | | | 98.92 | 81.43 | 1404 | 1933 | 2522 | 132970 |
| MG-1001 | 38.91 | 41.78 | 17.17 | 0.367 | 0.264 | 0.186 | | | 98.68 | 81.26 | 1460 | 2048 | 2620 | 133515 |
| MG-1001 | 39.1 | 42.19 | 17.2 | 0.375 | 0.264 | 0.187 | | | 99.32 | 81.38 | 1465 | 2043 | 2680 | 133748 |
| MG-1001 | 38.9 | 41.96 | 16.6 | 0.361 | 0.248 | 0.181 | | | 98.25 | 81.84 | 1423 | 1923 | 2583 | 129082 |
| MG-1001 | 40.05 | 43.63 | 16.74 | 0.364 | 0.249 | 0.191 | | | 101.22 | 82.29 | 1497 | 1929 | 2598 | 130171 |
| MG-1001 | 40.12 | 43.63 | 16.74 | 0.363 | 0.245 | 0.189 | | | 101.28 | 82.29 | 1483 | 1894 | 2591 | 130171 |
| MG-1001 | 39.85 | 43.38 | 16.78 | 0.366 | 0.249 | 0.184 | | | 100.81 | 82.17 | 1444 | 1928 | 2613 | 130482 |
| MG-1001 | 40.25 | 43.67 | 16.73 | 0.358 | 0.245 | 0.189 | | | 101.44 | 82.31 | 1485 | 1895 | 2557 | 130093 |
| MG-1001 | 38.21 | 40.14 | 18.12 | 0.367 | 0.286 | 0.172 | | | 97.29 | 79.79 | 1348 | 2215 | 2620 | 140902 |
| MG-1001 | 39.75 | 42.67 | 17.53 | 0.367 | 0.271 | 0.183 | | | 100.78 | 81.27 | 1434 | 2098 | 2622 | 136314 |
| MG-1001 | 39.99 | 42.82 | 17.45 | 0.37 | 0.268 | 0.18 | | | 101.07 | 81.39 | 1412 | 2074 | 2645 | 135692 |

| Sample | SiO2 | MgO | FeO | CaO | MnO | NiO | Cr2O3 | Al2O3 | Total | OL Mg# | Ni ppm | Mn ppm | Ca ppm | Fe ppm |
|---|---|---|---|---|---|---|---|---|---|---|---|---|---|---|
| MG-1001 | 39.4 | 42.15 | 17.49 | 0.369 | 0.27 | 0.184 | | | 99.86 | 81.12 | 1445 | 2094 | 2637 | 136003 |
| MG-1001 | 39.32 | 42.08 | 17.7 | 0.367 | 0.274 | 0.173 | | | 99.91 | 80.91 | 1360 | 2121 | 2620 | 137636 |
| MG-1001 | 39.36 | 42.2 | 17.69 | 0.369 | 0.276 | 0.173 | | | 100.07 | 80.96 | 1356 | 2138 | 2634 | 137558 |
| MG-1001 | 39.72 | 43.18 | 16.74 | 0.358 | 0.246 | 0.191 | | | 100.43 | 82.13 | 1501 | 1909 | 2558 | 130171 |
| MG-1001 | 39.66 | 43.14 | 16.76 | 0.357 | 0.247 | 0.19 | | | 100.35 | 82.1 | 1491 | 1910 | 2555 | 130327 |
| MG-1001 | 39.45 | 42.8 | 16.44 | 0.361 | 0.241 | 0.192 | | | 99.48 | 82.27 | 1505 | 1866 | 2579 | 127838 |
| MG-1001 | 39.56 | 42.76 | 16.38 | 0.363 | 0.243 | 0.189 | | | 99.49 | 82.31 | 1487 | 1885 | 2597 | 127372 |
| MG-1001 | 39.6 | 43.1 | 16.86 | 0.373 | 0.251 | 0.189 | | | 100.38 | 82 | 1483 | 1946 | 2666 | 131104 |
| MG-1001 | 39.63 | 43.12 | 16.87 | 0.373 | 0.249 | 0.191 | | | 100.42 | 82 | 1500 | 1925 | 2667 | 131182 |
| MG-1001 | 39.35 | 42.26 | 17.35 | 0.347 | 0.255 | 0.192 | | | 99.75 | 81.28 | 1511 | 1975 | 2481 | 134914 |
| MG-1001 | 39.49 | 42.48 | 17.37 | 0.344 | 0.253 | 0.197 | | | 100.12 | 81.34 | 1548 | 1961 | 2462 | 135070 |
| MG-1001 | 39.2 | 42.25 | 17 | 0.36 | 0.258 | 0.184 | | | 99.26 | 81.58 | 1444 | 1999 | 2576 | 132193 |
| MG-1001 | 38.98 | 42.1 | 17.04 | 0.362 | 0.257 | 0.188 | | | 98.93 | 81.49 | 1474 | 1988 | 2584 | 132504 |
| MG-1001 | 39.53 | 42.72 | 16.55 | 0.374 | 0.256 | 0.187 | | | 99.61 | 82.14 | 1465 | 1982 | 2672 | 128694 |
| MG-1001 | 39.6 | 42.73 | 16.51 | 0.374 | 0.25 | 0.189 | | | 99.66 | 82.18 | 1483 | 1934 | 2673 | 128383 |
| MG-1001 | 39.09 | 41.44 | 17.36 | 0.361 | 0.269 | 0.18 | | | 98.7 | 80.97 | 1415 | 2084 | 2582 | 134992 |
| MG-1001 | 39.33 | 41.85 | 17.53 | 0.361 | 0.272 | 0.18 | | | 99.52 | 80.97 | 1411 | 2103 | 2577 | 136314 |
| MG-1001 | 38.94 | 41.64 | 17.72 | 0.36 | 0.284 | 0.172 | | | 99.11 | 80.73 | 1350 | 2198 | 2570 | 137792 |
| MG-1001 | 38.73 | 41.18 | 17.59 | 0.355 | 0.282 | 0.175 | | | 98.32 | 80.67 | 1371 | 2187 | 2536 | 136781 |
| MG-1001 | 39.33 | 42.2 | 17.15 | 0.354 | 0.266 | 0.176 | | | 99.48 | 81.43 | 1379 | 2064 | 2529 | 133359 |
| MG-1001 | 39.39 | 42.24 | 17.14 | 0.354 | 0.269 | 0.175 | | | 99.58 | 81.46 | 1372 | 2084 | 2528 | 133281 |
| MG-1001 | 39.8 | 43.37 | 16.23 | 0.366 | 0.249 | 0.184 | | | 100.2 | 82.65 | 1448 | 1930 | 2619 | 126205 |
| MG-1001 | 39.95 | 43.46 | 16.14 | 0.365 | 0.247 | 0.182 | | | 100.34 | 82.76 | 1430 | 1913 | 2608 | 125505 |
| MG-1001 | 39.35 | 42.65 | 16.48 | 0.374 | 0.26 | 0.185 | | | 99.3 | 82.18 | 1451 | 2016 | 2674 | 128149 |
| MG-1001 | 39.27 | 42.74 | 16.52 | 0.374 | 0.262 | 0.183 | | | 99.34 | 82.18 | 1435 | 2029 | 2675 | 128460 |
| MG-1001 | 39.07 | 42.21 | 17.04 | 0.385 | 0.263 | 0.183 | | | 99.15 | 81.53 | 1438 | 2040 | 2754 | 132504 |
| MG-1001 | 38.85 | 42.08 | 17 | 0.382 | 0.266 | 0.182 | | | 98.76 | 81.52 | 1429 | 2063 | 2731 | 132193 |
| MG-1002 | 39.25 | 41.74 | 18.05 | 0.36 | 0.28 | 0.181 | | | 99.86 | 80.47 | 1422 | 2169 | 2573 | 140358 |

| Sample | SiO2 | MgO | FeO | CaO | MnO | NiO | Cr2O3 | Al2O3 | Total | OL Mg# | Ni ppm | Mn ppm | Ca ppm | Fe ppm |
|---|---|---|---|---|---|---|---|---|---|---|---|---|---|---|
| MG-1002 | 39.3 | 41.73 | 18.17 | 0.369 | 0.281 | 0.178 | | | 100.03 | 80.37 | 1398 | 2177 | 2638 | 141291 |
| MG-1002 | 38.82 | 41.82 | 17.15 | 0.373 | 0.255 | 0.2 | | | 98.63 | 81.29 | 1569 | 1976 | 2665 | 133359 |
| MG-1002 | 39.01 | 42.36 | 16.45 | 0.376 | 0.242 | 0.204 | | | 98.64 | 82.11 | 1602 | 1871 | 2685 | 127916 |
| MG-1002 | 38.73 | 40.7 | 18.97 | 0.384 | 0.288 | 0.171 | | | 99.25 | 79.27 | 1346 | 2228 | 2744 | 147512 |
| MG-1002 | 38.71 | 40.84 | 18.97 | 0.394 | 0.289 | 0.171 | | | 99.38 | 79.33 | 1342 | 2238 | 2814 | 147512 |
| MG-1002 | 38.28 | 40.17 | 19.28 | 0.412 | 0.304 | 0.162 | | | 98.61 | 78.78 | 1274 | 2357 | 2941 | 149922 |
| MG-1002 | 38.24 | 39.94 | 19.43 | 0.408 | 0.306 | 0.157 | | | 98.48 | 78.56 | 1233 | 2368 | 2916 | 151089 |
| MAGB-25 | 39.17 | 41.6 | 17.41 | 0.4 | 0.265 | 0.178 | | | 99.02 | 80.98 | 1398 | 2053 | 2859 | 135381 |
| MAGB-25 | 39.44 | 42.12 | 17.47 | 0.4 | 0.267 | 0.179 | | | 99.88 | 81.12 | 1408 | 2066 | 2856 | 135848 |
| MAGB-25 | 39.77 | 42.07 | 18.25 | 0.393 | 0.281 | 0.175 | | | 100.93 | 80.42 | 1375 | 2173 | 2808 | 141913 |
| MAGB-25 | 39.8 | 42.04 | 18.24 | 0.393 | 0.282 | 0.173 | | | 100.93 | 80.42 | 1360 | 2184 | 2809 | 141835 |
| MAGB-25 | 39.66 | 41.95 | 18.27 | 0.392 | 0.279 | 0.176 | | | 100.73 | 80.36 | 1379 | 2160 | 2800 | 142068 |
| MAGB-25 | 39.85 | 42.79 | 17.3 | 0.404 | 0.265 | 0.181 | | | 100.78 | 81.51 | 1419 | 2056 | 2885 | 134526 |
| MAGB-25 | 39.52 | 42.55 | 17.33 | 0.41 | 0.265 | 0.184 | | | 100.26 | 81.4 | 1447 | 2052 | 2930 | 134759 |
| MAGB-25 | 38.96 | 42.18 | 16.92 | 0.386 | 0.268 | 0.189 | | | 98.91 | 81.63 | 1485 | 2073 | 2762 | 131571 |
| MAGB-25 | 38.63 | 41.93 | 17.01 | 0.369 | 0.267 | 0.191 | | | 98.39 | 81.46 | 1499 | 2067 | 2640 | 132271 |
| MAGB-25 | 39.85 | 43.43 | 16.05 | 0.405 | 0.245 | 0.191 | | | 100.18 | 82.83 | 1504 | 1899 | 2897 | 124806 |
| MAGB-25 | 39.74 | 43.29 | 16.22 | 0.403 | 0.25 | 0.194 | | | 100.1 | 82.63 | 1522 | 1933 | 2881 | 126128 |
| MAGB-25 | 39.03 | 42.09 | 17.31 | 0.409 | 0.266 | 0.182 | | | 99.28 | 81.25 | 1429 | 2060 | 2921 | 134603 |
| MAGB-25 | 39.21 | 42.12 | 17.38 | 0.41 | 0.274 | 0.176 | | | 99.57 | 81.2 | 1386 | 2119 | 2929 | 135148 |
| MAGB-25 | 39.62 | 43.17 | 16.06 | 0.405 | 0.245 | 0.188 | | | 99.68 | 82.73 | 1474 | 1895 | 2896 | 124883 |
| MAGB-47 | 38.81 | 41.09 | 18.05 | 0.384 | 0.274 | 0.191 | | | 98.8 | 80.23 | 1502 | 2124 | 2743 | 140358 |
| MAGB-47 | 39.16 | 41.62 | 18.14 | 0.39 | 0.279 | 0.194 | | | 99.78 | 80.35 | 1522 | 2158 | 2791 | 141058 |
| MAGB-47 | 39.15 | 41.74 | 17.11 | 0.378 | 0.252 | 0.201 | | | 98.83 | 81.3 | 1580 | 1949 | 2705 | 133048 |
| MAGB-47 | 39.4 | 42.02 | 17 | 0.377 | 0.253 | 0.204 | | | 99.26 | 81.5 | 1601 | 1957 | 2695 | 132193 |
| MAGB-47 | 39.87 | 42.56 | 17.52 | 0.377 | 0.259 | 0.192 | | | 100.78 | 81.24 | 1509 | 2005 | 2691 | 136236 |
| MAGB-47 | 39.87 | 42.37 | 17.37 | 0.373 | 0.261 | 0.194 | | | 100.43 | 81.3 | 1523 | 2024 | 2663 | 135070 |
| MAGB-47 | 39.44 | 43.72 | 14.7 | 0.395 | 0.215 | 0.238 | | | 98.72 | 84.13 | 1867 | 1668 | 2824 | 114308 |

| Sample | SiO2 | MgO | FeO | CaO | MnO | NiO | Cr2O3 | Al2O3 | Total | OL Mg# | Ni ppm | Mn ppm | Ca ppm | Fe ppm |
|---|---|---|---|---|---|---|---|---|---|---|---|---|---|---|
| MAGB-47 | 39.48 | 43.48 | 14.63 | 0.395 | 0.218 | 0.237 | | | 98.44 | 84.12 | 1863 | 1689 | 2821 | 113764 |
| MAGB-47 | 39.53 | 41.76 | 17.55 | 0.39 | 0.263 | 0.19 | | | 99.67 | 80.92 | 1492 | 2039 | 2784 | 136470 |
| MAGB-47 | 39.19 | 41.67 | 17.65 | 0.395 | 0.272 | 0.19 | | | 99.37 | 80.8 | 1495 | 2106 | 2821 | 137247 |
| MAGB-47 | 40.26 | 44.85 | 14.83 | 0.363 | 0.219 | 0.229 | | | 100.75 | 84.35 | 1800 | 1692 | 2594 | 115319 |
| MAGB-47 | 40.63 | 45.21 | 14.71 | 0.379 | 0.22 | 0.225 | | | 101.38 | 84.56 | 1766 | 1700 | 2710 | 114386 |
| MAGB-47 | 39.11 | 43.1 | 15.52 | 0.376 | 0.23 | 0.222 | | | 98.55 | 83.19 | 1746 | 1784 | 2686 | 120684 |
| MAGB-47 | 38.97 | 42.9 | 15.45 | 0.382 | 0.229 | 0.22 | | | 98.16 | 83.19 | 1724 | 1770 | 2728 | 120140 |
| MAGB-47 | 40.47 | 46.03 | 13.42 | 0.359 | 0.19 | 0.253 | | | 100.72 | 85.94 | 1990 | 1474 | 2565 | 104355 |
| MAGB-47 | 40.56 | 46.12 | 13.43 | 0.364 | 0.192 | 0.253 | | | 100.92 | 85.96 | 1987 | 1490 | 2598 | 104432 |
| MAGB-47 | 39.38 | 41.81 | 18 | 0.413 | 0.272 | 0.195 | | | 100.08 | 80.54 | 1532 | 2108 | 2950 | 139969 |
| MAGB-47 | 39.44 | 41.85 | 18.14 | 0.418 | 0.277 | 0.192 | | | 100.31 | 80.44 | 1505 | 2143 | 2989 | 141058 |
| MAGB-47 | 40.21 | 44.83 | 14.76 | 0.398 | 0.222 | 0.226 | | | 100.64 | 84.41 | 1775 | 1718 | 2847 | 114774 |
| MAGB-47 | 40.17 | 44.82 | 14.8 | 0.398 | 0.22 | 0.231 | | | 100.64 | 84.37 | 1815 | 1706 | 2844 | 115086 |
| MAGB-47 | 39.23 | 41.79 | 18.31 | 0.356 | 0.278 | 0.198 | | | 100.16 | 80.27 | 1557 | 2156 | 2547 | 142379 |
| MAGB-47 | 39.31 | 41.81 | 18.34 | 0.357 | 0.277 | 0.196 | | | 100.29 | 80.25 | 1541 | 2143 | 2550 | 142613 |
| MAGB-47 | 39.34 | 44.94 | 13.01 | 0.42 | 0.196 | 0.254 | | | 98.16 | 86.03 | 1997 | 1517 | 3001 | 101166 |
| MAGB-47 | 40.08 | 45.97 | 12.88 | 0.407 | 0.194 | 0.253 | | | 99.77 | 86.42 | 1987 | 1505 | 2907 | 100156 |
| MAGB-47 | 40.1 | 45.44 | 13.02 | 0.373 | 0.199 | 0.242 | | | 99.38 | 86.15 | 1901 | 1541 | 2668 | 101244 |
| MAGB-47 | 39.96 | 45.34 | 13.03 | 0.375 | 0.2 | 0.247 | | | 99.15 | 86.11 | 1937 | 1551 | 2677 | 101322 |
| MAGB-47 | 39.73 | 44.37 | 14.83 | 0.371 | 0.226 | 0.228 | | | 99.75 | 84.21 | 1790 | 1750 | 2650 | 115319 |
| MG1006_Norm_Zone_Olivine1 | 39.65 | 43.01 | 16.55 | 0.318 | 0.247 | 0.209 | | | 99.99 | 82.24 | 1642 | 1913 | 2273 | 128694 |
| MG1006_Norm_Zone_Olivine1 | 39.29 | 41.68 | 18.12 | 0.399 | 0.278 | 0.189 | | | 99.95 | 80.39 | 1485 | 2153 | 2852 | 140902 |
| MG1006_Norm_Zone_Olivine1 | 39.46 | 42.33 | 17.53 | 0.345 | 0.267 | 0.207 | | | 100.14 | 81.15 | 1626 | 2068 | 2466 | 136314 |
| MG1006_Norm_Zone_Olivine1 | 39.51 | 42.67 | 16.99 | 0.35 | 0.253 | 0.203 | | | 99.98 | 81.74 | 1595 | 1960 | 2502 | 132115 |
| MG1006_Norm_Zone_Olivine1 | 39.3 | 41.68 | 18.34 | 0.45 | 0.286 | 0.191 | | | 100.25 | 80.2 | 1500 | 2215 | 3217 | 142613 |
| MG1006_Norm_Zone_Olivine2 | 39.72 | 43.65 | 16.19 | 0.337 | 0.238 | 0.211 | | | 100.35 | 82.77 | 1658 | 1844 | 2409 | 125894 |
| MG1006_Norm_Zone_Olivine2 | 39.6 | 43.4 | 16.31 | 0.343 | 0.244 | 0.209 | | | 100.1 | 82.59 | 1642 | 1890 | 2452 | 126827 |
| MG1006_Norm_Zone_Olivine2 | 39.43 | 42.61 | 17.22 | 0.365 | 0.26 | 0.2 | | | 100.08 | 81.52 | 1571 | 2014 | 2609 | 133904 |

| Sample | SiO2 | MgO | FeO | CaO | MnO | NiO | Cr2O3 | Al2O3 | Total | OL Mg# | Ni ppm | Mn ppm | Ca ppm | Fe ppm |
|---|---|---|---|---|---|---|---|---|---|---|---|---|---|---|
| MG1006_Norm_Zone_Olivine2 | 38.86 | 40.12 | 19.94 | 0.529 | 0.309 | 0.164 | | | 99.91 | 78.19 | 1288 | 2393 | 3781 | 155054 |
| MG1006_Norm_Zone_Olivine3 | 39.21 | 42.41 | 16.94 | 0.36 | 0.241 | 0.153 | | | 99.31 | 81.69 | 1202 | 1867 | 2573 | 131726 |
| MG1006_Norm_Zone_Olivine3 | 39.34 | 42.6 | 16.91 | 0.383 | 0.241 | 0.166 | | | 99.65 | 81.79 | 1304 | 1867 | 2738 | 131493 |
| MG1006_Norm_Zone_Olivine3 | 39.08 | 41.91 | 17.57 | 0.371 | 0.265 | 0.182 | | | 99.38 | 80.96 | 1430 | 2053 | 2652 | 136625 |
| MG1006_Norm_Zone_Olivine3 | 38.73 | 40.78 | 18.64 | 0.465 | 0.292 | 0.187 | | | 99.09 | 79.59 | 1469 | 2262 | 3324 | 144946 |
| MG1006_Norm_Zone_Olivine3 | 38.72 | 40.07 | 18.17 | 0.54 | 0.288 | 0.177 | | | 97.97 | 79.72 | 1390 | 2231 | 3860 | 141291 |
| MG1006_Norm_Zone_Olivine4 | 39.86 | 44.32 | 15.08 | 0.283 | 0.215 | 0.256 | | | 100.01 | 83.97 | 2011 | 1665 | 2023 | 117263 |
| MG1006_Norm_Zone_Olivine4 | 39.59 | 43.36 | 16.04 | 0.316 | 0.236 | 0.225 | | | 99.77 | 82.81 | 1767 | 1828 | 2259 | 124728 |
| MG1006_Norm_Zone_Olivine4 | 39.18 | 41.27 | 18.44 | 0.453 | 0.288 | 0.187 | | | 99.82 | 79.96 | 1469 | 2231 | 3238 | 143390 |
| MG1006_Norm_Zone_Olivine4 | 39.21 | 41.52 | 18.18 | 0.427 | 0.281 | 0.187 | | | 99.81 | 80.28 | 1469 | 2177 | 3052 | 141369 |
| MG1006_Norm_Zone_Olivine5 | 39.09 | 41.97 | 17.61 | 0.352 | 0.264 | 0.201 | | | 99.49 | 80.94 | 1579 | 2045 | 2516 | 136936 |
| MG1006_Norm_Zone_Olivine5 | 38.98 | 41.29 | 18.39 | 0.446 | 0.287 | 0.191 | | | 99.58 | 80.01 | 1500 | 2223 | 3188 | 143002 |
| MG1006_Norm_Zone_Olivine6 | 39.56 | 43.52 | 15.78 | 0.301 | 0.233 | 0.232 | | | 99.63 | 83.1 | 1822 | 1805 | 2152 | 122706 |
| MG1006_Norm_Zone_Olivine6 | 39.57 | 43.33 | 16.11 | 0.315 | 0.24 | 0.22 | | | 99.78 | 82.74 | 1728 | 1859 | 2252 | 125272 |
| MG1006_Norm_Zone_Olivine6 | 39.36 | 42.45 | 17.07 | 0.34 | 0.255 | 0.198 | | | 99.68 | 81.59 | 1555 | 1975 | 2430 | 132737 |
| MG1006_Norm_Zone_Olivine6 | 39.25 | 41.62 | 18.06 | 0.404 | 0.279 | 0.194 | | | 99.81 | 80.42 | 1524 | 2161 | 2888 | 140435 |
| MG1006_Norm_Zone_Olivine7 | 39.61 | 43.43 | 16.12 | 0.304 | 0.232 | 0.233 | | | 99.93 | 82.76 | 1830 | 1797 | 2173 | 125350 |
| MG1006_Norm_Zone_Olivine7 | 39.5 | 43.08 | 16.55 | 0.309 | 0.244 | 0.222 | | | 99.91 | 82.27 | 1744 | 1890 | 2209 | 128694 |
| MG1006_Norm_Zone_Olivine7 | 39.18 | 41.7 | 17.97 | 0.387 | 0.275 | 0.196 | | | 99.7 | 80.53 | 1540 | 2130 | 2766 | 139736 |
| MG1006_Norm_Zone_Olivine7 | 38.97 | 40.82 | 18.94 | 0.474 | 0.297 | 0.176 | | | 99.68 | 79.34 | 1383 | 2301 | 3388 | 147278 |
| MG1006_Norm_Zone_Olivine8 | 39.6 | 43.5 | 15.99 | 0.301 | 0.234 | 0.223 | | | 99.84 | 82.9 | 1752 | 1813 | 2152 | 124339 |
| MG1006_Norm_Zone_Olivine8 | 39.4 | 42.52 | 17.01 | 0.344 | 0.258 | 0.205 | | | 99.74 | 81.67 | 1610 | 1998 | 2459 | 132271 |
| MG1006_Norm_Zone_Olivine8 | 39.27 | 41.71 | 18.1 | 0.399 | 0.282 | 0.192 | | | 99.97 | 80.42 | 1508 | 2184 | 2852 | 140747 |
| MG1006_Norm_Zone_Olivine8 | 39.11 | 41.15 | 18.48 | 0.452 | 0.286 | 0.181 | | | 99.66 | 79.87 | 1422 | 2215 | 3231 | 143701 |
| MG1006_Norm_Zone_Olivine9 | 39.77 | 43.85 | 15.64 | 0.295 | 0.232 | 0.238 | | | 100.03 | 83.33 | 1870 | 1797 | 2109 | 121617 |
| MG1006_Norm_Zone_Olivine9 | 39.64 | 43.59 | 15.83 | 0.297 | 0.233 | 0.227 | | | 99.82 | 83.07 | 1783 | 1805 | 2123 | 123095 |
| MG1006_Norm_Zone_Olivine9 | 39.61 | 43.18 | 16.49 | 0.319 | 0.245 | 0.213 | | | 100.06 | 82.35 | 1673 | 1898 | 2280 | 128227 |
| MG1006_Norm_Zone_Olivine9 | 39.4 | 42.06 | 17.79 | 0.381 | 0.275 | 0.192 | | | 100.09 | 80.82 | 1508 | 2130 | 2723 | 138336 |

| Sample | SiO2 | MgO | FeO | CaO | MnO | NiO | Cr2O3 | Al2O3 | Total | OL Mg# | Ni ppm | Mn ppm | Ca ppm | Fe ppm |
|---|---|---|---|---|---|---|---|---|---|---|---|---|---|---|
| MG1006_Norm_Zone_Olivine10 | 39.4 | 42.69 | 16.96 | 0.333 | 0.254 | 0.202 | | | 99.84 | 81.77 | 1587 | 1967 | 2380 | 131882 |
| MG1006_Norm_Zone_Olivine10 | 39.47 | 43.22 | 16.31 | 0.333 | 0.247 | 0.199 | | | 99.78 | 82.53 | 1563 | 1913 | 2380 | 126827 |
| MG1006_Norm_Zone_Olivine10 | 39.36 | 42.75 | 16.86 | 0.336 | 0.249 | 0.201 | | | 99.76 | 81.88 | 1579 | 1929 | 2402 | 131104 |
| MG1006_Norm_Zone_Olivine11 | 39.4 | 42.59 | 17.04 | 0.336 | 0.256 | 0.204 | | | 99.83 | 81.67 | 1603 | 1983 | 2402 | 132504 |
| MG1006_Rev_Zone_Olivine0 | 38.01 | 38.12 | 21.31 | 0.3115 | 0.334 | 0.137 | | | 98.21 | 76.12 | 1079 | 2584 | 2227 | 165676 |
| MG1006_Rev_Zone_Olivine0 | 37.79 | 38.12 | 21.40 | 0.3110 | 0.331 | 0.138 | | | 98.09 | 76.05 | 1080 | 2564 | 2223 | 166424 |
| MG1006_Rev_Zone_Olivine0 | 38.70 | 38.62 | 21.79 | 0.2986 | 0.329 | 0.110 | | | 99.85 | 75.95 | 862 | 2549 | 2134 | 169469 |
| MG1006_Rev_Zone_Olivine0 | 38.46 | 38.41 | 21.80 | 0.3005 | 0.331 | 0.108 | | | 99.42 | 75.85 | 847 | 2564 | 2148 | 169517 |
| MG1006_Rev_Zone_Olivine0 | 38.72 | 39.21 | 21.11 | 0.2814 | 0.319 | 0.124 | | | 99.77 | 76.80 | 977 | 2472 | 2012 | 164163 |
| MG1006_Rev_Zone_Olivine0 | 38.60 | 39.13 | 21.09 | 0.2829 | 0.317 | 0.123 | | | 99.55 | 76.78 | 965 | 2458 | 2022 | 163998 |
| MG1006_Rev_Zone_Olivine1 | 38.85 | 39.84 | 20.39 | 0.27 | 0.283 | 0.154 | | | 99.79 | 77.69 | 1210 | 2192 | 1930 | 158554 |
| MG1006_Rev_Zone_Olivine1 | 38.78 | 39.79 | 20.34 | 0.269 | 0.279 | 0.153 | | | 99.6 | 77.71 | 1202 | 2161 | 1923 | 158165 |
| MG1006_Rev_Zone_Olivine1 | 38.86 | 39.98 | 20.29 | 0.272 | 0.28 | 0.15 | | | 99.83 | 77.84 | 1178 | 2169 | 1944 | 157776 |
| MG1006_Rev_Zone_Olivine1 | 39.05 | 40.77 | 19.29 | 0.274 | 0.274 | 0.167 | | | 99.83 | 79.02 | 1312 | 2122 | 1959 | 150000 |
| MG1006_Rev_Zone_Olivine1 | 39.26 | 41.51 | 18.35 | 0.374 | 0.28 | 0.189 | | | 99.96 | 80.13 | 1485 | 2169 | 2673 | 142691 |
| MG1006_Rev_Zone_Olivine2 | 38.51 | 38.65 | 21.95 | 0.279 | 0.337 | 0.097 | | | 99.82 | 75.84 | 762 | 2610 | 1994 | 170684 |
| MG1006_Rev_Zone_Olivine2 | 38.58 | 38.73 | 22.04 | 0.275 | 0.336 | 0.094 | | | 100.06 | 75.8 | 738 | 2603 | 1966 | 171384 |
| MG1006_Rev_Zone_Olivine2 | 38.5 | 38.83 | 21.76 | 0.273 | 0.332 | 0.094 | | | 99.79 | 76.08 | 738 | 2572 | 1951 | 169207 |
| MG1006_Rev_Zone_Olivine2 | 38.8 | 40.42 | 20.09 | 0.304 | 0.308 | 0.134 | | | 100.05 | 78.19 | 1053 | 2386 | 2173 | 156221 |
| MG1006_Rev_Zone_Olivine2 | 39.02 | 41.08 | 18.84 | 0.425 | 0.296 | 0.178 | | | 99.84 | 79.53 | 1398 | 2293 | 3038 | 146501 |
| MG1006_Rev_Zone_Olivine3 | 39.01 | 41.14 | 19.06 | 0.295 | 0.276 | 0.16 | | | 99.94 | 79.37 | 1257 | 2138 | 2109 | 148212 |
| MG1006_Rev_Zone_Olivine3 | 39.04 | 41.28 | 18.88 | 0.31 | 0.275 | 0.174 | | | 99.96 | 79.58 | 1367 | 2130 | 2216 | 146812 |
| MG1006_Rev_Zone_Olivine3 | 39.04 | 41.34 | 18.91 | 0.309 | 0.276 | 0.173 | | | 100.04 | 79.58 | 1359 | 2138 | 2209 | 147045 |
| MG1006_Rev_Zone_Olivine3 | 39.27 | 42.18 | 17.95 | 0.344 | 0.273 | 0.196 | | | 100.21 | 80.73 | 1540 | 2115 | 2459 | 139580 |
| MG1006_Rev_Zone_Olivine4 | 38.64 | 39.97 | 20.46 | 0.286 | 0.282 | 0.151 | | | 99.79 | 77.69 | 1186 | 2184 | 2044 | 159098 |
| MG1006_Rev_Zone_Olivine4 | 38.74 | 39.99 | 20.47 | 0.286 | 0.28 | 0.15 | | | 99.92 | 77.69 | 1178 | 2169 | 2044 | 159176 |
| MG1006_Rev_Zone_Olivine4 | 38.79 | 40.07 | 20.54 | 0.291 | 0.284 | 0.15 | | | 100.12 | 77.66 | 1178 | 2200 | 2080 | 159720 |
| MG1006_Rev_Zone_Olivine4 | 38.67 | 39.96 | 20.41 | 0.287 | 0.285 | 0.152 | | | 99.76 | 77.73 | 1194 | 2208 | 2051 | 158709 |

| Sample | SiO2 | MgO | FeO | CaO | MnO | NiO | Cr2O3 | Al2O3 | Total | OL Mg# | Ni ppm | Mn ppm | Ca ppm | Fe ppm |
|---|---|---|---|---|---|---|---|---|---|---|---|---|---|---|
| MG1006_Rev_Zone_Olivine4 | 38.9 | 40.9 | 19.38 | 0.307 | 0.288 | 0.163 | | | 99.94 | 79 | 1280 | 2231 | 2194 | 150700 |
| MG1006_Rev_Zone_Olivine4 | 38.96 | 41.24 | 18.67 | 0.403 | 0.286 | 0.185 | | | 99.75 | 79.74 | 1453 | 2215 | 2881 | 145179 |
| MG1006_Rev_Zone_Olivine5 | 38.92 | 40.81 | 19.54 | 0.253 | 0.279 | 0.147 | | | 99.95 | 78.82 | 1155 | 2161 | 1808 | 151944 |
| MG1006_Rev_Zone_Olivine5 | 39.21 | 41.86 | 18.23 | 0.276 | 0.269 | 0.151 | | | 100 | 80.36 | 1186 | 2084 | 1973 | 141757 |
| MG1006_Rev_Zone_Olivine5 | 39.44 | 43.18 | 16.49 | 0.308 | 0.245 | 0.193 | | | 99.86 | 82.35 | 1516 | 1898 | 2202 | 128227 |
| MG1006_Rev_Zone_Olivine5 | 39.08 | 41.72 | 18.02 | 0.393 | 0.279 | 0.19 | | | 99.69 | 80.49 | 1493 | 2161 | 2809 | 140124 |
| MG1006_Rev_Zone_Olivine6 | 38.63 | 39.48 | 20.93 | 0.321 | 0.304 | 0.139 | | | 99.79 | 77.07 | 1092 | 2355 | 2294 | 162753 |
| MG1006_Rev_Zone_Olivine6 | 38.71 | 39.61 | 20.93 | 0.317 | 0.301 | 0.143 | | | 100.02 | 77.13 | 1123 | 2332 | 2266 | 162753 |
| MG1006_Rev_Zone_Olivine6 | 38.65 | 39.54 | 20.94 | 0.316 | 0.302 | 0.141 | | | 99.89 | 77.09 | 1108 | 2339 | 2259 | 162830 |
| MG1006_Rev_Zone_Olivine6 | 38.7 | 39.6 | 20.94 | 0.312 | 0.304 | 0.142 | | | 100 | 77.12 | 1115 | 2355 | 2230 | 162830 |
| MG1006_Rev_Zone_Olivine6 | 38.71 | 39.57 | 20.94 | 0.308 | 0.303 | 0.141 | | | 99.98 | 77.11 | 1108 | 2347 | 2202 | 162830 |
| MG1006_Rev_Zone_Olivine6 | 38.76 | 39.61 | 21.01 | 0.31 | 0.304 | 0.139 | | | 100.13 | 77.06 | 1092 | 2355 | 2216 | 163375 |
| MG1006_Rev_Zone_Olivine6 | 38.65 | 39.51 | 20.98 | 0.3 | 0.299 | 0.137 | | | 99.88 | 77.05 | 1076 | 2316 | 2144 | 163142 |
| MG1006_Rev_Zone_Olivine6 | 38.91 | 40.51 | 19.84 | 0.301 | 0.292 | 0.143 | | | 100 | 78.44 | 1123 | 2262 | 2152 | 154277 |
| MG1006_Rev_Zone_Olivine6 | 39.07 | 41.23 | 18.71 | 0.466 | 0.289 | 0.186 | | | 99.96 | 79.71 | 1461 | 2239 | 3331 | 145490 |
| MG1006_Rev_Zone_Olivine7 | 38.76 | 39.95 | 20.39 | 0.283 | 0.283 | 0.152 | | | 99.82 | 77.74 | 1194 | 2192 | 2023 | 158554 |
| MG1006_Rev_Zone_Olivine7 | 38.77 | 40.04 | 20.42 | 0.279 | 0.281 | 0.154 | | | 99.94 | 77.75 | 1210 | 2177 | 1994 | 158787 |
| MG1006_Rev_Zone_Olivine7 | 38.79 | 40.41 | 19.88 | 0.281 | 0.282 | 0.156 | | | 99.79 | 78.37 | 1225 | 2184 | 2009 | 154588 |
| MG1006_Rev_Zone_Olivine7 | 38.92 | 41.32 | 18.71 | 0.395 | 0.284 | 0.184 | | | 99.81 | 79.74 | 1445 | 2200 | 2823 | 145490 |
| MG1006_Rev_Zone_Olivine8 | 38.9 | 40.6 | 19.79 | 0.265 | 0.278 | 0.173 | | | 100 | 78.52 | 1359 | 2153 | 1894 | 153888 |
| MG1006_Rev_Zone_Olivine8 | 38.88 | 40.73 | 19.41 | 0.282 | 0.275 | 0.17 | | | 99.74 | 78.9 | 1335 | 2130 | 2016 | 150933 |
| MG1006_Rev_Zone_Olivine8 | 39.06 | 41.29 | 18.62 | 0.344 | 0.272 | 0.176 | | | 99.77 | 79.81 | 1383 | 2107 | 2459 | 144790 |
| MG1006_Skeletal_Olivine1 | 39.09 | 41.77 | 18.28 | 0.338 | 0.246 | 0.049 | | | 99.77 | 80.29 | 385 | 1905 | 2416 | 142146 |
| MG1006_Skeletal_Olivine1 | 39.16 | 41.88 | 18.16 | 0.341 | 0.237 | 0.044 | | | 99.82 | 80.43 | 346 | 1836 | 2437 | 141213 |
| MG1006_Skeletal_Olivine1 | 39.15 | 41.91 | 18.15 | 0.335 | 0.236 | 0.043 | | | 99.81 | 80.45 | 338 | 1828 | 2395 | 141135 |
| MG1006_Skeletal_Olivine2 | 38.77 | 39.98 | 20.48 | 0.27 | 0.283 | 0.157 | | | 99.94 | 77.68 | 1233 | 2192 | 1930 | 159253 |
| MG1006_Skeletal_Olivine2 | 38.77 | 40 | 20.41 | 0.267 | 0.284 | 0.156 | | | 99.89 | 77.74 | 1225 | 2200 | 1909 | 158709 |
| MG1006_Skeletal_Olivine2 | 38.88 | 40.19 | 20.3 | 0.271 | 0.288 | 0.152 | | | 100.09 | 77.92 | 1194 | 2231 | 1937 | 157854 |

| Sample | SiO2 | MgO | FeO | CaO | MnO | NiO | Cr2O3 | Al2O3 | Total | OL Mg# | Ni ppm | Mn ppm | Ca ppm | Fe ppm |
|---|---|---|---|---|---|---|---|---|---|---|---|---|---|---|
| MG1006_Skeletal_Olivine2 | 38.87 | 40.32 | 20.04 | 0.285 | 0.281 | 0.148 | | | 99.94 | 78.19 | 1163 | 2177 | 2037 | 155832 |
| MG1006_Skeletal_Olivine2 | 39.12 | 41.17 | 18.93 | 0.388 | 0.289 | 0.175 | | | 100.06 | 79.49 | 1375 | 2239 | 2773 | 147201 |
| MG1006_Skeletal_Olivine2 | 39.1 | 41.25 | 18.67 | 0.43 | 0.288 | 0.188 | | | 99.92 | 79.75 | 1477 | 2231 | 3074 | 145179 |
| MG1006_Skeletal_Olivine3 | 39.48 | 43.32 | 16.07 | 0.325 | 0.234 | 0.217 | | | 99.65 | 82.77 | 1705 | 1813 | 2323 | 124961 |
| MG1006_Skeletal_Olivine3 | 39.3 | 42.6 | 16.99 | 0.35 | 0.25 | 0.202 | | | 99.68 | 81.71 | 1587 | 1936 | 2502 | 132115 |
| MG1006_Skeletal_Olivine3 | 39.1 | 41.89 | 17.82 | 0.379 | 0.267 | 0.189 | | | 99.64 | 80.73 | 1485 | 2068 | 2709 | 138569 |
| MG1006_Skeletal_Olivine4 | 38.8 | 39.84 | 20.55 | 0.41 | 0.296 | 0.11 | | | 100.01 | 77.55 | 864 | 2293 | 2931 | 159798 |
| MG1006_Skeletal_Olivine4 | 38.77 | 40.01 | 20.34 | 0.412 | 0.297 | 0.113 | | | 99.94 | 77.81 | 888 | 2301 | 2945 | 158165 |
| MG1006_Skeletal_Olivine4 | 39.01 | 41.03 | 19.02 | 0.441 | 0.294 | 0.132 | | | 99.93 | 79.36 | 1037 | 2277 | 3152 | 147900 |

# Chapter 4

## Nickel and helium evidence for melt above the core–mantle boundary

### 1. Introduction

High $^{3}He/^{4}He$ ratios in some basalts have generally been interpreted as originating in an incompletely degassed lower-mantle source (Kurz et al., 1982; Class and Goldstein, 2005; Tolstikhin and Hofmann, 2005; Labrosse et al., 2007; Gonnermann and Mukhopadhyay, 2009; Kurz et al., 2009; Jackson et al., 2010; Coltice et al., 2011; Jackson and Carlson, 2011). This helium source may have been isolated at the core–mantle boundary region since Earth's accretion (Tolstikhin and Hofmann, 2005; Labrosse et al., 2007; Coltice et al., 2011). Alternatively, it may have taken part in whole-mantle convection and crust production over the age of the Earth (Class and Goldstein, 2005; Gonnermann and Mukhopadhyay, 2009; Jackson and Carlson, 2011); if so, it is now either a primitive refugium at the core–mantle boundary or is distributed throughout the lower mantle (Class and Goldstein, 2005; Gonnermann and Mukhopadhyay, 2009). Here we constrain the problem using lavas from Baffin Island, West Greenland, the Ontong Java Plateau, Isla Gorgona and Fernandina (Galapagos). Olivine phenocryst compositions show that these lavas originated from a peridotite source that was about 20 per cent higher in nickel content than in the modern mid-ocean-ridge basalt source. Where data are available, these lavas also have high $^{3}He/^{4}He$. We propose that a less-degassed nickel-rich source formed by core–mantle interaction during the crystallization of a melt-rich layer or basal magma ocean (Labrosse et al., 2007; Coltice et al., 2011), and that this source continues to be sampled by mantle plumes. The spatial distribution of this source

may be constrained by nickel partitioning experiments at the pressures of the core–mantle boundary.

**2. Results**

Primitive mantle has been estimated to contain 1,960 p.p.m. nickel (Ni) (McDonough and Sun, 1995), and this is similar to estimates for depleted peridotite (Salters and Stracke, 2004), which makes up the average mid-ocean-ridge basalt (MORB) source. It is also similar to the Ni content of fertile peridotite (which has less basalt than primitive peridotite but more melt than depleted peridotite so more basalt can be extracted during partial melting) obtained from recent high-quality measurements (Ionov, 2007) (Supplementary Fig. 1 and Supplementary section 1), which can be described by:

$$\text{Ni (p.p.m.)} = 568.6\text{MgO (weight per cent)} - 630 \quad (1)$$

Equation (1) fits the Ni contents of 110 fertile and depleted peridotite compositions to 92 p.p.m. ($\pm 2\sigma$); we refer to this as normal Ni peridotite. High-precision olivine analyses from these fertile and depleted peridotites12 yield 2,800–3,100 p.p.m. Ni and magnesium (Mg)-numbers of 89–92 (that is, 100MgO/(MgO + FeO) in mole per cent; Fig. 1a, Supplementary Table 1 and Supplementary Information section 2). These olivines from mantle peridotite are very similar to primitive olivine phenocryst compositions from East Pacific Rise (EPR) basalts (Fig. 1a). They are also very similar to model Ni contents (Herzberg, 2011) shown by the black line in Fig. 1, which is appropriate for olivine

phenocrysts of primary magmas having 8%–38% MgO and for melting of both fertile and depleted upper-mantle peridotite. Model olivines are also similar to observed olivine phenocrysts in hot Archaean komatiites from Alexo (Sobolev et al., 2007; Arndt et al., 2008) (Fig. 1b) and other occurrences of high-temperature magmas (Methods), demonstrating restricted compositions over a broad temperature range (Sobolev et al., 2007).

Olivines from the Palaeocene-epoch picrites in Baffin Island and West Greenland, on the other hand, have higher Ni contents (up to 3,800 p.p.m.) than those from MORBs, Archaean komatiites, and mantle peridotite (Fig. 1c). Those with high Mg-numbers are also higher in Ni than olivines that are expected to crystallize from any partial melt of normal mantle peridotite, as indicated by Ca, Mn and Fe/Mn (Fig. 2). Primary magma major-element compositions were estimated from modelling of whole-rock lava compositions (Herzberg and Gazel, 2009), but sorting of olivine phenocrysts in lava flows compromises reliable Ni estimates with this method. However, the Ni contents and Mg-numbers of the olivine phenocrysts themselves are unaffected by crystal sorting. We estimated a typical Ni content of the primary magma that is required to crystallize olivines with the observed Ni and highest Mg-numbers. The high-Ni olivines require a fertile peridotite source having 2,360 p.p.m. Ni (Methods Summary). This is about 20% higher than normal Ni peridotite with 1,960 p.p.m. Ni and is well outside the 2σ uncertainty bounds of equation (1). The range of olivine compositions at low Mg-numbers and Ni contents is a consequence of variable olivine and clinopyroxene fractionation from primary magmas (Fig. 1c and Supplementary Information section 4).

The excess-Ni problem is not confined to Baffin Island and West Greenland. Although high-precision Ni data for olivine in intraplate occurrences are limited, we find high Ni in olivines from the Ontong Java plateau, Gorgona komatiites, and the Fernandina volcano in the Galapagos Islands (Fig. 3). In all cases a peridotite source provenance is indicated by Ca, Mn and Fe/Mn (Sobolev et al., 2007; Herzberg, 2011) in olivine (Fig. 2 and Supplementary Information). The high Ni in Gorgona olivines is clearly seen because the sample suite includes olivines with very high Mg-numbers, close to those expected for early crystals from the primary magmas. The high Ni in olivines from the other occurrences is less clear, owing to their lower Mg-numbers. For these we modelled the Ni contents of olivines that would crystallize from primary magmas and their liquid lines of descent. Using primary magma compositions from Herzberg and Gazel, 2009 with the Ni contents adjusted to those expected in melts from normal fertile peridotite containing 1,960 p.p.m. Ni (Fig. 1), the Ni contents of olivines that crystallize along liquid lines of descent are always lower than those observed in olivines from the Ontong Java plateau or the Fernandina volcano, regardless of the proportions of crystallizing olivine and clinopyroxene. Rather, all successful solutions require Ni-rich fertile peridotite sources having Ni contents up to 2,360 p.p.m.

Mantle that has been depleted by prior melting events can be high in both MgO and NiO compared with more fertile sources (see equation (1)). However, the Ni contents of partial melts of highly depleted peridotite and fertile peridotites are indistinguishable at liquid MgO < 25 weight per cent (Herzberg, 2011) (Supplementary Fig. 1) and the

olivines of primary melts shown in Fig. 1c should be generally applicable. Therefore, Ni-rich olivine phenocrysts cannot crystallize from melts of normal depleted peridotite.

Excess Ni in olivine has also been attributed to high temperatures and pressures of melting (Putirka et al., 2011). However, this is not consistent with olivines from Archaean komatiites from Alexo (Sobolev et al., 2007) (Fig. 1b) and Barberton (see Methods), which are thought to be among the hottest magmas ever erupted on Earth (Arndt et al., 2008), and yet have normal Ni concentrations. Appealing to the formation of Alexo komatiites in a cool and wet environment does not solve the problem because they are compositionally similar to komatiites from the Belingwe greenstone belt (Puchtel et al., 2009) for which melt inclusion studies point to a hot and dry origin (Berry et al., 2008). Furthermore, Barberton komatiites separated from a deep garnet-bearing residue that was hot and dry, and yet there is no excess Ni (Methods); low-temperature hydrous melting models are also not consistent with olivine phenocryst compositions (Methods). Consequently, the high Ni contents of the Baffin Island and West Greenland olivines are more plausibly related to composition rather than temperature-pressure effects.

Shield volcanoes from Hawaii also contain olivine phenocrysts with increased Ni (Arndt et al., 2008; Putirka et al., 2011), and there is general agreement that Hawaii is melting from a source that is hotter than the ambient mantle (Herzberg and Gazel, 2009; Putirka et al., 2011). High Ni contents in Hawaiian olivines have been used to infer both pyroxenite melting in the source (Sobolev et al., 2007; Herzberg, 2011) and high temperatures and pressures of peridotite melting (Putirka et al., 2011). Comparably high

mantle potential temperatures have been inferred for both Hawaii and West Greenland occurrences (1,500–1,600 °C; (Herzberg and Gazel, 2009)) and both erupted through thick lithosphere (Supplementary Information). If increased temperature and pressure is the main mechanism for producing olivine phenocrysts with high Ni contents (Putirka et al., 2011), there should be similar Ni, Mn, Fe/Mn and Ca contents in olivines from Hawaii and from Baffin Island and West Greenland. This is not observed (Supplementary Fig. 8). Hawaiian olivines are higher in Ni by ~1,000 p.p.m. and they have substantially lower calcium (Ca) and manganese (Mn) and higher Fe/Mn contents than those from West Greenland and Baffin Island. For the latter, a peridotite source provenance is clearly indicated (Fig. 2 and Supplementary Fig. 8). By contrast, low Ca and low Mn and high Fe/Mn contents for Hawaiian olivines are an expected consequence of pyroxenite source melting, owing to residuum retention of Ca in clinopyroxene and Mn in garnet (Supplementary Fig. 5). It is pyroxenite that contributes to high Ni in Hawaiian olivines (Sobolev et al., 2007; Herzberg, 2011), not temperature and pressure effects (Putirka et al., 2011). However, a possible role for mixed Ni-rich and Ni-poor peridotite with pyroxenite remains to be evaluated for Hawaii.

We conclude that high Ni coupled to peridotite-generated levels of Ca, Mn and Fe/Mn (Figs 1–3 and Supplementary Figs 6 and 7) point to Ni-rich peridotite sources for Baffin Island, West Greenland, Ontong Java plateau, Isla Gorgona and Fernandina in the Galapagos Islands. By ‘Ni-rich’, we refer to Ni contents that are significantly higher than those described by equation (1), in contrast with normal-Ni peridotite sources that melt to make modern oceanic crust at mid-ocean ridges (Fig. 1a).

Current estimates of the Ni content of fertile mantle peridotite (McDonough and Sun, 1995; Salters and Stracke, 2004) are based on averages which can vary by about 300 p.p.m. (Herzberg, 2011); the Ni content of olivine in such peridotites obtained from open-access web sources is also large (Putirka et al., 2011). Although our estimated Ni content for Ni rich peridotite is roughly within this range, we emphasize that this coincidence has no meaning because whole-rock and olivine Ni data are often compiled from sources of questionable accuracy (Herzberg, 2011), and there is much less uncertainty in our more recent work (Ionov, 2007) (Fig. 1 and Supplementary Fig. 1). Random 6300 p.p.m. variations in the Ni content of peridotite can result in olivines with Ni as low as 2,200 p.p.m. (Herzberg, 2011). Such low Ni contents have never been reported from high precision olivine analyses in unmetasomatized mantle peridotite (Fig. 1a) and, when found in olivine phenocrysts (Sobolev et al., 2007), other explanations are more plausible. For example, some MORB olivines can be low in Ni (Fig. 1a), but this is plausibly explained by sequestration of Ni into a residual sulphide phase (Herzberg, 2011), which can remain stable in the residue up to 15% melting (Bezos et al., 2005).

Lavas exhibiting Ni excess are also associated with elevated $^{3}He/^{4}He$. Picrites from Baffin Island and West Greenland have $^{3}He/^{4}He$ up to 50 times the atmospheric value (Ra) (Starkey et al., 2009), and they also have primitive Nd and Pb isotopic compositions (Jackson et al., 2010). For the others, the maximum $^{3}He/^{4}He$ (Ra) is 29 for Fernandina (Kurz et al., 2009) and 18 for Gorgona (Revillon et al., 2002). No helium data are currently available for lavas from the Ontong Java plateau, but they also have primitive Nd and Pb isotopic ratios (Jackson and Carlson, 2011).

We now explore a model that might produce a Ni-rich peridotite with increased $^{3}He/^{4}He$. We have tested the formation of Ni-rich peridotite in a magma ocean by perovskite subtraction and/or ferropericlase addition. Although such models can yield high Ni contents, they produce a peridotite source that is too low in $SiO_2$ and Fe/Mn that is too high. More work on intra-mantle differentiation scenarios informed by accurate high-pressure phase equilibria and partitioning data are warranted (Coltice et al., 2011), but here we propose a core–mantle interaction model.

Evidence for melting at the present-day core–mantle boundary includes the coincidence of recent determinations of the peridotite solidus with the estimated temperature at the top of the outer core (Fiquet et al., 2010) and seismic observations of ultralow-velocity zones (Williams and Garnero, 1996). As even more melt is expected in an early hotter Earth, present-day ultralow-velocity zones may represent the terminal stages in the crystallization of a long-lived magma ocean, and they provide a possible mechanism for preserving primitive mantle (Labrosse et al., 2007; Coltice et al., 2011). This model predicts an equilibrium exchange of Ni between liquid metal in the core and liquid silicate in the mantle, which can be described by :

$$FeO^{silicate} + Ni^{metal} = NiO^{silicate} + Fe^{metal} \quad (2)$$

The present-day Ni content of fertile mantle peridotite (1,960 p.p.m.) may have been established by core formation at, 30–60 GPa (Siebert et al., 2012). Silicate melt in contact

with liquid metal would be enriched in Ni at 135 GPa as the exchange is driven from left to right with increasing pressure at constant oxidation state of iron (Walker, 2005; Rubie et al., 2011; Siebert et al., 2012). We propose that a Ni-rich and less-degassed domain was formed by core–mantle interaction during the late stages of the crystallization of a basal magma ocean (Labrosse et al., 2007) or melt layer, and that some part of this source continues to be sampled by mantle plumes. Another tracer for core–mantle interaction may be the addition of tungsten and osmium (Os) isotopes from the core to the mantle (Brandon et al., 2003; Walker, 2005). Gorgona is the only location examined here with available $^{186}Os/^{188}Os$ data, and there is an $^{186}Os$ anomaly that has been attributed to core influence (Brandon et al., 2003). There is no shortage of plausible mechanisms of core–mantle interaction, and the challenge is to understand how they are geochemically expressed (Walker, 2005).

Earth's mantle may have become oxidized by disproportionation of FeO in a deep magma ocean during crystallization of $Fe^{3+}$ -rich Mg-perovskite and loss of metallic Fe to the core (Wade and Wood, 2005). The Ni-rich peridotite source for West Greenland is also oxidized, having produced melts more oxidizing than MORB and within one log unit of the nickel–nickel oxide oxygen fugacity buffer (Larsen and Pedersen, 2000). Although it is counterintuitive, we propose that these oxidized magmas had an origin that began above the core–mantle boundary, in a location where Ni-rich silicate melt and $Fe^{3+}$ -rich Mg-perovskite were in equilibrium with the outer core. Mantle plumes that sample this region and ascend above the melting zone would solidify to Ni-rich ferropericlase, Ca perovskite and $Fe^{3+}$ -rich Mg-perovskite, transforming further to Ni-rich and oxidized

peridotite in the upper mantle. Partial melting will yield magmas like those from West Greenland that are both Ni-rich and more oxidizing than MORB.

The spatial distribution of elevated $^{3}He/^{4}He$ in the mantle might be constrained by understanding the origin of a Baffin Island and West Greenland source with 2,360 p.p.m. Ni. Although core formation in a single stage is not likely (Rubie et al., 2011), its prediction of 3,580 p.p.m. Ni (Rubie et al., 2011) in the mantle at 135 GPa may be a guide to the Ni content of silicate melt at the present time. A source with 2,360 p.p.m. Ni would then require mixing of this high-Ni endmember with the canonical, 1,960 p.p.m. Ni from elsewhere in the mantle. In this scenario, the Ni-rich and high-$^{3}He/^{4}He$ source may be widely distributed (Class and Goldstein, 2005; Gonnermann and Mukhopadhyay, 2009) or it may take the form of a halo around the core. Alternatively, the isolation of the Baffin Island and West Greenland source as a refuge from convection near the core–mantle boundary (Tolstikhin and Hofmann, 2005; Jackson et al., 2010; Coltice et al., 2011; Jackson and Carlson, 2011) is plausible if it can be demonstrated that 2,360 p.p.m. Ni in a silicate melt is in equilibrium with the core. In any case, interaction of the core with a silicate melt is a plausible mechanism for production of oxidized Ni rich peridotite, and it provides evidence for a long-lived melt layer or basal magma ocean (Labrosse et al., 2007; Coltice et al., 2011).

**3. Methods Summary**

The method for calculating model olivine Ni compositions is given elsewhere (Herzberg, 2011) and in the Supplementary Information. Primary magma compositions are calculated first, followed by the olivines that they crystallize. The compositions of Ni

in liquids extracted from dunite [liquid+olivine] and harzburgite [liquid+olivine+orthopyroxene] residues were computed by mass balance solutions to the equation for accumulated fractional melting:

$$C_L = C_o[1 - (1-F)^{1/D}]/F$$

where $C_L$ is weight per cent NiO in the liquid (primary magma), $C_o$ is the initial NiO in the peridotite source composition (0.25%, (McDonough and Sun, 1995); 1,960 p.p.m.), F is the melt fraction, and D is the bulk distribution coefficient from the Beattie–Jones model (Supplementary Information). Ni contents for near-solidus melts were calculated from the MgO contents of near-solidus melts, together with a solidus olivine composition having 0.36% NiO (Herzberg, 2011) (Supplementary Information). Ni contents of near-solidus primary magmas are nearly indistinguishable from those of primary magmas for liquid+olivine and liquid+olivine+orthopyroxene assemblages, and the full range of possible Ni contents are shown in Supplementary Fig. 1.

The Ni content of olivine that crystallizes as a phenocryst at one atmosphere from a primary magma $C_L$ was calculated using olivine/liquid Ni distribution coefficients from the Beattie–Jones model (Supplementary Information). Results are displayed in Figs 1 and 3 for a fertile peridotite having $C_o$ = 1,960 p.p.m. Ni. Olivines have 2,800–3,100 p.p.m. Ni, and they provide an excellent description of olivine in normal mantle peridotite, primitive olivine phenocrysts in modern MORB, and olivine phenocrysts in

Archaean komatiites. However, they fail to describe the much higher Ni contents of olivines from Baffin Island, West Greenland, the Ontong Java Plateau, Isla Gorgona and Fernandina (Galapagos) (Figs 1c and 3). For these, excellent agreement between computed and observed olivine Ni contents could be obtained with $C_o$ = 0.30% NiO (2,360 p.p.m. Ni), a Ni-rich peridotite source.

**4. References:**

Arndt, N., C.M. Lesher and S.J. Barnes (2008), Komatiite, Cambridge University Press, p. 363-389.

Berry, A. J., D.V. Danyushevsky, H.S,C. O'Neil, M. Newville and S.R. Sutton, (2008), Oxidation state of iron in komatiitic melt inclusions indicates hot Archaean mantle, Nature, v. 455, no. 7215, p. 960-963.

Bezos, A., J. Lorand, E. Hummler and M. Gros, (2005), Platinum-group element systematics in Mid-Oceanic Ridge basaltic glasses from the Pacific, Atlantic, and Indian Oceans, Geochimica Et Cosmochimica Acta, v. 69, p. 2613-2627.

Brandon, A.D., R.J. Walker, I.S. Puchtel, H. Becker, M. Humayun and S. Revillon, (2003), Os-186-Os-187 systematics of Gorgona Island komatiites: implications for early growth of the inner core, Earth and Planetary Science Letters, v. 206, p. 411-426.

Class, C. and S. L. Goldstein, (2005), Evolution of helium isotopes in the Earth's mantle, Nature, v. 436, p. 1107-1112.

Coltice, N., M. Moreira, J. Hernlund and S. Labrosse, (2011), Crystallization of a basal magma ocean recorded by Helium and Neon, Earth and Planetary Science Letters, v. 308, p. 193-199.

Fiquet, G., A.L. Auzende, J. Siebert, A. Corgne, H. Bureau, H. Ozawa and G. Garbarino, (2010), Melting of Peridotite to 140 Gigapascals, Science, v. 329, p. 1516-1518.

Gonnermann, H.M. and S. Mukhopadhyay, (2009), Preserving noble gases in a convecting mantle, Nature, v. 459, p. 560-588.

Herzberg, C., (2011), Identification of Source Lithology in the Hawaiian and Canary Islands: Implications for Origins, Journal of Petrology, v. 52, p. 113-146.

Herzberg, C. and E. Gazel, (2009), Petrological evidence for secular cooling in mantle plumes, Nature v. 458, p. 619-622.

Ionov, D.A., (2007), Compositional variations and heterogeneity in fertile lithospheric mantle: peridotite xenoliths in basalts from Tariat, Mongolia, Contributions to Mineralogy and Petrology, v. 154, p. 455-477.

Jackson, M.G. and R.W. Carlson, (2011), An ancient recipe for flood-basalt genesis, Nature, v. 476, p. 316-377.

Jackson, M.G., R.W. Carlson, M.D. Kurz, P.D. Kempton, D. Francis and J. Blusztajn, (2010), Evidence for the survival of the oldest terrestrial mantle reservoir, Nature, v. 466, p. 853-884.

Kurz, M.D., J. Curtice, D. Fornari, D. Geist and M. Moreira, (2009), Primitive neon from the center of the Galapagos hotspot, Earth and Planetary Science Letters, v. 286, p. 23-34.

Kurz, M.D., W.J. Jenkins and S.R. Hart, (1982), Helium Isotopic Systematics of Oceanic Islands and Mantle Heterogeneity, Nature, v. 297, p. 43-47.

Labrosse, S., J.W. Hernlund and N. Coltice, (2007), A crystallizing dense magma ocean at the base of the Earth's mantle, Nature, v. 450, p. 866-869.

Larsen, L.M. and A. K. Pedersen (2000), "Processes in high-mg, high-T magmas: Evidence from olivine, chromite and glass in palaeogene picrites from West Greenland." Journal of Petrology, v. 41, no. 7, p. 1071-1098.

McDonough, W.F. and S. S. Sun, (1995), THE COMPOSITION OF THE EARTH, Chemical Geology, v. 120, p. 223-253.

Puchtel, I.S., R.J. Walker, A.D. Brandon and E.G. Nisbet, (2009), Pt-Re-Os and Sm-Nd isotope and HSE and REE systematics of the 2.7 Ga Belingwe and Abitibi komatiites, Geochimica Et Cosmochimica Acta, v. 73, p. 6367-6389.

Putirka, K., F.J. Ryerson, M. Perfit and W.I. Ridley, (2011), Mineralogy and Composition of the Oceanic Mantle, Journal of Petrology, v. 52, p. 279-313.

Revillon, S., C. Chauvel, N.T. Arndt, R. Pik, F. Martineau, S. Fourcade and B. Marty, (2002), Heterogeneity of the Caribbean plateau mantle source: Sr, O and He isotopic compositions of olivine and clinopyroxene from Gorgona Island, Earth and Planetary Science Letters, v. 205, p. 91-106.

Rubie, D.C., D.J. Frost, U. Mann, Y. Asahara, F. Nimmo, K. Tsuno, P. Kegler, A. Holzheid and H. Palme, (2011), Heterogeneous accretion, composition and core-mantle differentiation of the Earth, Earth and Planetary Science Letters, v. 301, p. 31-42.

Salters, V.J.M. and A. Stracke (2004), "Composition of the depleted mantle." Geochemistry Geophysics Geosystems 5.

Siebert, J., J. Badro, D. Antonangeli and F.J. Ryerson, (2012), Metal-silicate partitioning of Ni and Co in a deep magma ocean, Earth and Planetary Science Letters, v. 321, p. 189-197.

Sobolev, A.V., A.W. Hofmann, D.V. Kuzmin, G.M. Yaxley, N.T. Arndt, S.L. Chung, L.V. Danyushevsky, T. Elliot, F.A. Frey, M.O. Garcia, A.A. Gurenko, V.S. Kamenetsky, A.C. Kerr, N.A. Krivolutskaya, V.V. Matvienkov, I.K. Nikogosian, A. Rocholl, I.A. Sigurdsson, N.M. Sushchevskaya and M. Teklay, (2007), The amount of recycled crust in sources of mantle-derived melts, Science, v. 316, p. 412-417.

Starkey, N.A., F.M. Stuart, R.M. Ellam, J.G. Fitton, S. Basu and L.M. Larsen, (2009), Helium isotopes in early Iceland plume picrites: Constraints on the composition of high He-3/He-4 mantle, Earth and Planetary Science Letters, v. 277, p. 91-100.

Tolstikhin, I. and A.W. Hofmann, (2005), Early crust on top of the Earth's core, Physics of the Earth and Planetary Interiors, v. 148, p. 109-130.

Wade, J. and B.J. Wood, (2005), Core formation and the oxidation state of the Earth, Earth and Planetary Science Letters, v. 236, p. 78-95.

Walker, D. , (2005), CORE–MANTLE CHEMICAL ISSUES, The Canadian Mineralogist, v. 43, p. 1553-1564.

Williams, Q. and E.J. Garnero, (1996), Seismic evidence for partial melt at the base of Earth's mantle, Science, v. 273, p. 1528-1530.

**5. Figure Captions:**

**Figure 1:** Mg-numbers and Ni content for calculated (Herzberg, 2011) and observed olivine. An Mg-number is defined as 100MgO/(MgO + FeO)) in mole per cent. The black curve represents the calculated Ni content in olivines that crystallize from all primary melts derived from a fertile peridotite source having a whole-rock Ni content of 1,960 p.p.m. (Herzberg, 2011); the ±1σ uncertainty (grey shading) is discussed in Supplementary Information section 3. The black hatched area represents the calculated Ni content in olivines from olivine fractionated derivative liquids from primary magmas having 8–13% MgO. **a,** The green circles are 203 high-precision analyses of olivine in mantle peridotite from various tectonic settings (Supplementary Information); the blue and red circles are high-precision olivine phenocrysts in MORBs from the Pacific (the

EPR) and Indian oceans (Sobolev et al., 2007; Putirka et al., 2011). **b,** The red circles are high-precision olivine phenocrysts from the Archaean Alexo komatiites (Sobolev et al., 2007). The green curves are calculated Ni contents in olivines from olivine-fractionated derivative liquids from primary magmas having 20–30% MgO (Herzberg, 2011), as indicated (green numbers); primary magmas for Alexo contained 26–30% MgO (Herzberg, 2011; Arndt et al., 2008). **c,** The white circles are high-precision olivine phenocrysts from West Greenland and Baffin Island (Sobolev et al., 2007); the uncertainty is only slightly greater than the size of the open circles. The red crosses are the Ni contents of olivine phenocrysts expected to crystallize from primary melts derived from Ni-rich fertile peridotite having 2,360 p.p.m. Ni. The green and blue lines are olivine compositions that will crystallize from these primary magmas by fractionation of olivine and clinopyroxene in the weight proportions indicated (Supplementary Information). A low-Ni population comes from one sample (ID 27142) from West Greenland (Sobolev et al., 2007), and it represents 28% of the database, having Mg number. 90. There is little overlap between this sample and the more Ni-rich types. The difference between the low- and high-Ni populations most probably reflects mantle source heterogeneity, but there are no independent geochemical data for these samples with which to test this possibility.

**Figure 2: Mg-numbers and Ca, Mn and Fe/Mn contents for calculated (Herzberg, 2011) and observed olivine phenocrysts from MORBs (right panels) compared with Baffin Island and West Greenland (Sobolev et al., 2007) (left panels).** The black regions are calculated olivines from primary melts (8–38% MgO) derived by peridotite

melting (Herzberg, 2011). The black hatched area in **f** and the grey shading in **c** and **d** represent the calculated olivines from olivine-fractionated derivative liquids from primary magmas having 8–20% MgO. The green and blue lines in **a, c** and **e** are olivine compositions that crystallize from primary magmas that fractionated olivine and clinopyroxene in the weight proportions indicated (Supplementary Information). The inset in **b** shows how Ca in olivine changes owing to olivine and clinopyroxene fractionation from the primary magmas. The MORBs in **b, d** and **f** are from the EPR (white circles) and Indian Ocean (yellow circles). Although a wide range of Ca contents are theoretically possible for olivines that crystallize from peridotite-source primary magmas, most have ~2,000 p.p.m. Ca—similar to those found in MORBs, Baffin Island and West Greenland. Primitive and depleted peridotites contain ~1,000 p.p.m. Mn (McDonough and Sun, 1995; Salters and Stracke, 2004) and, although olivines with Fe/Mn = 55–70 can crystallize from primary magmas, more usually the range is restricted to 60–65 (Herzberg, 2011).

**Figure 3: Mg-numbers and Ni contents for calculated olivine (Herzberg, 2011) and observed olivine phenocrysts. a,** Gorgona (Sobolev et al., 2007), **b,** the Ontong Java Plateau (Sobolev et al., 2007), and **c,** Fernandina (this work; Supplementary Information section 5 and Supplementary Table 2). The black curves represent the calculated Ni content in olivines of primary magmas of fertile peridotite having 1,960 p.p.m. Ni (Herzberg, 2011); the grey shaded regions (±1σ) represent a possible range of Ni contents in olivine that may arise from uncertainties in the calculation (Supplementary Information). The red crosses are olivines that would crystallize from Ni-rich fertile

peridotite-source primary magmas; the green and blue lines are olivine compositions that crystallize from primary magmas that fractionated olivine and clinopyroxene in the weight proportions indicated (Supplementary Information section 4).

## 6. Figures

**Figure 1:**

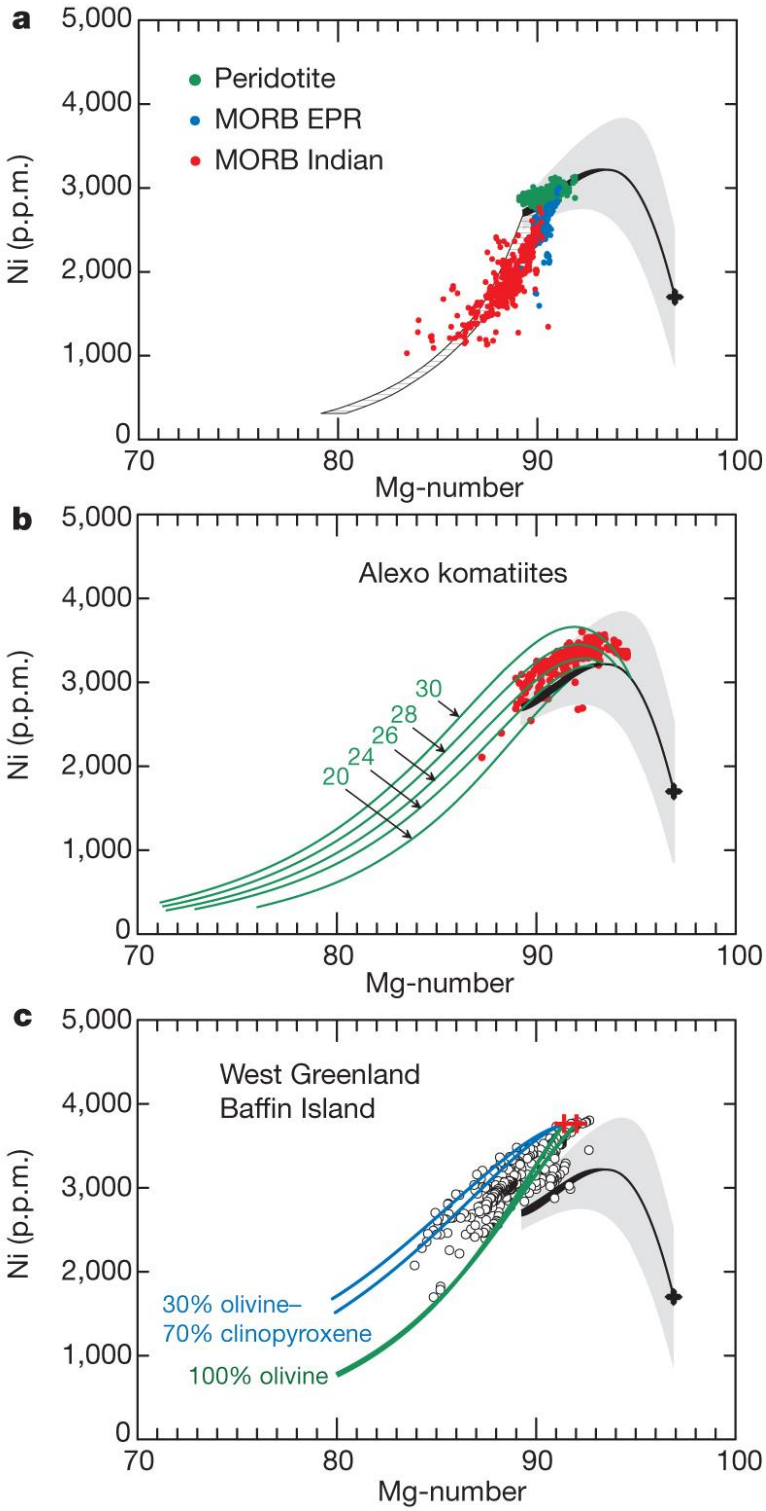

**Figure 2:**

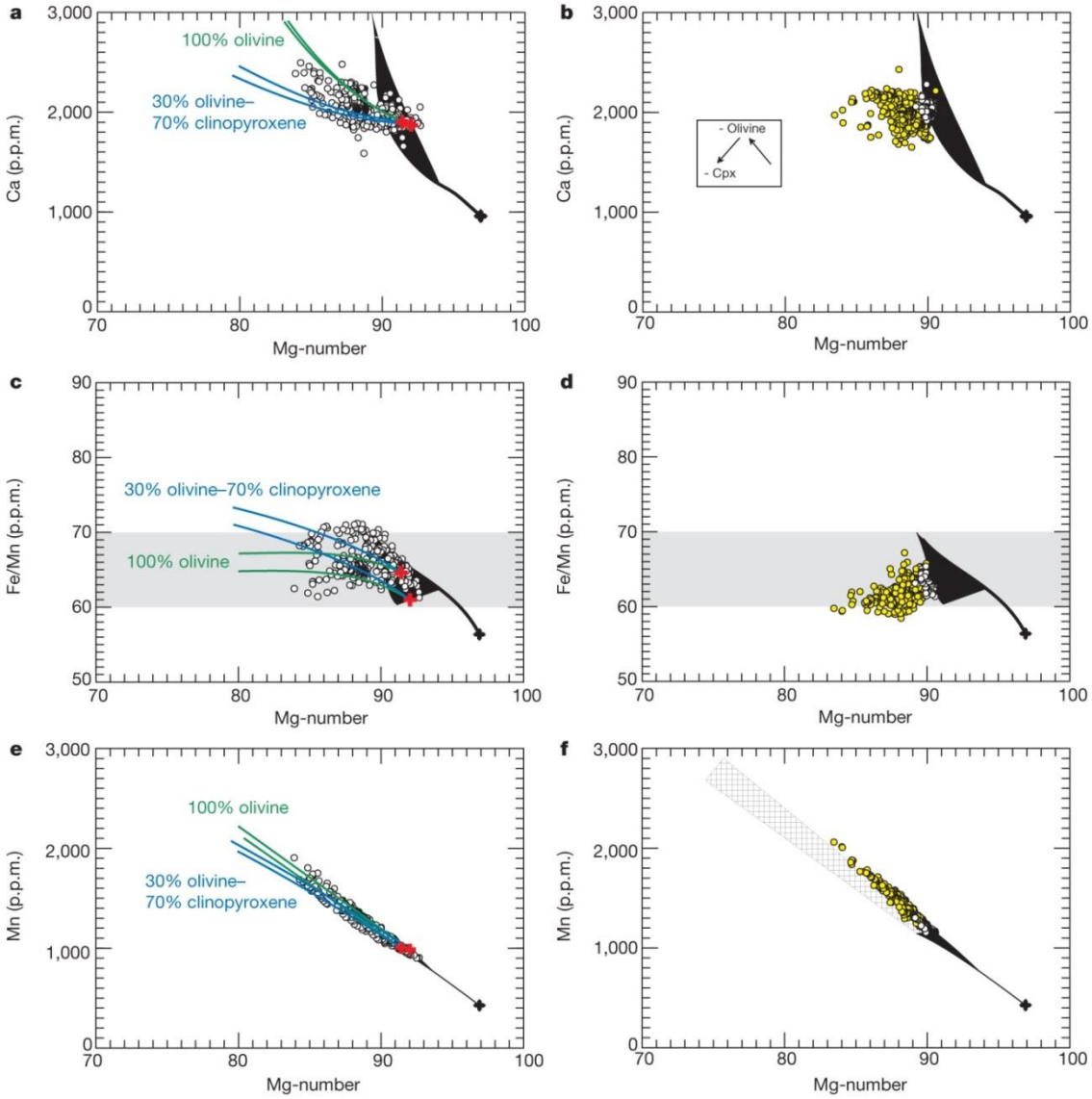
a
b
c
d
e
f
100% olivine
30% olivine–
70% clinopyroxene
- Olivine
- Cpx
Ca (p.p.m.)
Fe/Mn (p.p.m.)
Mn (p.p.m.)
Mg-number
3,000
2,000
1,000
0
90
80
70
60
50
100

**Figure 3:**

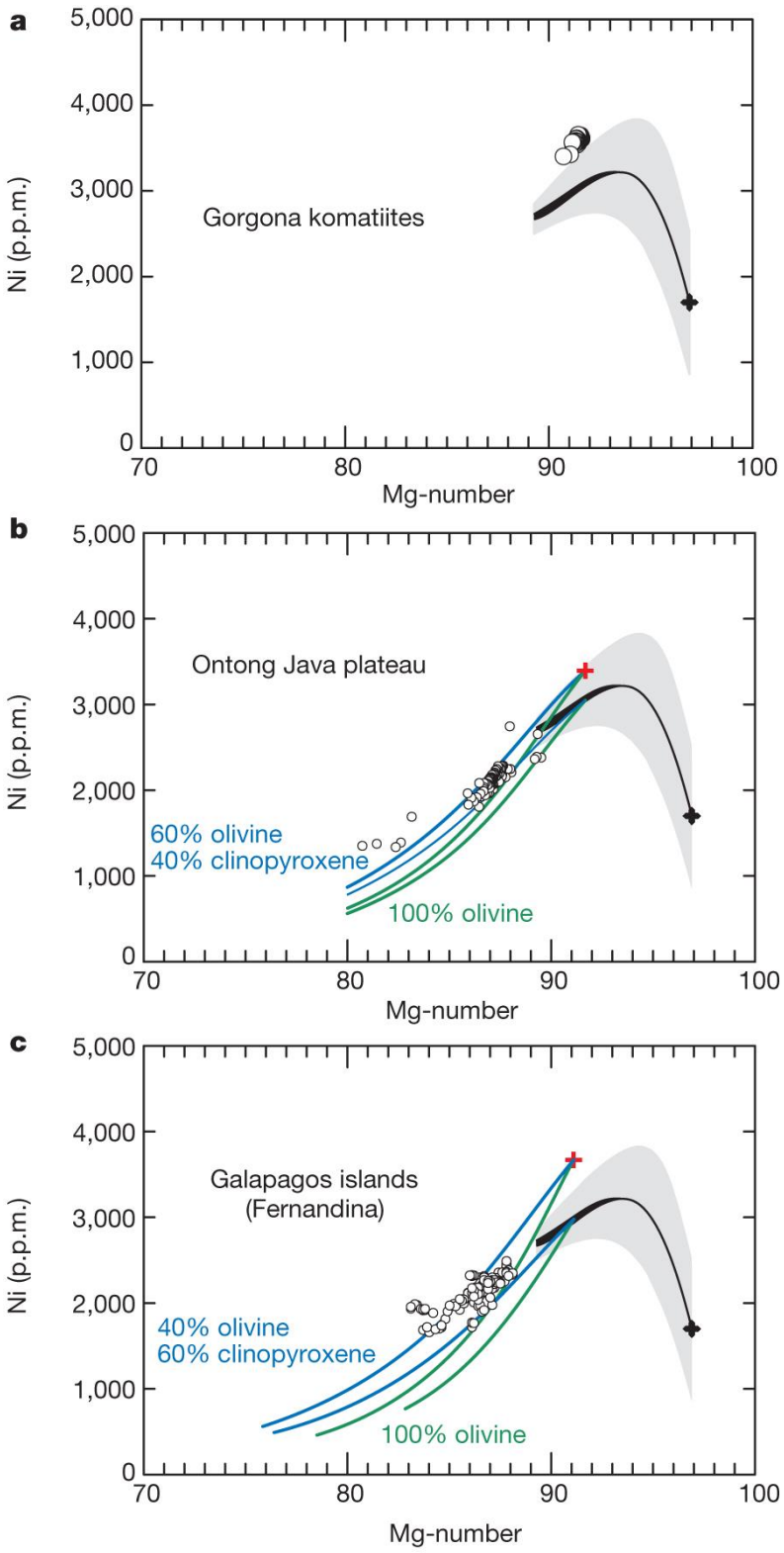
a
Ni (p.p.m.)
5,000
4,000
3,000
2,000
1,000
0
Gorgona komatiites
70
80
90
100
Mg-number
b
Ni (p.p.m.)
Ontong Java plateau
60% olivine
40% clinopyroxene
100% olivine
Mg-number
c
Ni (p.p.m.)
Galapagos islands
(Fernandina)
40% olivine
60% clinopyroxene
100% olivine
Mg-number

**Supplimental Information:**

**S.1. The Ni Content of Mantle Peridotite and Its Primary Magmas**

Of the 590 whole rock spinel and garnet peridotite analyses from off-craton xenolith and tectonic occurrences compiled by Herzberg (1993), 407 contain Ni data and these are shown in Fig. S1. Fertile peridotite has 0.03% K2O (McDonough and Sun, 1995), and most of the peridotites have higher K2O, indicating that they were modified by metasomatism. There are 264 analyses with K2O < 0.03%, and these generally have more uniform NiO contents than the metasomatised types. Nevertheless, many of the measurements in this database were obtained in the 1960s by analytical methods that predated the XRFS, and the variation in Ni shown in Fig. S1 likely reflects uncertainties in analytical method. For example, peridotites with K2O < 0.03% can be described by the equation: Ni (ppm) = 71.7MgO – 844, and the uncertainty is ± 254 ppm (1σ).

The old database of Herzberg (1993) can now be compared with the more recent determinations of off-craton peridotite xenoliths from Asia (Ionov, 2007; 2010; Ionov and Hofmann, 2007; Ionov et al., 2005). Most Ionov data were obtained using wavelength-dispersive X-ray fluorescence spectrometry at the University of Mainz. Data quality is greatly improved (Fig. S1), and can be described by the equation: Ni (ppm) = 68.6MgO – 630 where the uncertainty of 110 fertile and depleted peridotite compositions is ± 46 ppm (1σ). Using this equation and 37.7% MgO in pyrolite (McDonough and Sun, 1995), we obtain 1957 ppm Ni, virtually indistinguishable from the McDonough and Sun (1995) canonical value of 1960 ppm.

## S.2. High Precision Olivine Analyses in Peridotite

Ionov (2007, 2010) and Ionov et al. (2005) published high-precision analyses of olivine in intraplate peridotite xenoliths from Tariat (Mongolia) and Tok (SE Siberia), and subduction xenoliths from Avacha (Kamchatka), using protocols similar to those reported by Sobolev et al. (2007). We have compiled these data and add high precision analyses of olivine from other off-craton spinel and garnet peridotites from Asia. Results from abyssal peridotites will be reported by Ionov and Sobolev separately, and are similar to intraplate and subduction occurrences, demonstrating homogeneity of Ni in all tectonic settings. Table S1 lists individual olivine analyses in some cases and also averages. Replicate analyses using the method of Sobolev et al. (2007) are in good agreement, and will be reported elsewhere by Ionov and Sobolev. Results of 203 analyses shown in Fig. 1 of the text reveal substantial homogeneity of Ni in peridotite olivine. They are in excellent agreement with model Ni contents of olivine (Fig. 1; Herzberg, 2011), although they are slightly higher in Ni in some cases, indicating the possible influence of Ni exchange with orthopyroxene on cooling (Herzberg, 1999). Overall olivine Ni homogeneity is in contrast with a wide range of Ni contents in olivines from peridotites compiled by Putirka et al. (2011) from GEOROC. While we concur that Ni-rich peridotite sources can be important in intraplate magmatism, we conclude the evidence for it can be weak in existing peridotite databases owing to questionable accuracy.

## S.3. The Effects of Temperature, Pressure and Composition on the Partitioning of Ni between Olivine and Liquid

The partitioning of Ni between olivine and liquid depends on temperature, pressure, and composition of the melt (Hart and Davis, 1978; Beattie et al., 1991; Herzberg and Zhang, 1996; Wang and Gaetani, 2008; Filiberto et al., 2009; Putirka et al., 2011; Li and Ripley, 2010; Longhi et al., 2010; Niu et al., 2011). In particular, $D_{Ni}$ Ol/L goes down with increasing MgO content of the melt. But as increasing temperatures and pressures of melting yield melts with higher MgO contents (O'Hara, 1968), it can be difficult to resolve the separate T-P-X effects. This problem has given rise to a plethora of parameterizations of experimental data that have calibrated $D_{Ni}$ Ol/L as a function of T-P-X. It is important to resolve because elevated Ni contents of olivine phenocrysts have been used to infer pyroxenite melting in the source (Sobolev et al., 2005; 2007; Herzberg, 2011), elevated temperatures and pressures in mantle plumes (Li and Ripley, 2010; Putirka et al., 2011; Matzen et al., 2012) and elevated pressures (Niu et al., 2011).

We adopt a model of Ni partitioning that provides the minimum error when recovering experimental data. This is a temperature-independent model first formulated by Jones (1984), later calibrated by Beattie et al. (1991), and corroborated in subsequent studies (Wang and Gaetani, 2008; Filberto et al., 2009; Longhi et al., 2010). We call this a Beattie-Jones model, which is described by:

$$D_{NiO}^{Ol/L} = NiO^{OL}/NiO^{L} \quad (1)$$

$$D_{MgO}^{OL} = MgO^{Ol}/MgO^{L} \quad (2)$$

and

$$D_{NiO}^{Ol/L} = 3.346\ D_{MgO}^{Ol/L} - 3.665 \quad (3)$$

where $NiO^{OL}$, $Ni^{OL}$, $MgO^{Ol}$, $Mg^{OL}$ refer to mole fractions of NiO and MgO in the phases liquid (L) and olivine (Ol), based on one metal cation per oxide (i.e., $SiO_2$, MgO, $AlO_{1.5}$, $NaO_{0.5}$ etc.; Beattie et al., 1991). The constants in equation (3) have been obtained from a parameterization of experimental data (Beattie et al., 1991), which we have tested using the experimental database on Fe-bearing compositions collated by Li and Ripley (2010). To this database was added:

- 11 experiments of Longhi et al. (2010; 1554 to 2015ºC and 1.6 to 6.0 GPa).

- 11 experiments of Taura et al. (1998; 1600 to 2000ºC and 3.0 to 14.4 GPa using both electron microprobe and SIMS analyses)

- 6 experiments of Le Roux et al. (2011; 1300 to 1500 ºC and 1.5 to 2.0 GPa)

- 10 experiments of Matzen et al. (2011; 1301 to 1500 ºC and 1 atmosphere)

There are a total of 271 experiments with temperatures in the 1122-2050ºC range and pressures in the 1 atmosphere to 13 GPa range. To these experiments, the olivine/liquid

distribution coefficients $D_{NiO}^{Ol/L}$ were calculated according to the Beattie-Jones equation (3). For the entire database (N = 271) we calculate:

$$1 \text{ standard deviation } (1\sigma) = (\Sigma(D_{NiO},\text{calculated} - D\ D_{NiO},\text{observed})^2/(N-1))^{0.5} \quad (4)$$

and obtain $1\sigma = 1.1$. However, the difference between calculated and observed $D_{NiO}^{Ol/L}$ is clearly related to temperature as shown in Fig. S2. This likely reflects the effects of temperature on promoting equilibrium during the course of an experiment, and differences between calculated and observed partitioning are minimized and approximately constant at T > 1500°C. We have developed an empirical expression for computing the effects of temperature on σ by binning the experimental database in 100°C increments. At T > 1500°C:

$$1 \text{ standard deviation } (1\sigma) = 0.4 \quad (5)$$

and T < 1500°C:

$$1 \text{ standard deviation } (1\sigma) = -9.308 + 0.0179T - 0.0000075T^2 \quad (6)$$

The results of this uncertainty analysis on the Ni content of olivine in equilibrium with partial melts of mantle peridotite was shown in Fig. 1 of the main body of this paper.

It was shown by Herzberg (2011) that the method of Beattie et al. (1991; equation 3) provides a better description of experimental data than the method of Li and Ripley (2010) which contains independently adjustable temperature and composition terms. Similarly, Putirka et al. (2011) have expressed the partitioning of NiO on a weight % basis, and parameterized it according to both temperature (°C) and composition (wt%). They parameterized 81 experiments with:

$$D_{NiO}^{Ol/L} = \exp[-3.257 + 6800/T] \quad (7a)$$

49 experiments with:

$$D_{NiO}^{Ol/L} = \exp[-4.75 + 0.033(SiO_2)^{L} + 6829/T] \quad (7b)$$

and 81 experiments with:

$$D_{NiO}^{Ol/L} = \exp[-1.78 + .04(SiO_2)^{L} - 0.04(MgO)^{L} + 3236/T] \quad (7c)$$

These equations were labeled as 2a, 2b, and 2c in Putirka et al. (2011). Results shown in Fig. S3 demonstrate that the Beattie – Jones parameterization of equation (3) yields a more accurate description of the experimental database than Putirka et al. (2011). For mantle peridotite having 1960 ppm Ni that melts at high temperatures appropriate to a mantle plume, use of the Putirka et al. (2011) parameterization will yield primary magmas with Ni contents that are too high.

Niu et al. (2011) suggested that the Ni content of olivine is a function of the pressure at which melting stops at the base of the lithosphere, which covers the 0 to 3 GPa range. They provided the following parameterization of a limited and unspecified number of experiments:

$$D_{NiO}^{Ol/L} = 4.6914P^{-0.5357} \quad (8)$$

As their equation (8) intercepts the y-axis at infinity, we restrict this analysis to experiments in the 0.5 to 3.2 GPa. Results shown in Fig. S4 demonstrate that the Niu et al. (2011) parameterization is not as successful as the method of Beattie et al. (1991) in describing the experimental database.

The most successful method for describing the Ni content of olivine phenocrysts to crystallize from magmas is provided by Beattie et al. (1991), and it is the one we have adopted in this work. The method has the advantage of requiring only the composition of the melt from which olivine crystallizes. There are no independently adjustable temperature and pressure terms, which are themselves model-dependent. We conclude that the high Ni contents of olivines in Baffin Island, Disko Island, West Greenland, the Ontong Java Plateau, Isla Gorgona, and Fernandina originated from a Ni-rich peridotite source, and are not artifacts of elevated temperatures and pressures of melting.

## S.4. Forward Models of Liquid Lines of Descent Involving Olivine and Clinopyroxene

The problem of inferring source lithology is tractable when Mg-numbers of olivine phenocrysts are high, generally > 89 (Herzberg, 2011). For example, olivine phenocrysts for shield building lavas on Hawaii are higher in Ni and Fe/Mn, and lower in Mn and Ca than those expected of a normal peridotite source (Sobolev et al., 2005; 2007; Herzberg, 2011). In contrast, maximum Mg-numbers for olivine phenocrysts from many intraplate volcanoes are typically in the 80-88 range, and can result from the crystallization of both olivine and clinopyroxene from primary magmas. The problem is to compare high precision olivine analyses with those that are expected to crystallize from such magmas. This is solved by a forward model of the liquid line of descent, and the calculation of olivine that crystallizes along it.

The importance of sub Moho clinopyroxene fractionation in ocean island and MORB petrogenesis has been recognized previously (Albarède et al., 1997; Geist et al., 1998; Herzberg, 2004a; Herzberg and Asimow, 2008). The effect of decompression is to expand the liquidus crystallization fields of olivine and clinopyroxene (O'Hara, 1968; Herzberg, 1992), and both can crystallize when primary magmas interact with wall rocks during transit. Relative to olivine only crystallization, deep fractionation of clinopyroxene can produce derivative magmas with lower CaO, $SiO_2$, higher FeO, lower MnO, and higher NiO. Olivine that crystallizes from such melts at the surface will exhibit depletions in Ca and Mn, elevated Fe/Mn, and elevated Ni. The erroneous interpretation can be made that this olivine points to a pyroxenite source lithology even if the primary magmas melted from a peridotite source. The problem is how to distinguish the effects of

clinopyroxene as a crystallizing phase from clinopyroxene a residual phase in pyroxenite source.

The method for calculating a liquid line of descent begins with identification of a primary magma composition. Primary magma compositions for peridotite-sources have been computed from primitive lava compositions that differed by olivine addition and subtraction using PRIMELT2 (Herzberg and Asimow, 2008). Results for many ocean islands and large igneous provinces were reported by Herzberg and Gazel (2009). In most cases it was sufficient to obtain primary magmas from the raw lava compositions. For Fernandina, most lava compositions were too differentiated to obtain primary magma compositions owing to plagioclase and augite fractionation. The few remaining primitive samples had unusually variable Mn, and primary magma Mn was adjusted slightly to optimize the match with observed olivine phenocryst compositions. Additionally, whole rock NiO contents often provide unreliable primary magma NiO contents due to olivine sorting; for primary magmas of peridotite-sources, we use Ni (ppm) = $21.6MgO - 0.32MgO^2 + 0.051MgO^3$ (Herzberg, 2011).

From these identified primary magmas, both olivine and clinopyroxene were permitted to crystallize along a liquid line of descent. The Ol:Cpx proportions have been varied arbitrarily because the exact T-P paths at which melts interact with wall rocks are not known. We assume perfect fractional crystallization, and the extraction of olivine and clinopyroxene was accomplished computationally by removing them incrementally by 0.1%. Of course, the compositions of olivine and clinopyroxene need to be computed at

each step in order to compare with observed phenocryst compositions. This is accomplished with partition coefficients as discussed now.

The method for computing the compositions of Ni, Ca, Mn, and Fe in olivine in equilibrium with both the primary magmas and their derivative liquids was reported in Herzberg (2011), and is repeated here because it is an appropriate introduction to the calculation of clinopyroxene composition. As discussed above, we make use of the partition coefficient:

$$D_i^{Ol/L} = X_i^{Ol} / X_i^{L} \quad (9)$$

where $X_i$ refers to the mole fraction of oxide component i in the phases liquid (L), olivine (Ol), based on one metal cation per oxide (i.e., $SiO_2$, MgO, $AlO_{1.5}$, $NaO_{0.5}$ etc.). We used the temperature-independent Beattie-Jones parameterization model (Jones, 1984; Beattie et al., 1991):

$$D_i^{Ol/L} = A_i^{Ol/L} D_{MgO}^{Ol/L} + B_i^{Ol/L} \quad (10)$$

where $D_{MgO}^{OL} = MgO^{Ol}/Mg^{OL}$ and the A and B constants have been parameterized from experimental data. Parameterized results for Ni reported by Beattie *et al*. (1991) were

discussed above (equation 3). Results for Mn and Ca are from Herzberg and O'Hara (2002), and we use a 1 atmosphere Fe/Mg exchange coefficient from Toplis (2005).

The method for calculating Cpx fractionation is similar to that for Ol addition/subtraction calculations (Herzberg and Asimow, 2008; Herzberg, 2011) except that the partition coefficients are different. We have parameterized high quality high pressure experimental data for Cpx/L from the following sources: Walter (1998), Longhi (2002), Pertermann and Hirschmann (2003), Keshav et al. (2004), Gerbode and Dasgupta (2010) and Le Roux et al. (2011). For Fe and Mn, we follow the Jones-Beattie method of parameterizing partition coefficients as discussed above for olivine:

$$DFeO\ Cpx/L = 0.215\ DMgOCpx/L + 0.181\ (R = 0.98) \quad (11)$$

$$DMnO\ Cpx/L = 0.284\ DMgOCpx/L + 0.294\ (R = 0.91) \quad (12)$$

And

$$DCaO\ Cpx/L = 0.395\ DMgOCpx/L + 0.503\ (R = 0.85) \quad (13)$$

where R refers to the correlation coefficient. Results show that D for FeO and MnO are well-correlated with D for MgO (Fig. S5), as indicated also by the high correlation coefficients. Equations (11) and (12) describe equally well the partitioning of Fe and Mn in melting experiments for which 3-4% $H_2O$ was reported in the liquid (Balta et al., 2011). However, as discussed by Balta et al. (2011), clinopyroxene in these wet experiments contain unusually high CaO compared with anhydrous experiments; as it is

not likely that intraplate magmas are this wet (Herzberg and Asimow, 2008), the Balta results for CaO were not included in the parameterization. For all other experiments, the lower correlation coefficients for CaO may result in part from vacant sites (Hirschmann and Petermann, 2003). But there are also less satisfactory correlations of $D_{MgO}^{Cpx/L}$ with Ds for $TiO_2$, $AlO_{1.5}$, and $NaO_{0.5}$, indicating limitations in application of the Jones-Beattie method to coupled ionic substitutions. Improved correlations were obtained empirically with the following equations:

$$D_{TiO2}^{Cpx/L} = 0.215\ D_{CaO}^{Cpx/L} - 0.047\ (R = 0.87)\ (14)$$

$$D_{AlO1.5}^{Cpx/L} = -1.114\ D_{SiO2}^{Cpx/L} + 1.859\ (R = 0.77)\ (15)$$

and

$$D_{NaO0.5}^{Cpx/L} = 1.304\ D_{AlO1.5}^{Cpx/L} - 0.412\ (R = 0.93)\ (16)$$

D values for CaO, $SiO_2$ $AlO_{1.5}$ , and $NaO_{0.5}$ are computed from mole fractions of these components in Cpx and Liquid in the usual manner; however, sodium partitioning depends on aluminum partitioning and equation (15) must be solved before equation (16).

Clinopyroxene compositions that were computed with the above partition coefficients were assumed to be stoichiometric, with no site vacancies, and all plot exactly within the pyroxene-garnet plane.

It is useful to compare the partitioning behavior of garnet and clinopyroxene, and results are shown in Fig. S5 and listed below.

| | $A^{Gt/L}$ | $B^{Gt/L}$ | R (correlation coefficient) |
|---|---|---|---|
| FeO | 0.589 | -0.135 | 0.99 |
| MnO | 1.169 | -0.375 | 0.98 |
| CaO | 0.20 | 0.31 | 0.96 |
| NiO (see below) | | | |

Included in Fig. S5 are data for majorite garnet/liquid from experiments in the range 15.5-22.5 GPa and 2135-2375°C (Herzberg and Zhang, 1996). These extreme T-P data are fully consistent with others in the 2.5 to 7.0 GPa range, demonstrating the success of the Jones-Beattie model in capturing the partitioning of Fe, Mn, Mg, and Ca between garnet and liquid over all conditions of magma genesis.

Manganese is strongly partitioned into garnet, whereas it displays both compatible and incompatible behavior in clinopyroxene. Furthermore, MnO is more compatible in Cpx and Gt than is FeO (Fig. S5). The ability of garnet and clinopyroxene to preferentially accept Mn over Fe during melting and crystallization will yield liquids with elevated Fe/Mn. Olivines that crystallize from such liquids will also be elevated in Fe/Mn and can indicate a garnet pyroxenite source during partial melting (Sobolev et al., 2007; Herzberg, 2011). Alternatively, olivines with elevated Fe/Mn can indicate garnet pyroxenite crystallization from melts of a peridotite source.

There are very few experiments that constrain the partitioning of Ni for Cpx/L and Gt/L. However, Canil (1999) reported variable $D_{NiO}^{Gt/Ol}$ in subsolidus experiments, reaching a maximum of 0.11 at 1500°C and 5 GPa. Using Canil's data, Sobolev et al. (2005) estimated $D_{NiO}^{Gt/Ol}$ in the 0.10-0.14 range appropriate to Walter's (1998) experiments for which no NiO data were reported; similarly, they estimated $D_{NiO}^{Gt/Cpx}$ of about 0.5. For the case of L + Ol + Cpx ± Gt, we can estimate $D_{NiO}^{Cpx/L}$ and $D_{NiO}^{Gt/L}$ from $D_{NiO}^{Gt/Ol}$ and $D_{NiO}^{Cpx/Ol}$ and $D_{NiO}^{Ol/L}$ (Beattie et al., 1991; equation 1). Results are:

$$D_{NiO}^{Cpx/Ol} = 0.250\ D_{NiO}^{Ol/L} \quad (17)$$

and

$$D_{NiO}^{Gt/L} = 0.125\ D_{NiO}^{Ol/L} \quad (18)$$

There is only one experiment for which high quality Ni data are reported for all phases for L + Ol + Cpx, that being G107 of Le Roux et al. (2011). Results show $D_{NiO}^{Cpx/Ol}$ = 0.28 $D_{NiO}^{Ol/L}$ using Ni in olivine and liquid in experiment G107. The distribution of Ni between Ol and L in this experiment (8.32) is in good but not perfect agreement with the parameterization of Beattie et al. (1991; 9.32) at the $D_{MgO}^{Ol/L}$ in G107 (3.88). Using Beattie's parameterized $D_{NiO}^{Ol/L}$, we obtain for experiment G107 $D_{NiO}^{Cpx/Ol}$ = 0.250 $D_{NiO}^{Ol/L}$, in excellent agreement with equation (17).

**S.5. Olivine Phenocrysts from Isla Gorgona, Ontong Java Plateau and Fernandina**

Olivine phenocryst compositions from Isla Gorgona komatiites were provided by Sobolev et al. (2007) and are shown in Fig. S6. These have very high *Mg*-numbers, similar to those expected for early crystals from the primary magmas, and peridotite source provenance is indicated by Ca, Mn, and Fe/Mn (Herzberg, 2011; Sobolev et al., 2007). However, they distinctly enriched in Ni, and require crystallization of magmas of a Ni-rich peridotite source.

Olivine phenocryst compositions from the Ontong Java Plateau were also provided by Sobolev et al. (2007) and are also shown in Fig. S6. They have lower *Mg*-numbers than olivines from Gorgona, and there is some indication that both olivine and clinopyroxene fractionation has affected their compositions. Relative to olivine-only fractionation, the effects of variable clinopyroxene fractionation is to lower Ca and Mn, and raise both Ni and Fe/Mn.

Olivine phenocryst compositions for Fernandina are new and reported in Table S2 and shown in Fig. S7. These were obtained from a submarine sample D38A from Fernandina in the Galapagos Islands (Geist et al., 2006). Major and trace element data were obtained using the method of Sobolev 2007 on Rutgers University's Joel JXA-8600 electron microprobe. Detection limits were obtained from the Probe for Windows for all elements. Average detection limits for Si, Mg and Fe are 53, 36 and 40 ppm respectively. Average detection limits for trace elements Ni, Mn and Ca are 26, 28 and 16 ppm respectively. 2σ error for all elements was calculated from repeated analyses of the San Carlos olivine standard. Analyses of Si, Mg and Fe have a relative 2σ error of ~1.75%,

~0.51% and ~0.57% respectively. Analyses of trace elements Ni, Mn and Ca have a relative 2σ error of 2.02%, 2.68% and 3.06% respectively. The relative 2σ error for the Fo# is ~0.12%. Analyses with oxide totals > ± 2% deviation from 100% were excluded. Chemical formulas were calculated for all analyses. Analyses with deviations in stoichiometry > ± 1% were excluded. Relative to olivine-only fractionation, the effects of variable clinopyroxene fractionation (Geist et al., 1998) is to lower Ca and Mn, and raise both Ni and Fe/Mn.

**S.6. Examples of Peridotite and Pyroxenite Source Lithologies Inferred from Olivine Phenocryst Composition**

Comparably high mantle potential temperatures have been inferred for both Hawaii and West Greenland occurrences (TP = 1500-1600°C; Herzberg and Asimow, 2008; Herzberg and Gazel, 2009), and both erupted over thick lithosphere (Larsen and Pedersen, 2000; Li et al., 2000; 2004). If elevated temperature and pressure is the main mechanism for producing olivine phenocyrsts with high Ni contents, then it is to be expected olivine phenocryst compositions from Hawaii and West Greenland occurrences will have similar Ni, Mn, Fe/Mn, and Ca. This is not observed (Fig. S8). Hawaiian olivines are higher in Ni by ~ 1000 ppm, they are substantially lower Ca and Mn and higher Fe/Mn compared with those from West Greenland, Baffin Island and Disko Island.

Olivine phenocrysts from Alexo komatiites of Archean age have Ni contents that are somewhat higher than those of expected from olivines of primary peridotite-source magmas with 26-30% MgO (Fig. S9). However, the effect of minor olivine fractionation is to initially raise Ni then lower it, producing an array that is concaved toward the Mg-

number axis (Herzberg, 2011). This sense of curvature computed from the Beattie-Jones Ni partitioning model is captured in olivines from Alexo (Fig. S9), a remarkable level of agreement. It is also clear from Fig. S9 that olivine phenocrysts from Hawaii and Alexo komatities have very different Ca, Mn, and Fe/Mn. For Alexo, a peridotite source provenance is clearly indicated (Fig. S9). In contrast, low Ca and Mn and high Fe/Mn for Hawaiian olivines are not consistent with peridotite-source melting.

Olivine phenocrysts in subduction zone andesites from the Mexican Volcanic Belt have the highest Ni contents ever reported (Straub et al., 2008), and greatly exceed the Ni contents of normal mantle peridotite (Fig. S10). Straub et al. (2008) interpreted these high Ni contents with a pyroxenite source lithology that formed by reaction of $SiO_2$-rich slab fluids with peridotite in the mantle wedge. Ni maxima are observed for 4 sub parallel arrays, and those with the lowest Mg-numbers exclude the possibility of formation from a peridotite source lithology. Most relevant to the present discussion is that it is not probable that these olivine Ni contents can be interpreted by any temperature- and pressure-melting and crystallization process that operated on a normal Ni peridotite source.

**S.7. References:**

Albarède, F., B. Luais, G. Fitton, M. Semet, E. Kaminski, B.G.J. Upton, P. Bachèlery, and J.L. Cheminée, (1997), The geochemical regimes of Piton de la Fournaise volcano (Réunion) during the last 530000 years. Journal of Petrology, v. 38, p. 171-201.

Balta, J.B., P.D. Asimow and J.L. Mosenfelder, (2011), Hydrous, low-carbon melting of garnet peridotite. Journal of Petrology, v. 52, p. 2079-2105.

Beattie, P., C. Ford and D. Russell, (1991), Partition coefficients for olivine-melt and orthopyroxene-melt systems. Contributions to Mineralogy and Petrology, v. 109, p. 212-224.

Canil, D., (1996), The Ni-in-garnet geothermometer: calibration at natural abundances. Contributions to Mineralogy and Petrology, v. 136, p. 240-246.

Filiberto, J., C. Jackson, L. Le and A.H. Treiman, (2009), Partitioning of Ni between olivine and an iron-rich basalt: experiments, partition models, and planetary implications. American Mineralogist, v. 94, p. 256-261.

Geist, D., T. Naumann and P. Larson, (1998), Evolution of Galapagos magmas: mantle and crustal fractionation without assimilation. Journal of Petrology, v. 39, p. 953-971.

Geist, D., D.J. Fornari, M.D. Kurz, K.S. Harpp, S.A. Soule, M.R. Perfit and A.M. Koleszar, (2006), Submarine Fernandina: Magmatism at the leading edge of the Galápagos hot spot. Geochemistry Geophysics Geosystems 7, Q12007, doi:10.1029/2006GC001290.

Gerbode, C. and R. Dasgupta, (2010), Carbonate-fluxed melting of MORB-like pyroxenite at 2.9 GPa and genesis of HIMU ocean island basalts. Journal of Petrology, v. 51, p. 2067-2088.

Hart, S.R. and K.E. Davis, (1978), Nickel partitioning between olivine and silicate melt. Earth and Planetary Science Letters, v. 40, p. 203-219.

Herzberg, C.T., (1993), Lithosphere peridotites of the Kaapvaal craton. Earth and Planetary Sciences Letters, v. 120, p. 13-29.

Herzberg, C., (1999), Phase equilibrium constraints on the formation of cratonic mantle. In: Mantle Petrology: Field Observations and High Pressure Experimentation: A Tribute to Francis R. (Joe) Boyd. The Geochemical Society, Special Publication 6, Fei, Y., Bertka, C.M., Mysen, B.O., eds, p. 241-257.

Herzberg, C., (2004a), Partial crystallization of mid-ocean ridge basalts in the crust and mantle. Journal of Petrology, v. 45, p. 2389-2405.

Herzberg, C., (2004b), Geodynamic information in peridotite petrology. Journal of Petrology, v. 45, p. 2507-2530.

Herzberg, C., (2011), Identification of Source Lithology in the Hawaiian and Canary Islands: Implications for Origins. Journal of Petrology, v. 52, p. 113-146.

Herzberg, C. and J. Zhang, (1996), Melting experiments on anhydrous peridotite KLB-1: Compositions of magmas in the upper mantle and transition zone. Journal of Geophysical Research, v. 101, p. 8271-8295.

Herzberg, C. and M.J. O'Hara, (2002), Plume-associated ultramafic magmas of phanerozoic age. Journal of Petrology, v. 43, p. 1857-1883.

Herzberg, C. and P.D. Asimow, (2008), Petrology of some oceanic island basalts: PRIMELT2.XLS software for primary magma calculation. Geochemistry Geophysics Geosystems 8, Q09001, doi:10.1029/2008GC002057.

Ionov, D.A., (2007), Compositional variations and heterogeneity in fertile lithospheric mantle: peridotite xenoliths in basalts from Tariat, Mongolia. Contributions to Mineralogy and Petrology, v. 154, p. 455–477.

Ionov, D.A., (2010), Petrology of mantle wedge lithosphere: New data on supra-subduction zone peridotite xenoliths from the andesitic Avacha volcano, Kamchatka. Journal of Petrology v. 51, p. 327-361.

Ionov, D.A., I. Ashchepkov and E. Jagoutz, (2005), The provenance of fertile off-craton lithospheric mantle: Sr-Nd isotope and chemical composition of garnet and spinel peridotite xenoliths from Vitim, Siberia. Chemical Geology, v. 217, p. 41-74.

Ionov, D.A., V. Prikhodko, J.-L. Bodinier, A.V. Sobolev and D. Weis, (2005), Lithospheric mantle beneath the south-eastern Siberian craton: petrology of peridotite xenoliths in basalts from the Tokinsky Stanovik. Contributions to Mineralogy and Petrology, v. 149, p. 647-665.

Ionov, D.A. and A.W. Hofmann, (2007), Depth of formation of subcontinental off-craton peridotites. Earth and Planetary Science Letters, v. 261, p. 620-634.

Jones, J.H., (1984), Temperature and pressure- independent correlations of olivine-liquid partition coefficients and their application to trace element partitioning. Contributions to Mineralogy and Petrology, v. 88, p. 126-132.

Keshav, S., G.H. Gudfinnsson, G. Sen and Y.-W. Fei, (2004), High-pressure melting experiments on garnet clinopyroxenite and the alkalic to tholeiitic transition in ocean-island basalts. Earth and Planetary Science Letters, v. 223, p. 365-379.

Larsen, L.M. and A.K. Pedersen, (2000), Processes in high-Mg, high-T magmas: evidence Fro m olivine, chromite and glass in Palaeogene picrites from West Greenland. Journal of Petrology, v. 41, p. 1071-1098.

Le Roux, V., R. Dasgupta and C.-T.A. Lee, (2011), Mineralogical heterogeneities in the Earth's mantle: Constraints from Mn, Co, Ni and Zn partitioning during partial melting. Earth and Planetary Science Letters, v. 307, p. 395-408.

Li, X., R. Kind, K. Priestley, S.V. Sobolev, F. Tilmann, X. Yuan and M. Weber, (2000), Mapping the Hawaiian plume conduit with converted seismic waves. Nature, v. 405, p. 938-941.

Li, X. R. Kind, X. Yuan, I. Wölbern and W. Hanka, (2004), Rejuvenation of the lithosphere by the Hawaiian plume. Nature, v. 427, p. 827-829.

Li, C. amd E.M. Ripley, (2010), The relative effects of composition and temperature on olivine-liquid Ni partitioning: Statistical deconvolution and implications for petrologic modeling. Chemical Geology, v. 275, p. 99-104.

Longhi, J., (2002), Some phase equilibrium systematics of lherzolite melting: I, Geochemistry Geophysics Geosystems 3, 10.1029/2001GC000204.

Longhi, J., S.R. Durand and D. Walker, D, (2010), The pattern of Ni and Co abundances in lunar olivines. Geochimica et Cosmochimica Acta, v. 74, p. 784-798.

Matzen, A.K., M.B. Baker, J.R. Beckett and E.M. Stolper, (2011), Fe-Mg Partitioning between olivine and high-magnesian melts and the nature of Hawaiian parental liquids. Journal of Petrology, v. 52, p. 1243-1263.

Niu, Y., M. Wilson, E.R. Humphreys and M.J. O'Hara, (2011), The origin of intra-plate ocean island basalts (OI B): the lid effect and its geodynamic implications. Journal of Petrology, v. 52, p. 1443-1468.

O'Hara, M.J., (1968), The bearing of phase equilibria studies in synthetic and natural systems on the origin of basic and ultrabasic rocks. Earth Science Reviews, v.4, p.69-133.

Pertermann, M. and M.M. Hirschmann, (2003), Anhydrous partial melting experiments on MORB-like eclogite: phase relations, phase compositions and mineral-melt partitioning of major elements at 2-3 GPa. Journal of Petrology, v. 44, p. 2173-2201.

Putirka, K.D., F.J. Ryerson, M. Perfit and W.I. Ridley, (2011), Mineralogy and composition of oceanic mantle. Journal of Petrology, v. 52, p. 279-313.

Salters, V.J.M and A. Stracke, (2004), Composition of depleted mantle. Geochemistry,Geophysics, Geosystems 5, Q05004, doi:10.1029/2003GC000597.

Sobolev, A.V., A.W. Hofmann, S.V. Sobolev and I.K. Nikogosian, (2005), An olivine-free mantle source of Hawaiian shield basalts, Nature, v. 434, p. 590-597.

Sobolev, A.V., A.W. Hofmann, D.V. Kuzmin, G.M. Yaxley, N.T. Arndt, S.L. Chung, L.V. Danyushevsky, T. Elliott, F.A. Frey, M.O. Garcia, A.A. Gurenko, V.S. Kamenetsky, A.C. Kerr, N.A. Krivolutskaya, V.V. Matvienkov, I.K. Nikogosian, A. Rocholl, I.A. Sigurdsson, N.M. Sushchevskaya and M. Teklay, (2007), The amount of recycled crust in sources of mantle-derived melts. Science v. 316, p. 412-417.

Straub, S.M., A.B. LaGatta, A.L.M.-D. Pozzo and C.H. Langmuir, (2008), Evidence from high Ni olivines for a hybridized peridotite/pyroxenite source for orogenic andesites from the central Mexican Volcanic Belt. Geochemistry Geophysics Geosystems 9, Q03007, doi: 10.1029GC001583.

Taura, H., H. Yurimoto, K. Kurita and S. Sueno, (1998), Pressure dependence on partition coefficients for trace elements between olivine and coexisting melts. Physics and Chemistry of Minerals v. 25, p. 469-484.

Toplis, M.J. (2005), The thermodynamics of iron and magnesium partitioning between olivine and liquid: criteria for assessing and predicting equilibrium in natural and

experimental systems. Contributions to Mineralogy and Petrology, v. 149, p. 22-39.

Wang, Z. and G.A. Gaetani, (2008), Partitioning of Ni between olivine and siliceous eclogite partial melt: experimental constraints on the mantle source of Hawaiian basalts. Contributions to Mineralogy and Petrology, v. 156, p. 661-678.

**S.8. Figure Captions:**

**Figure S1:**

MgO and Ni contents of mantle peridotite and partial melts of mantle peridotite (Herzberg, 2011).

**Figure S2:**

A comparison of model and experimentally observed partition coefficients for nickel.

**Figure S3:**

Measured versus calculated $D_{NiO}^{Ol/L}$ for equation (3) of Beattie et al. (1991) and equations 7a,b,c of Putirka et al. (2011).

**Figure S4:**

Measured versus calculated $D_{NiO}^{Ol/L}$ for equation (8) of Niu et al. (2011).

**Figure S5:**

Partition coefficients determined for clinopyroxene/liquid (blue squares) and garnet/liquid (red circles) from experimental data listed in the text. Note that FeO contents of garnets in experimental data from Keshav et al.(2004; orange circles) are highly discrepant, unlike MnO, and were not included in the regression.

**Figure S6:**

Mg-numbers and Ni, Ca, Mn, and Fe/Mn for calculated olivine (Herzberg, 2011) and observed olivine phenocrysts from Gorgona komatiites and basalts from the Ontong Java Plateau (Sobolev et al., 2007). Black regions are calculated olivines from primary magmas of peridotite (Herzberg, 2011). Green and blue lines are olivine compositions that crystallize from primary magmas that fractionated olivine and clinopyroxene in the weight proportions indicated. Hi Ni refers to olivine crystallization from a primary melt of a high Ni mantle peridotite.

**Figure S7:**

Mg-numbers and Ni, Ca, Mn, and Fe/Mn for calculated olivine (Herzberg, 2011) and observed olivine phenocrysts from a submarine sample D38A from Fernandina in the Galapagos Islands (Table S1). Black regions are calculated olivines from primary magmas of peridotite (Herzberg, 2011). Green and blue lines are olivine compositions that crystallize from primary magmas that fractionated olivine and clinopyroxene in the weight proportions indicated. Hi Ni refers to olivine crystallization from a primary melt of a high Ni mantle peridotite.

**Figure S8:**

A comparison of olivine phenocryst compositions for Hawaii, West Greenland, Baffin Island and Disko Island. All data are from Sobolev et al. (2007).

**Figure S9:**

A comparison of olivine phenocryst compositions for Hawaii and Alexo komatiites of Archean age. All data are from Sobolev et al. (2007).

**Figure S10:**

Olivine phenocryst compositions from the Mexican Volcanic Belt (Straub et al., 2008).

**Figure S11:**

Olivine phenocryst compositions from the Komati Formation of the Barberton greenstone belt compared with olivines expected to crystallize from primary magmas of dry fertile peridotite (black form; 3.45% CaO). Red arrow labeled F reflects lower Ca content of olivine with increasing melt fraction F. Low Ca olivine outliers may have grown in heterogeneous melts formed at high melt fractions or from melts of more depleted peridotite (grey form; 2.14% CaO; melt solutions in Herzberg (2004b) except calculated for accumulated fractional melting). It is notable that depleted isotopic compositions do not correlate with depleted major element compositions of peridotite sources (e.g., Salters and Stacke, 2004), and the olivine Ca contents should cover the full range of possibilities. Model depleted and fertile peridotite compositions have ~ 8% FeO (Herzberg and O'Hara, 2002). An ancient FeO-depleted source is expected to yield olivines with similar CaO but higher Mg-numbers.

**Figure S12:** Ca contents of olivine in experimental melts with various $H_2O$ contents.

**S.9. Figures:**

**Figure S1:**

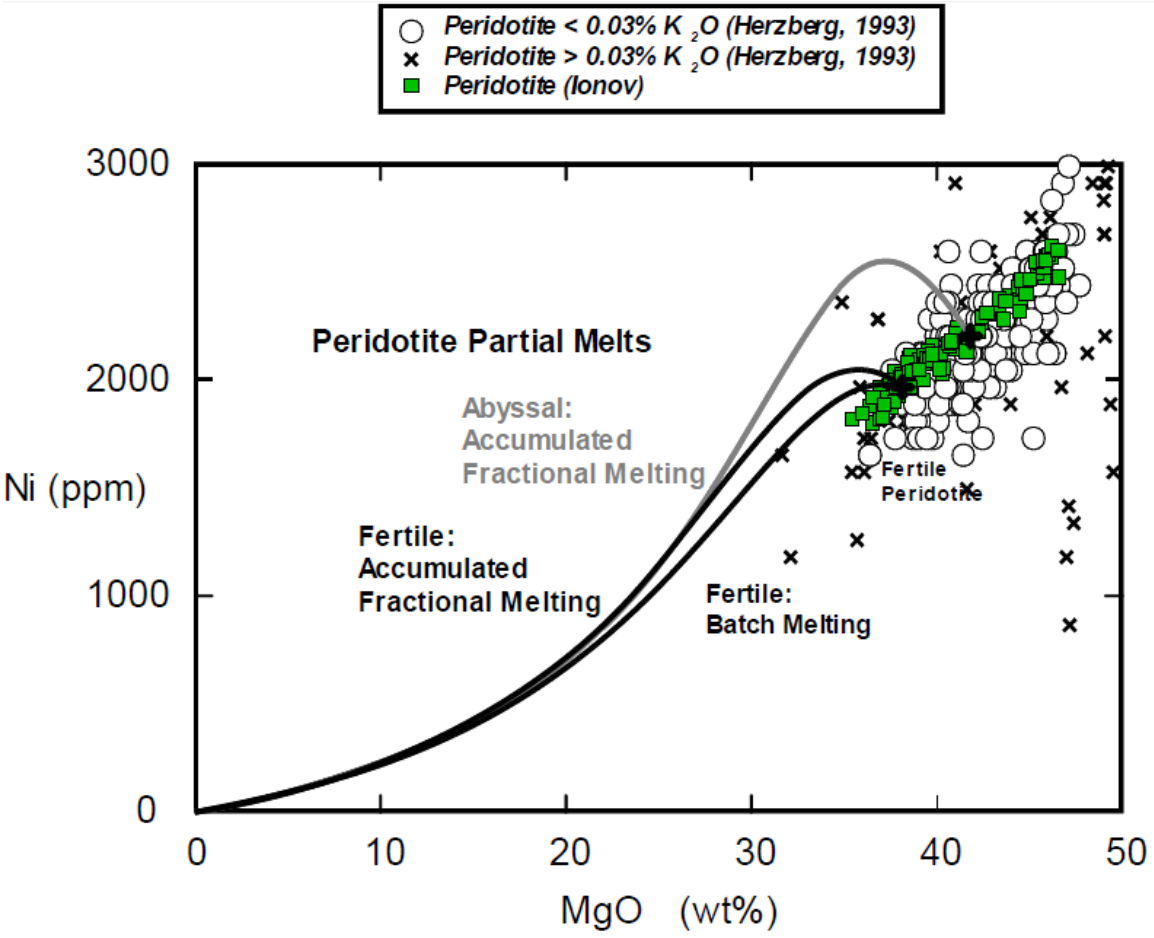

**Figure S2:**

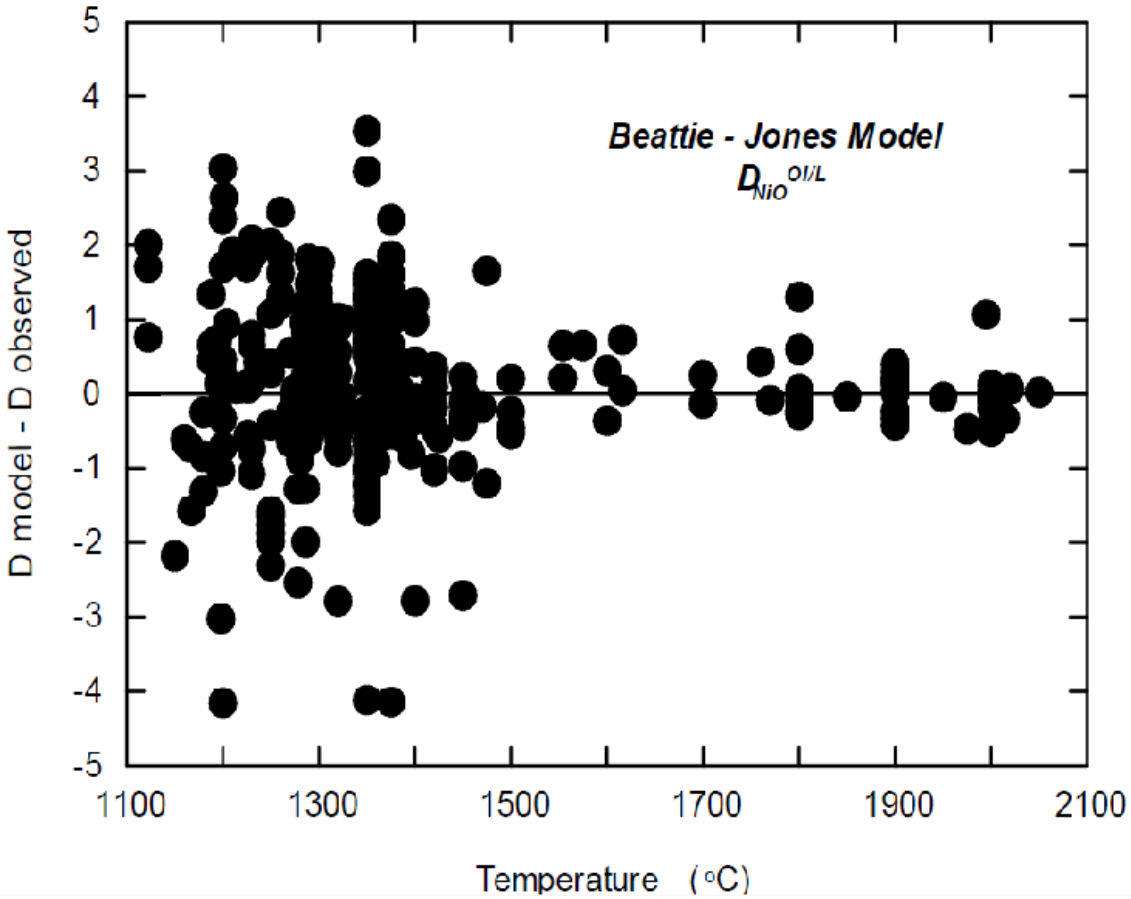
Beattie - Jones Model
$D_{NiO}^{Ol/L}$
D model - D observed
5
4
3
2
1
0
-1
-2
-3
-4
-5
1100
1300
1500
1700
1900
2100
Temperature (°C)

**Figure S3:**

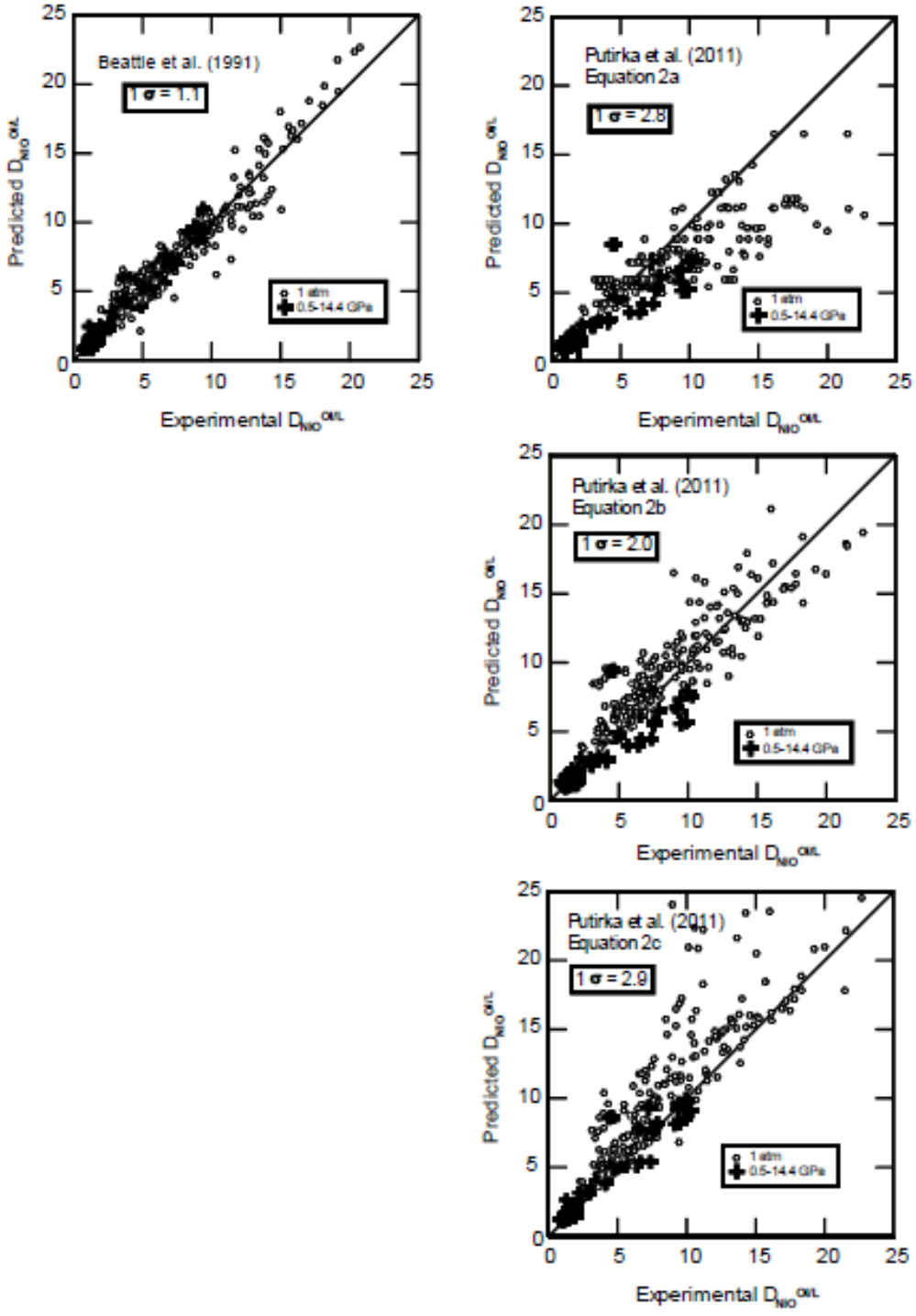
Beattie et al. (1991)
1 σ = 1.1
Putirka et al. (2011)
Equation 2a
1 σ = 2.8
Putirka et al. (2011)
Equation 2b
1 σ = 2.0
Putirka et al. (2011)
Equation 2c
1 σ = 2.9
1 atm
0.5-14.4 GPa
Predicted D_NiO^ol/L
Experimental D_NiO^ol/L
0
5
10
15
20
25

**Figure S4:**

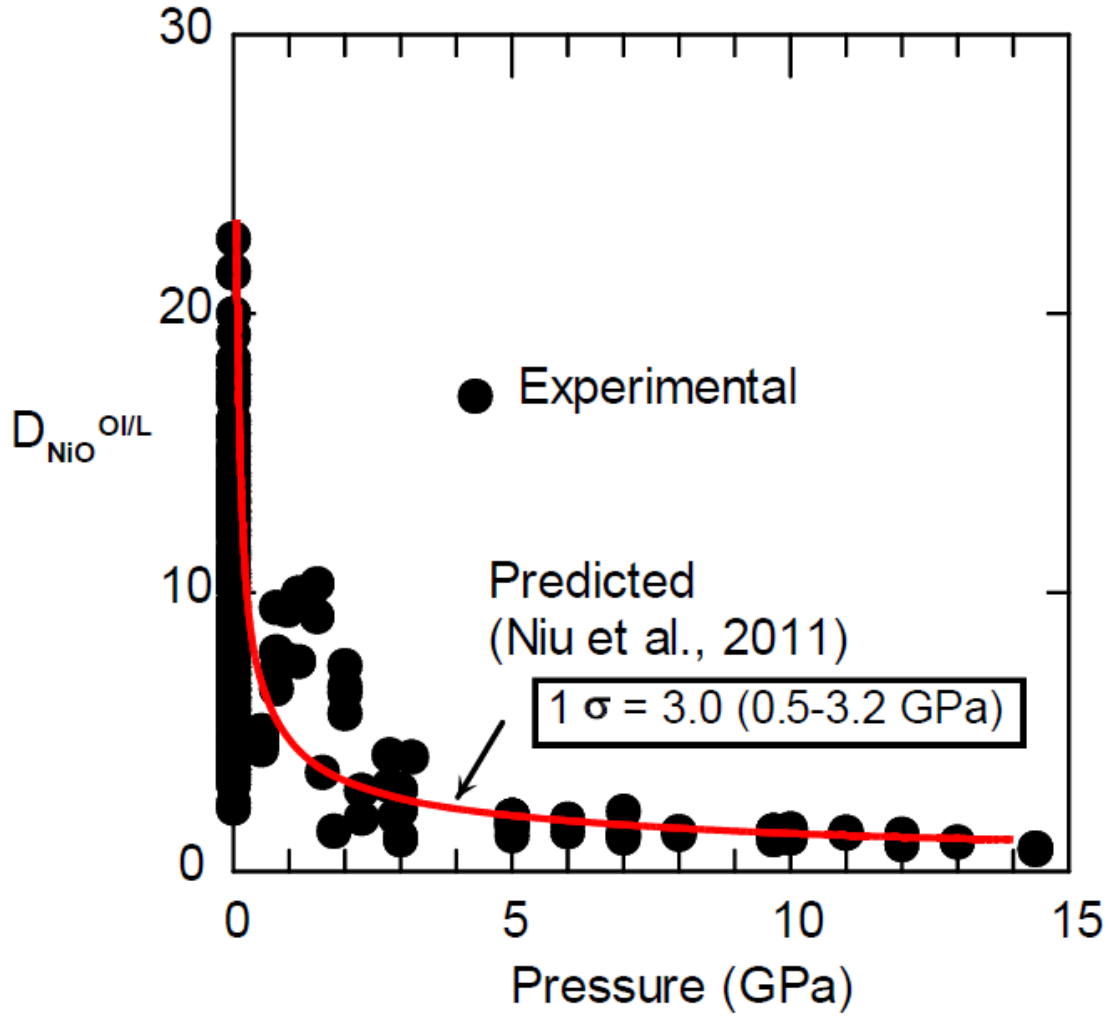
30
20
10
0
$D_{NiO}^{Ol/L}$
Experimental
Predicted
(Niu et al., 2011)
1 σ = 3.0 (0.5-3.2 GPa)
0
5
10
15
Pressure (GPa)

**Figure S5:**

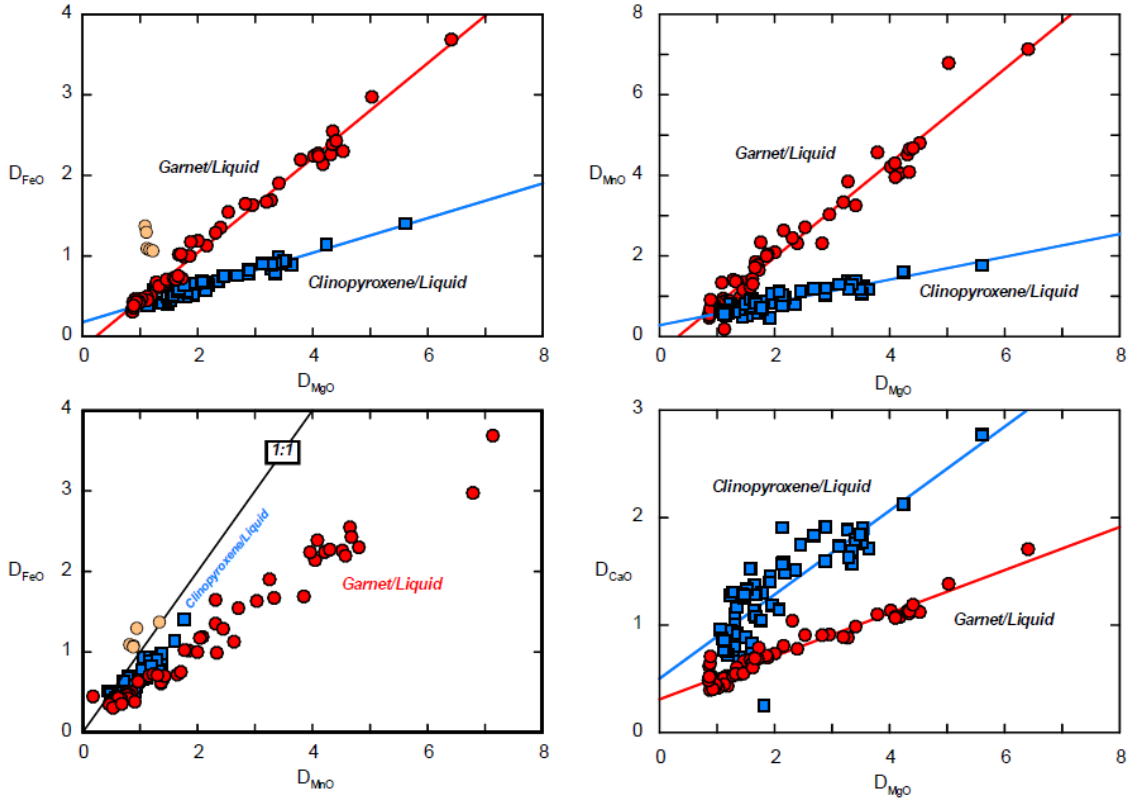
Garnet/Liquid
Clinopyroxene/Liquid
D_FeO
D_MgO
Garnet/Liquid
Clinopyroxene/Liquid
D_MnO
D_MgO
1:1
Clinopyroxene/Liquid
Garnet/Liquid
D_FeO
D_MnO
Clinopyroxene/Liquid
Garnet/Liquid
D_CaO
D_MgO

**Figure S6:**

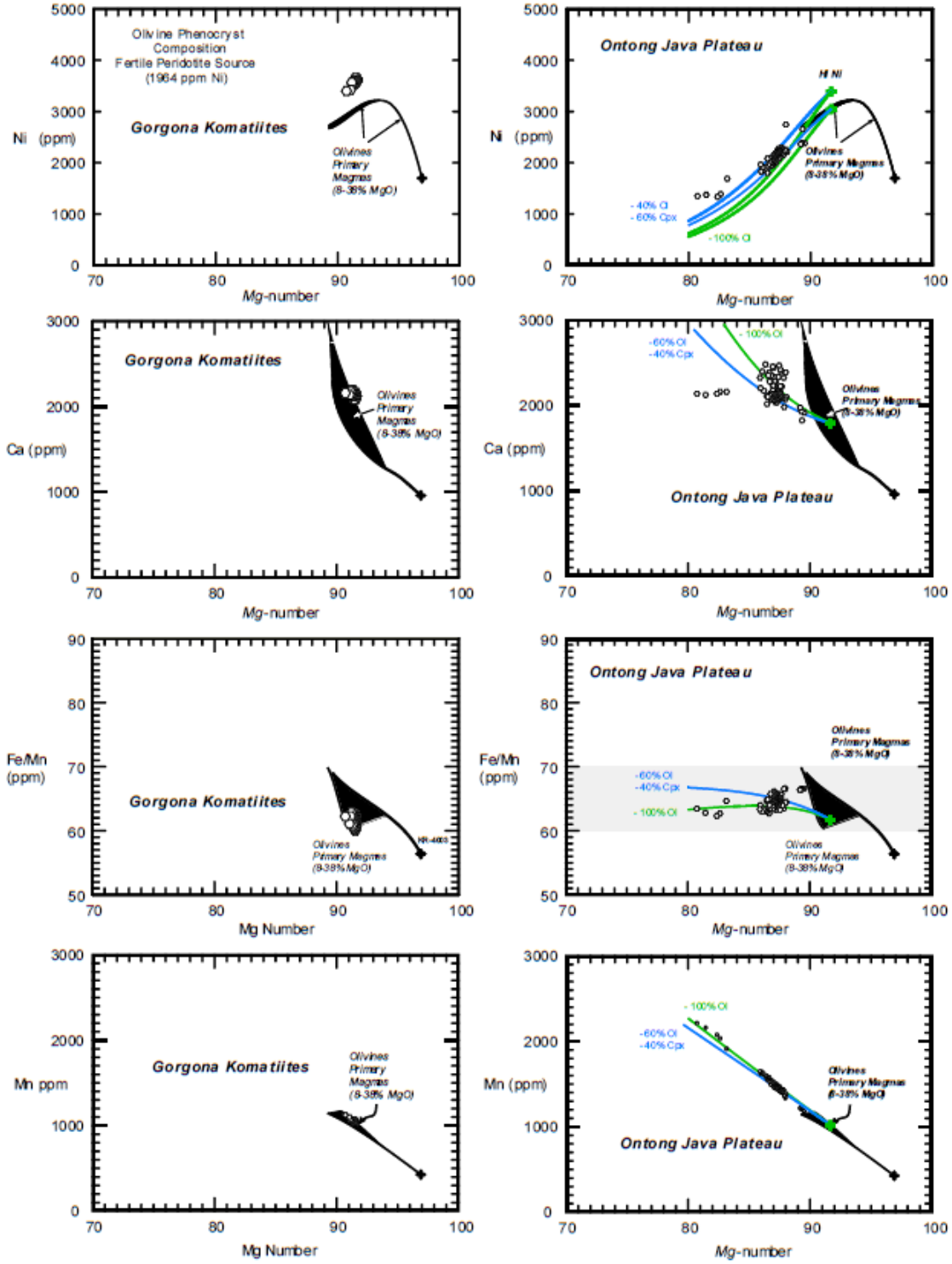
Olivine Phenocryst Composition
Fertile Peridotite Source
(1964 ppm Ni)
Gorgona Komatiites
Olivines Primary Magmas (8-38% MgO)
Ni (ppm)
Mg-number
Ontong Java Plateau
Hi Ni
- 40% Ol
- 60% Cpx
- 100% Ol
Ca (ppm)
Fe/Mn (ppm)
Mg Number
Mn ppm
Mn (ppm)

**Figure S7:**

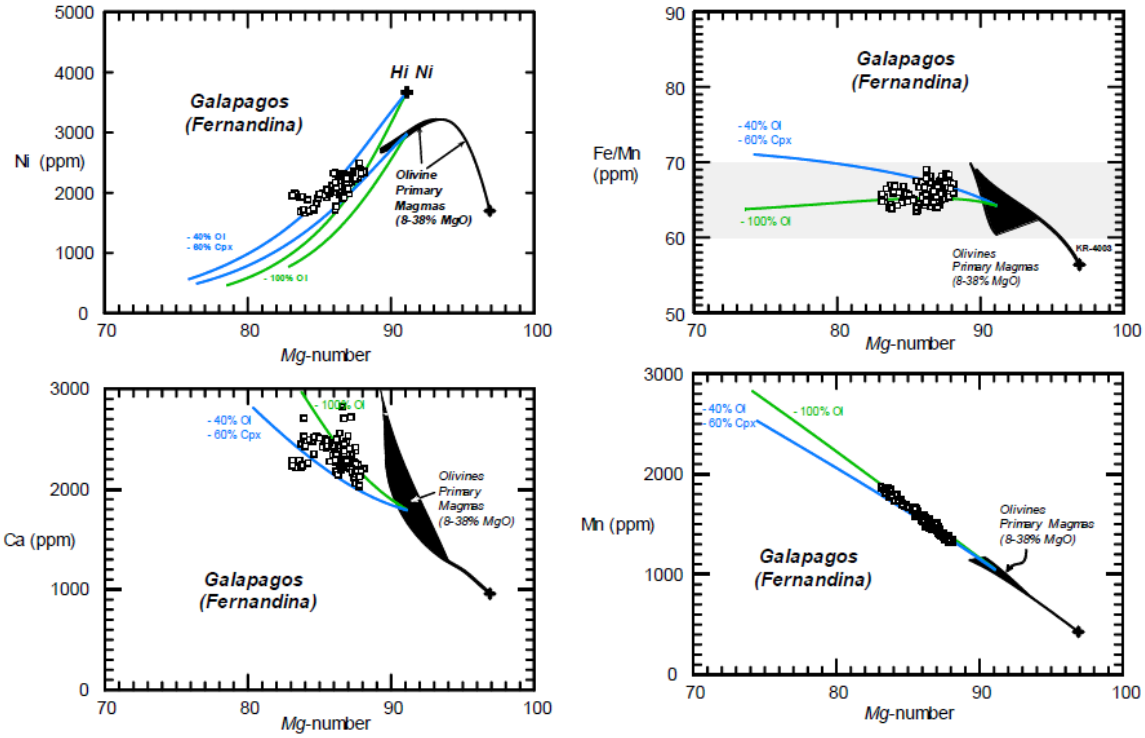
Galapagos
(Fernandina)
Hi Ni
Olivine
Primary
Magmas
(8-38% MgO)
- 40% Ol
- 60% Cpx
- 100% Ol
Ni (ppm)
Mg-number
Fe/Mn
(ppm)
Olivines
Primary Magmas
(8-38% MgO)
KR-4008
Ca (ppm)
Mn (ppm)

**Figure S8:**

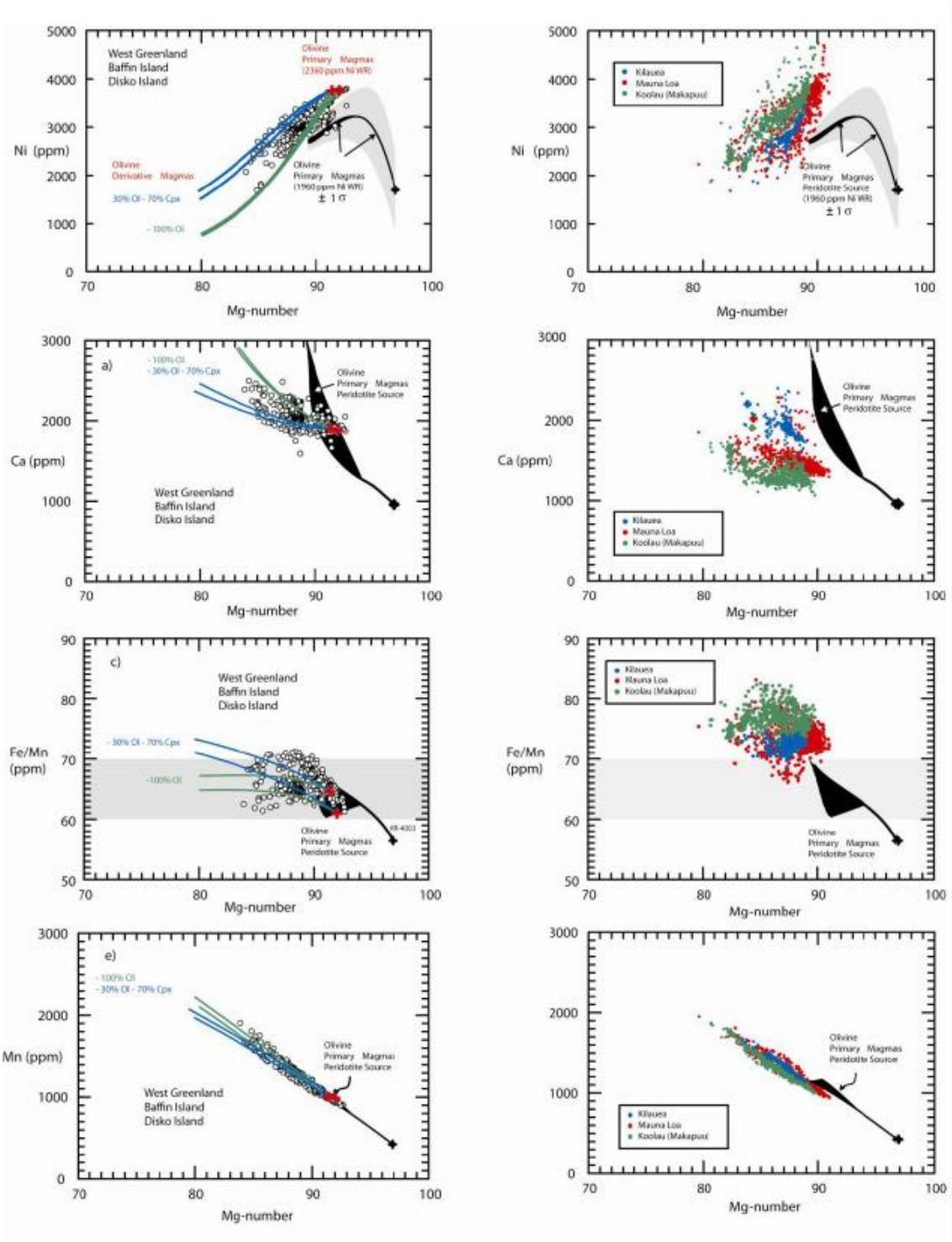
West Greenland
Baffin Island
Disko Island
Olivine Primary Magmas (2340 ppm Ni WR)
Olivine Derivative Magmas
30% Ol - 70% Cpx
- 100% Ol
Olivine Primary Magmas (1960 ppm Ni WR)
± 1 σ
Ni (ppm)
Mg-number
Kilauea
Mauna Loa
Koolau (Makapuu)
Olivine Primary Magmas Peridotite Source
a)
Ca (ppm)
c)
Fe/Mn (ppm)
e)
Mn (ppm)

**Figure S9:**

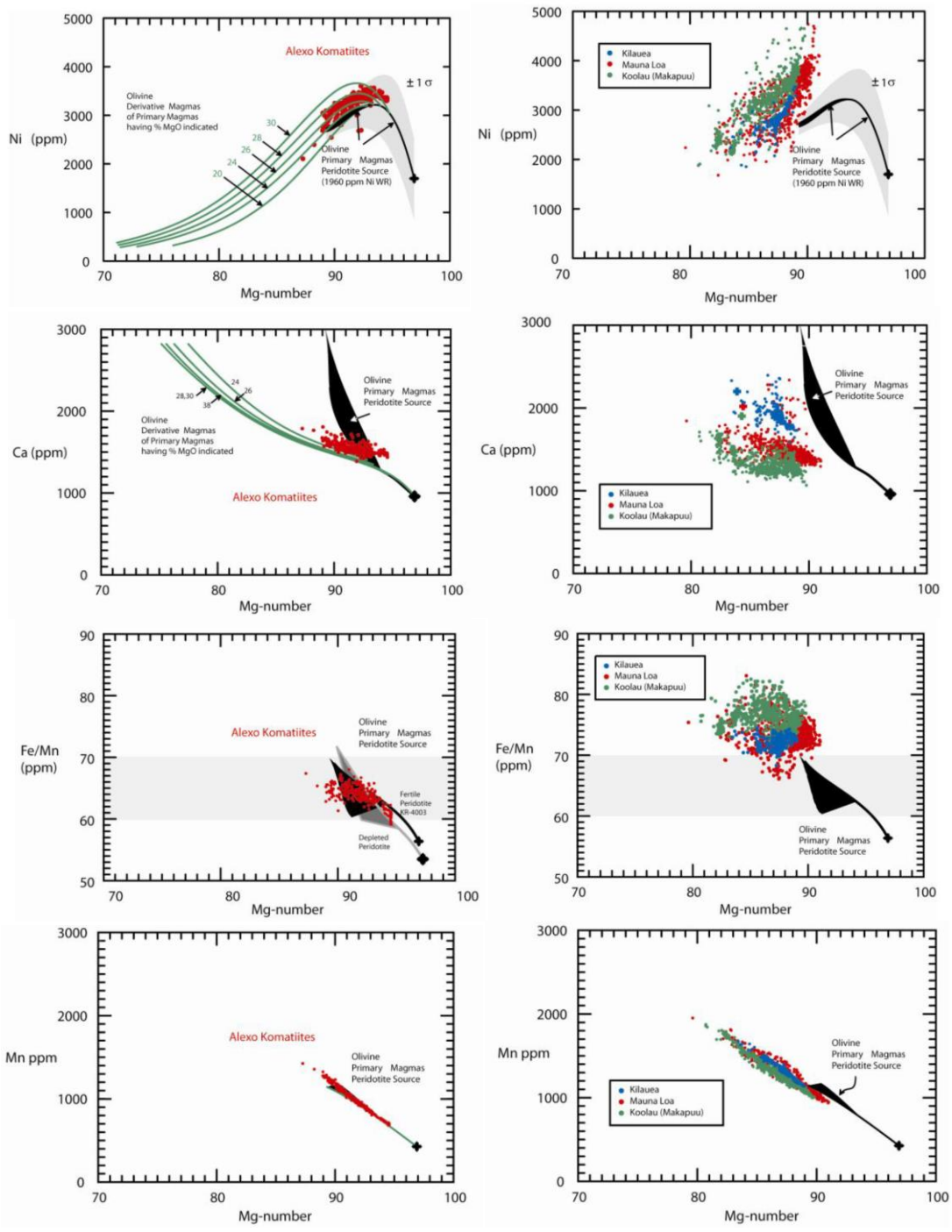
Alexo Komatiites
Olivine Derivative Magmas of Primary Magmas having % MgO indicated
Olivine Primary Magmas Peridotite Source (1960 ppm Ni WR)
±1σ
Ni (ppm)
Mg-number
Kilauea
Mauna Loa
Koolau (Makapuu)
Ca (ppm)
Fe/Mn (ppm)
Fertile Peridotite KR-4003
Depleted Peridotite
Mn ppm

**Figure S10:**

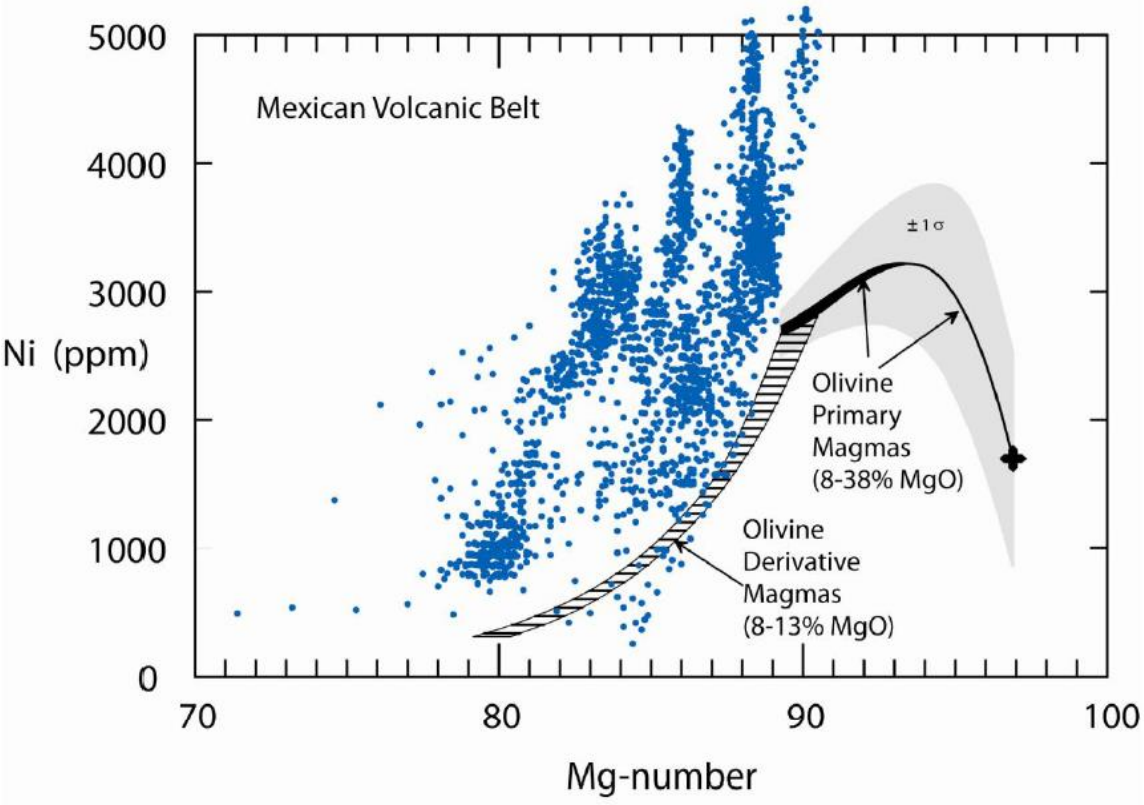
Mexican Volcanic Belt
±1σ
Olivine
Primary
Magmas
(8-38% MgO)
Olivine
Derivative
Magmas
(8-13% MgO)
Ni (ppm)
5000
4000
3000
2000
1000
0
70
80
90
100
Mg-number

**Figure S11:**

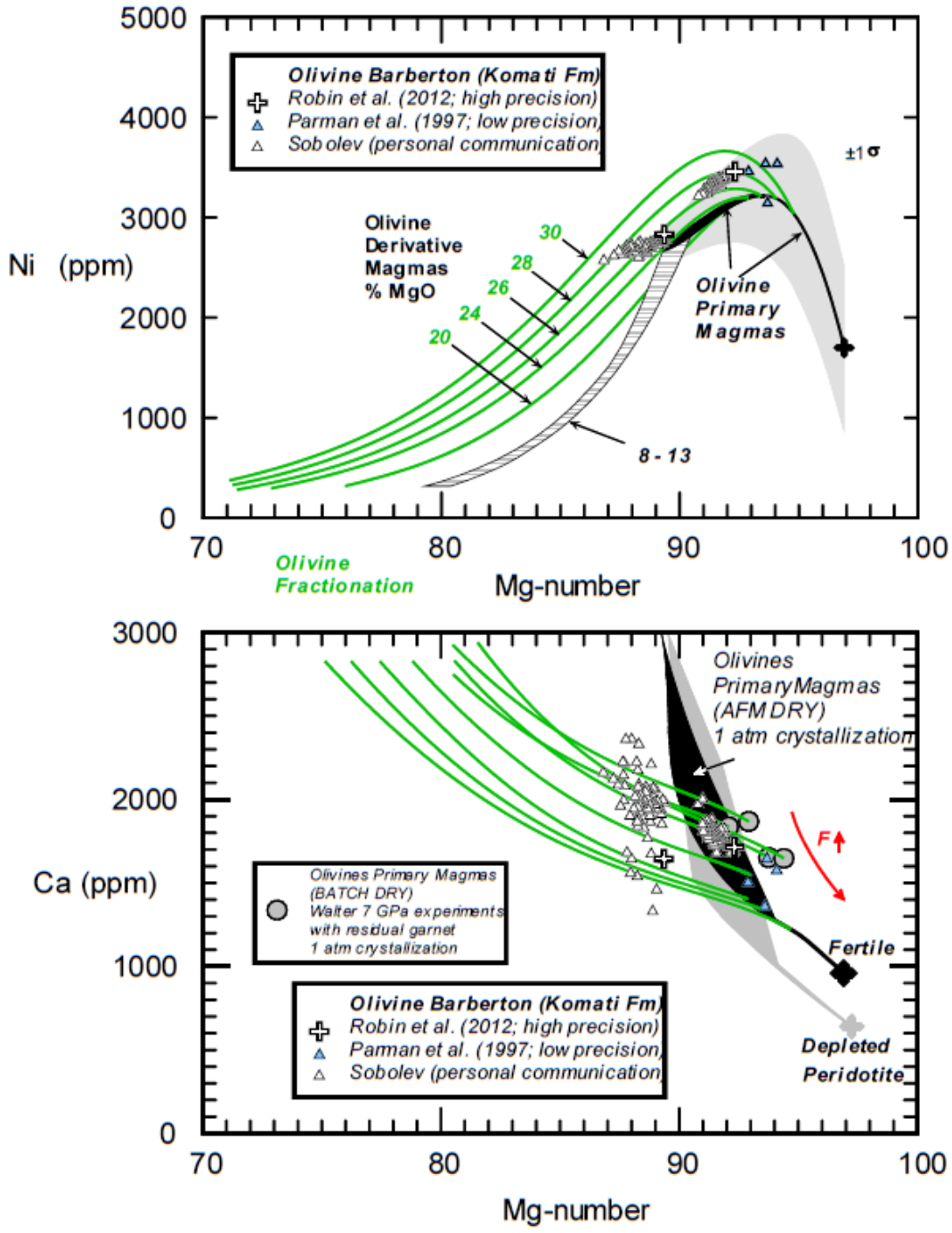
Olivine Barberton (Komati Fm)
Robin et al. (2012; high precision)
Parman et al. (1997; low precision)
Sobolev (personal communication)
±1σ
Olivine Derivative Magmas % MgO
30
28
26
24
20
Olivine Primary Magmas
8 - 13
Olivine Fractionation
Ni (ppm)
Mg-number
Olivines Primary Magmas (AFM DRY) 1 atm crystallization
F
Olivines Primary Magmas (BATCH DRY) Walter 7 GPa experiments with residual garnet 1 atm crystallization
Fertile
Depleted Peridotite
Ca (ppm)
Mg-number

**Figure S12:**

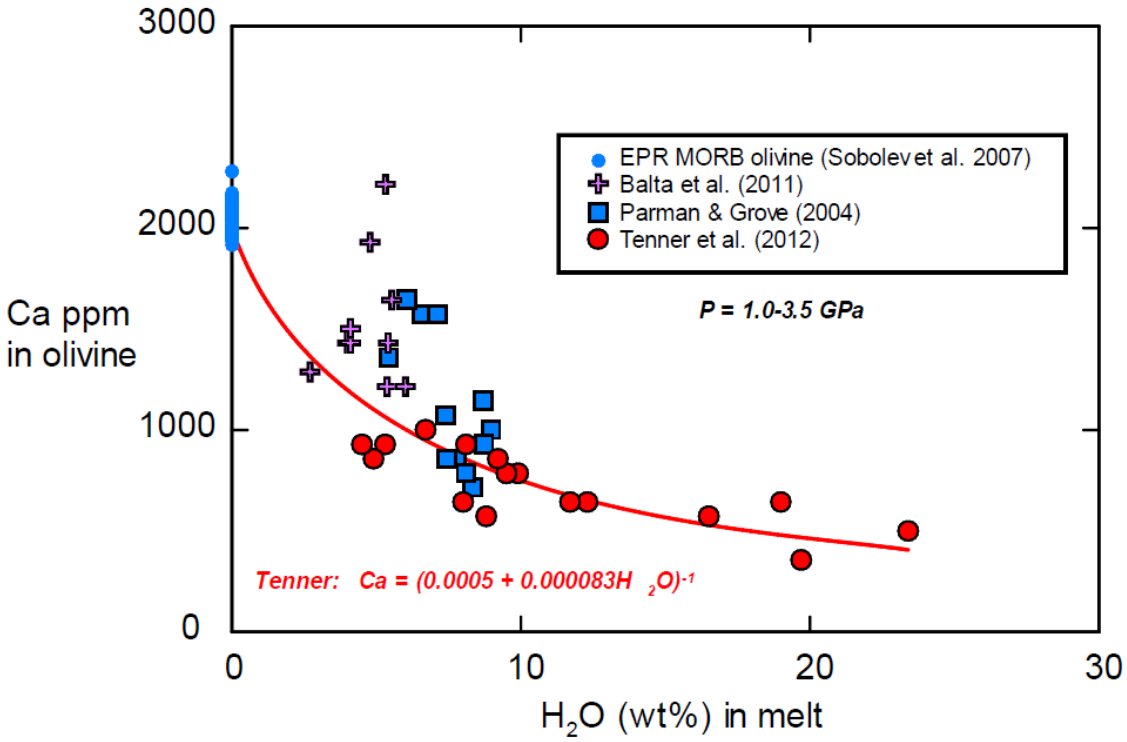
3000
2000
1000
0
Ca ppm
in olivine
0
10
20
30
H2O (wt%) in melt
EPR MORB olivine (Sobolev et al. 2007)
Balta et al. (2011)
Parman & Grove (2004)
Tenner et al. (2012)
P = 1.0-3.5 GPa
Tenner: Ca = (0.0005 + 0.000083H2O)-1

**S.10. Tables:**

**Table S1: High Precision Olivine Analyses for Peridotites**

| Off-Craton Spinel Peridotites<br>Sample Number | SiO2 | NiO | MgO | Total | *Mg*-number | Ni (ppm) |
|---|---|---|---|---|---|---|
| Vitim, southern Siberia, (east of Lake Baikal): | | | | | | |
| Spinel lherzolites in Miocene tuffs | | | | | | |
| 314-56ol7 | 40.28 | 0.373 | 49.03 | 100.4 | 89.3 | 2933 |
| 314-58ol7 | 40.39 | 0.371 | 49.42 | 100.3 | 89.9 | 2915 |
| 314-59ol8 | 40.52 | 0.368 | 49.77 | 100.3 | 90.4 | 2888 |
| 314-71ol7 | 40.37 | 0.374 | 50.11 | 100.0 | 91.0 | 2938 |
| 314-72ol7 | 40.48 | 0.375 | 49.83 | 100.3 | 90.4 | 2945 |
| Spl lherzolites in young basaltic lavas | | | | | | |
| 86-1ol7 | 40.45 | 0.357 | 49.49 | 100.3 | 90.0 | 2807 |
| 302-10 ol7 | 40.49 | 0.371 | 49.16 | 100.4 | 89.6 | 2913 |
| 302-403 ol9 | 40.71 | 0.364 | 49.23 | 100.7 | 89.6 | 2861 |
| 559-43 ol8 | 40.79 | 0.373 | 49.49 | 100.5 | 90.1 | 2933 |
| 621-11 ol10 | 40.69 | 0.370 | 49.16 | 100.7 | 89.5 | 2905 |
| 621-24 ol9 | 40.68 | 0.364 | 49.37 | 100.4 | 90.0 | 2863 |
| 621-36 ol8 | 40.90 | 0.381 | 50.54 | 100.4 | 91.5 | 2990 |
| 623-10 ol7 | 40.75 | 0.372 | 49.47 | 100.5 | 90.0 | 2923 |
| 623-14 ol9 | 40.79 | 0.359 | 49.58 | 100.5 | 90.3 | 2823 |
| 625-1 ol av6 | 40.88 | 0.352 | 49.31 | 100.7 | 89.9 | 2764 |
| Southern Baikal region, southern Siberia: | | | | | | |
| 8601-13 ol7 | 40.96 | 0.386 | 50.03 | 100.8 | 90.7 | 3033 |
| 8603-2ol7 | 40.64 | 0.362 | 49.00 | 100.7 | 89.3 | 2846 |
| 83-36ol7 | 40.72 | 0.366 | 49.34 | 100.7 | 89.7 | 2873 |
| 83-50ol7 | 40.86 | 0.362 | 49.55 | 100.8 | 90.0 | 2847 |
| 601-1 ol av8 | 40.98 | 0.386 | 50.24 | 100.6 | 91.1 | 3033 |
| 604-2 ol av8 | 40.94 | 0.374 | 49.75 | 100.4 | 90.7 | 2936 |

| | | | | | | |
|---|---|---|---|---|---|---|
| Mongolia: | | | | | | |
| Dariganga (SE Mongolia) | | | | | | |
| bn8ol7 | 41.12 | 0.389 | 50.90 | 100.6 | 91.8 | 3059 |
| bn9ol8 | 40.98 | 0.377 | 50.31 | 100.6 | 91.1 | 2960 |
| bn10ol8 | 40.99 | 0.375 | 49.87 | 100.7 | 90.6 | 2946 |
| bn12ol6 | 40.97 | 0.363 | 50.36 | 100.6 | 91.1 | 2853 |
| bn24ol7 | 40.67 | 0.370 | 49.41 | 100.5 | 89.9 | 2909 |
| bn38ol6 | 40.56 | 0.369 | 49.87 | 100.4 | 90.4 | 2902 |
| by24 ol6 | 40.92 | 0.382 | 50.04 | 100.5 | 90.8 | 2998 |
| by26ol7 | 40.89 | 0.372 | 50.11 | 100.5 | 91.0 | 2921 |
| by31ol7 | 40.51 | 0.379 | 49.80 | 100.1 | 90.6 | 2975 |
| by35ol7 | 40.44 | 0.394 | 50.14 | 100.1 | 90.9 | 3095 |
| by36ol7 | 40.68 | 0.378 | 49.76 | 100.5 | 90.3 | 2965 |
| by40ol7 | 40.42 | 0.377 | 49.48 | 100.2 | 90.0 | 2960 |
| db10ol8 | 40.81 | 0.375 | 50.27 | 100.6 | 91.0 | 2946 |
| db11ol7 | 40.86 | 0.382 | 50.06 | 100.8 | 90.6 | 3002 |
| db12ol7 | 40.89 | 0.392 | 50.22 | 100.7 | 90.8 | 3079 |
| db15ol7 | 41.14 | 0.387 | 50.64 | 100.9 | 91.4 | 3040 |
| db17ol7 | 40.97 | 0.369 | 50.28 | 100.7 | 91.0 | 2901 |
| db18ol7 | 41.11 | 0.393 | 50.52 | 101.1 | 91.0 | 3088 |
| db19ol7 | 41.01 | 0.375 | 50.27 | 101.0 | 90.7 | 2948 |
| db22 ol6 | 40.80 | 0.364 | 49.94 | 100.7 | 90.5 | 2858 |
| db23ol7 | 41.04 | 0.382 | 50.31 | 100.8 | 91.0 | 3001 |
| db24ol7 | 40.99 | 0.372 | 50.16 | 100.9 | 90.7 | 2923 |
| ats68 ol av7 | 40.26 | 0.365 | 49.44 | 99.9 | 90.1 | 2870 |
| ats73 ol av6 | 40.42 | 0.384 | 49.53 | 99.8 | 90.5 | 3017 |
| ats76 ol av6 | 40.47 | 0.378 | 49.35 | 99.9 | 90.2 | 2972 |
| ats77 ol av4 | 40.53 | 0.365 | 49.06 | 99.9 | 90.0 | 2865 |
| ats78 ol av4 | 40.14 | 0.367 | 49.28 | 99.2 | 90.4 | 2887 |
| ats79 ol av3 | 40.64 | 0.373 | 49.69 | 100.0 | 90.7 | 2930 |

| | | | | | | |
|---|---|---|---|---|---|---|
| Dariganga (SE Mongolia) | | | | | | |
| Ats80 ol av3 | 40.56 | 0.375 | 49.21 | 100.3 | 89.7 | 2944 |
| 9429-7ol6 | 40.89 | 0.381 | 49.74 | 100.8 | 90.2 | 2990 |
| 9429-11 ol7 | 41.04 | 0.388 | 50.27 | 100.8 | 91.0 | 3047 |
| 9429-12ol7 | 40.98 | 0.384 | 50.03 | 100.6 | 90.8 | 3013 |
| 9429-13 ol5 | 40.81 | 0.377 | 49.99 | 100.5 | 90.6 | 2965 |
| 9429-36ol7 | 41.11 | 0.373 | 50.23 | 100.8 | 90.9 | 2929 |
| Tariat, central Mongolia: | | | | | | |
| Shavaryn-Tsaram eruption center | | | | | | |
| Mo-79-4 ol7 | 41.20 | 0.370 | 49.78 | 100.9 | 90.5 | 2905 |
| Mo-88 ol8 | 41.10 | 0.395 | 50.00 | 100.5 | 91.0 | 3102 |
| Mo-89 ol9 | 41.03 | 0.372 | 49.98 | 100.6 | 90.8 | 2924 |
| mo90ol6 | 40.70 | 0.377 | 49.93 | 100.1 | 90.9 | 2960 |
| mo91ol5 | 40.40 | 0.367 | 49.60 | 99.8 | 90.5 | 2883 |
| mo92ol5 | 40.40 | 0.378 | 50.13 | 99.6 | 91.3 | 2973 |
| mo93ol5 | 40.30 | 0.377 | 50.02 | 99.4 | 91.3 | 2962 |
| Mo-94a ol6 | 41.19 | 0.371 | 50.26 | 100.7 | 91.1 | 2915 |
| mo94a ol6 | 40.53 | 0.357 | 49.64 | 99.9 | 90.6 | 2808 |
| Mo-95 ol6 | 41.09 | 0.378 | 50.23 | 100.8 | 90.9 | 2969 |
| Mo-96 ol11 | 41.03 | 0.366 | 49.95 | 100.7 | 90.7 | 2872 |
| Mo-99 ol6 | 40.89 | 0.366 | 48.93 | 100.7 | 89.4 | 2875 |
| Mo-101 ol7 | 41.09 | 0.366 | 48.77 | 100.9 | 89.3 | 2875 |
| Mo-102 ol8 | 40.95 | 0.384 | 49.86 | 100.5 | 90.7 | 3015 |
| Mo-103 ol8 | 40.91 | 0.374 | 49.51 | 100.5 | 90.3 | 2937 |
| Mo-104 ol8 | 41.13 | 0.385 | 49.93 | 100.6 | 90.8 | 3027 |
| MOG-1 ol7 | 40.85 | 0.379 | 49.56 | 100.5 | 90.3 | 2978 |
| MOG-2 ol7 | 40.70 | 0.367 | 48.78 | 100.6 | 89.2 | 2880 |
| MOG-3 ol7 | 40.92 | 0.369 | 49.48 | 100.4 | 90.3 | 2896 |
| MOG-4 ol7 | 41.12 | 0.373 | 49.05 | 101.0 | 89.6 | 2928 |
| MOG-5 ol7 | 40.95 | 0.365 | 48.79 | 100.6 | 89.5 | 2871 |

| | | | | | | |
|---|---|---|---|---|---|---|
| Shavaryn-Tsaram eruption center | | | | | | |
| MOZ-1 ol7 | 40.69 | 0.371 | 48.84 | 100.5 | 89.3 | 2911 |
| 4399-23 ol8 | 41.12 | 0.382 | 50.23 | 100.5 | 91.3 | 3003 |
| 4500-8 ol7 | 40.83 | 0.367 | 48.77 | 100.7 | 89.3 | 2886 |
| 4500-17 ol8 | 41.00 | 0.376 | 50.00 | 100.6 | 90.8 | 2956 |
| 4500-18 ol av9 | 41.33 | 0.392 | 50.94 | 100.8 | 91.9 | 3082 |
| 4500-21 ol7 | 40.87 | 0.371 | 48.98 | 100.6 | 89.6 | 2917 |
| 4594-4 ol8 | 41.14 | 0.395 | 50.63 | 100.3 | 91.9 | 3103 |
| 4594-6 ol7 | 40.84 | 0.370 | 49.13 | 100.7 | 89.6 | 2907 |
| Other Tariat volcanoes, averages of 6-7 analyses (Ionov 2007) | | | | | | |
| Z-5 | 40.79 | 0.368 | 49.07 | 100.6 | 89.6 | 2891 |
| Z-6 | 40.82 | 0.373 | 49.21 | 100.7 | 89.7 | 2930 |
| Z-7 | 40.81 | 0.358 | 49.14 | 100.6 | 89.8 | 2812 |
| Z-8 | 40.88 | 0.372 | 49.07 | 100.6 | 89.7 | 2922 |
| Z-11 | 40.77 | 0.365 | 48.85 | 100.5 | 89.5 | 2867 |
| Z-12 | 40.98 | 0.365 | 49.49 | 100.7 | 90.2 | 2867 |
| Z-14 | 40.72 | 0.368 | 48.67 | 100.6 | 89.1 | 2891 |
| Z-15 | 40.81 | 0.367 | 48.95 | 100.5 | 89.6 | 2883 |
| Z-16 | 40.65 | 0.375 | 49.06 | 100.5 | 89.6 | 2946 |
| Z-17 | 40.74 | 0.372 | 49.15 | 100.5 | 89.7 | 2922 |
| Z-18 | 40.74 | 0.357 | 48.9 | 100.7 | 89.3 | 2804 |
| Z-65 | 40.71 | 0.368 | 48.86 | 100.6 | 89.3 | 2891 |
| Z-71 | 40.78 | 0.361 | 49.24 | 100.7 | 89.7 | 2836 |
| Z-72 | 40.72 | 0.365 | 49.01 | 100.6 | 89.5 | 2867 |
| Hr-4 | 41.16 | 0.372 | 49.29 | 100.9 | 89.9 | 2922 |
| Hr-6 | 40.98 | 0.365 | 48.66 | 100.7 | 89.3 | 2867 |
| Hr-12 | 41.07 | 0.363 | 48.6 | 100.9 | 89.1 | 2852 |
| Hr-18 | 41.15 | 0.371 | 49.34 | 100.8 | 90.0 | 2914 |
| Hr-20 | 40.9 | 0.360 | 48.8 | 100.7 | 89.4 | 2828 |
| Hr-22 | 40.78 | 0.365 | 48.59 | 100.3 | 89.4 | 2867 |

Other Tariat volcanoes, averages of 6-7 analyses (Ionov 2007)

| | | | | | | |
|---|---|---|---|---|---|---|
| Hr-26 | 41.06 | 0.364 | 48.9 | 100.9 | 89.4 | 2859 |
| St-0 | 40.77 | 0.367 | 48.89 | 100.7 | 89.3 | 2883 |
| St-3 | 40.7 | 0.375 | 49.06 | 100.4 | 89.6 | 2946 |
| St-23 | 40.71 | 0.369 | 48.9 | 100.6 | 89.4 | 2899 |
| Ts-14 | 40.86 | 0.365 | 49.19 | 100.6 | 89.8 | 2867 |
| Ts-21 | 40.84 | 0.366 | 48.85 | 100.8 | 89.2 | 2875 |

Russian Far East:

Tok, LH series, averages of 8 analyses each (Ionov et al. 2005)

| Sa.N° | SiO2 | NiO | MgO | Total | Mg# | Ni, ppm |
|---|---|---|---|---|---|---|
| 9501-2 | 40.97 | 0.390 | 50.41 | 100.5 | 91.3 | 3067 |
| 9501-3 | 41.00 | 0.371 | 50.29 | 100.5 | 91.2 | 2917 |
| 9502-9 | 41.14 | 0.376 | 50.51 | 100.7 | 91.4 | 2956 |
| 9505-3 | 41.45 | 0.365 | 50.07 | 101.6 | 90.4 | 2870 |
| 9506-0 | 40.74 | 0.367 | 50.46 | 99.7 | 91.9 | 2879 |
| 9506-1 | 41.24 | 0.361 | 49.38 | 101.6 | 89.5 | 2836 |
| 9506-2 | 41.27 | 0.363 | 49.39 | 101.6 | 89.5 | 2849 |
| 9506-3 | 41.43 | 0.394 | 50.54 | 101.6 | 90.9 | 3097 |
| 9507-1 | 41.27 | 0.375 | 50.53 | 101.2 | 91.1 | 2947 |
| 9507-5 | 40.75 | 0.365 | 49.42 | 100.4 | 90.1 | 2866 |
| 9508-1 | 40.82 | 0.373 | 49.58 | 100.4 | 90.4 | 2928 |
| 9508-2 | 40.88 | 0.378 | 49.69 | 100.3 | 90.6 | 2967 |
| 9508-5 | 40.73 | 0.363 | 49.38 | 100.4 | 90.1 | 2853 |
| 9508-6 | 40.73 | 0.360 | 49.01 | 100.5 | 89.6 | 2825 |
| 9508-7 | 40.95 | 0.373 | 49.97 | 100.2 | 91.1 | 2933 |
| 9508-11 | 40.98 | 0.381 | 50.10 | 100.2 | 91.3 | 2994 |
| 9508-31 | 41.01 | 0.382 | 50.50 | 100.3 | 91.6 | 2997 |
| 9508-39 | 40.63 | 0.359 | 48.91 | 100.4 | 89.4 | 2820 |
| 9508-40 | 41.12 | 0.383 | 50.27 | 100.5 | 91.3 | 3008 |

| | | | | | | |
|---|---|---|---|---|---|---|
| 9508-50 | 40.82 | 0.376 | 50.08 | 100.2 | 91.2 | 2952 |
| Tok, LH series, averages of 8 analyses each (Ionov et al. 2005) | | | | | | |
| 9510-2 | 41.12 | 0.371 | 50.48 | 100.5 | 91.5 | 2911 |
| 9510-4 | 41.03 | 0.382 | 50.41 | 100.5 | 91.4 | 3001 |
| 9510-8 | 40.87 | 0.375 | 50.07 | 100.6 | 90.8 | 2948 |
| 9510-17 | 40.97 | 0.354 | 49.90 | 100.6 | 90.7 | 2781 |
| 9510-19 | 41.14 | 0.380 | 50.28 | 100.7 | 91.1 | 2988 |
| River Ussuri: | | | | | | |
| 8802-1ol7 | 40.56 | 0.363 | 49.51 | 100.5 | 90.0 | 2850 |
| 8802-2ol7 | 40.64 | 0.354 | 49.31 | 100.7 | 89.7 | 2782 |
| 8803-1ol8 | 40.87 | 0.376 | 50.67 | 100.5 | 91.6 | 2955 |
| 8803-2ol9 | 40.79 | 0.375 | 50.34 | 100.4 | 91.2 | 2942 |
| 8803-3ol8 | 40.81 | 0.373 | 50.30 | 100.5 | 91.0 | 2929 |
| 8803-4ol9 | 40.78 | 0.377 | 50.21 | 100.5 | 90.9 | 2962 |
| Zeya-Amur region (averages of 7 analyses each) | | | | | | |
| f1 | 40.67 | 0.388 | 49.77 | 100.0 | 90.8 | 3048 |
| f2 | 40.67 | 0.395 | 50.01 | 99.9 | 91.1 | 3103 |
| f3 | 40.42 | 0.375 | 49.13 | 100.0 | 89.9 | 2946 |
| f4 | 40.52 | 0.377 | 49.55 | 99.8 | 90.6 | 2962 |
| f5 | 40.26 | 0.383 | 48.89 | 99.7 | 89.8 | 3009 |
| f6 | 40.32 | 0.374 | 48.74 | 99.8 | 89.5 | 2938 |
| f7 | 40.34 | 0.370 | 48.72 | 99.9 | 89.4 | 2907 |
| f8 | 40.83 | 0.399 | 50.53 | 99.9 | 91.9 | 3134 |
| f9 | 40.63 | 0.374 | 49.57 | 100.1 | 90.5 | 2938 |
| fev-1 ol5 | 40.67 | 0.366 | 49.32 | 100.4 | 89.9 | 2938 |
| en-1 ol4 | 40.80 | 0.369 | 49.44 | 100.6 | 90.0 | 2938 |
| en-2 ol5 | 40.66 | 0.375 | 49.30 | 100.4 | 90.0 | 2938 |
| sv-1 ol6 | 40.76 | 0.376 | 49.38 | 100.5 | 90.0 | 2938 |

Sources of published data: Ionov (2007; 2010); Ionov et al., (2005)

Off-Craton Garnet and Garnet-Spinel Peridotites

| Sample Number | SiO2 | NiO | MgO | Total | *Mg*-number | Ni (ppm) |
|---|---|---|---|---|---|---|
| Vitim, southern Siberia (east of lake Baikal) | | | | | | |
| 313-1ol6 | 40.88 | 0.371 | 49.67 | 100.8 | 90.1 | 2912 |
| 313-2ol10 | 40.74 | 0.376 | 49.61 | 100.3 | 90.4 | 2954 |
| 313-3 ol9 | 40.92 | 0.368 | 49.56 | 100.8 | 90.1 | 2892 |
| 313-5ol6 | 40.79 | 0.361 | 49.64 | 100.7 | 90.2 | 2836 |
| 313-6ol7 | 40.82 | 0.363 | 49.46 | 100.5 | 90.2 | 2848 |
| 313-7ol6 | 40.92 | 0.366 | 49.49 | 100.8 | 90.0 | 2876 |
| 313-8 ol11 | 40.81 | 0.369 | 49.50 | 100.5 | 90.3 | 2898 |
| 313-37ol7 | 40.68 | 0.374 | 49.56 | 100.6 | 90.1 | 2938 |
| 313-54ol7 | 40.83 | 0.368 | 49.40 | 100.6 | 90.0 | 2892 |
| 313-102ol9 | 40.67 | 0.362 | 49.29 | 100.5 | 89.9 | 2844 |
| 313-104ol8 | 40.59 | 0.361 | 49.28 | 100.4 | 89.9 | 2838 |
| 313-106ol7 | 40.38 | 0.363 | 49.50 | 100.1 | 90.1 | 2855 |
| 313-110ol6 | 40.81 | 0.364 | 49.92 | 100.7 | 90.4 | 2859 |
| 313-112ol7 | 40.82 | 0.374 | 49.53 | 100.6 | 90.1 | 2941 |
| 313-240ol7 | 40.37 | 0.352 | 49.43 | 100.0 | 90.2 | 2765 |
| 313-241ol7 | 40.69 | 0.356 | 49.43 | 100.4 | 90.1 | 2795 |
| 31474ol6 | 40.90 | 0.370 | 50.15 | 100.7 | 90.9 | 2909 |
| 314-230 av.3 | 40.98 | 0.375 | 49.45 | 100.7 | 90.2 | 2946 |
| 314-580 av.3 | 40.84 | 0.371 | 49.34 | 100.4 | 90.2 | 2914 |
| 621-10 ol9 | 40.89 | 0.362 | 49.35 | 100.7 | 89.9 | 2840 |
| 621-19 ol10 | 40.63 | 0.363 | 48.67 | 100.7 | 89.1 | 2855 |
| Dariganga (SE Mongolia) | | | | | | |
| 8508-6ol7 | 40.92 | 0.364 | 49.67 | 100.7 | 90.3 | 2859 |
| by18ol7 | 40.95 | 0.374 | 50.19 | 100.8 | 90.8 | 2940 |
| by27ol7 | 40.52 | 0.366 | 49.14 | 100.3 | 89.7 | 2876 |
| 8504-24ol7 | 40.57 | 0.365 | 49.58 | 100.5 | 90.0 | 2866 |

| | | | | | | |
|---|---|---|---|---|---|---|
| Dariganga (SE Mongolia) | | | | | | |
| db8ol7 | 40.82 | 0.367 | 49.78 | 100.8 | 90.3 | 2882 |
| db13ol7 | 40.90 | 0.369 | 50.11 | 100.8 | 90.7 | 2896 |
| db20ol7 | 40.60 | 0.369 | 49.73 | 100.6 | 90.2 | 2898 |
| db21ol7 | 40.88 | 0.375 | 49.95 | 100.9 | 90.4 | 2944 |
| Shavaryn-Tsaram, Tariat (central Mongolia) | | | | | | |
| 4334-11 ol9 | 40.82 | 0.358 | 48.81 | 100.6 | 89.4 | 2815 |
| 53389 ol8 | 40.84 | 0.361 | 48.93 | 100.5 | 89.6 | 2836 |
| 200-81 ol av8 | 40.87 | 0.379 | 49.36 | 100.7 | 90.0 | 2974 |

Spinel peridotite xenoliths from subduction zones

| Sample Number | SiO2 | NiO | MgO | Total | *Mg*-number | Ni (ppm) |
|---|---|---|---|---|---|---|
| Subduction zone peridotites: Avacha volcano, Kamchatka, Russia (Ionov et al. 2010) | | | | | | |
| Av-1 | 40.70 | 0.38 | 50.08 | 100.10 | 91.0 | 2975 |
| Av-2 | 40.72 | 0.39 | 50.19 | 100.26 | 91.1 | 3080 |
| Av-3 | 40.58 | 0.38 | 50.05 | 100.07 | 90.9 | 3012 |
| Av-4 | 40.77 | 0.40 | 49.89 | 100.31 | 90.7 | 3107 |
| Av-5 | 40.65 | 0.40 | 50.20 | 100.35 | 90.9 | 3122 |
| Av-6 | 40.53 | 0.39 | 50.16 | 100.07 | 91.0 | 3024 |
| Av-7 | 40.67 | 0.38 | 50.16 | 100.21 | 91.0 | 2991 |
| Av-8 | 40.80 | 0.39 | 50.27 | 100.12 | 91.3 | 3024 |
| Av-9 | 40.77 | 0.38 | 50.20 | 100.27 | 91.1 | 2963 |
| Av-10 | 40.74 | 0.39 | 50.09 | 100.10 | 91.1 | 3043 |
| Av-11 | 40.74 | 0.38 | 50.18 | 100.11 | 91.2 | 3013 |
| Av-12 | 40.67 | 0.38 | 50.20 | 100.16 | 91.1 | 3006 |
| Av-13 | 40.77 | 0.39 | 50.21 | 100.21 | 91.2 | 3027 |
| Av-14 | 40.67 | 0.38 | 50.25 | 100.21 | 91.1 | 2985 |
| Av-15 | 40.67 | 0.38 | 50.10 | 100.11 | 91.0 | 2949 |
| Av-16 | 40.87 | 0.40 | 50.62 | 100.16 | 91.8 | 3124 |
| Av-17 | 40.76 | 0.39 | 50.37 | 100.10 | 91.4 | 3038 |

Table S2: Olivine Analyses from Fernandina Sample D38A

| | SiO2 % | MgO % | FeO % | CaO % | MnO % | NiO % | OL Mg# | Ni ppm | Mn ppm | Ca ppm | Fe ppm |
|---|---|---|---|---|---|---|---|---|---|---|---|
| D38A Phen 1 | 40.44 | 46.58 | 11.53 | 0.302 | 0.175 | 0.303 | 87.8 | 2380 | 1352 | 2156 | 89640 |
| D38A Phen 1 | 40.52 | 46.80 | 11.57 | 0.298 | 0.174 | 0.308 | 87.8 | 2420 | 1349 | 2132 | 89936 |
| D38A Phen 1 | 40.43 | 46.86 | 11.56 | 0.298 | 0.170 | 0.311 | 87.8 | 2446 | 1318 | 2127 | 89890 |
| D38A Phen 1 | 40.19 | 45.61 | 12.65 | 0.324 | 0.190 | 0.291 | 86.5 | 2284 | 1468 | 2312 | 98383 |
| D38A Phen 2 | 40.64 | 47.17 | 11.65 | 0.299 | 0.179 | 0.311 | 87.8 | 2442 | 1386 | 2138 | 90623 |
| D38A Phen 3 | 39.73 | 44.99 | 13.03 | 0.336 | 0.202 | 0.258 | 86.0 | 2029 | 1561 | 2398 | 101287 |
| D38A Phen 4 | 40.07 | 45.71 | 13.36 | 0.328 | 0.205 | 0.270 | 85.9 | 2121 | 1586 | 2344 | 103890 |
| D38A Phen 5 | 40.35 | 46.77 | 11.87 | 0.287 | 0.177 | 0.288 | 87.5 | 2266 | 1369 | 2053 | 92339 |
| D38A Phen 6 | 40.26 | 46.62 | 11.85 | 0.332 | 0.180 | 0.287 | 87.5 | 2255 | 1394 | 2371 | 92161 |
| D38A Phen 6 | 40.35 | 46.62 | 11.92 | 0.337 | 0.179 | 0.291 | 87.5 | 2290 | 1384 | 2411 | 92707 |
| D38A Phen 6 | 40.47 | 46.59 | 12.15 | 0.380 | 0.184 | 0.286 | 87.2 | 2243 | 1426 | 2719 | 94483 |
| D38A Phen 7 | 40.55 | 46.93 | 11.51 | 0.298 | 0.172 | 0.303 | 87.9 | 2378 | 1330 | 2133 | 89481 |
| D38A Phen 8 | 40.22 | 45.72 | 13.16 | 0.334 | 0.201 | 0.274 | 86.1 | 2149 | 1557 | 2386 | 102305 |
| D38A Phen 8 | 40.13 | 45.55 | 13.12 | 0.334 | 0.199 | 0.268 | 86.1 | 2107 | 1541 | 2388 | 102052 |
| D38A Phen 8 | 40.12 | 44.96 | 13.93 | 0.338 | 0.215 | 0.253 | 85.2 | 1986 | 1662 | 2418 | 108310 |
| D38A Phen 9 | 40.39 | 46.33 | 12.15 | 0.329 | 0.186 | 0.276 | 87.2 | 2171 | 1440 | 2349 | 94502 |
| D38A Phen 9 | 40.37 | 45.76 | 12.86 | 0.328 | 0.190 | 0.265 | 86.4 | 2083 | 1474 | 2342 | 99968 |
| D38A Phen 9 | 40.36 | 45.60 | 13.75 | 0.339 | 0.204 | 0.246 | 85.5 | 1931 | 1584 | 2421 | 106903 |
| D38A Phen 10 | 40.36 | 46.28 | 12.10 | 0.327 | 0.187 | 0.276 | 87.2 | 2169 | 1450 | 2337 | 94085 |
| D38A Phen 12 | 40.04 | 44.06 | 15.28 | 0.343 | 0.229 | 0.215 | 83.7 | 1691 | 1775 | 2454 | 118854 |
| D38A Phen 13 | 40.61 | 46.29 | 12.39 | 0.347 | 0.187 | 0.275 | 86.9 | 2162 | 1447 | 2483 | 96338 |
| D38A Phen 14 | 40.29 | 46.45 | 11.93 | 0.294 | 0.177 | 0.298 | 87.4 | 2345 | 1374 | 2104 | 92763 |
| D38A Phen 15 | 40.54 | 46.43 | 12.14 | 0.319 | 0.182 | 0.283 | 87.2 | 2226 | 1409 | 2279 | 94415 |
| D38A Phen 16 | 40.38 | 45.74 | 12.74 | 0.331 | 0.188 | 0.269 | 86.5 | 2114 | 1453 | 2367 | 99059 |
| D38A Phen 18 | 40.53 | 46.85 | 11.92 | 0.305 | 0.179 | 0.288 | 87.5 | 2262 | 1387 | 2179 | 92664 |
| D38A Phen 19 | 40.34 | 46.33 | 12.29 | 0.333 | 0.189 | 0.274 | 87.0 | 2151 | 1466 | 2378 | 95598 |
| D38A Phen 19 | 40.41 | 46.40 | 12.26 | 0.321 | 0.184 | 0.277 | 87.1 | 2177 | 1427 | 2296 | 95337 |
| D38A Phen 19 | 40.53 | 45.71 | 13.09 | 0.318 | 0.190 | 0.256 | 86.2 | 2011 | 1476 | 2273 | 101797 |

| | SiO2 % | MgO % | FeO % | CaO % | MnO % | NiO % | OL Mg# | Ni ppm | Mn ppm | Ca ppm | Fe ppm |
|---|---|---|---|---|---|---|---|---|---|---|---|
| D38A Phen 21 | 40.65 | 46.69 | 12.01 | 0.318 | 0.181 | 0.289 | 87.4 | 2272 | 1400 | 2270 | 93419 |
| D38A Phen 21 | 40.75 | 46.96 | 11.77 | 0.314 | 0.178 | 0.288 | 87.7 | 2259 | 1380 | 2246 | 91499 |
| D38A Phen 21 | 40.56 | 45.84 | 12.93 | 0.319 | 0.198 | 0.279 | 86.3 | 2189 | 1534 | 2283 | 100537 |
| D38A Phen 22 | 40.53 | 45.71 | 12.79 | 0.326 | 0.198 | 0.250 | 86.4 | 1964 | 1530 | 2327 | 99422 |
| D38A Phen 22 | 40.74 | 46.15 | 12.86 | 0.333 | 0.200 | 0.253 | 86.5 | 1986 | 1552 | 2381 | 100034 |
| D38A Phen 22 | 40.74 | 46.36 | 12.27 | 0.337 | 0.192 | 0.252 | 87.1 | 1981 | 1484 | 2407 | 95403 |
| D38A Phen 23 | 40.62 | 44.14 | 15.64 | 0.314 | 0.236 | 0.255 | 83.4 | 2004 | 1829 | 2248 | 121603 |
| D38A Phen 23 | 40.57 | 43.85 | 15.69 | 0.313 | 0.241 | 0.255 | 83.3 | 2005 | 1867 | 2236 | 122043 |
| D38A Phen 23 | 40.75 | 43.90 | 15.91 | 0.317 | 0.243 | 0.250 | 83.1 | 1964 | 1882 | 2267 | 123717 |
| D38A Phen 23 | 40.50 | 43.55 | 15.77 | 0.322 | 0.244 | 0.251 | 83.1 | 1970 | 1891 | 2305 | 122606 |
| D38A Phen 23 | 41.04 | 44.76 | 15.29 | 0.360 | 0.233 | 0.223 | 83.9 | 1752 | 1804 | 2574 | 118884 |
| D38A Phen 24 | 41.42 | 46.17 | 13.33 | 0.323 | 0.206 | 0.222 | 86.1 | 1748 | 1593 | 2309 | 103630 |
| D38A Phen 24 | 41.23 | 46.03 | 13.27 | 0.331 | 0.202 | 0.229 | 86.1 | 1796 | 1568 | 2365 | 103218 |
| D38A Phen 24 | 41.29 | 46.08 | 13.25 | 0.335 | 0.205 | 0.229 | 86.1 | 1796 | 1590 | 2393 | 103028 |
| D38A Phen 24 | 41.21 | 46.04 | 13.17 | 0.340 | 0.200 | 0.228 | 86.2 | 1790 | 1549 | 2428 | 102385 |
| D38A Phen 24 | 40.90 | 44.43 | 15.09 | 0.344 | 0.227 | 0.214 | 84.0 | 1681 | 1755 | 2457 | 117303 |
| D38A Phen 25 | 41.32 | 46.44 | 12.05 | 0.315 | 0.182 | 0.291 | 87.3 | 2288 | 1411 | 2249 | 93733 |
| D38A Phen 26 | 41.26 | 46.32 | 12.36 | 0.328 | 0.191 | 0.283 | 87.0 | 2225 | 1477 | 2342 | 96097 |
| D38A Phen 27 | 40.93 | 45.65 | 13.06 | 0.333 | 0.199 | 0.269 | 86.2 | 2109 | 1541 | 2377 | 101548 |
| D38A Phen 28 | 41.27 | 46.02 | 13.17 | 0.335 | 0.201 | 0.271 | 86.2 | 2133 | 1553 | 2395 | 102404 |
| D38A Phen 28 | 41.19 | 45.86 | 13.07 | 0.334 | 0.202 | 0.271 | 86.2 | 2128 | 1561 | 2389 | 101600 |
| D38A Phen 28 | 40.88 | 45.69 | 12.78 | 0.325 | 0.196 | 0.269 | 86.4 | 2117 | 1518 | 2326 | 99375 |
| D38A Phen 28 | 40.92 | 45.88 | 12.50 | 0.323 | 0.188 | 0.270 | 86.7 | 2125 | 1453 | 2310 | 97227 |
| D38A Phen 29 | 40.84 | 44.54 | 14.40 | 0.302 | 0.221 | 0.253 | 84.6 | 1986 | 1709 | 2159 | 111961 |
| D38A Phen 30 | 41.07 | 45.66 | 13.26 | 0.346 | 0.199 | 0.268 | 86.0 | 2102 | 1544 | 2472 | 103107 |
| D38A Phen 31 | 41.13 | 46.20 | 12.42 | 0.322 | 0.192 | 0.285 | 86.9 | 2240 | 1490 | 2305 | 96555 |
| D38A Phen 32 | 41.18 | 46.86 | 12.09 | 0.308 | 0.180 | 0.290 | 87.4 | 2282 | 1398 | 2202 | 94044 |
| D38A Phen 33 | 40.97 | 46.55 | 12.12 | 0.306 | 0.182 | 0.293 | 87.3 | 2303 | 1406 | 2190 | 94266 |
| D38A Phen 34 | 40.97 | 46.57 | 12.06 | 0.308 | 0.181 | 0.290 | 87.3 | 2275 | 1405 | 2199 | 93752 |
| D38A Phen 35 | 40.32 | 44.45 | 14.43 | 0.329 | 0.220 | 0.218 | 84.6 | 1716 | 1707 | 2349 | 112194 |

| | SiO2 % | MgO % | FeO % | CaO % | MnO % | NiO % | OL Mg# | Ni ppm | Mn ppm | Ca ppm | Fe ppm |
|---|---|---|---|---|---|---|---|---|---|---|---|
| D38A Phen 36 | 40.38 | 44.50 | 14.57 | 0.348 | 0.226 | 0.218 | 84.5 | 1710 | 1752 | 2485 | 113262 |
| D38A Phen 37 | 40.76 | 45.44 | 13.56 | 0.320 | 0.204 | 0.256 | 85.7 | 2008 | 1581 | 2289 | 105475 |
| D38A Phen 38 | 40.82 | 46.44 | 12.23 | 0.310 | 0.186 | 0.294 | 87.1 | 2308 | 1438 | 2213 | 95070 |
| D38A Phen 38 | 41.03 | 46.68 | 12.28 | 0.311 | 0.187 | 0.291 | 87.1 | 2289 | 1445 | 2221 | 95461 |
| D38A Phen 38 | 40.86 | 46.66 | 12.24 | 0.317 | 0.187 | 0.290 | 87.2 | 2282 | 1446 | 2267 | 95169 |
| D38A Phen 38 | 40.55 | 46.24 | 11.75 | 0.313 | 0.181 | 0.283 | 87.5 | 2226 | 1403 | 2236 | 91336 |
| D38A Phen 38 | 40.61 | 44.89 | 14.34 | 0.355 | 0.219 | 0.233 | 84.8 | 1827 | 1694 | 2540 | 111500 |
| D38A Phen 39 | 40.59 | 46.27 | 12.27 | 0.315 | 0.182 | 0.276 | 87.1 | 2168 | 1413 | 2254 | 95395 |
| D38A Phen 39 | 40.62 | 46.69 | 12.25 | 0.309 | 0.182 | 0.284 | 87.2 | 2232 | 1408 | 2210 | 95241 |
| D38A Phen 39 | 40.50 | 46.74 | 12.07 | 0.304 | 0.178 | 0.286 | 87.3 | 2243 | 1379 | 2172 | 93888 |
| D38A Phen 39 | 40.45 | 46.21 | 12.63 | 0.318 | 0.190 | 0.272 | 86.7 | 2136 | 1470 | 2272 | 98218 |
| D38A Phen 40 | 40.70 | 46.99 | 11.97 | 0.302 | 0.179 | 0.285 | 87.5 | 2239 | 1387 | 2161 | 93088 |
| D38A Phen 41 | 39.93 | 45.36 | 13.07 | 0.314 | 0.197 | 0.292 | 86.1 | 2295 | 1529 | 2246 | 101636 |
| D38A Phen 41 | 40.16 | 45.74 | 13.16 | 0.304 | 0.198 | 0.295 | 86.1 | 2314 | 1534 | 2173 | 102308 |
| D38A Phen 41 | 40.25 | 45.87 | 13.14 | 0.304 | 0.194 | 0.296 | 86.2 | 2325 | 1506 | 2173 | 102190 |
| D38A Phen 41 | 39.78 | 44.03 | 15.07 | 0.378 | 0.229 | 0.219 | 83.9 | 1716 | 1774 | 2699 | 117165 |
| D38A Phen 42 | 40.22 | 46.19 | 12.29 | 0.321 | 0.184 | 0.283 | 87.0 | 2221 | 1424 | 2296 | 95534 |
| D38A Phen 43 | 40.23 | 45.82 | 13.18 | 0.325 | 0.205 | 0.297 | 86.1 | 2330 | 1586 | 2323 | 102505 |
| D38A Phen 44 | 40.23 | 45.53 | 13.23 | 0.335 | 0.205 | 0.295 | 86.0 | 2320 | 1592 | 2393 | 102900 |
| D38A Phen 45 | 40.06 | 45.54 | 13.11 | 0.332 | 0.202 | 0.269 | 86.1 | 2112 | 1566 | 2376 | 101953 |
| D38A Phen 46 | 40.03 | 45.52 | 13.07 | 0.330 | 0.199 | 0.269 | 86.1 | 2113 | 1540 | 2362 | 101671 |
| D38A Phen 47 | 40.33 | 46.46 | 12.41 | 0.318 | 0.187 | 0.287 | 87.0 | 2253 | 1446 | 2276 | 96530 |
| D38A Phen 48 | 40.07 | 45.91 | 12.67 | 0.325 | 0.190 | 0.279 | 86.6 | 2189 | 1474 | 2324 | 98549 |
| D38A Phen 49 | 40.25 | 46.55 | 11.67 | 0.304 | 0.176 | 0.297 | 87.7 | 2335 | 1362 | 2174 | 90768 |
| D38A Phen 50 | 40.28 | 46.76 | 11.84 | 0.304 | 0.174 | 0.300 | 87.6 | 2353 | 1344 | 2174 | 92070 |
| D38A Phen 51 | 40.42 | 47.02 | 11.66 | 0.296 | 0.177 | 0.317 | 87.8 | 2489 | 1375 | 2118 | 90646 |
| D38A Phen 52 | 40.46 | 45.93 | 13.39 | 0.329 | 0.200 | 0.265 | 85.9 | 2085 | 1546 | 2349 | 104148 |
| D38A Phen 53 | 40.54 | 46.07 | 12.87 | 0.327 | 0.192 | 0.276 | 86.4 | 2169 | 1487 | 2336 | 100112 |
| D38A Phen 53 | 40.45 | 45.81 | 13.12 | 0.330 | 0.203 | 0.268 | 86.2 | 2104 | 1573 | 2360 | 102024 |
| D38A Phen 53 | 40.61 | 46.09 | 12.95 | 0.340 | 0.195 | 0.269 | 86.4 | 2115 | 1509 | 2433 | 100674 |

| | SiO2 % | MgO % | FeO % | CaO % | MnO % | NiO % | OL Mg# | Ni ppm | Mn ppm | Ca ppm | Fe ppm |
|---|---|---|---|---|---|---|---|---|---|---|---|
| D38A Phen 54 | 40.75 | 45.90 | 13.14 | 0.325 | 0.200 | 0.270 | 86.2 | 2118 | 1552 | 2320 | 102188 |
| D38A Phen 54 | 40.51 | 45.69 | 13.03 | 0.321 | 0.198 | 0.270 | 86.2 | 2120 | 1531 | 2293 | 101294 |
| D38A Phen 54 | 40.61 | 45.91 | 13.20 | 0.332 | 0.200 | 0.272 | 86.1 | 2139 | 1552 | 2376 | 102650 |
| D38A Phen 54 | 40.37 | 45.14 | 13.24 | 0.339 | 0.204 | 0.268 | 85.9 | 2106 | 1578 | 2421 | 102928 |
| D38A Phen 55 | 41.02 | 46.01 | 13.27 | 0.327 | 0.201 | 0.273 | 86.1 | 2142 | 1557 | 2334 | 103180 |
| D38A Phen 56 | 40.86 | 46.13 | 13.25 | 0.334 | 0.207 | 0.273 | 86.1 | 2143 | 1603 | 2385 | 103022 |
| D38A Phen 57 | 40.60 | 45.74 | 12.90 | 0.300 | 0.192 | 0.275 | 86.3 | 2164 | 1490 | 2143 | 100331 |
| D38A Phen 58 | 40.61 | 45.04 | 13.79 | 0.350 | 0.213 | 0.251 | 85.3 | 1970 | 1649 | 2503 | 107215 |
| D38A Phen 58 | 40.73 | 45.31 | 13.62 | 0.345 | 0.215 | 0.262 | 85.6 | 2057 | 1665 | 2467 | 105908 |
| D38A Phen 58 | 41.05 | 45.69 | 13.64 | 0.348 | 0.212 | 0.264 | 85.7 | 2070 | 1646 | 2490 | 106032 |
| D38A Phen 58 | 40.93 | 44.98 | 14.22 | 0.356 | 0.220 | 0.245 | 84.9 | 1923 | 1707 | 2543 | 110606 |
| D38A Phen 59 | 40.83 | 45.43 | 13.64 | 0.343 | 0.214 | 0.260 | 85.6 | 2043 | 1660 | 2451 | 106064 |
| D38A Phen 59 | 40.84 | 45.46 | 13.76 | 0.342 | 0.218 | 0.263 | 85.5 | 2066 | 1686 | 2447 | 106990 |
| D38A Phen 59 | 40.73 | 45.27 | 13.70 | 0.349 | 0.215 | 0.262 | 85.5 | 2057 | 1665 | 2498 | 106565 |
| D38A Phen 59 | 40.69 | 44.32 | 14.77 | 0.350 | 0.225 | 0.217 | 84.3 | 1707 | 1740 | 2505 | 114820 |
| D38A Phen 60 | 42.01 | 47.61 | 11.16 | 0.287 | 0.167 | 0.307 | 88.4 | 2409 | 1291 | 2048 | 86769 |
| D38A Phen 61 | 41.53 | 46.33 | 12.92 | 0.318 | 0.201 | 0.270 | 86.5 | 2121 | 1554 | 2276 | 100484 |
| D38A Phen 61 | 41.09 | 45.96 | 12.92 | 0.319 | 0.194 | 0.272 | 86.4 | 2133 | 1499 | 2280 | 100486 |
| D38A Phen 61 | 40.75 | 46.15 | 12.85 | 0.318 | 0.198 | 0.271 | 86.5 | 2128 | 1536 | 2272 | 99925 |
| D38A Phen 61 | 40.66 | 46.25 | 12.97 | 0.315 | 0.198 | 0.274 | 86.4 | 2151 | 1535 | 2251 | 100884 |
| D38A Phen 61 | 40.68 | 46.25 | 12.88 | 0.318 | 0.202 | 0.271 | 86.5 | 2128 | 1561 | 2270 | 100165 |
| D38A Phen 62 | 40.80 | 46.32 | 12.74 | 0.399 | 0.195 | 0.244 | 86.6 | 1915 | 1512 | 2848 | 99104 |
| D38A Phen 62 | 40.56 | 46.13 | 12.60 | 0.379 | 0.193 | 0.244 | 86.7 | 1921 | 1492 | 2709 | 98012 |
| D38A Phen 62 | 40.64 | 46.10 | 12.93 | 0.360 | 0.194 | 0.261 | 86.4 | 2048 | 1506 | 2572 | 100533 |
| D38A Phen 63 | 40.81 | 46.15 | 12.87 | 0.309 | 0.199 | 0.284 | 86.5 | 2232 | 1540 | 2210 | 100092 |
| D38A Phen 63 | 41.01 | 46.32 | 12.92 | 0.313 | 0.193 | 0.287 | 86.5 | 2258 | 1497 | 2236 | 100500 |
| D38A Phen 63 | 40.85 | 46.09 | 12.68 | 0.314 | 0.195 | 0.283 | 86.6 | 2220 | 1509 | 2242 | 98626 |
| D38A Phen 63 | 41.04 | 46.42 | 12.48 | 0.313 | 0.193 | 0.280 | 86.9 | 2203 | 1496 | 2240 | 97060 |
| D38A Phen 63 | 40.90 | 46.12 | 12.60 | 0.316 | 0.194 | 0.288 | 86.7 | 2260 | 1504 | 2256 | 97976 |
| D38A Phen 64 | 40.19 | 45.91 | 12.87 | 0.328 | 0.197 | 0.267 | 86.4 | 2101 | 1529 | 2342 | 100095 |

| | SiO2 % | MgO % | FeO % | CaO % | MnO % | NiO % | OL Mg# | Ni ppm | Mn ppm | Ca ppm | Fe ppm |
|---|---|---|---|---|---|---|---|---|---|---|---|
| D38A Phen 64 | 40.01 | 46.06 | 12.87 | 0.325 | 0.194 | 0.273 | 86.4 | 2143 | 1504 | 2321 | 100106 |
| D38A Phen 64 | 40.22 | 46.03 | 12.92 | 0.333 | 0.199 | 0.278 | 86.4 | 2181 | 1545 | 2379 | 100435 |
| D38A Phen 64 | 40.24 | 45.75 | 13.06 | 0.349 | 0.203 | 0.273 | 86.2 | 2141 | 1569 | 2493 | 101571 |
| D38A Phen 65 | 40.61 | 46.67 | 11.56 | 0.283 | 0.177 | 0.300 | 87.8 | 2357 | 1373 | 2020 | 89856 |
| D38A Phen 66 | 40.58 | 46.81 | 11.64 | 0.284 | 0.171 | 0.299 | 87.8 | 2346 | 1324 | 2033 | 90520 |
| D38A Phen 67 | 40.21 | 45.65 | 12.81 | 0.319 | 0.196 | 0.267 | 86.4 | 2095 | 1516 | 2278 | 99592 |
| D38A Phen 67 | 40.44 | 45.80 | 13.10 | 0.329 | 0.194 | 0.273 | 86.2 | 2147 | 1500 | 2349 | 101847 |
| D38A Phen 67 | 40.38 | 45.69 | 13.00 | 0.319 | 0.199 | 0.264 | 86.2 | 2075 | 1539 | 2281 | 101114 |
| D38A Phen 67 | 40.76 | 46.62 | 12.55 | 0.331 | 0.192 | 0.278 | 86.9 | 2180 | 1490 | 2365 | 97626 |
| D38A Phen 68 | 40.21 | 44.70 | 14.53 | 0.353 | 0.218 | 0.222 | 84.6 | 1746 | 1692 | 2523 | 113021 |
| D38A Phen 69 | 40.41 | 46.07 | 12.61 | 0.326 | 0.195 | 0.294 | 86.7 | 2311 | 1512 | 2332 | 98041 |
| D38A Phen 69 | 40.13 | 45.95 | 12.58 | 0.328 | 0.194 | 0.290 | 86.7 | 2278 | 1499 | 2343 | 97813 |
| D38A Phen 69 | 40.27 | 46.28 | 12.68 | 0.333 | 0.193 | 0.293 | 86.7 | 2300 | 1492 | 2382 | 98592 |
| D38A Phen 69 | 39.98 | 45.90 | 12.53 | 0.340 | 0.195 | 0.287 | 86.7 | 2254 | 1508 | 2432 | 97426 |
| D38A Phen 69 | 39.67 | 44.24 | 13.87 | 0.346 | 0.212 | 0.248 | 85.0 | 1946 | 1641 | 2472 | 107833 |
| D38A Phen 70 | 39.67 | 43.71 | 15.21 | 0.310 | 0.237 | 0.242 | 83.7 | 1904 | 1837 | 2219 | 118250 |
| D38A Phen 71 | 39.66 | 43.52 | 15.20 | 0.317 | 0.239 | 0.244 | 83.6 | 1918 | 1849 | 2269 | 118224 |
| D38A Phen 71 | 39.75 | 43.73 | 15.05 | 0.310 | 0.236 | 0.243 | 83.8 | 1907 | 1828 | 2214 | 117055 |
| D38A Phen 71 | 39.92 | 43.92 | 15.21 | 0.311 | 0.239 | 0.245 | 83.7 | 1926 | 1848 | 2220 | 118259 |
| D38A Phen 71 | 39.89 | 43.84 | 15.09 | 0.312 | 0.237 | 0.245 | 83.8 | 1928 | 1836 | 2233 | 117318 |
| D38A Phen 71 | 39.81 | 43.96 | 14.74 | 0.314 | 0.230 | 0.238 | 84.2 | 1873 | 1783 | 2244 | 114584 |
| D38A Phen 72 | 40.41 | 46.93 | 11.28 | 0.306 | 0.169 | 0.295 | 88.1 | 2318 | 1307 | 2189 | 87727 |
| D38A Phen 72 | 40.47 | 46.61 | 11.27 | 0.306 | 0.172 | 0.297 | 88.1 | 2331 | 1331 | 2187 | 87660 |
| D38A Phen 72 | 40.40 | 46.66 | 11.40 | 0.303 | 0.172 | 0.293 | 87.9 | 2298 | 1333 | 2163 | 88665 |
| D38A Phen 72 | 39.86 | 45.24 | 12.98 | 0.317 | 0.195 | 0.274 | 86.1 | 2150 | 1514 | 2264 | 100965 |
| D38A Phen 73 | 39.97 | 46.01 | 12.33 | 0.313 | 0.189 | 0.285 | 86.9 | 2241 | 1467 | 2240 | 95878 |
| D38A Phen 74 | 39.76 | 46.03 | 12.33 | 0.316 | 0.194 | 0.281 | 86.9 | 2209 | 1499 | 2258 | 95911 |
| D38A Phen 75 | 39.68 | 45.88 | 12.24 | 0.349 | 0.192 | 0.259 | 87.0 | 2035 | 1487 | 2497 | 95192 |